

**“STUDIES ON SYNTHESIS, CHARACTERIZATION AND
BIOCOMPATIBILITY TESTING OF BIOCERAMICS MATERIAL”**

**A THESIS SUBMITTED TO
BHARATI VIDYAPEETH UNIVERSITY, PUNE
FOR AWARD OF DEGREE OF
DOCTOR OF PHILOSOPHY IN CHEMISTRY
UNDER THE FACULTY OF SCIENCE**

SUBMITTED BY

MR. PRAMOD NIVAS JAGADALE
M.Sc.

**UNDER THE GUIDANCE OF
PRIN. DR. SAMHAJI R. BAMANE**

M.Sc. Ph.D., D.I.T.

**RESEARCH CENTRE
BHARATI VIDYAPEETH DEEMED UNIVERSITY
YASHWANTRAO MOHITE COLLEGE,
ERANDWANE, PUNE – 411038.**

JULY 2015

CERTIFICATE

This is to certify that the work incorporated in the thesis entitled
**“STUDIES ON SYNTHESIS, CHARACTERIZATION AND
BICOMPATIBILITY TESTING OF BIOCERAMICS MATERIAL”** for
the degree of ‘Doctor of Philosophy’ in the subject of **Chemistry** under the
faculty of **Science** has been carried out by **Mr. Pramod Nivas Jagadale** in
the Department of **Chemistry** at Bharati Vidyapeeth Deemed University, **Y.
M. College**, Pune during the period from **Aug 2010** to **July 2015** under the
guidance of **Prin. Dr. Sambhaji R. Bamane**.

Place: Pune

Prin. Dr. K. D. Jadhav

Date: /07/2015

CERTIFICATION OF GUIDE

This is to certify that the work incorporated in the thesis entitled

**“STUDIES ON SYNTHESIS, CHARACTERIZATION AND
BIOCOMPATIBILITY TESTING OF BIOCERAMICS MATERIAL”**

Submitted by **Mr. Pramod Nivas Jagadale** for the degree of ‘Doctor of Philosophy’ in the subject of **Chemistry** under the faculty of **Science** has been carried out in the Department of **Chemistry**, Bharati Vidyapeeth’s **Y. M. College, Pune** during the period from **Aug 2010 to July 2015** under my direct supervision/guidance.

Place: Pune

Prin. Dr. Sambhaji R. Bamane

Date: /07/2015

(Research Guide)

DECLARATION BY THE CANDIDATE

I hereby declare that the thesis entitled “**STUDIES ON SYNTHESIS, CHARACTERIZATION AND BIOCOMPATIBILITY TESTING OF BIOCERAMICS MATERIAL**” submitted by me to the Bharati Vidyapeeth University, Pune for the degree of **Doctor of Philosophy (Ph.D.) in Chemistry** under the **faculty of Science** is original piece of work carried out by me under the supervision of **Prin. Dr. Sambhaji R. Bamane**. I further declare that it has not been submitted to this or any other university or Institution for the award of any degree or Diploma.

I also confirm that all the material which I have borrowed from other sources and incorporated in this thesis is duly acknowledged. If any material is not duly acknowledged and found incorporated in this thesis, it is entirely my responsibility. I am fully aware of the implications of any such act which might have been committed by me advertently or inadvertently.

Place: Pune

Date: /07/2015

Pramod N. Jagadale

(Research Student)

Dedicated to My Grandfather Late Shri.
Baburao Jagadale
(Dada)



*Who is the real source of encouragement,
strength and has brought great deal of
happiness to my life*

ACKNOWLEDGEMENT

Words are inadequate to express my feeling while recording my deep sense of gratitude and respect to my guide Dr. S. R. Bamane, Principal, Raja Shripatrao Bhagwantrao Mahavidyalaya, Aundh (Satara). It was really an experience to work with and to learn from my guide. I salute him for his unbroken faith in experimentation and deep quest for scientific knowledge. I thank him not only for the guidance, he rendered in the field of research but also for enlightening the path of my life with deep love for science. It was his support with which I could overcome my personal and scientific problems and this work could not have been completed without his inspiring guidance, constructive criticism and sustained encouragement during the course of my research programme.

I owe to Prof. Dr. K. D. Jadhav, Principal, Yashwantrao Mohite Arts, Science and Commerce College, Pune for providing necessary facilities and encouragement during research work. I take this opportunity to special thanks Prof. Dr. V. V. Dhapte, Head, Department of Chemistry for the inspiration, scientific guidance, earnest suggestions and encouragement during this work.

I keep on record my deep sense of gratitude to Dr. Patangrao Kadam, Founder of Bharati Vidyapeeth, Pune, and Prof. Dr. Shivajirao Kadam, Vice chancellor, Bharati Vidyapeeth Deemed University, Pune. My special thanks are due to Dr. P. M. Bulakh, Director, BCUD, Bharati Vidyapeeth Deemed University, Pune and Dr. M. G. Bodhankar, Dean, faculty of Science, Bharati Vidyapeeth Deemed University, Pune for their co-operation and help in every aspect throughout this work.

My special thanks are due to my colleagues to Dr. A. B. Pawar, Dr. V. B. Jadhav, Dr. S. R. Kulal, Dr. S. M. Khetre, Dr. H. V. Jadhav, Dr. S. V. Bangale. Dr. S. T. Mane, Dr. A. S. Sapkal, Adhik Bhat, S. N. Kamble, Pramod Jagtap, R. N. Dhale, M.

V. Kamble, Mrs. K. A. Khamkar, for their keen interest and encouragement during the research period.

I believe, it is my pleasant duty to offer thanks to my Friends, Nandkumar Jagadale, Bajarang Pawar, Sachin Salunkhe, Amol Pawar, Rohant Dhabbe, Abhijeet Kumbhar, Santosh Yadav, Rupesh Sawant, Prashant Phadatare, Navanath Chavan, Bhagwan Jagadale, Ramchandra Deshmukh, Dipak Jagadale, Suryakant Jagadale, Shahaji Jagadale, and Shankar Jagadale for their help.

I am also thankful to IIT Bombay, Department of Physics, Pune University, Pune, Dr. Meghand Joshi (Stem One Laboratory, Pune), Shri. Sachin Kalash, CFC Shivaji University Kolhapur, for their help and cooperation.

I am greatly indebted to my father Nivas Baburao Jagadale and mother Sou. Sunanda N. Jagadale who is the real source of encouragement and strength and have brought great deal of happiness to my life. As parents, they provided me the encouragement not only for the period of this thesis but throughout my life. The inspiration and affection of my granny, Sister Dipali, Akka, bhauji Jalindar Jadhav, Bapu, Bhau, Tatya, and brothers Mayur and Vaibhav have provided me all type of moral and emotional support throughout my work.

Lastly, I would like to express my thanks to Prof. S. B. Ballal, Dept. of Microbiology Y. M. College, Pune for his fruitful discussion and co-operation in the patent publications.

Mr. Pramod N. Jagadale

CHAPTER - 1

<u>Introduction</u>	1-21
1.1 Introduction to bioceramics	1-4
1.2 Types of bioceramics	5-6
1.3 Bioceramics in the initial phase	6-7
1.4 Properties of bioceramics	8-9
1.4.1 Biocompatibility	8
1.4.2 Biocompatibility with its components	8-9
1.5 Significant study of biocompatibility of bioceramics	10
1.6 Types of biocompatibility tests	10-11
1.7 Biodegradation	11
1.8 Drug delivery	12
1.9 Applications of bioceramics	12
1.10 Clinical uses of bioceramics	12-14
1.10.1 Orthopedics	12-13
1.10.2 Cardiovascular function	13
1.10.3 Scaffolds for bone tissue engineering	13
1.10.4 Dentistry	14
1.10.5 Drug- Delivery systems	14
1.11 Other applications	14-15
1.12 Preparation of bioceramics	15
1.13 Combustion synthesis	15-20
1.14 Wet chemical technique	20
1.15 Aim and objectives	20-21

CHAPTER - 2

<u>Characterization Techniques</u>	22-47
2.1 Thermal analysis techniques (TG/DTA)	22-25
2.1.1 Thermogravimetry (TGA)	22-23
2.1.2 Differential Thermal Analysis (DTA)	23-25
2.2 X-Ray Diffraction (XRD) analysis	25-31
2.2.1 X-ray Powder photograph	28

2.2.2 X-ray powder Diffractometer	28-30
2.2.3 Identification of substances by X-ray diffraction	30-31
2.2.4 Calculation of crystallite size (t)	31
2.3 Energy Dispersive X-Ray analysis (EDAX)	32
2.4 Scanning Electron Microscope (SEM)	33-35
2.5 Transmission Electron Microscopy (TEM)	36-40
2.6 Fourier transform infrared (FTIR) spectroscopy	40-41
2.7 Wettability measurement,	42-44
2.8 UV-visible Spectroscopy	44-47
2.9 Pellet preparation	47

CHAPTER - 3

<u>Synthesis, characterization and applications of CaSiO₃</u>	48-69
3.1 Introduction	48-49
3.2 Experimental and chemical details	49-55
3.2.1 Cell culture experiments	51-52
3.2.2 MTT cytotoxicity test	52
3.2.3 Cell adhesion test	52-53
3.2.4 In vitro biodegradation behavior	53-54
3.2.5 In vitro drug loading experiment	54-55
3.2.6 In vitro drug release experiment	55
3.3 Results and discussion	55-68
3.3.1 TGA/DTA analysis	55-56
3.3.2 Phase identification	56-58
3.3. 3 TEM analysis	58-59
3.3.4 SEM Analysis	59-60
3.3.5 EDAX analysis	60-61
3.3.6 FTIR analysis	61-62
3.3.7 Wettability studies	62-63
3.3.8 Cell growth measurement	63-64
3.3.9 Cell adhesion studies	64-65
3.3.10 Degradation study	65-66

3.3.11 Drug loading	66-67
3.3.12 In vitro drug release	67-68
3.4 Conclusions	68-69
CHAPTER - 4	
<u>Synthesis, characterization and applications of hydroxyapatite (HAP)</u>	70-90
4.1 Introduction	70-71
4.2 Experimental and chemical details	71-77
4.2.1 Cell culture experiments	73
4.2.2 MTT cytotoxicity test	73-74
4.2.3 Cell adhesion test	74
4.2.4 In vitro biodegradation behavior	74-76
4.2.5 In vitro drug loading experiment	77
4.2.6 In vitro drug release experiment	77
4.3 Result and Discussion	77-90
4.3.1 TGA-DTA Analysis	77-78
4.3.2 Phase identification	78-80
4.3.3 TEM Analysis	80-81
4.3.4 SEM Analysis	81-82
4.3.5 EDAX Analysis	82-83
4.3.6 FTIR Analysis	83-84
4.3.7 Wettability studies	84-85
4.3.8 Cell growth measurement	85-86
4.3.9 Cell adhesion studies	86-87
4.3.10 Degradation study	87-88
4.3.11 Drug loading	88-89
4.3.12 In vitro drug release	89-90
4.5 Conclusions	90

CHAPTER - 5

<u>Synthesis, characterization and applications of Zn doped hydroxyapatite</u>	91-122
5.1 Introduction	91-92
5.2 Experimental and chemical details	92-99
5.2.1 Cell culture experiments	95
5.2.2 MTT cytotoxicity test	95-96
5.2.3 Cell adhesion test	96-97
5.2.4 In vitro biodegradation behavior	97-98
5.2.4 Drug loading experiment	98-99
5.2.5 In vitro drug release experiment	99
5.3 Results and Discussion	99-121
5.3.1 TGA-DTA Analysis	99-101
5.3.2 Phase identification	101-107
5.3.3 TEM Analysis	107-109
5.3.4 SEM Analysis	109-112
5.3.5 EDAX Analysis	112-114
5.3.6 FTIR Analysis	115
5.3.7 Wettability test	116
5.3.8 Cell growth measurement	116-117
5.3.9 Cell adhesion studies	118
5.3.10 Degradation study	119-120
5.3.11 Drug loading	120
5.3.12 In vitro drug release	121
5.4 Conclusion	122

CHAPTER - 6

<u>Synthesis, characterization and applications of Fe doped hydroxyapatite</u>	123-138
6.1 Introduction	123-124
6.2 Experimental and chemical details	124-127
6.2.1 Cell adhesion test	126
6.2.2 Drug loading experiment	126-127
6.2.3 Drug release-in vitro study	127

6.3 Results and Discussion	127-138
6.3.1 TGA-DTA Analysis	127-129
6.3.2 Phase identification	129-134
6.3.3 FTIR Analysis	134-135
6.3.4 Cell adhesion studies	135-136
6.3.5 Drug loading	136-137
6.3.6 In vitro drug release	137-138
6.4 Conclusion	138
CHAPTER - 7	
Summary and conclusions	139-142
Bibliography	143-173
Patents filed, Publications and Conferences attended	174-176

List of Figures

Fig. No.	Title	Page No.
1.1	Several examples of commercial bioceramics	2
1.2	The fire triangle	16
1.3	Combustion synthesized HAP product	20
2.1	Typical (a) DTA and (b) TG curve	23
2.2	Block diagram for DTA	24
2.3	DTA curve	24
2.4	Schematic representation of Bragg's law	27
2.5	Layout of powder diffractometer	29
2.6	Typical XRD pattern	30
2.7	Interaction of the electrons beam with the specimen	34
2.8	Scanning electron microscope	35
2.9	Schematic diagram of TEM	37
2.10	Schematic showing the basic principle behind Michelson's interferometer	41
2.11	The contact angle instrument sketch	43
2.12	Schematic of the energy levels of the various possible electronic transitions	45
2.13	Schematic representation of the UV-Visible spectrophotometer	46
3.1	CaSiO ₃ powder calcined at 1250°C	50
3.2	Thermal behavior of the CaSiO ₃ obtained from TG-DTA measurements	56
3.3	X-ray diffraction pattern of CaSiO ₃ nanoparticles	57
3.4	TEM (A-D) micrographs of the CaSiO ₃ sintered at 1250°C	59
3.5	SEM images of synthesized nanocrystalline CaSiO ₃ ceramic	60
3.6	Energy Dispersive Spectra (EDAX) of CaSiO ₃ Powder	61
3.7	FTIR spectrum of CaSiO ₃ powder	62
3.8	Water droplet on the superhydrophilic of CaSiO ₃	63
3.9	MTT assay results showing the human bone marrow mesenchymal stem cells (BMMSCs) and cord blood mesenchymal stem cells (CBMSCs) proliferation on CaSiO ₃	64

	sample after 12, 24 and 48 h of culturing	
3.10	The morphological behavior of BMMSCs cells without CaSiO ₃ as positive control (A). BMMSCs cells adhering and spreading on CaSiO ₃ surface after 3 days (B) and 7 days (C-D)	65
3.11	Changes in weight loss of CaSiO ₃ after immersion in SBF	66
3.12	Drug loading behavior on CaSiO ₃ at different Drug concentration (A) different temperature (B) and at different stirring time (C)	67
3.13	Drug release percentage from CaSiO ₃	68
4.1	TGA-DTA curve of HAP as synthesized powder	78
4.2	XRD patterns of the HAP samples prepared by auto-combustion method	79
4.3	(A-B) Transmission electron microscopy images of HAP calcined at 1000°C for 4 h	81
4.4	SEM micrographs of the porous HAP bioceramics	82
4.5	Energy dispersive spectra of HAP	83
4.6	FTIR spectrum of HAP powder	84
4.7	Water droplet on the superhydrophilic of HAP	85
4.8	MTT assay results showing the human bone marrow mesenchymal stem cells (BMMSCs) and cord blood mesenchymal stem cells (CBMSCs) proliferation on HAP sample after 12, 24 and 48 h of culturing	86
4.9	The morphological behavior of BMMSCs cells without HAP as positive control (A). BMMSCs cells adhering and spreading on HAP surface after 3 days (B) and 7 days (C-D)	87
4.10	Changes in weight loss of HAP after immersion in SBF	88
4.11	Drug loading behavior on HAP at different Drug concentration (A) different temperature (B) and at different stirring time (C)	89
4.12	Drug release percentage from HAP	90
5.1	Zn-HAP powder calcined at 1000°C	94
5.2	TGA-DTA curve of Ca _{10-x} Zn _x (PO ₄) ₆ (OH) ₂ system (x=0.5)	100
5.3	TGA-DTA curve of Ca _{10-x} Zn _x (PO ₄) ₆ (OH) ₂ system (x=1.0)	101
5.4	TGA-DTA curve of Ca _{10-x} Zn _x (PO ₄) ₆ (OH) ₂ system (x=2.0)	101

5.5	XRD pattern for $\text{Ca}_{10-x}\text{Zn}_x(\text{PO}_4)_6(\text{OH})_2$ system ($0 \leq x \leq 2$)	102
5.6	Transmission electron spectrum of $\text{Ca}_{10-x}\text{Zn}_x (\text{PO}_4)_6(\text{OH})_2$ system ($x=0.5$)	108
5.7	Transmission electron spectrum of $\text{Ca}_{10-x}\text{Zn}_x (\text{PO}_4)_6(\text{OH})_2$ system ($x=1.0$)	108
5.8	Transmission electron spectrum of $\text{Ca}_{10-x}\text{Zn}_x (\text{PO}_4)_6(\text{OH})_2$ system ($x=1.5$)	109
5.9	Transmission electron spectrum of $\text{Ca}_{10-x}\text{Zn}_x (\text{PO}_4)_6(\text{OH})_2$ system ($x=2.0$)	109
5.10	SEM micrograph of the $\text{Ca}_{10-x}\text{Zn}_x (\text{PO}_4)_6(\text{OH})_2$ system ($x=0.5$)	110
5.11	SEM micrograph of the $\text{Ca}_{10-x}\text{Zn}_x (\text{PO}_4)_6(\text{OH})_2$ system ($x=1.0$)	111
5.12	SEM micrograph of the $\text{Ca}_{10-x}\text{Zn}_x (\text{PO}_4)_6(\text{OH})_2$ system ($x=1.5$)	111
5.13	SEM micrograph of the $\text{Ca}_{10-x}\text{Zn}_x (\text{PO}_4)_6(\text{OH})_2$ system ($x=2.0$)	112
5.14	Energy dispersive spectra of the $\text{Ca}_{10-x}\text{Zn}_x (\text{PO}_4)_6(\text{OH})_2$ system ($x=0.5$)	113
5.15	Energy dispersive spectra of the $\text{Ca}_{10-x}\text{Zn}_x (\text{PO}_4)_6(\text{OH})_2$ system ($x=1.0$)	113
5.16	Energy dispersive spectra of the $\text{Ca}_{10-x}\text{Zn}_x (\text{PO}_4)_6(\text{OH})_2$ system ($x=1.5$)	114
5.17	Energy dispersive spectra of the $\text{Ca}_{10-x}\text{Zn}_x (\text{PO}_4)_6(\text{OH})_2$ system ($x=2.0$)	114
5.18	FTIR spectrum of $\text{Ca}_{10-x}\text{Zn}_x (\text{PO}_4)_6(\text{OH})_2$ system	115
5.19	(a–b) Photograph of measured contact angle on surface of $\text{Ca}_{10-x}\text{Zn}_x (\text{PO}_4)_6(\text{OH})_2$ ($x=0.5$ and 1.5) (Pellet)	116
5.20	MTT assay results showing the human bone marrow mesenchymal stem cells (BMMSCs) and cord blood mesenchymal stem cells (CBMSCs) proliferation on zinc doped HAP sample after 12, 24 and 48 h of culturing	117
5.21	The morphological behavior of BMMSCs cells without nanoparticles as positive control (a). BMMSCs cells adhering and spreading on $\text{Ca}_{10-x}\text{Zn}_x (\text{PO}_4)_6(\text{OH})_2$ system after 3 days [b–($x=0.5$), c–($x=1.0$), d–($x=1.5$), e– $x=2.0$)] and after 7 days [f–($x=0.5$), g–($x=1.0$), h–($x=1.5$), i– $x=2.0$)]	118

5.22	Changes in weight loss of $\text{Ca}_{10-x}\text{Zn}_x(\text{PO}_4)_6(\text{OH})_2$ system with ($x=0.5, x=1.0, x=1.5, x=2.0$) after immersion in SBF	120
5.23	Drug loading behavior on Zn-HAP system	120
5.24	Drug release percentage from $\text{Ca}_{10-x}\text{Zn}_x(\text{PO}_4)_6(\text{OH})_2$	121
6.1	Fe-HAP powder calcined at 1000°C	125
6.2	TGA-DTA curve of $\text{Ca}_{10-2x}\text{Fe}_{2x}(\text{PO}_4)_6(\text{OH})_2$ system ($x=0.1$)	128
6.3	TGA-DTA curve of $\text{Ca}_{10-2x}\text{Fe}_{2x}(\text{PO}_4)_6(\text{OH})_2$ system ($x=0.2$)	128
6.4	TGA-DTA curve of $\text{Ca}_{10-2x}\text{Fe}_{2x}(\text{PO}_4)_6(\text{OH})_2$ system ($x=0.4$)	129
6.5	XRD patterns of the pure HAP sample	130
6.6	XRD pattern for $\text{Ca}_{10-2x}\text{Fe}_{2x}(\text{PO}_4)_6(\text{OH})_2$ system ($0.1 \leq x \leq 0.4$)	130
6.7	FTIR spectrum of $\text{Ca}_{10-2x}\text{Fe}_{2x}(\text{PO}_4)_6(\text{OH})_2$ system ($x=0.1$ to 0.4)	135
6.8	The morphological behavior of BMMSCs cells without nanoparticles as positive control (a). BMMSCs cells adhering and spreading on $\text{Ca}_{10-2x}\text{Fe}_{2x}(\text{PO}_4)_6(\text{OH})_2$ system after 3 days [b-($x=0.1$), c-($x=0.2$), d-($x=0.3$), e- $x=0.4$)] and after 7 days [f-($x=0.1$), g- ($x=0.2$), h-($x=0.3$), i- $x=0.4$)]	136
6.9	Drug loading behavior on Fe-HAP system	137
6.10	Drug release percentage from $\text{Ca}_{10-2x}\text{Fe}_{2x}(\text{PO}_4)_6(\text{OH})_2$ ($x = 0.1$ to 0.4)	138

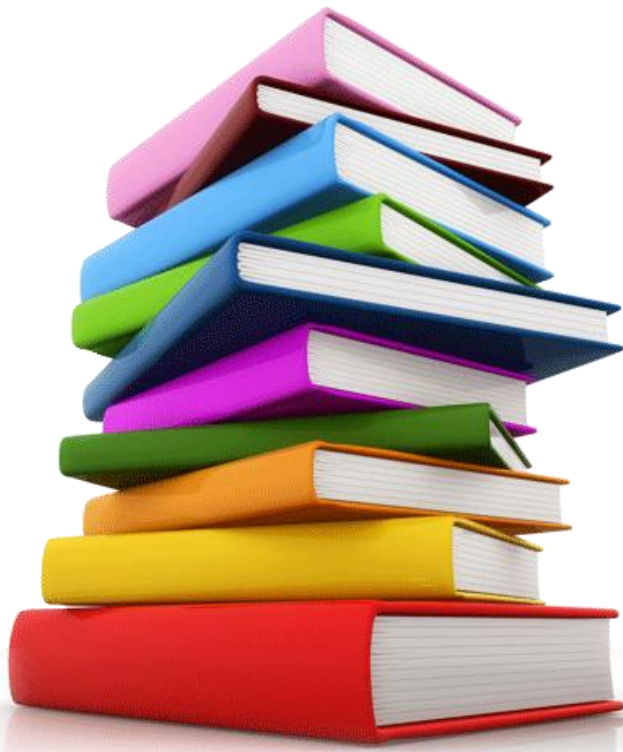
List of Tables

Table No.	Title	Page No.
1.1	Components of biocompatibility	9
1.2	Commonly used fuels in auto combustion synthesis are	18
2.1	Typical JCPD card for TiO_2	31
3.1	Ion concentrations (mmol/dm^3) of SBF and human blood plasma	54
3.2	Reagent used for preparing SBF (1l, pH 7.4)	54
3.3	Indexed X-ray diffraction pattern of CaSiO_3	58
4.1	Ion concentrations (mmol/dm^3) of SBF and human blood plasma	76
4.2	Reagent used for preparing SBF (1l, pH 7.4)	76
4.3	Indexed X-ray diffraction pattern of HAP	80
5.1	Ion concentrations (mmol/dm^3) of SBF and human blood plasma	98
5.2	Reagent used for preparing SBF (1l, pH 7.4)	98
5.3	Indexed X-ray diffraction pattern of $\text{Ca}_{10-x}\text{Zn}_x(\text{PO}_4)_6(\text{OH})_2$ ($x = 0.0$)	103
5.4	Indexed X-ray diffraction pattern of $\text{Ca}_{10-x}\text{Zn}_x(\text{PO}_4)_6(\text{OH})_2$ ($x = 0.5$)	104
5.5	Indexed X-ray diffraction pattern of $\text{Ca}_{10-x}\text{Zn}_x(\text{PO}_4)_6(\text{OH})_2$ ($x = 1.0$)	105
5.6	Indexed X-ray diffraction pattern of $\text{Ca}_{10-x}\text{Zn}_x(\text{PO}_4)_6(\text{OH})_2$ ($x = 1.5$)	106
5.7	Indexed X-ray diffraction pattern of $\text{Ca}_{10-x}\text{Zn}_x(\text{PO}_4)_6(\text{OH})_2$ ($x = 2.0$)	107
6.1	Indexed X-ray diffraction pattern of $\text{Ca}_{10-2x}\text{Fe}_{2x}(\text{PO}_4)_6(\text{OH})_2$ ($x = 0.1$)	131
6.2	Indexed X-ray diffraction pattern of $\text{Ca}_{10-2x}\text{Fe}_{2x}(\text{PO}_4)_6(\text{OH})_2$ ($x = 0.2$)	132
6.3	Indexed X-ray diffraction pattern of $\text{Ca}_{10-2x}\text{Fe}_{2x}(\text{PO}_4)_6(\text{OH})_2$ ($x = 0.3$)	133

6.4	Indexed X-ray diffraction pattern of $\text{Ca}_{10-2x}\text{Fe}_{2x}(\text{PO}_4)_6(\text{OH})_2$ ($x = 0.4$)	134
-----	---	-----

Chapter - 1

INTRODUCTION



1.1 Introduction

Analyzing through the last 3-4 decades and considering especially the medical materials, equipments, machines, etc., the sector has been advancing, developing with respect to different need. Specifically mentioning, the technological advancement into the innovative ceramics is generally used for skeletal repair and reconstruction. “Bioceramics” is the technical word (so-called) referring to the materials used for distinguishes the class of medical implants. Nowadays, expansion and biologically, technically and professionally upgradation of information has been seen via application of Bioceramics. These applications are does having noteworthy hike in the publications and the patents relating to it. Talking about the late 1960s, the medical sector found heavy concern especially with the use ceramics biologically. At its initiation phase, it was considered as a substitute to the metals basically being used to increase a biocompatibility of implants. It has been classified as an assorted category of biomaterials. If you glance through the period of last 30-40 years, we do find a varied and miscellaneous development in this sector irrespective of it’s biological, mechanical and the commercial aspect. Initially, the innovation of bioceramics could endure comfortably the physiological environment. Afterwards, more emphasis was given onto the use of bioceramics, which leads to start the interaction with the human bones. The interaction of bioceramic with human bones occurs via chemical bonding. The current scenario relating to the bioceramics and its formation, function, quality, etc. is considered as an outstanding innovation that can regenerate the bone tissues. Hips, teeth, knees, ligaments and tendons are the major body parts where in we find the major implications of the bioceramics. The concern bioceramic directly replaces the mentioned body parts. In addition to this periodontal disease, maxillofacial reconstruction, augmentation of jawbone especially the bones filled and the spinal fusion are treated through the bioceramics.

In modern Periodic table, the counting of elements reach up to 100+ but, it is quite interesting that only few elements are used for synthesis of the bioceramics viz. zirconia, silica, alumina, carbon and many are enlisted with others also [1]. The development suggests that the materials used, specifically based on the bioceramics, does have versatile significance into the human body usage; it covers the total skeleton of the human body. The bioceramics materials due to its unique factor lead to versatile uses of it in human body covering all body parts of human skeleton. It



There are varieties of definitions have been explained for 'bioceramics'. And as per as the human body is concern with its very well functioning with biomedical materials which confirms that it is well suited with human body environment. These provide proper immunity and the operative facilities to the human body as per the application and the need. Bioceramics are defined as the substances that confirm completely to the human body's environment are those manufactured by the body itself (autogenous) and any other substance that is recognized as foreign, and initiate some type of reaction [6]. On the conclusive terms, the bioceramics are anticipated to line with biological systems for evaluating, treating or replacing a tissue. Same is used in different application as per as the body is concern [7]. Unique feature when concerning about bioceramics comparing it with the other corresponding and usable materials is the potential to remain in any usual and unusual biological environment with no any damage to the surroundings and to itself. Hence, bioceramics is absolutely coupled properly with the province caring for health; imbibe the interface, most needy as far as tissues are concern.

As far as the bioceramics discipline is concern it is said to be synergistic interaction of biological science, material science, chemical science, medical science, also there is requirement of the input of comprehension from all these areas so that, smooth and adequate functioning of the implanted bioceramics in a living body occurs and interrupt normal body functions [8]. The ultimate expected aim through this process is to get the right procedural interaction with biologically implanted bioceramics and concerning living tissues. The bioceramics must pass through different stages such as synthesis of the material, its varied design and then the prosthesis especially for the manufacturing. Additionally mentioning bioceramics should possess the potential to undergo all the research examinations that are looked through its purpose of clinics and the other regulations [9].

Bioceramics because of its uniqueness and the applicative characteristics should have some unique differences comparing with the other materials known biologically. Reason being, 'used material' were healthily acknowledged by the tissues (living) and so can have their usage into replacing the concern tissue, despite that the materials being produced are passing through different steps to be made biological viz. cotton, wood, chitin, bones, etc. [10]. The observation also include the materials made without any help or the constructive involvement of the living organisms, they are so-called biomimetic materials. These biomimetic materials

comprises of the same composition, structure and properties that the bioceramic materials. A step ahead, bioceramics material or the ceramics that is biomedical can be explained as the biomaterials with its ceramic initiation and involvement. To be mentioned in the simple terms that the bioceramics can follow through the structural functions especially for those tissues that needs to be joined or replaced, be applied as coating helping in developing the biocompatibility of implanted metals. In addition is the utility of lattices resorbable, provisionally providing arrangements and frame-works those are dissolved and or replaced as the body rebuilds the damaged tissues [11-16].

To assuage sting and restore function, bioceramics is the needy material for to the tissues that are unhealthy or injured with calcification (bone, teeth, etc.) and its right functioning through the body. Progressive weakening of all the tissues considering it with the human body age is the benefactor majorly to the spares that are necessary. Bone, for any living body is most susceptible part for getting fractured especially to the aged people because the density, immunity and strength get weaker with age. Feminine gender (women) with their varied hormonal changes especially the menopause, are more prone to this. The available theoretical literature reads and represents graphically the timed effect on the strength and density both of the bone for the age by 30s [15]. It is because of the bone-growing cells (osteoblasts) the density decreases and progressively becomes less immune with the productive making of new bone and repairing micro-fractures.

The most common characteristic of the bioceramics is its concerned surface activity. This has the worthy contribution for their ability in binding the bones and so also the enhancing effect on the formation of the bone. While in the process of implantation there can be a reactive affect at the material/tissue been interfaced. This might lead to the changes dependent on time especially into the characteristics concerning only with the surface when implanted material and obviously the tissues surrounding by it [17]. There is a great challenge that is been faced by the bioceramics and its therapeutic relevance so as to put back the aged, weakening of the specified bone although had been the functioning of the material for the life to be lived ideally in the future. So should be substituted with the bone, must be the new.

1.2 Types of bioceramics (Biomimetics and Bioceramics):

A part from the human body undergoing the process of replacement of the synthetic material, it is factual that the reactions observed through do carry versatility about the available resources. It is totally dependent on the material used, its quality, life and the effect. The mechanism of interaction and the response of the tissue results with the surface being implanted. We can define that the use of bioceramics or biomaterials can be classified into three concerning the needy factors and the functions. When named these are called as bioinert, bioresorbable and bioactive [18-21].

1.2, A) Bioresorbable:

Bioresorbable is a biomaterial referring when placed inside the body of a human being; initiate to get melt and the characteristics of coping up makes it gradually substituted by tissue development on medical terms. As an example commonly taken of bioresorbable materials named as tricalcium phosphate [$\text{Ca}_3(\text{PO}_4)_2$] and copolymers with polylactic polyglycolic acid. And others enlisted are calcium carbonate (coral), calcium oxide and gypsum. This all data refers to last three decades.

1.2, B) Bioactive:

Bioactive, the other method relating to the material used for human body, upon its augmentation, has interactions with all the bones responsibly surrounding or cases apart even help in softening tissue. Reaction considering when in the implants of the bioactive process and is been exchanged with an ion and the fluids of the body being surrounded thoroughly outcomes with the biological configuration of active carbonate apatite (CHA) layer that has been implanted on whether chemically or the system named crystallographically both. These methods are similar and comparable into the bone structure especially the phase of mineral into it. Synthetic hydroxyapatite [$\text{Ca}_{10}(\text{PO}_4)_6(\text{OH})_2$] [22, 23], Glass ceramic A-W [24,25], and bioglass [26] are defined as the main components for the same.

1.2, C) Bioinert:

It is the substance when positioned into the body of a human being results in the dealings that are negligible to its nearby corresponding tissues. It is named as bioinert. Mostly a capsule, fibrous in making, mends around forming implantations bioinert in its structure. This is the reason the bio-functionality, considering the

implants based on the integration of tissue. Stabilized zirconia, stainless steel, alumina, cobalt chromium molybdenum alloy (Zimmer alloy), titanium, modern zirconia and alumina alloys and polyethylene with ultra high weight at molecular level are the sector examples of the bioinert materials.

Referring the last four decades, we find the researchers have generated interest into the applications of biomedical supplies especially the ceramics. Mentioning about ceramics, implants in human body with more of the medically oriented facilities including aluminium oxide (alumina), bioglass, calcium phosphates (hydroxyapatite and β -tricalcium phosphate) stabilized zirconia but partially (PSZ), glass-ceramics, and crystalline or carbon in its glassy form and compounds [27].

1.3 Bioceramics – in the initial phase:

Skeleton and the bones it is made of are major part of human body, is also seems to be living tissue with complexity, having a elegant format even when we consider the variables with scales hierarchical mentioned. On the basic terms, composite comprises of phase organically specified (collagen) wherein the inorganic crystals containing calcium [28] is embedded. Comparing the mammals and the body with their bone structure, the last, skeleton does play an important role when you need sustain and motion based support both. It protects body from the organs that are very important; it is vulnerable when the fracture is resulting into grievance with degenerative disease does follow with the age of the concern. This makes mandatory about the repair of the damaged hard tissues right since the earliest time.

The attempt made for the issues of repair of the damaged bones in the earlier era could reinstate tissues that are hard with biomaterials functioning basically and aiming towards restoration. But repair had the causes defective to the grievance and ailment. Now, basic motive is bringing out fully biological response to minimal level helping through the physiological environment and hence the complete absence of the poisonous reaction might be recognized as the ending with triumphant [3].

De Jong [29], the first person who worked over the parallel aspects that X-ray diffraction patterns has, studied the mineral bone and compound called calcium phosphate, hydroxyapatite (HAP) in the late 1920s then after Posner and coworkers identified the same through the methodical process of crystallographic relating to the mineral bone and hydroxyapatite [30-32]. The research (1960s) reveals about

carbonate accessible through bone and also the mineral tooth. Hydroxyapatite, the process, can have its observation directly for spectroscopy reporting infra red.

1960s is been recognized as one of the most momentous period for bioceramics and its corresponding development. Technology had played very fortunate role into this scheme. There have been huge numbers of researchers into this sector with name and fame both. It is genuinely considered that all these had begun with seminal work-process during the contemporary time phase. The names include Prof. Kokubo Hench, Prof. DeGroot and Prof. Bonfield with Prof Aoki, Prof. Jarcho, and Prof. Zhang. All these researchers benefited Europe, China, USA, Japan and UK with all the needy development.

The research with the bioceramics does carry some interested topics viz. the studies on biocompatibility, development of new bioceramics components that will be beneficial for tissue engineering and many more. The metals with their respective biological and mechanical properties doped with hydroxyapatite bioceramics, have emerged as versatile and promising materials for their use in biomedical applications [33-38]. Complexion of different chemicals (bonding) and tissue on other side stands facilitating factor to HAP. This is specifically with purposes clinically termed in comparison with almost all of the other substituted bones viz. allografts/(metallic) implants. Taniguchi, with research, proved HAP sintered displays outstanding cope up biologically to tissues (soft) like muscle, skin, gums, etc. With these, the HAP has been considered as perfect method operative to orthopaedic, dental (implants), components (implants), etc [39-45]. If there is HAP ceramics with low mechanical potency then the application obstructs its facility available for load bearing (low).

Creative development on the recent terms especially with the subject matter such as nano-science and nano-technology has reignited curiosity of different properties of nano-sized HAP such as enhanced sinterability and densification due to huge surface area. This helps smoothening fractural pains and mechanical properties in relation [46]. Engineered tissue with biocompatibility on implants can make use of nano sized HAP particles. Nanotechnology has the considerable capacity and potential both to appreciably benefit the development of HAP biomedical materials.

1.4 Properties of bioceramics:

1.4.1 Biocompatibility:

Biocompatibility is very well been defined as the extensively used biomaterials or bioceramics materials although there exists ambiguity in its definition, when thinking about involved mechanisms with phenomena collectively constituting biocompatibility [47]. Biocompatibility is defined as “ability of material performing with host response appropriately with specific application” [48]. Then factually, the appropriate response from host is vital. Bioceramics materials were at first had selection, development with factors that it would be non-carcinogenic, non-thrombogenic, non-immunogenic, non-irritant and non-toxic. There were two important factors found while in the period of re-evaluation. Firstly, an increasing number of applications required that the material should specifically react with the tissues rather than be ignored by them, as required in the case of an inert material. Secondly, and in a similar context, some applications required that the material should degrade over time in the body rather than remain indefinitely. So the ultimate solution edicts biocompatibility equals biological safety. It means material should be harmless for patient in any respect. This when considered pre-requisite was absolutely of no any need. In the year 2008, biocompatibility was redefined and stated that, “capacity based material must execute its function directing to medical way, with no any elicit undesirably local or has systematic effect to beneficiary of therapy generating appropriate favorable reply from cell or tissue with concern circumstances medically optimizing the performance of treatment [49].

1.4.2 Biocompatibility with its components:

The five components named immunogenicity, mutagenicity, Cytotoxicity, carcinogenicity and genotoxicity that can be considered as the materials with “biocompatibility” and this is with their factorial outcomes to the tissue and the pertinent for the clinical presentation as bioceramics [47].

Table 1.1**Components of biocompatibility**

Beneficial tissue response and the clinically relevant performance
Cytotoxicity (systematic and local)
Genotoxicity
Mutagenicity
Carcinogenicity
Immunogenicity

Toxicity, this term describes that the material has the aptitude damaging biological system because of its chemical processing. The higher level animals, like human beings, etc., with adverse reactions emerging at the application site is local toxicity and it is differentiated from systematic toxicity, in which adverse reaction appear in an area distinct from the application site. Cytotoxicity is for spoiling individual cells and cell culture which vanish due to necrosis or apoptosis.

Immunogenicity, term refers about the competence of material or substance giving aggravating response to immunity. There might be the chances of an allergic reaction. It may get triggered with the substance only if concern organism was earlier been sensitized to substance. Concentrations that elicit a reaction in person, fluctuates with the subjects. The dose levels which are responsible for allergic reactions are generally significantly lower than those causing toxic reactions. Alteration of base pair of the DNA genome is described as the genotoxicity. For repair of the genotoxic damages the affected cells follow through several mechanisms. Even so, situational base, if these hierarchical injuries are taken to generation ahead, then effect is defined as mutagenicity. Carcinogenicity and Mutagenicity both are not equivalent when feature, characters and applications is taken into consideration. Carcinogenicity, here in this affect suggests about the modification in DNA which causes inappropriate cell growth, leads to generation of malignant tumors. One should be importantly aware in understanding all (not) mutagenic event leads carcinogenesis. However, mutagenicity can be used indicator to monitor carcinogenicity of substances that directly attack DNA.

1.5 Significant study of biocompatibility of bioceramics

Bioceramics and biocompatibility both are serious points when referring to three reasons. First, materials are cherished with human tissues with its longevity. Once implanted then no role of patient. The second, process of biocompatibility is still ongoing, had not been processed static. (e.g when considering future dental implants named osseointegrated may not be). The third, it is needed to be concentrated about the biocompatibility and its property of being the item with fixed prosthodontic especially ceramics because it frequently examined by process makers taking it for granted, if segment is on commercial market then there is negligence biocompatibility. The proofs analyzed for quality, consists clinical tests, in-vivo tests (animal experiments) and in-vitro tests (cell culture).

1.6 Types of biocompatibility test:

Bioceramics is innovated with the very first thought to appraise, supplement or substitute tissues of human beings. Biocompatibility is prerequisite (safe) for their safe use in medical devices. Battery of tests is must for assessing biocompatibility. Biocompatibility is done in three methods: in-vitro tests, animal experiments and clinical tests [47]. It starts with in-vitro tests because it has the simple way for testing of biological behavior. The experiments and investigations made finds that the material has efficiency then more comprehensive studies on animal experiments and clinical trials will be performed.

1.6 I) In-vitro tests:

These tests are the used to examine newly developed materials. The test simulates biological reactions onto the segment item when positioned on the tissues. It is worked into test tube (cell culture dish) if not then external structure of living organism where the testing items (cell or bacteria) are linked well to the concern. As an example, bacterial injuries might be judging capability of experimenting segment for mutations (the Ames test). There are a few advantages carried by this test viz,

- experimentally controllable
- repeatable
- fast
- relatively inexpensive
- simple

Most advantageous factor is, avoids ethical and legalities comprising animals and humans for testing.

1.6 II) Animal Experiments (In-vivo):

When an animal undergoes the experiments, then component is positioned to the animal body part (e.g. component is tested against mouse or tooth of monkey, rat, sheep, goat, dog or cat). Animal as experimenting element undergoes reaction taking sufficient time duration that too having versatility with experimenting tissues (e.g. osteopenic bone).

1.6 III) Clinical tests:

These tests need the clinical trials too and are very essential. Clinical segment to be tested is experimented in to volunteer (human being) as intended use to final. Parallel to this testing and controlling elements are examined. High level of significance in comparison to research must be possessed by the controlled clinical. Here during the test only one material is investigated. It is mandatory that for 'Clinical tests' the other two sequential tests are successful.

1.7 Biodegradation:

The presence of body fluids and cells, bioceramics tested has degradation; appearance, physical properties, chemical structure, etc. keeps changing [50]. Bioceramics with its degradation totally depends on crystallinity (reflecting crystal size), particle (size), composition, preparation conditions and porosity. Ca and P containing ceramics and bioactive glasses degrade by dissolution and cellular mechanisms (osteoclastic). Polymers mortify by mechanism of metabolization, erosion and chain scission [51]. When linked with fluids (biology based), bioceramics degrade via dissolution/re-precipitation [52]. Transferring ions passes from solid phase and then to aqueous (liquid) finally to (surface) hydration. Physiology mentions, this process of disbanding is nature dependent of material and its thermodynamic stability. The composition of reaction in-vitro tests [53-55] influences dissolution-reprecipitation mechanism. Biodegradation of biomaterials or bioceramics is achieved by simulated body fluid (SBF), which is blood plasma. This checks release of ions in time. In bone tissue engineering; biocompatible and degradable bioceramics have been extensively experimented on primary carrier for implants [56], also used for controlled drug delivery systems.

1.8 Drug delivery:

Repairs of the bone defects are substituted with materials because of the pains like trauma, arthritis, cancer treatment or other skeletal diseases is often expensive and persistent. If used extensively the materials mentioned might be responsible to cause the major blockade. These devices carry the possibilities for the bacterial adhesion to biomaterials resulting into the biomaterial centered infection (BCI), and the lack of successful tissue integration or compatibility controlled manner [57]. On talks, reads, etc. commented recently, the nano sized and porous bioceramics have gained enhanced interest with biomaterial surfaces [58]. The incidence of BCI is of 2% for hip prosthesis and 4% for knee replacement [59, 60]. If defected by BCI, it causes many severe problems that are very difficult to treat even. The use of antibiotics in orthopaedic surgery has been shown to be beneficial [61]. System of delivery efficient enough must be capable to carry antibiotics to targeted cells or tissues, and release them in keeping in interest as drug stores.

1.9 Applications of bioceramics:

Bioceramics is getting its fame into wide range of medicinal applications especially during the period passing by at this stage. At a primer level the reason for the same is, bioceramics are used for physically to reinstate hard tissues or soft tissues that are said to be hurt through any process of pathology [62]. Year 1920, the first victorious therapeutic applications of bioceramics in human beings were reported by Albee [63]. Two decades just passed, significant advances are found and are have been made in the development of biocompatible and biodegradable bioceramics materials.

1.10 Clinical uses of bioceramics:

An overview of areas where bioceramics can be used-

1.10.1 Orthopedics:

Orthopedic, a medical field needs to have an implant device. This is also one of the most prominent application areas for bioceramics. Bioceramics are used for orthopedic implant devices. Since 30 years that the bioceramics is medically operated for orthopedics and concern surgeries. This is only for the sake that if the calcified tissues having chemical resemblance of mammals therefore with their surprising biocompatibility [43, 64, 65]. Nanotechnology is faster growing technology, and finds its commercial application by forming probable nanocrystalline bioceramics e.g.

bioceramics may be self-setting cement for bone because of better bioactivity, enhanced densification and improved sinterability in comparison with coarser crystal and nanocrystalline calcium orthophosphates [66, 67].

In general there are two directions for the orthopedics application when it is seen through nano-sized and nano-crystalline bioceramics ways:

- (i) Powder form as fillers imparting bioactivity to biocomposites and hybrid biomaterial [68-70]; and
- (ii) Bioceramics with thickness satisfying properties (mechanical) frequently implicated for surgeries like maxillofacial and orthopedic [69].

1.10.2 Cardiovascular function:

Cardiovascular, during body functioning (e.g process of circulating blood into concern body parts like vessels and heart), problems regarding non-functionality can occur with arteries and valves of heart. This body parts can effectively be treated by implanting bioceramics. The valves relating to operative heart suffer with structure based changes preventing valve either being kept open or close. Then on damaged valve has varieties of substitutions.

1.10.3 Scaffolds for bone tissue engineering:

When we mention about bone tissue engineering, the most important aspects is introduction of bioactive material in porous scaffold [71]. Mesenchymal Stem Cells (MSCs) as suggested have their presence by direct extraction through the bone marrow. MSCs, when seen commercially are available with all needy factors. It is sourced cells that cannot be differed considering capacity of raising it to tissues diversified. That can be muscle, cartilage, bone, etc. [72]. The other important fact is MSCs and immune system, are accepted rather it allows production at large-scale and characterization. It supports easiness of accessibility to (allogeneic) tissue repair [73]. Due to the more advantageous character MSCs are widely been used in bone tissue engineering as compared to the other cells [74]. Also biocompatible and a degradable scaffold used as a temporary carrier for implanted cells [56]. This scaffold makes available space needed for processed cells having their own growth [75]. Bone tissue engineering is sector with unique interest of seeding MSCs to porosity defects reconstructing bone [76].

1.10.4 Dentistry:

The tooth/dental pain is ubiquitous worldwide oral disease. Nery et al. (1975) researched on bioceramics having dental application, first was an animal experimented [63]. Today, we find a wide variety of oxide based bioceramics systems used for dental reinstatement and implants with ceramic [77-79]. Superior biocompatibility and outstanding aesthetics are the basic factors with which the materials work through and are very simply fabricated with any shape having considerable sarcastic and mechanical resistance [80-84]. Dense HAP in tooth form has been used as an immediate tooth root replacement to minimize alveolar ridge resorption, which follows tooth loss, and to maintain ridge width and height.

1.10.5 Drug- Delivery systems:

For any of the fastest growing applicative sector we are referring to implants applications, the need is of its delivery, how fast and accurate? The concern devices for controlled or targeted delivery of drugs must be delivered sooner the possible. Several technologies are used for bioceramics as a vehicle for delivering drugs [85-88].

1.11 Other applications:

There is progressive growth in the manufacturing of the bioceramics irrespective of the medical sector. We find its applications in many other sectors too. Some of them are discussed ahead. There had been a test for surface modification of bioceramics nanoparticles for knowing the modulating low pH value which prevents dissolution, inflammation, structured stabilized collusion then serving as intermediary allowing strength based formation of bond between bioceramics/polymer matrices. Ultimately there will be enhancement into potential of its bioactivity [89-91]. On the other aspect with the same approach, bioceramics nano-particle do served as carriers for drug delivering purpose. It is because, in simplified terms, for ease in established biocompatibility, especially handling with affinity about notorious adsorption [92-94]. Nano-sized bioceramics with loading by genes or drugs through adsorption process make available an ambience of protective environment shielding it degrading and providing suitable way for incursion of cell covering the forbidden release of gene/drugs [95]. Through experiments proves nano dimensional bioceramics with its penetration rate high into the membranes also its transfixion efficiency when compared to conventional particles could be 25-fold or higher. HAP, that are nano-

structured handles large and the specific surface area compared to the particles (coarsers) results to potential indication of nano-structured bioceramics may be through delivery of gene and as drug carriers [95-97].

Transferring of nucleic acids (DNA or RNA) to (living) cells (transfection) is primary technique concerning to recent biochemistry with molecular biology. The property mentions that the nucleic acids are really incapable for penetrating cell wall and there is requirement of efficient carriers [98]. Bioceramic nanoparticles exceptional class of non-viral vector, for delivery of genes beleaguered, serve as alternative DNA carriers [99-102] and cells [103-105]. The experimental demonstration had mentioned that the surface modified bioceramic nanoparticles are feasible enough reacting in in-vivo tests targeting specifically liver genes [106]. Modification of surface makes it conventional site for specific gene delivery [106].

1.12 Preparation of bioceramics:

The process used for the preparation of bioceramics can have a great influence over the performance of the materials. There are two or more metals consisting in the ceramic material. The proper mixing of the same will play major role in the preparation. Many systems are available for the synthesis of bioceramics materials including sol-gel, spark plasma sintering, solid state reaction, microwave-assisted method, and ultrasound assisted method, freezing organic-inorganic soft solution, co-precipitation method and auto combustion method [107-114]. There are varieties of bioceramics materials that had been under process of preparation or have already been processed with their conventional methods. These methods involve mixing of the powders of constituent carbonates, precursors, nitrates, etc. as compounds and are thermally maintained at high temperatures. Wide range of conditions have been considered while synthesis for experimental segments; these include rapid quenching, very low oxygen fugacities and maintained high temperature/pressure. It is with the thought achieving stoichiometry, control over structure and phase purity. In the present study, wet chemical precipitation method and auto combustion are employed for synthesis of calcium silicate, hydroxyapatite (HAP), zinc and iron ion doped HAP bioceramics.

1.13 Combustion synthesis:

Year 1967, there was an initiation of the combustion synthesis of advanced materials. Russian scientists Merzhanov Skiniro and Borovinsskaya had led the

experiments. They all used the word ‘self-propagating high temperature synthesis (SHS)’ for synthetic combustion. Main characteristics of this method are short reaction time, high temperatures and fast heating rate. There are two modes signified with the combustion synthesis on the basis of characters. The first was the SHS mode. It was self propagating high temperature synthesis (SHS) mode where the reactants in powder form are heated well continuing reaction converting into wavelike propagation. The other method is combustion synthesis (CS), in which the reactants are well heated consistently with mixture. Ceramics, ceramic composites, intermetallic compounds etc. are the advanced materials for which this CS method was used for synthesizing. Combustion synthesis on its basic level relies mainly on highly exothermic reactions that are self-sustaining. Exothermic reaction starts with ignited temperature using some form of heating source e.g. resistance wire, laser arc etc. and generates heat to maximum level for combustion (1000 to 6500K).

Process of synthetically combustion when alternated, with its aqueous combustion synthesis using precursors like nitrates from desired metals and fuel like citric acid, urea, hydrazine or glycine. Method used for manufacturing various mixed oxides viz. zirconia, ferrites, chromates, [115-119] etc. Aqueous combustion synthesis process when the powder is prepared, in general, they need chemical composition huge pure phase and surface areas.

Combustion synthesis is also known as fire synthesis or self-propagating high temperature synthesis (SHS). For SHS, the needs are right temperature, fuel and oxidizer. CS works as the triangle with all the three elements. Fire had been described as combustion (uncontrolled) producing outputs like heat, light and ash (Fig.1.2). Highly exothermic and redox chemical reactions occur between oxidizer and fuel.

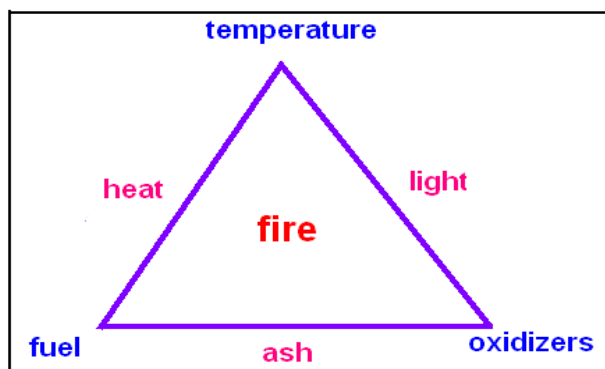


Fig.1.2 The fire triangle

Redox reactions are nothing but the self-propagating high-temperature synthesis reactions; but even though all the redox reactions do not need to be

considered as SHS reactive. For the reactions based on self-propagating the heat generated must be more compared to requirement for initiating combustion. Redox reaction engrosses concurrent process of reduction and oxidation. Defining it at classical level, then, oxygen added or any electronegative element (nonmetal), hydrogen or any electropositive element (metal) is added for controlling. Combustion means flaming (gas-phase) and smouldering (solid-gas). It can either be linear combustion or volume combustion. First method of combustion involves burning surface at whole in layers. Second, combustion is only mixture igniting flames.

SHS process (by Merzhanov), is now, used for preparing technologically based oxides e.g. sensors, refractories, catalysts, semiconductors, magnetic, dielectric, phosphors, etc. and non-oxide materials like silicides, carbides, borides and nitrides by reaction with solid-state between metals and nonmetals [120]. Process is immaterial until and unless it satisfies the requirement like high-purity precursors igniting at temperatures $>1000^{\circ}\text{C}$. Process is exothermic ($T_{\text{ad}} \sim 4000^{\circ}\text{C}$), self-propagating resulting in to coarse products. Russia is using same method at successful level and is preparing many useful items and technologically [121,122], which includes preparation of oxides. The process of combustion is solid-state reaction but on other side homogeneous products are not made. Hence the result is coarse powder. Auto combustion prepares undoped hydroxyapatite (HAP) and doped hydroxyapatite bioceramics with desired properties, structure and composition.

Role of fuels:

Urea an element, by day had been known as fuel for synthetic combustion, oxides like alumina and alkaline, there is need of high temperatures. The necessity is work over the alternates in the process of preparing ceramics, it must be stable at 1000°C , likewise as hydroxyapatite (HAP) and different metal doped HAP. With the same applicative factors hydrazine-based fuels like dihydrazide (MDH), carbohydrazide (CH), maloni and oxalyl dihydrazide (ODH), with its temperature at low ignition. Presence of N–N bond makes it combustible helping in decomposing exothermically to N_2 ($\text{N}\equiv\text{N}$). Investigated and used fuels are enlisted with summary Table 1.2.

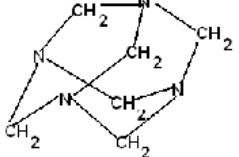
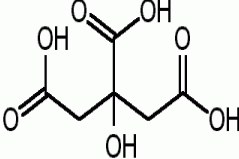
Overall, the fuels mentioned above does follow the purposes written below:

1. These are the sources of C and H, when combusted through the process forms simple gaseous molecules called as CO_2 and H_2O . This combustion liberates heat.

2. They have a complex form of metallic ions assisting the mixing of cations converting into required soluble.
3. It broke off through the components concern. This helps decomposing combustible gases like HNCO, NH₃.

Table 1.2

Commonly used fuels in auto combustion synthesis are-

Sr.No.	Fuel	Formula	Reactants for preparation	Structure
1	Urea (U)	CH ₄ N ₂ O	Commercially available	H ₂ N CO NH ₂
2	Glycine (G)	C ₂ H ₅ NO ₂	Commercially available	NH ₂ CH ₂ COOH
3	Hexamethylene tetramine (HMT)	C ₆ H ₁₂ N ₄	4NH ₃ + 6HCHO Commercially available	
4	Carbohydrazide (CH)	CH ₆ N ₄ O	(C ₂ H ₅) ₂ CO + 2N ₂ H ₄ H ₂ O	H ₃ N ₂ CO N ₂ H ₃
5	Oxalic acid dihydrazide (ODH)	C ₂ H ₆ N ₄ O ₂	(COOC ₂ H ₅) ₂ + 2N ₂ H ₄ H ₂ O (Ref. 9)	H ₃ N ₂ COCON ₂ H ₃
6	Citric acid	C ₆ H ₈ O ₇	Commercially available	

Compounds like citric acid, urea and glycine are simple enough to get acknowledgment of fuels. Compounds with N–N bonds are found assisting combustion well mannered. Important regulatory qualifying for fuel is as mentioned below-

- Being water soluble
- Pertain low ignition temperature (<500°C)
- Compatible with metals like nitrates because the combustion reaction should be smooth enough to be controlled without any explosion.

- Evolves larger amount of gases with low molecular weight and are harmless during the combustion process.
- Easily available and more easy to prepare.

The synthesis via combustion is basically encouraged by fuel and fuel-to-oxidizer ratio. 1000°C to 1500°C is the variable exothermic temperature for redox reaction (T_{ad}), which depends on fuel and metal ion involved. Combustion differs from flaming (gas phase) and non-flaming (smouldering and heterogeneous) type. Flaming reactions during execution of gaseous products like nitrogen oxides (NO_x) by metal nitrates and HNCO, NH_3 , CO, etc., these are made off urea. Mentioned fuels were examined as being specific regarding oxides and ceramics. Urea when considered as an example is generally used for alumina. CH is for zirconia; ODH for Fe_2O_3 and ferrites; TFTA for TiO_2 and related materials; glycine for chromium, etc.

Characteristics of fuel or its specialty is dictated by metal–ligand complexity; the reactions with its thermodynamics and thermal stability. Theoretically mentioning any of the redox mixture if once ignited sure to undergo combustion. Addition of fuel lowers decomposition temperature of the metal nitrates. Hence it makes us to choose the fuel which is again a critical factor in deciding exothermicity of redox reaction examined through metal nitrate and fuel. It totally depends on exothermicity of reaction. Combustion is explosive, flaming or smoldering, e.g aluminum nitrate–urea reaction is exothermic (T_{ad} 1500°C) but is not explosive. Probably, thermal insulating nature of the alumina formed. Here, the changeover between metal nitrate–urea reactions is aggressive. Urea as a fuel being changed to CH or citric acid then the combustion process is more controlled. This because of the complex formation of the metal ions with a ligand like CH and nature of combustion powder is shown in Fig.1.3.



Fig.1.3 Combustion synthesized HAP product

1.14 Wet chemical technique:

This is one more available method by which the preparations of nanostructured bioceramic materials are made. The process involves in preparing an aqueous solution of desired cations and mixing them with other solution containing precipitating agent. Then this precipitated compound is filtered separately. They are consequently calcined at the defined temperatures; finally, yielding powder as product. Solubility of precipitated metal cations must be kept close achieving high homogeneity.

Advantages:

1. Homogeneous mixing of the reactants precipitates and reduces the temperature while in the reaction process.
2. It is a process with simplicity and helping the direct impact on synthesis of powders that are reactive with sintering at low temperature even.

1.15 Aim and objectives:

As far as the current situation of the bioceramic material is concern, we find researchers showing interest and hence there has been a great deal in synthesis of different types of bioceramic materials for biomedical usage. Hydroxyapatite (HAP) with chemical formula $\text{Ca}_{10}(\text{PO}_4)_6(\text{OH})_2$ has been concentrated more [123,124]. It is used as bioceramic because of the properties of osteoconductivity and bioactivity [125,126]. Compared to the other bioceramics like bioglass, the advantage of HAP use as a bioceramic or biomaterial is its chemical similarity to the inorganic component of bone and tooth. HAP or based materials does have no any cytotoxic

effects showing biocompatibility with tissues, skin and muscle [127]. So the conclusive talks about the HAP have been that, it is applied clinically as dense, sintered material with its coating on metallic implants [128,129]. Recently, an enormous number of substitutions, especially the composites resulting from the cationic substitution are of potential application in the fields of dental and bone substitution, luminescence, drug delivery, and catalysis because of the high stability and flexibility of the apatitic structure, [130-133].

The use of HAP does have its limitations in biomedical fields due to relatively slow rate of biological interaction, hence study is focused on success rate of HAP implants. Proper methodology and technique to improve osseointegration is obtained via chemical modification of HAP which is possible through doping it with beneficial elements observed in human bone. Metals like Zn and Fe are considered to have great potential among all the other elements that have been substituted. Also the nanoparticles of calcium silicate (CaSiO_3) ceramics are investigated as bioceramics [109]. Preparative method is more dependent on the distribution of metallic ions and properties [134].

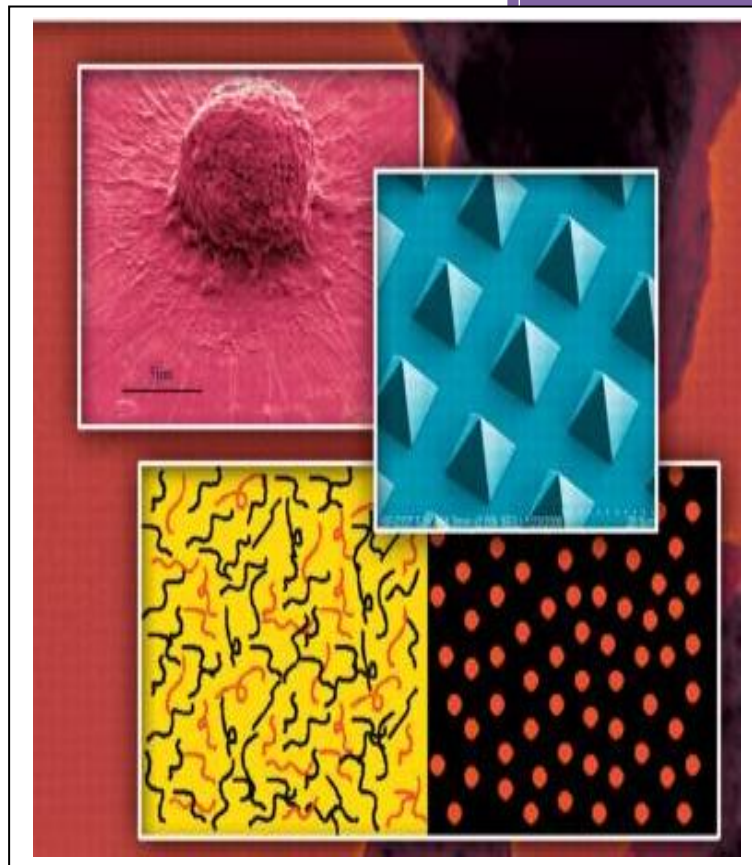
Research mainly focuses on synthesis of bioceramics by auto-combustion and wet chemical precipitation method. Properties considered such as crystal structure, biocompatibility, biodegradability, drug delivery and spectral properties are influenced by ions being in HAP. Therefore, to find out the effect of substitution of Zn and Fe ions on the properties of HAP, various techniques such as scanning electron microscopy (SEM), transmission electron microscopy (TEM), energy dispersive X-ray analysis (EDAX), X-ray diffraction analysis (XRD), thermogravimetric analysis (TGA), differential thermal analysis (DTA) and IR spectroscopy are used.

Auto-combustion process is executed during synthesis of Zn and Fe ion doped HAP, and wet chemical precipitation technique is for synthesis of calcium silicate bioceramics. In vitro biocompatibility, in vitro biodegradation, drug delivery and in vitro wettability properties of these bioceramics have also been investigated.

- a) CaSiO_3
- b) $\text{Ca}_{10}(\text{PO}_4)_6(\text{OH})_2$
- c) $\text{Ca}_{10-x}\text{Zn}_x(\text{PO}_4)_6(\text{OH})_2$ where ($x = 0.5, 1.0, 1.5, 2.0$)
- d) $\text{Ca}_{10-2x}\text{Fe}_{2x}(\text{PO}_4)_6(\text{OH})_2$ where ($x = 0.1, 0.2, 0.3, 0.4$).

Chapter - 2

CHARACTERIZATION TECHNIQUES



2.1. Thermal analysis techniques (TG/DTA):

Considering the last century with this field, we find that the thermal analysis techniques are the most dominant experimental tool developed. This technique starts processing with analyzing the changes in the properties of material likewise function of temperature when it is being heated at the consistent and predetermined rate specified under the ambient of the atmospheric conditions. The analyzed properties that it possess are mass, energy, dimension, modulus of elasticity, dielectric constant, etc. All these properties keep changing with the calculated temperature. Each of the thermal technique is specifically identified with all the potential property measured. There are varieties of theoretical book resource and monographs too that takes a bit deeper for the coverage of the techniques [1-7]. Most commonly and more frequently used thermal analysis techniques are TGA, DTA, DSC and TD. For this research work the techniques used are TGA and DTA mentioned here.

2.1.1. Thermogravimetry (TGA):

Thermogravimetry is defined as the “technique where the mass of the sample element is monitored through functioning of temperature or time when it is targeted to a programmed temperature change in specified atmosphere”. A typical TGA curve referring to the mass loss type reactions as shown in Fig.2.1(b). Into the practicality of the TGA method, the mass change in the sample element is monitored consistently being the function temperature especially avoiding the possibility of missing any phase match to the formation of weakly stable intermediates, stable over a limited temperature range. The plot of mass change against temperature is termed as thermogravimetric or TGA curve. The derivative resulting from thermogravimetric curve is termed as DTA; this has specific use in resolving the partially overlapping multistep reactions that involves the formation of weakly stable intermediates. The ordinates of DTA plot represents rate of mass change ($d\Delta m/dT$) and temperature T is plotted as abscissa. Fig. 2.1 (a) represents the DTA curve. TGA curve Fig.2.1 can be described by characteristic temperatures called the inception temperature (T_i) and the final temperature (T_f). The temperature T_i refers to the temperature where the increasing mass change of the sample element surpass the sensitivity of the recording system and the plot begins to show the removal from the horizontal baseline and T_f representing the temperature at which reaction is said to be complete. The difference

between the steady baselines before and after the transformation analyzes the mass change in DTA is calculated referring the area under the peak.

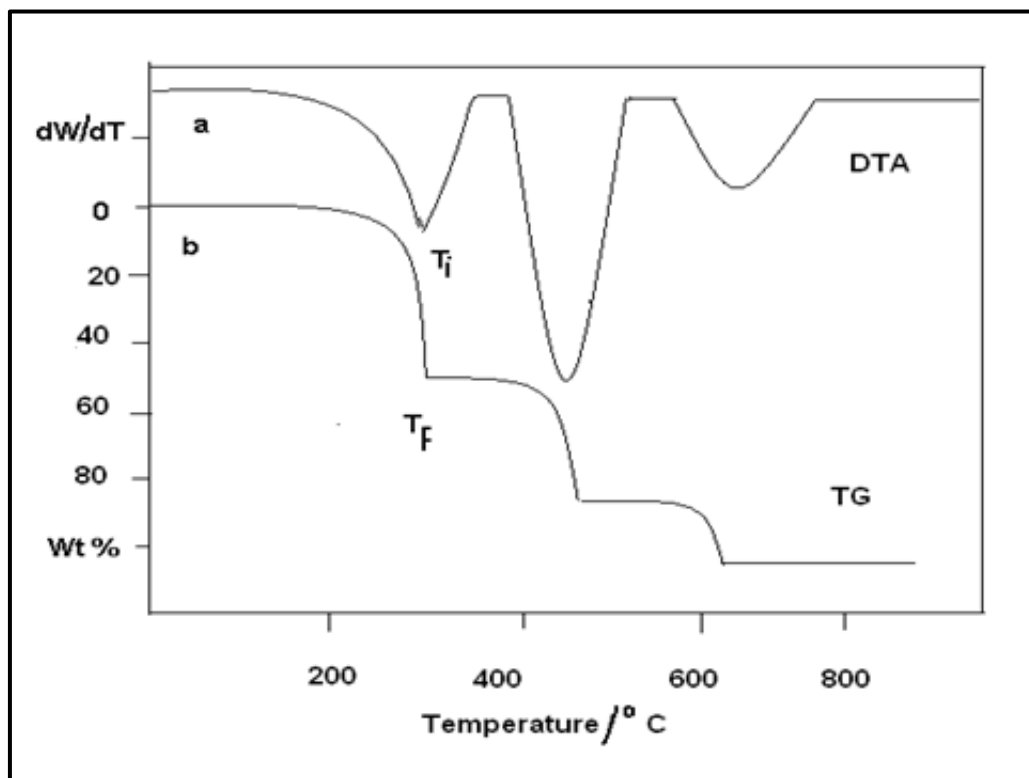


Fig.2.1 Typical (a) DTA and (b) TG curve

TG and DTA curves both seen in the graph are prejudiced by different instrumental factors like heating rate, sample size, ambient atmosphere, type of sample holder and sample characteristics such as particle size etc. [1-3, 7-8].

2.1.2. Differential Thermal Analysis (DTA):

DTA, the chemical process, while progress of processing the temperature dissimilarity (ΔT) compared with sample element and material that is thermally referred and inert enough are endlessly verified as utility of temperature (furnace) (T_f), or time (t), sample temperature (T_s) and reference temperature (T_r). The schematic diagrams for a differential thermal analyzer with its analyzed DTA curve are shown in Fig.2.2 and 2.3 respectively. During the initial stage of the processing temperature represents exactly the beginning of the DTA signal so as to deviate it from a steady base line. The extrapolated onset temperature (T_e) corresponding to the intersection to the base line along the tangent drawn to rising part of the DTA observed at the maximum slope point is often preferred to the initiation temperature.

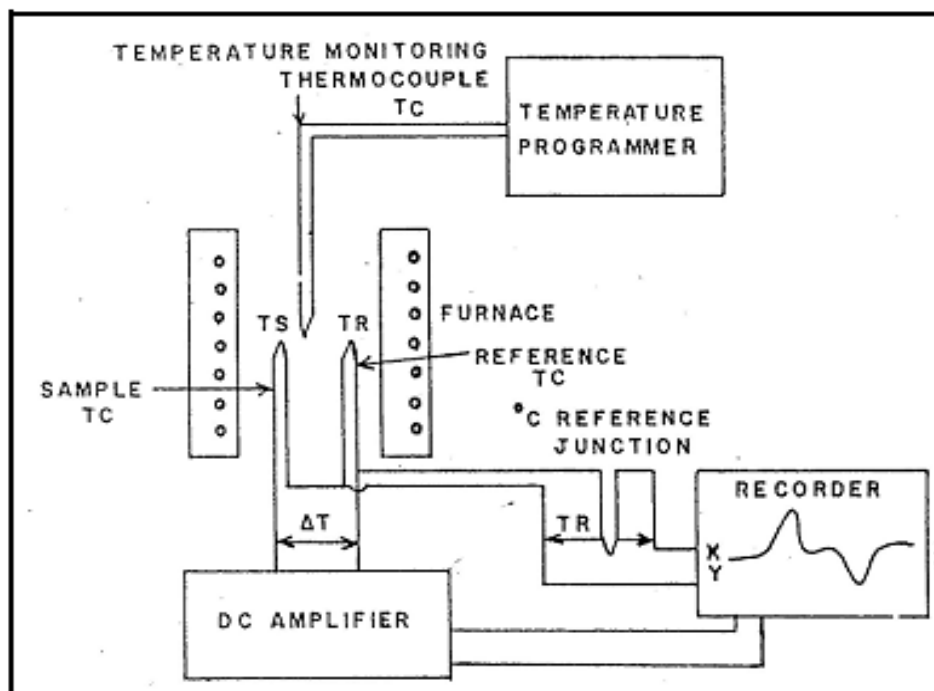


Fig.2.2 Block diagram for DTA

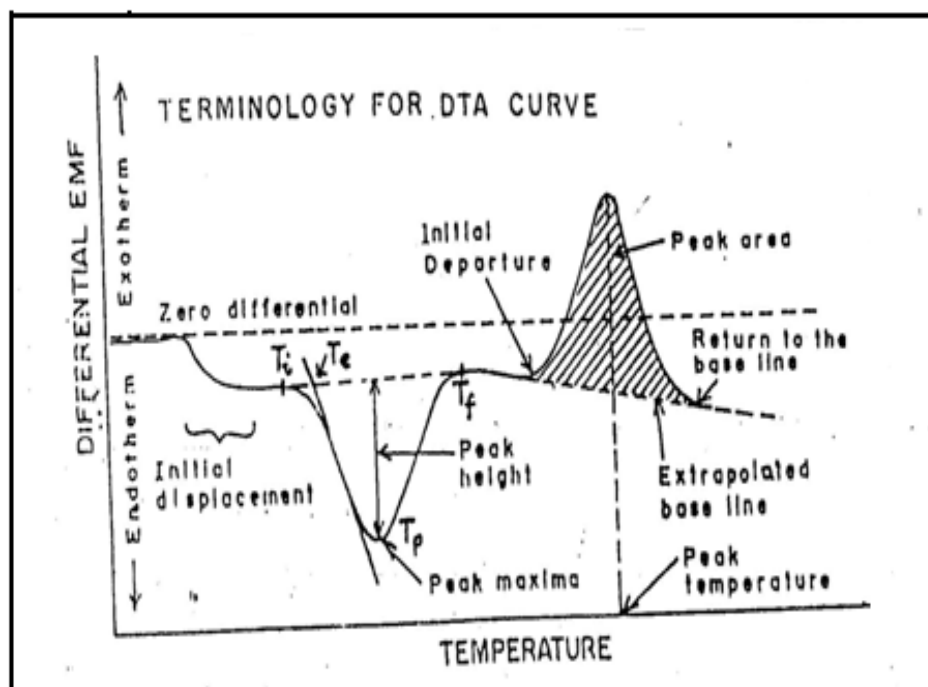


Fig.2.3 DTA curve

The peak of the graph indicates that the temperature is either at the end phase of the reaction or transformation or the stage where the transformation temperature is at its maximum. Finally, T_f indicates that the temperature at which the signal returns to the base line. The changes in the calculated temperature may be because of the

enthalpy changes caused by phase transitions, fusion decomposition reaction, oxidation or reduction reactions, etc. Number of instrumental factors and also the sample element with its characteristics determines the nature of the DTA curve and the magnitude of the peak.

For this investigation Modern instruments used was SDT Q-600. It has been mentioned that the instrumental factors such as geometry and material of the sample element holder, nature and location of the thermocouple, the heating rate and the ambience atmosphere around the sample influences the DTA signal. The particle size, amount of sample used, its heat capacity, thermal conductivity and packing density are the sample characteristics taken under consideration and plays role important enough in affecting DTA curve. The delineation of phase boundary in DTA Technique, measured by evolution or absorption of heat accompanying phase changes, when the sample is heated or cooled at constant rate. Melting and freezing of pure compounds or eutectics is done through the changes into phase.

For operating DTA technique, instrument requires calibrating factor such as temperature and enthalpy. Only the quality based, pure compounds with the required standard materials are recommended for these purposes. The melting point of metals like In, Zn, Sn, Sb, Ag and Au and phase transitions in Li_2SO_4 , BaCO_3 etc. can be used for temperature calibration. Enthalpy calibration can be done using the heats of solid–solid transitions or fusion of the above materials or organic compounds of high purity.

2.2. XRD analysis

X-ray diffraction technique mainly deals with characterization of different crystalline solids. The location and strengths of X-ray when diffracted by a crystalline solid does make available more information about,

1. Crystalline nature of materials
2. Structure of crystalline materials i.e. Crystal axes,
3. Number of atoms per unit cell

Mainly three methods of X-ray diffraction are used namely,

The X-rays is defined with the electromagnetic radiation with a very short wavelength ranging from 0.1 \AA to 100 \AA . These electromagnetic waves or the X-rays are nothing but the sudden obstructive reflection to any of the solidifying object. In this process, initially the rays are generated with the help of X-ray tube and the

electrons are formed by an electrically heated tungsten filament and accelerated towards the target pertaining large variable prospective with target and filament. Further in the process, atoms of the target acts as obstacles for these high speed electrons and these are responsible for formation of X-rays. These X-rays are thoroughly being produced from the faces of the objective. The basic target materials are transition metals such as Mo, W, Cr, Fe, Mn and Cu. The electron on hitting the obstacle target seizes sufficient energy for displacing an electron from the target atom. This hitting then produces an ion with unstable atom and the processing electron with its outer shell acquires the vacancy. The whole transition process is accompanied by the emission of a characteristic photon of a definite wavelength known as X-ray.

The diffraction with its typical phenomenon occurs when the light ways itself through a narrow slit or grating consisting of parallel slits. Considering the crystal with its different atoms and molecules are mostly arranged in several planes with the proper system and the repetitive manner. These inter- planer distances are of the same order of magnitude as the wavelength of the characteristic X-rays are emitted by target. Hence the crystal planes act as a diffraction grating to the X-ray and diffraction occurs. The necessary condition for X-ray diffraction to occur is represented by Bragg's equation (2.1).

$$n \lambda = 2d \sin \theta \quad (2.1)$$

Where n is integer (1,2,3,4.....) called order of refraction, θ is glancing angle of incident X-ray beams on crystal surface, d is inter-planar spacing between crystals planes and λ is the wavelength of X-rays.

Fig.2.4 represents to the ray diagram to satisfy Braggs condition. The path difference especially between the two monochromatic parallel beams that too after the diffraction and can be calculated as $2d \sin \theta$.

The narrow X-ray beam is progressing and when it strikes the surface of the crystal like NaCl at glancing angle θ then the meaning is that the array of ions are in parallel planes AA, BB but are separated with the distance 'd'. LM, the incident ray is converted as MN, the reflected ray; that too from the plane AA similarly PQ, the incident ray is converted into QR, the reflected ray; that too from the plane BB and so on so forth. Now, the second ray PQR needs to pass through a longer distance compared with the first ray LMN, the extra path SQT is being given the work which with the help of geometry of the crystal planes and the laws of the optical reflection brings to just $2d \sin \theta$. When the reflected rays are in same phase with incident ray

there will be reinforcement. Also, the path difference created must be an integral multiple of λ , the X-ray wavelength. Bragg's law needs to be considered with the acquired importance when the issue regarding the diffraction confines with particular family of planes. Bragg's condition is satisfied only when the crystal is rotated and sooner or later the position reaches to particular family of planes.

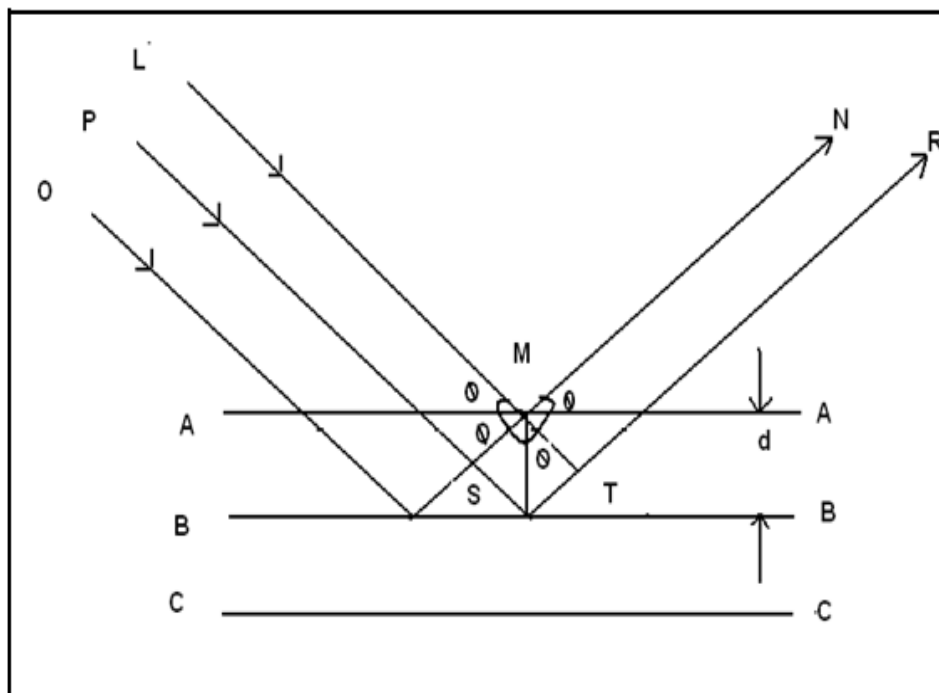


Fig.2.4 Schematic representation of Bragg's law

The XRD Pattern of powder (as said), the intensity of the diffracted beam is plotted against 2θ . And the reflection with its particular intensity totally depends upon the atomic number of atoms, the arrangement of atoms within the unit cell, the unit cell volume of diffracting crystal and the absorption of X-rays by crystal. Talking practically about the X-ray diffraction pattern right since its position of the reflection with observed size and shape of unit cell; all can be well determined.

There are two different ways of obtaining X-ray diffraction data

- 1) X-ray powder photograph by employing the powder camera
- 2) X-ray powder diffraction pattern employing powder diffractometer.

The diffractograms of the concern calculations were reported having 2θ between 10° and 100° . In general, diffraction peak from a lattice plane is labeled as Miller indices (hkl) and these indices are related to inter-atomic spacing or d spacing.

For the hexagonal system (i.e., $a = b \neq c$), the d spacing for any set of planes is given by [9];

$$\frac{1}{d^2} = \frac{(h^2 + k^2 + l^2)}{a^2} \quad (2.2)$$

where a, b, and c are the cell edges.

For hexagonal crystals,

$$\frac{1}{d^2} = \frac{4}{3} \left(\frac{h^2 + hk + k^2}{a^2} \right) + \frac{l^2}{c^2} \quad (2.3)$$

These notations, when used, the Miller indices are assigned for each diffraction peak obtained in a diffractogram.

2.2.1. X-ray Powder photograph:

In this technique, one obtains the complete spectrum and the results of the diffraction are visible on the film after development. The intensity data obtained by this method is much more accurate as all the planes in the crystal are exposed to X-ray radiation repeatedly. The powder photograph of X-ray diffractogram serves as fingerprint in the identification of the compound. Although the film techniques are capable of producing X-ray powder diffraction data, it is time consuming. In addition to long exposure times and time spent in processing the film, it takes several hours to measure the pattern and perform the subsequent calculations for derivation of θ and d values.

2.2.2. X-ray powder Diffractometer:

Diffractometer dealing mainly with the powder, for which it is possible to scan the whole spectrum or only some part of spectrum. The accuracy calculated through this method of the intensity data obtained is comparatively lesser from the photographic method. Interestingly mentioning that the powder diffractometer, with its activeness feature, might develop the needed data for which half an hour is enough and hence it is less time consuming.

Fig.2.5 drawn below is the typical layout of powder diffractometer. For analyzing the same, a flat specimen is positioned at the top, on a moving circled turntable along with movable detector. Bragg's condition is said to be satisfied only when the X-rays are reflected in phase to the detector. This detector is generally technically linked to the specimen table and then is geared. Now, rotating of the table scrolls through θ degrees, the detector rotates through 2θ degrees. This suggests that

the detector is always in specified position so that it receives rays reflected by sample. To record the diffraction pattern, the detector is positioned at or near 0° on the graduated 2θ scale, and then driven by a motor at constant speed e.g. 2° per minute. Alternatively, the detector may be driven clockwise from about 170° .

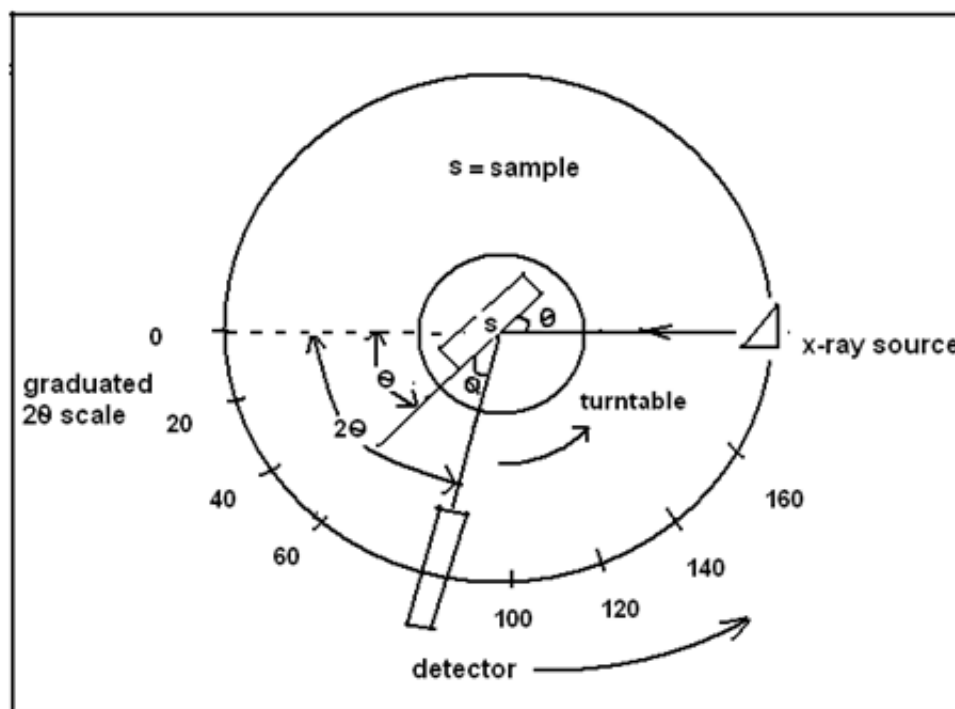


Fig.2.5 Layout of powder diffractometer

As mentioned in the Fig.2.6 about the diffraction of the angles. Generally, a linear intensity scale is used in monitoring the trace and also 2θ scale is printed automatically over it. When the appropriate approximation of the intensities are concerned for qualitative phase analysis then it is very normal in the practice point of view to measure the peak height above the background in mm and to scale the values up or down such that the tallest peak has a value of 100. If the accurate values of intensities are required e.g. for quantitative phase analysis, the peak areas have to be measured.

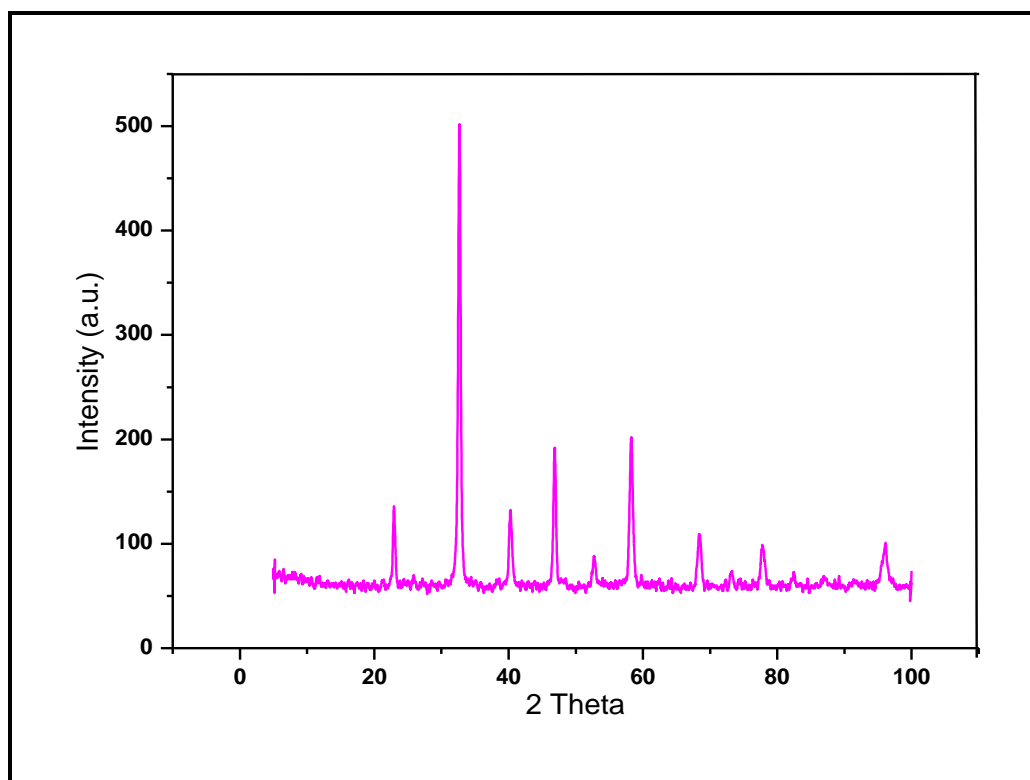


Fig.2.6 Typical XRD pattern

The available diffractometer are gadgetry equipment, can be called as microcomputer and are controlled by the same. Such instruments are basically programmed keeping in view the Bragg's angle for to scan the selected angular range and/or print out actual value ' d ' and so also the intensities in the form of count per second. When the count is in the cardinal or the ordinal form, it should be accurate enough. For such accurate intensity concerning measurement, then the instrument is set stationary so that the detector is receiving diffracted X-rays corresponding to a particular peak. The intensity measured is then part apart for the selected length of time using counting circuitry built into the instrument.

The details of working, application and instrumentation are discussed in several books [10-11]. In the present study Philips Analytic X-ray B.V. (PW-3710 Based Model) Advanced X-ray diffraction is referred.

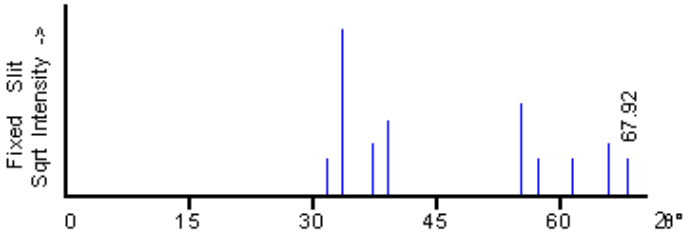
2.2.3. Identification of substances by X-ray diffraction:

The diffraction X-ray method has autonomously proved to be invaluable specifically with the identification of thousands of crystalline phases. This can be considered through its application of the finger-print where this type of pattern is displayed with each sample being the characteristic of that sample. Thus by matching the patterns of a known compound, unknown can be identified. This system was

devised by Hanawalt [12]. Hanawalt selected the specified quantity spacing ‘d’ of lattice plane forming by each line instead of 2θ . Although he found more than one substance can have the same or nearly the same ‘d’ values, Hanawalt characterized each substance by ‘d’ values with its three very meaningful lines. A data bank consisting of d-spacing and intensities of different peaks recorded in the XRD patterns are listed along with the ‘hkl’ Miller indices for each plane. Left-top of each card lists ‘d’ values of three very meaningful lines of a compound. Addition to it is the other parameter like type of unit cell, length of a, b and c axis and the angle between them are also available in the compilation for each compound. Data shall be made available for years together with the new compounds each year to the existing one which is generally referred to as JCPD (Joint Commission on Powder Diffraction) data file.

The X-ray pattern recorded for the compound is compared with that available in JCPD file for its identification. A typical card for TiO_2 is reproduced and presented in Table 2.1.

Table: 2. 1 Typical JCPD card for TiO_2

33-1381	Quality: I	TiO2													
CAS Number:		Titanium Oxide													
Molecular Weight: 79.90		Ref: Liu, L., Science, 199, 422 (1978)													
Volume[CD]: 418.53															
Dx: 5.072 Dm:															
S.G.:															
Cell Parameters:															
a 9.22 b c 5.685															
α β γ															
SS/FOM: F 9=5(0.037, 51)															
I/lor:															
Rad: MoKa															
Lambda: 0.710688															
Filter:															
d-sp:															
2θ	int-f	h	k	l	2θ	int-f	h	k	l	2θ	int-f	h	k	l	
31.589	5	0	0	2	39.098	20	2	2	0	65.701	10	0	0	4	
33.575	100	2	1	1	55.150	30	4	1	1	67.915	5	4	0	3	
33.575	100	3	0	0	57.205	5	2	1	3						
37.280	10	3	0	1	61.344	5	4	2	0						

2.2.4 Calculation of crystallite size (t):

The width counted full at half maxima (FWHM) was calculated for crystallite size referring Scherrers formula in equation 2.4.

$$\tau = 0.94 * \lambda / \beta * \cos \theta \quad (2.4)$$

Where, β = FWHM $\times \pi/180$ in radian

2.3 Energy Dispersive X-Ray analysis (EDAX):

It has primary components counted four of the EDAX:

- 1) Beam source
- 2) X-ray detector
- 3) Pulse processor
- 4) Analyzer

EDAX is a method analytically applied to element based scrutiny or the specified characterization chemically processed with sample. When considered or compared it with the spectroscopy, it is based on sample's examination with electromagnetic radiation. Specifically, examining X-rays released due to hitting through charged particles of matter. To stimulate the emission of characteristic X-rays from a specimen, a high energy beam of charged particles such as electrons, or a beam of X-rays, is focused into the sample being studied. At rest, an atom within the sample contains ground state or unexcited electrons in discrete energy levels or electron shells bound to the nucleus. Beam (incident) for the inner shell might excite an electron and then helping it in ejecting out from shell. This is specifically done by ejecting electron there by generating hole at the actual location of electron. Subsequently the outer shelled electron with the energy of heavy state fills the so-called vacant hole. Finally diversity carried by the energy source considering shell with higher-energy and shell with lower energy might get unconfined into X-ray. Power dispersive spectrometer is an instrument used for measuring X-rays with the count and actual energy that emits through specimen. X-rays with its energy, we are well known, is characteristic disparity of energy between those shells leads to elemental atomic structure from where were they emitted. Factor does allow instrument to get measuring of specimen.

EDAX spectrum and the accuracy talked about get affected with variants. EDAX detectors have some limitations that it can only detect the elemental having atomic number greater than 5 as, meaning that EDAX cannot identify Be, Li, H or He [13]. EDAX when supplied with over-voltage shall upshots with graphical peaks variance and also elevate this voltage to more readings about EDAX budge spectrum to large energies showing the peaks to high and vice versa. Some elements like Mn $K\beta$, Ti $K\beta$, Fe $K\alpha$ and V $K\alpha$ might overlies peaks.

2.4 Scanning Electron Microscope (SEM):

It is an instrument with its versatility in the applicative and the availability especially for analysis of morphological surface and compositions through chemicals. This instrument configured by cathode linked to magnetic lenses; this creates and focuses beam. From period of late 1960s, it has outfitted with capabilities relating to analysis. This detector is basically, used for converting energy of X-ray into voltaic signals. The voltage signals generated transfer the information to processed pulse that at first stage actions signals then overtake into analyzer displaying and stating data.

Mostly available analytical method provides an average composition of a sample. However, the properties of many solids depend not only on the average composition, but also on the composition of the individual grain boundaries, etc. The scanning electron microscope is suitable to study the samples at microscopic levels [14]. The instruments SEM operates with the electrical current at lower electron beam. The result of the instruments is that it can produce an electron image of specimen's surface of up to X160000 magnification with resolution better than 100 Å. SEM's are more comfortable with the X-ray spectrophotometers for the energy dispersion. During its initial phase, the technique designed well resolved high magnification of specimen's surface. It is basically concerned with the surface of topography. The mentioned technique has priorities for the investigation of shape, size and surface texture. It does support in determining the micro cracking of the fractured ceramic and study of diffusion and corrosion of alloys. SEM is also been utilized for to study the local based enrichment in bones, tissues and membranes which may be related to body functioning or the disease involved.

This SEM technique is used in the study of surface morphology of the sample. For the SEM's practical studies, samples are positioned on top of the holder with double-sided adhesive tape. The samples, which are very sensitive to electron beam cause artifacts and also create focusing problems in the SEM. The sample specimen is generally has coat of thin layered (250-300Å) material for conducting just to avoid charging. Coating to the sample helps in surveillance of example's topography. Thermal special effects and insufficient grounding does not disturb through caused blaze and buckle. Coatings are generally made of carbon, gold and gold-palladium and carbon. Often used because of its property of high conduction, easy to apply and can be applied on the specimen thin film either by evaporation/sputtering.

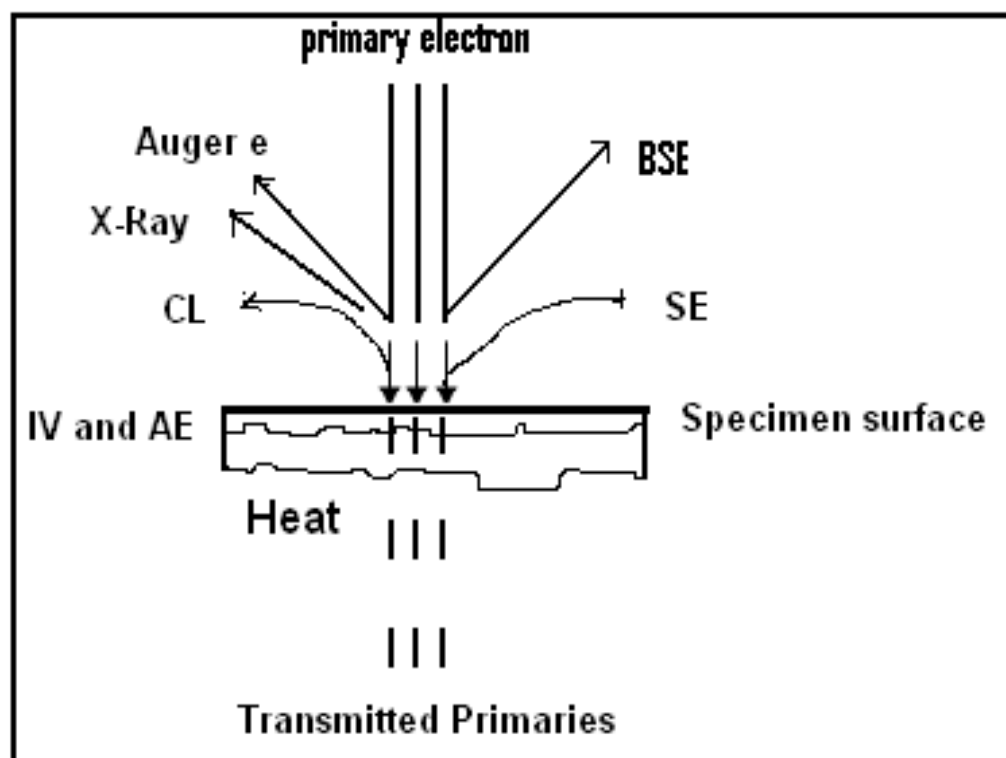


Fig.2.7 Interaction of the electrons beam with the specimen

Beam with interface of specimen results variety of phenomena (physical) such as (1) emission of secondary electrons (SE), (2) reflection of backscattered electrons (BSE), (3) Characteristic X-ray emission, (4) emission of Auger electrons, (5) cathode luminescence (CL), (6) conduction of current, (7) charging from induced voltage (IV) or absorbed electrons (AE), (8) electron transmission, and (9) heat generation Fig.2.7. Of all the enlisted, SE and BSE most priority for making SEM images so also the X-ray emission analysis used in elemental analysis of the selected part of the sample. Secondary electrons (SE) are low energy electrons (5 to 20 eV) emitted by the elemental surface resulting metallic collisions. This collision is of the specimen's primary (incident) electrons (PE) and electrons possessed by it. These electrons are generally originated by 2 – 30 nm on surface with high resolution images. Back scattered electrons (BSE) are PE. PE, undergoes collisions that are multiple irrespective of its existence from the specimen; so is the reason that BSEs have energies over a broad range (15 to 25 keV). BSE compared to SE, are gathered efficiently less because images yielded are by resolution a bit poor. The resourceful reflection of BSE is purpose of specimen's atomic count (Z) (atoms). Hence, contrast between BSE (images) focuses on composed elements. BSE materialize with deeper infiltration (0.1 to 5 μm). The depth referring to the penetration of electrons is

moreover upsets the density of specimen, composition of element, etc. images from the BSE with high/low light elemental phase, or species mixture, demonstrate contrast that represents heterogeneity of element [15].

The SEM in conjugation of energy-dispersive X-ray (EDAX) or wavelength-dispersive-X-ray spectrometry (WDS) is surely an extremely important equipment to characterize specimens (microscopic), size and morphology helping to obtain the information mentioned below in the materials prepared under varying experimental conditions.

The details regarding the procedural working, instrumentation and applications of SEM are very well being discussed in the theoretical different books [11, 14]. The present investigation involves JEOL JSM 6360 Scanning Electron Microscope for the experimental proceedings that helps in the characterization of bioceramics powder for microstructure and morphological characteristics Fig.2.8.



Fig.2.8 Scanning electron microscope

2.5 Transmission Electron Microscopy (TEM):

TEM is one more concern process related with subject, its spatiality being its microscopic method of analyzing under it. The process is likewise that the specimen (ultra thin) has to pass through beam of electrons while this passing the electrons keeps interacting with the specimen and these electrons get transmitted through it Fig.2.9. This image is an output of communication between transmitted electrons by specimen and information due to interaction. The this process, first the magnification of the image is done and then it is focused to imaging device called as fluorescent screen then it is on a photographic film layer where it is the sensor that detects it, and may be CCD. TEM, the process does carry the potential for resolution (high) than any other microscopic devise (light), owing to de Broglie wavelength. Characteristics makes operator of machine to research through any fact (as micro to column of atoms) which is micro in size to the least one resolvable object into (light) microscope. TEM, while comparing bit through the technical terminology can be said, it operates major analytical method within range of fields scientifically made either physical or biological both (sciences). It does have various usages in a few researches like material science, virology, cancer with it is the research made through semiconductor and pollution [16]. When a smaller magnification of an image, there is contrast because of the electron material's absorption with properties like composition and thickness.

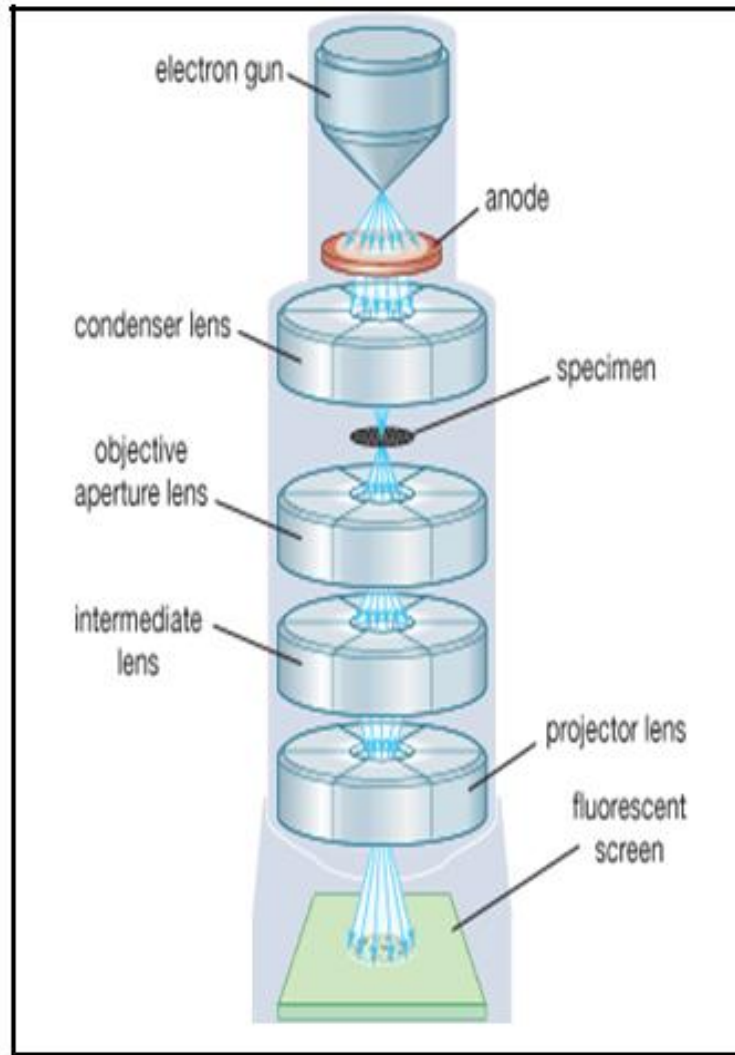


Fig.2.9 Schematic diagram of TEM

While in processing the images with higher magnifications, the interaction that modulates the complex wave with considerable intensity the image is of in respect of expert investigation required by the images scrutinized. There are many alternatives also that are permitted by TEM to monitor electronic structure, crystal orientation, induced electron phase shift, chemical identity, regular absorption based on imaging, etc. It was in year 1931; the TEM, ranked first, was invented by Max Knoll and Ernst Ruska. This team innovated TEM with factors like greater resolving power than that of light (1933) and the first commercial TEM was configured in 1939.

Electrons:

Maximum resolution, d , can be achieved from (light) microscope with limitation to its photon wavelength used for probing sample in equation 2.5, λ and numerical put-up of system, NA [17].

$$d = \frac{\lambda}{2n \sin \alpha} \approx \frac{\lambda}{2NA} \quad (2.5)$$

Scientists from the early twentieth century theorized about the sources available to get limitations of large wavelength considering visible light (400–700 nanometers) using electrons. Unlike everything, electrons do have properties of particle and wave both (by Louis-Victor de Broglie). Here the property of wave meant that beam can perform like beam for radiation of electromagnetic. Electron wavelength is described by equating it to de Broglie equation made for kinetic energy of electron. There is basic need of correction and is must for effects called relativistic. TEM electron's velocity looms the speed of light c , equation 2.6 refers to the same

$$\lambda_e \approx \frac{h}{\sqrt{2m_0E(1 + \frac{E}{2m_0c^2})}} \quad (2.6)$$

Where, h , m_0 and E are the Planck's constant, rest mass of an electron and energy of the accelerated electron, respectively. There is a process named as thermionic emission from the filaments wherein the electrons are generated from microscope. Usually the tungsten is used as Filament. It is parallel as a light bulb. If not, then the alternative process is on field emission of electron. Now mentioned electrons gets acceleration through its electric potential (unit is Volts) and concentrated with the lenses that are electrostatic and electromagnetic too with respect to sample. Procedural transmission of the beam carries the information for phase, periodicity and density of electron respectively; the fact of image for which the beam is used.

Analyzing the process of TEM from initiation to end, it does have the so-called emission source; this source might be filament generated through tungsten or lanthanum hexaboride (LaB_6), etc. When the foundation is tungsten filament then the form may either be like a hairpin-style filament or you can shape it and name it as a small spike. LaB_6 composition is resource accepted as crystal which is small in size and single. Now the gun is connected with high voltage generating source (100-300 kV), is supplied with need based electric current. This process progresses to initiate the emission of electrons through different ways. It either by method called thermionic or vacuum that too emits field electron. Wehnelt cylinder is frequently

supported for this extraction. After it is being extracted from the last, instrument has upper lenses allocation where from the next phase of the process starts.

Manipulation of the electron beam is performed using two physical effects. The interaction of electrons with a magnetic field will cause electrons to move according to the right hand rule, thus allowing for electromagnets to manipulate the electron beam. The use of magnetic fields allows for the formation of a magnetic lens of variable focusing power, the lens shape originating due to the distribution of magnetic flux. Additionally, electrostatic fields can cause the electrons to be deflected through a constant angle. Coupling of two deflections in opposing directions with a small intermediate gap allows for the formation of a shift in the beam path, this being used in TEM for beam shifting, subsequently this is extremely important to STEM. From these two effects, as well as the use of an electron imaging system, sufficient control over the beam path is possible for TEM operation. The optical configuration of a TEM can be rapidly changed, unlike that for an optical microscope, as lenses in the beam path can be enabled, have their strength changed, or be disabled entirely simply via rapid electrical switching, the speed of which is limited by effects such as the magnetic hysteresis of the lenses.

Optics:

Lens, considering its usage into the TEM procedure is allowed especially during the convergence of beam where convergence angle is different constraint and gives TEM its capability of magnification changed process just adjusting supplied electric current flowing by lenses so called hexapole, coil or quadrupole. Hexapole is a mechanical configuration enhancing symmetry of the lens which use of either six or four coils. While, quadrupole is systematic display of coils that are electromagnetic especially at vertices of square. This enables generation throughout into magnetic fields of lens.

In conclusion, the TEM has three stages of the image to be transmitted through the lens namely condenser, objective and projector. A condenser lens, at an initial phase are dependable on primary level of formation of beam, next is objective lenses concentrates more on beam passing through sample and finally projector lenses, basically are made to enlarge beam to screen (phosphor made) or a film. Magnification of TEM is calculated on the basis of ratio between distance of specimen and image plane of objective lens. In addition the quad or hexapole lenses

permits correcting asymmetrical distortion of beam. This is termed as astigmatism. TEM has the optical configurations differing considerably to its accomplishment.

Display:

TEM and its operative system when considered chemically, it contains screen made of phosphor screen. This is made from micro sized (10-100 μm) zinc sulphide and the motive being, operator can have direct observation. The mentioned device or the materials either used or not? as per requirement of analysis of the image in the TEM procedure.

2. 6 Fourier transform infrared (FTIR) spectroscopy:

Currently available on the commercial basis the modern spectrometers having its procedural factor in relation to the infrared region normally make use of the Fourier transform technique. It is mainly for the spectral detection and analysis. The electromagnetic radiation between 400 cm^{-1} to 4000 cm^{-1} falls under infra red region. The mentioned range of the electromagnetic radiation causes transitions in the bond on the vibrating factor. It takes place while the frequency of incident IR radiation matches with the difference between vibration levels. Optical systems in an FTIR spectrophotometer consists of interferometer, infrared light source, an infrared detector and beam splitter [18]. FTIR instrument as we are discussing about, its most essential part is the Michelson's interferometer. This has its static and a movable mirror as has been shown in Fig.2.10. The source for the operation of the same is a Nernst filament. While in the process, the beam of the mentioned Nernst filament is then routed and helped to pass through a beam splitter. Now the beam bifurcates into two parts and then again recombines in constructive mode or destructive mode, fully dependent on variations of path in respect of mirror available is movable. The main signal through it focuses on wave count consisting into process of spanning radiation with full force. Now, it is easy getting integrated contributions of single. The movable mirror with its relative change in the position compared with the immovable mirror there is a special prototype of interference generation. Resultant beam gets dissolved into sample and is detector gets eventually focused. The whole process and their amplitudes from the waves set starts getting absorbed meaning reduction. This is possible only when waves with the set frequency equal even single frequency of being examined. Interferogram has content over entire IR where detector replies for result. Fourier transformation is mathematical calculation helps in converting the

interferogram (that displays intensity v/s time) to the final IR spectrum (intensity v/s frequency). Pyroelectric substance, deuterated triglycine sulfate (DTGS) are the detectors commonly used in the FTIR instruments. Inclusion mercury cadmium telluride (MCT) is other photoconductive detectors. These are highly sensitive to the action in respect of the faster response time [19]. There are four normal modes of vibration when any linear molecule is with 3 atoms. It is on the theoretical basis. These vibrations are symmetric stretching and bending and asymmetric stretching and binding. Hence it is possible to identify the presence of functional groups in a molecule [20]. So has the FTIR its unique feature. It is an indispensable tool in the detection of the presence of capping agents, their interaction with the formed nanoparticles and so on. Almost all samples for FTIR measurements have been drop-coated onto Si (111) wafers and air-dried off which some of the samples have been taken in the form of powder and are thus combined with the KBr powder of the standard. FTIR of samples are processed out in JASCO FT/IR-6100 type. An operative spectrometer is maintained at resolution of 4 cm^{-1} disperses for replication. A total counts 256 scan yielded signal to noise ratio by IR spectra.

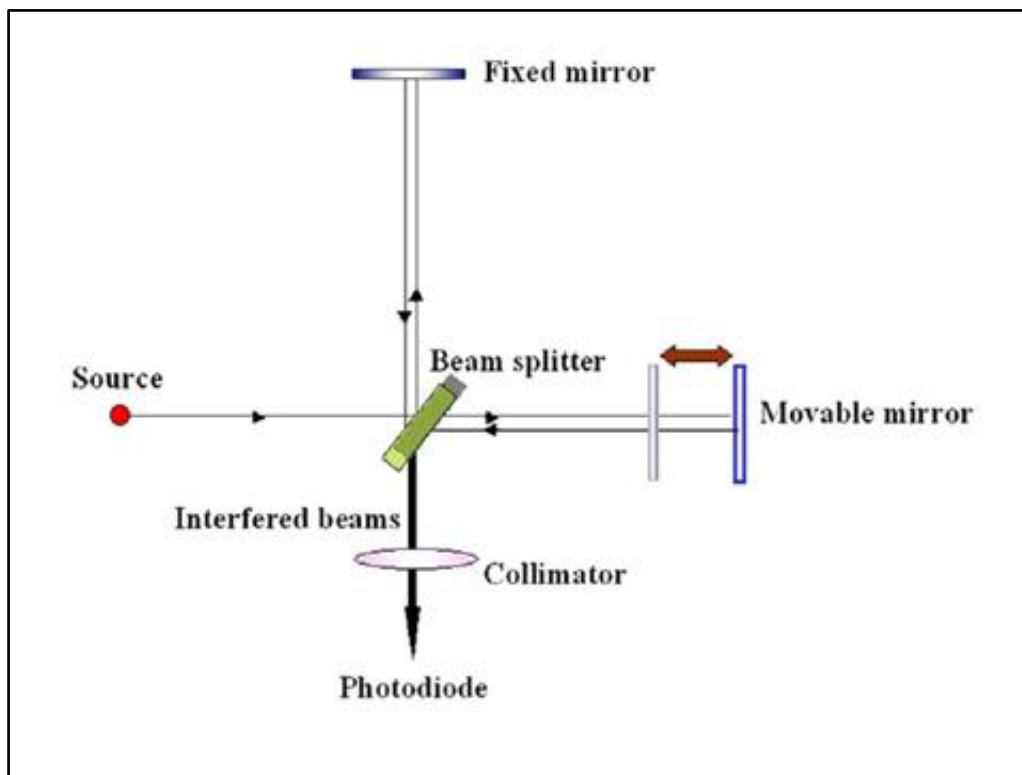


Fig.2.10 Schematic showing the basic principle behind Michelson's interferometer

2.7 Wettability measurement:

Our daily life experiences the wet behaviour of solid surfaces, similarly the science and the engineering does follow the key-ness of this wet behavior. Wettability is one of the property of hard facade. This has generated curiosity in a lot of the commercial applications and does depend on power at surface and structural geometry solid façade [21-23]. On the similar terms, when considering the biomaterials, the wetting states on solid surfaces can be of different advantages like in the biotechnology, bone tissue engineering and biomedical fields. Wettability of solid surface is known by contact angle (CA). This angle is defined as angle made by solid and liquid exterior. If any surface gets wet due to liquid then value of angle is $0^\circ \leq \theta \leq 90^\circ$, whereas if in case any surface does not get wet then value of angle is $90^\circ \leq \theta \leq 180^\circ$. Here the surface termed is believed to be super-hydrophobic like if θ is more than 150° and super-hydrophilic if θ is less than 5° . Although with any science only a few factors can not define the needs. Surface with properties termed as hydrophobic or hydrophilic does not satisfy the needs for devices into development. Here the dominant factors are its surface energy and surface roughness as per the wettability of the surface is concerned. There is specification of contact angle for any of the mentioned system. It is exposed by interactive methods it applies over 3 interfaces. Angle plays significant responsibility for boundary condition. The unit is recognized through goniometer.

We have adhesive and cohesive forces, when finding result oriented it will help to define contact angle. Force with the adhesive character carried by liquid and solid makes liquid converted to drops and broaden over surface. Force with cohesive properties carried by liquid causes drops converted to a ball and rolls down over surface circumvents contact. As drop with tendency of spreading over flat surface with solid structure increase then so called angle starts decreasing. Hence angle mentioned in the situation contrasts with wettability. With the angle less than 90° generally assumes property of getting wet over surface is common and the fallen fluid shall soaked huge surface area. When angle is greater than 90° (high) pretends the process to vice versa. Hence spreading of the fluid to certain level shall decrease affecting physical contact with surface and will get converted to droplet. Chemical terms mentions that the wettable surface is termed hydrophilic whereas, non-wettable as hydrophobic. Energy at surface of experimenting solid is low then surface repels

water from it and vice versa does explaining hydrophobicity or hydrophilicity. Superhydrophilic and super-hydrophobic both are the important factors for any practical applications. Painting, drying, cleaning, pesticide, adhesion and coating heat transfer are the applications where we find wetting phenomenon and its importance.

Consider liquid drop on solid surface. Now, if drop gets attached to surface (water spread over hydrophilic solid surface), then droplet fully widen over considered surface with angle of 0° . With the similar experiment, the hydrophilic (surface) solids with less strength shall attain an angle of 90° . For Hydrophobic surface 90° angles are generally observed. We might observe the angles counting from 150° to 180° on hydrophobic surfaces (high) too. Droplets rest on surface although not wetting any significance if the property of it is as mentioned. These are named superhydrophobic and are obtained by fluorinated surfaces (Teflon-like coatings) which are micropatterned. Lotus effect- the term mentioned for this. Angle provides direct information of energy interacted by surface and liquid. Fig.2.11 shows the sketch of the contact angle instrument.

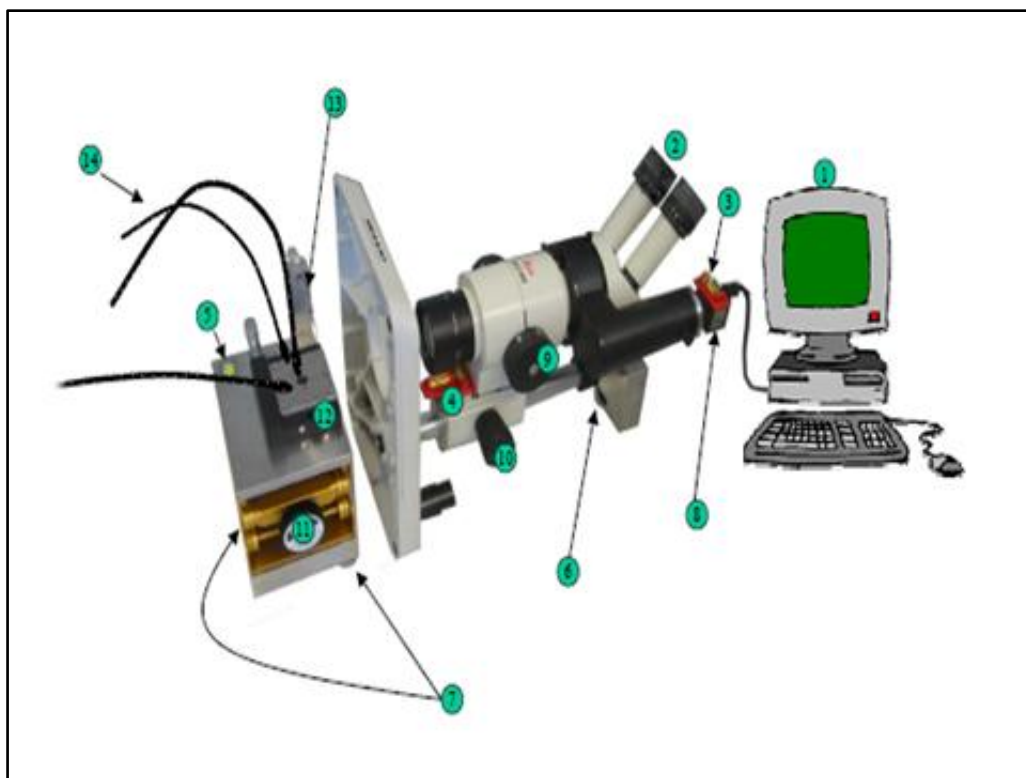


Fig.2.11 The contact angle instrument sketch

1. PC, 2. Eyepiece, 3, 4, 5. Water-level, 6, 7. Leveling screws, 8. CCD Camera, 9, 10. Focus Knobs, 11. Leveling mount, 12. Micro-stage (Sample holder), 13. Micro syringe, 14. Eliminating fibers.

Dynamic sessile drop method was used for the measurement of the contact angle in this case. Distilled droplets (0.01ml) were sent to surface of ceramic material with goniometer (Model 110, Ram hart Instrument Co., USA).

2.8 UV-Visible Spectroscopy

Spectroscopy in relation with absorption where the area is visible has been imperative apparatus for analyst [24]. The colour appeared is signified with appearance and with property of coloured substance absorbing selective colours and reflecting the opposite. This is recognized by electromagnetic spectrum. Energy absorption heads changeover of electron from zero state to excited state. This is governed by equation mentioned below,

$$\Delta E = h\nu = hc/\lambda \quad (2.7)$$

Equation predicts that the UV-energy is properly been quantized and as a result a single discrete line should be obtained from a single electronic spectrum but is not true to the practical aspect of the same because of the case of reality as excitation of electronic energy levels would also involve excitation of the embedded vibrations and rotational energy levels of an atom, thus giving rise to a broad absorption band [25].

The absorption intensity of the band depends on three factors namely

- (a) transition probability
- (b) population of states
- (c) Concentration or path length.

Calculation of transition probability does require an exact knowledge of the waves functioning at initial to final and is generally governed by selection rules. The selection rules, (eg. Laporte's selection rule) with its help, it is possible to predict whether a transition will be allowed or forbidden [26]. Population of states is also an important factor when intensity is concerned because the absorption process from the most populated state shall give rise to the most intense spectrum. If we consider N number of molecules to be divided into the excited (final state) and ground states (initial state) named as f and i respectively, then statistically following Boltzmann distribution,

$$\frac{N_f}{N_i} = \exp(-\Delta E/kT) \quad (2.8)$$

where, $\Delta E = E_{\text{final}} - E_{\text{initial}}$

T is the Temperature in Kelvin

k is Boltzmann's constant

Almost all relationships between intensities of incident and transmitted radiation and the concentration and path-length is governed by Beer-Lambert's law which is written as,

$$I = I_0 \exp(-\kappa cl) \quad (2.9)$$

Where, I = Intensity of the emitted radiation, I_0 = Intensity of the incident radiation, ϵ = constant called as molar extinction coefficient c = concentration and l = path length.

The equation can be recast into,

$$\log(I_0/I) = A = \kappa cl \quad (2.10)$$

Where, the ratio $\log(I_0/I) = A$ is known as the Absorbance or the optical density.

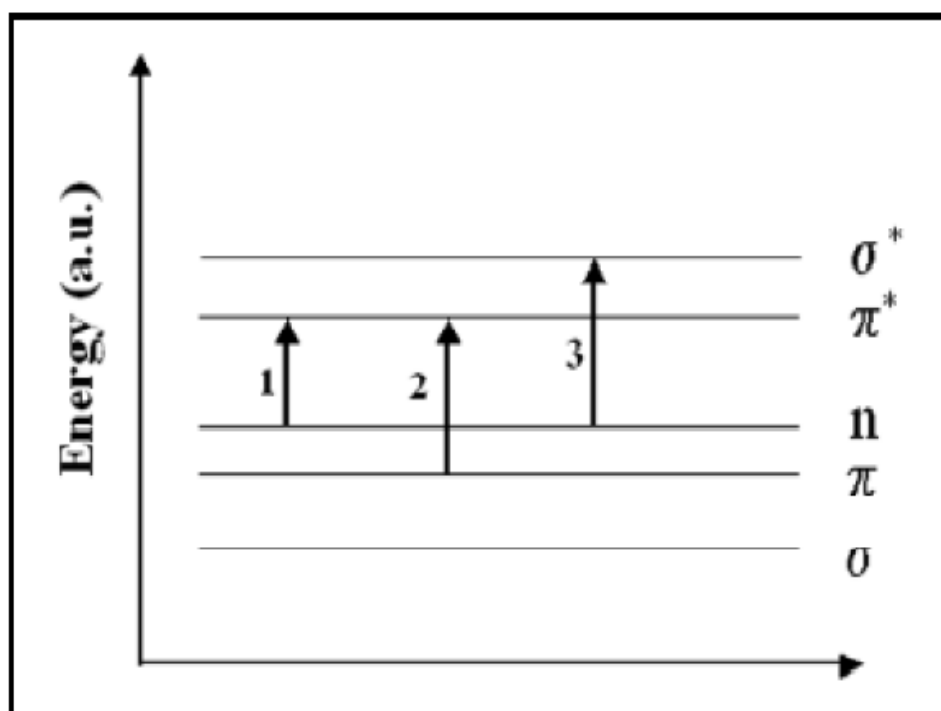


Fig.2.12 Schematic of the energy levels of the various possible electronic transitions

The process of absorbance with the mentioned wavelength is because of the electronic transition which might occur with the following means:

- a) Transition between the bonding and anti-bonding levels of n , π or σ electrons.

- b) Charge-transfer transitions which include ligand-metal, ligand-ligand and metal-metal intervalent transitions.
- c) d-d transitions which are mostly weak in intensity and are prohibited with respect to centrosymmetric rule.

From all the possible electronic transitions, $n-\pi^*$ and $\pi-\pi^*$ transition carries the most intensifying nature and is achieved in case of compounds having either lone pair of electrons or an unsaturated carbon atom (double bonds or conjugated systems) is shown in the Fig.2.12. The requirement of the energy for such transitions is relatively low as compared to the other $\sigma-\sigma^*$ and $n-\sigma^*$, hence their absorption is red-shifted and falls well within the visible range of the electromagnetic spectrum.

As per the recent commercial status of the market, the spectrophotometer available, deuterium and tungsten lamp both are used as the source for characterization in the UV and visible regions respectively [27]. Although xenon arc lamp with all its properties and characteristics can also be used serving the purpose for both UV and visible region. In such a dual beam spectrophotometer, light from either the visible or the ultraviolet source enters the grating monochromator before it reaches the filter.

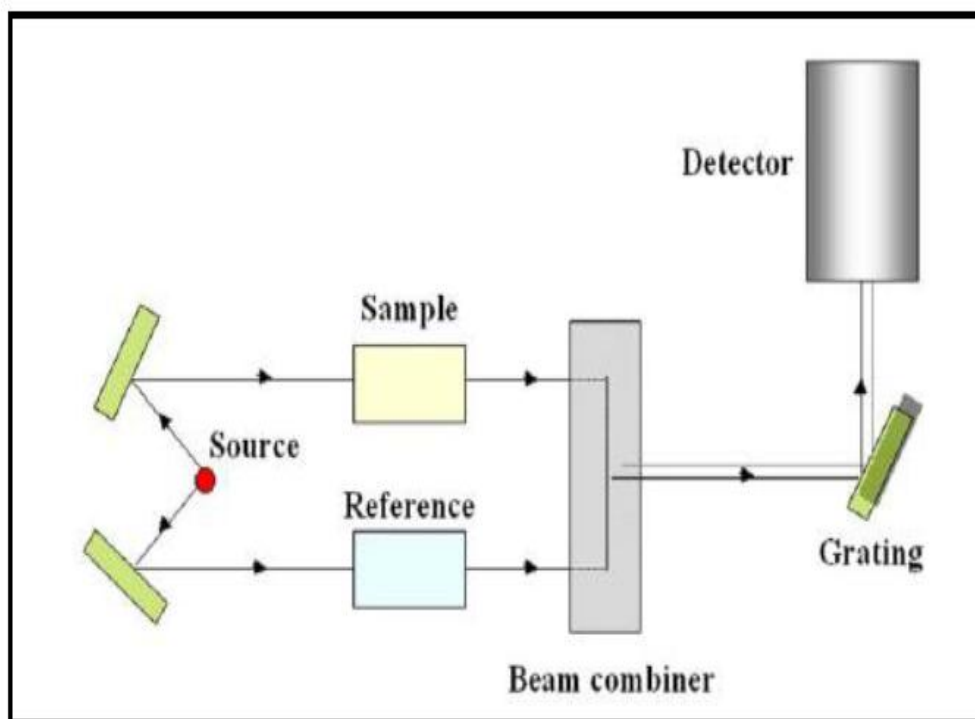


Fig.2.13 Schematic representation of the UV-Visible spectrophotometer

Filter wheel containing the broadband filters are automatically indexed into position at the required wavelengths because this helps in reducing the amount of stray light and unwanted orders from the diffraction grating. The source light is obvious that it gets alternatively bifurcated into one of two beams by the process of rotating mirror called as chopper shown in the schematic of Fig.2.13. From the bifurcated beams, the beam passes through sample and referral sources. Spectrophotometer is double beam – sample and reference. Here both beams are recorded at an instant. The other gadget available, in those, both beams routes through beam chopper works as obstacle for a beam. Photodiode utilized often as detector that keeps on alternating between unit counts of both beams.

UV-Visible spectroscopy is also one more method, widely been used during the characterization of the formation of bioceramics nano-particles. All the experiments have been performed on Systronic UV-Vis double beam AU-2700 UV-visible spectrophotometer in the range of 190nm to 1100 nm.

2.9 Pellet preparation:

For achieving fine particle size of the prepared bioceramic powder, therefore, as prepared powder is ground in an agate pastel mortar. Afterward, powder was sintered at fixed temperature, in muffle furnace. The sintered powder of bioceramics was mixing with PVA (2%) as a binder and then pressed into pellets [28]. The pellets formed through the reactive process then were gradually heated to about 250°C-400°C so as to remove the binder. These pellets when ready were utilized for evaluation biodegradation and wettability property of the ceramics materials.

Chapter - 3

**SYNTHESIS, CHARACTERIZATION AND
APPLICATIONS OF CaSiO_3**

3.1 Introduction:

Bone substitutes are extensively used to overcome different bone damages, reconstructive surgery and degenerative syndrome or disease [1]. Historical three decades had witnessed noteworthy rise in the use of bioceramics especially for bone based surgical operations. Bioceramics is not a drug but is used for the augmentation or replacement of the needy functioning of living tissue or organs. Coping up with the physiological environment, the different type of tissues as well as body fluid gets connected with bioceramics. The process ends with the interaction of the tissues. Bioinert, bioactive and bioresorbable, whichever for the reference, totally depends on the tissue (type) and bioceramics interaction [2].

The ongoing research with the present time have specified that inorganic materials containing CaO-SiO_2 like bioactive glasses [3-5], CaSiO_3 ceramics [6], Apatite–Wollastonite glass ceramics [7, 8] can very well be used to produce bonds with living bones [9]. The bioactivity of CaSiO_3 sample in vivo and vitro can be increased due to creation of apatite layer [10, 11]. Materials meant as bioactive which extract formation of normal tissue and helps in forming a direct bond with the bone have been broadly examined to improve osteointegration. Silica containing ceramics are more bioactive, degradable, and have shown higher bioactivity than calcium phosphate materials [12]. An agent, the silicon is so-called for promoting the formation of new bones [13]. The present research reads more about calcium silicate (CaSiO_3) ceramics with its processed investigation as a new bioceramics for bone regeneration [14, 15].

Previous research reports about calcium silicate make us understand the potential use of calcium silicate such as Portland cements. This is probably related with their load bearing capabilities and bioactivity [16]. However, the major confront to be defeated, on using CaSiO_3 based materials, in biomaterial applications is related to its in vitro cellular functionality. The biological activity of engineered nanosized bioceramics material is improved due to decrement in the particle size. The presence of grain like bioceramics leads to growth of bone [17]. There are important evidences collected through the papers mentioning about the polymer and metal based ceramics nanocomposites specifically used for the improved functioning of osteoblast, which leads to extensive bone growth compared to biomaterial with micrometer range [18]. From reported papers, only a few have been published on in vitro bioactivity

evaluation of nanostructured CaSiO_3 ceramics. Hence this suggests the necessity and importance for synthesizing nano sized CaSiO_3 and investigating there in vitro biodegradation and cellular biocompatibility.

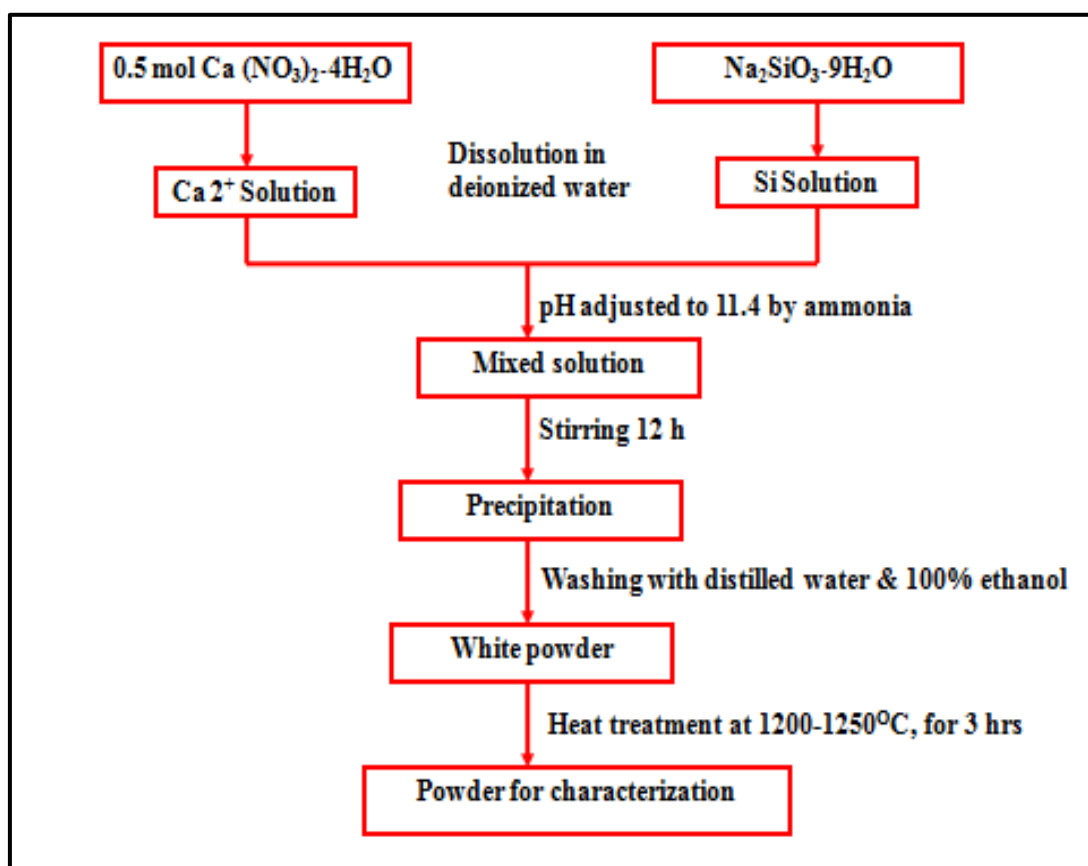
Theoretically referring there have been many methods reported for synthesizing calcium silicate, including sol–gel [19] spark plasma sintering [6], solid state reaction [20], and microwave-assisted method [21]. In use with the need, the nano-sized CaSiO_3 particles are being synthesized by some methods viz. sol-gel and microwave-assisted methods. The most convenient method for the making of nano-sized calcium silicate particles is the ‘wet-chemical method’ [22]. The simplicity in its operation, reactive speed and suitable for large scale production makes this process the most convenient.

Wet-chemical method because of its simplicity and low cost has been used for synthesizing nano-sized calcium silicate. Systematic characterization of these materials was done by different techniques such as XRD, TG/DTA, FTIR, EDAX, TEM, SEM, and wettability to explore their structural properties. The present researches are taking efforts for developing biocompatible, biodegradable materials for their potentials biomedical applications. The current research work is focuses on yields, stability as well as reusability of bioceramics.

3.2 Experimental and material details:

Analytical grade chemical reagents were used as it is without any purification. The nanocrystalline CaSiO_3 powder was prepared by wet-chemical method. Briefly, 0.5 mol sodium silicate [$\text{Na}_2\text{O}_3\text{Si}.9\text{H}_2\text{O}$; Loba] was added in 0.5 mol calcium nitrate [$\text{Ca}(\text{NO}_3)_2.4\text{H}_2\text{O}$] purchased from Merck under continuous stirring. The pH equal to 11.4 is adjusted by adding ammonia. The special arrangement was made to add drop wise sodium precursor (0.5 ml/min.) into the calcium precursor at constant stirring to form a white precipitate. Washing of synthesized precipitate with distilled water was done in order to ensure complete removal of Na^+ and NO_3^- . Then, the precipitate was finally washed with 100% ethyl alcohol to develop the dispersion characteristics. After washing, the precipitate was dried at 60°C to 80°C for 24 h, and then calcined at 1200 and 1250°C for 3 h in a muffle furnace. The pellets were prepared by mixing of calcined CaSiO_3 with polyvinyl alcohol (1-2%) as a binder. The removal of the binder was done by calcinations of pellets at 250 - 400°C . CaSiO_3 in powdered form was used for biological and structural analysis while the pellets were utilized for in vitro

biodegradation behavior and wettability test. Wet chemical precipitation route for preparation of CaSiO_3 sample is shown by flow chart and appearance of powder after calcinations is shown in Fig.3.1. For this synthesis we propose following reaction.



Flowchart of Wet-chemical precipitation route for CaSiO_3 preparation



Fig.3.1 CaSiO_3 powder calcined at 1250°C

Weight loss of CaSiO₃ ceramics was checked by thermogravimetric analysis on the SDT Q-600 instrument by heating the dried powder in air atmosphere from 20° to 1000°C at the rate of 10°C per min. The X-ray diffraction analysis was used to know phase purity of synthesized material by using PW3710 (Model- Philips) with CuK α radiation ($\lambda = 1.5406\text{\AA}$). Debye Scherrer's formula was used to estimate crystallite size of synthesized material [23-25]:

$$\tau = 0.94 * \lambda / \beta * \cos \theta \quad (3.2)$$

Where, crystallite size (τ) depends upon wavelength λ (1.54 Å for CuK α) of the X-ray and the FWHM (β) of the XRD peak at 2θ . Morphology of synthesized nanostructure sample was studied by TEM analysis (Philips CM-200) at 200 kV. The surface topography and microstructure of the sample was examined by means of electron microscopy scanned with different magnifications (JEOL JSM-6360). These nanoparticles were evaluated for the qualitative determination of different elements by energy-dispersive X-ray spectroscopy (JEOL JSM-6360). JASCO FT/IR-6100 type 'A' was used for FTIR study of these nanoparticles. In vitro wetting property of CaSiO₃ sample was evaluated by sessile drop technique using contact angle measurement. A distilled water droplet (0.01 mL) was diffused to the upper surface of CaSiO₃ and examined with sophisticated goniometer (Model110, R. hart Instrument Co., USA). UV-Visible spectral measurements of this sample carried out by using UV/Visible spectrophotometer (Systronic AU-2700). The pH of the solution was carried out by using HANNA phep (model H 19).

3.2.1 Cell culture experiments:

In vitro test is an important parameter to study the biocompatibility of CaSiO₃ sample. Therefore, the present study mainly focuses on in vitro test of as synthesized CaSiO₃ sample. The human bone marrow mesenchymal stem cells (BMMSCs) and cord blood mesenchymal stem cells (CBMSCs) from a passage 4-6 were analyzed as a test subject. Prior to bioceramic surface cell seeding, cells were revived and cultured in Dulbecco's minimum essential medium (DMEM, Make-Sigma Aldrich) with fetal bovine serum (FBS) 10%, 1mM sodium pyruvate, 2mM L-glutamine, streptomycin (50 mg/mL) and penicillin (50 U/mL) as a supplement. The concentration of 5×10^5 cells per well were used for seeding in 6-well plates with 2 mL of DMEM. Further, incubation of the cells was done for growth and proliferation in CO₂ incubator optimized at 5% CO₂, 90% humidity with temperature at 37°C. The cells were

cultured with 20, 60, and 80 µg CaSiO₃/ml for 12, 24 and 48 hours (70% confluency) before the assays.

3.2.2 MTT cytotoxicity test:

MTT cytotoxicity test is very important to evaluate cell viability and cell proliferation of bioceramic materials. As synthesized CaSiO₃ sample was therefore analyzed by MTT cytotoxicity test to study cell cytotoxicity, proliferation and viability. Well-characterized BMMSCs and CBMSCs cells were used and cultured by culture method described previously [26]. Each composition was taken in three replicate. Initially, autoclaved samples were positioned in the well plate and consequently washed with PBS. After that, 96 well plates were seeded with concentration of 5×10^5 cells per mL. Afterward, the incubation of culture plate in CO₂ incubator was done for 12, 24 and 48 hours. Subsequently, the medium was aspirated and then samples were washed with PBS twice. 20 µL of MTT dye solution [(3-(4,5-dimethylthiazol-2-yl) -2,5 diphenyltetrazolium bromide: Make-SIGMA, USA, Cat no.M5655)] and 5 mg per mL phosphate buffer was added to each well so as to pH =7.4. Lastly, the incubation of plate for 15 min and 4 h was done for steady-state confluent cells and exponentially growing cells respectively. After the incubation, the samples were taken off from the well and the crystals were solubilized with help of DMSO (200 µL) and this solution was energetically stirred for dissolution of the reacted dye. ELISA automated microplate reader was used to check the absorbance of each well at 550 nm (Biorad). All data were given in form of mean \pm SD for three group samples. The culture medium without cells is used as blank to calibrate the spectrophotometer at zero.

The viability of the cell in percentage is related to control wells containing cell culture medium without any addition of nanoparticles and was analyzed using the formula:

$$\text{Cell Viabilities (\%)} = [A] / [AB] \times 100 \quad (3.3)$$

Where, A and [AB] is the absorbance of the test sample and control sample respectively.

3.2.3 Cell adhesion test:

Cell adhesion property of bioceramic samples provides basic information due to which bioceramics were widely used in tissue engineering. Therefore, in vitro cell adhesion test of CaSiO₃ sample was evaluated using microscopic methods. This property is carried out to examine whether the CaSiO₃ sample is capable to sustain

morphology of the MMSCs. The cells were cultivated in direct contact with the CaSiO_3 sample. Therefore, mesenchymal stem cells (MMSCs) derived from bone marrow of sheep and plated in to the 50 mL hard glass test tube. The cells were moderately immersed in Dulbecco's modified Eagle medium with 10% serum of animal, 100 U per mL penicillin G, 100 μg per mL streptomycin (invitrogen) and 15 mg of CaSiO_3 (calcined powder) sprayed on the surface of cultured cells which acts as supplement. These cultured medium was incubated in CO_2 incubator operated at optimized conditions (5% CO_2 , 90% humidity) at 37°C for 7 days respectively. After selected time points, for morphological examination surface layer of cultured medium was removed and dried in air after washed with distilled water. The adherent cells on CaSiO_3 sample were visualized under 40X magnification microscope (Coslab, Model HL-9). Additionally, one culture medium containing MMSCs without studied sample considered as positive control.

3.2.4 In vitro biodegradation behavior:

Degradability of bioceramics is most important parameter in the biomedical field. Therefore, in vitro biodegradation behavior of CaSiO_3 sample was carried out in simulated body fluid (SBF). Ionic concentrations were used to prepare the SBF solution which is nearly similar to human blood plasma. It is prepared as per the procedure developed by Kokubo [27-29]. The comparison of human blood plasma with ion concentration of SBF prepared by Kokubo method was displayed in Table 3.1, and Table 3.2 provides appropriate quantities of reagents to be added in de-ionized water to have desired ionic concentration. Reagents are added in stepwise manner Table 3.2. Further, pH of this solution was adjusted to 7.4. The temperature of the SBF solution is maintained at 37°C .

To assess in vitro biodegradation tests the CaSiO_3 pellets (3 wt%) were added in closed bottle of SBF solution maintained at body temperature and are incubated for 5, 15, 20, 35, and 50 days. Afterwards, the pellets of sample are taken out from SBF solution subsequently rinsing with de-ionized water, and drying in an oven at 100°C - 150°C for 24 h was done. At last, weight loss (%) of sample and particulates was calculated by precise electronic balance. Two pellets of each group were rested under the above mentioned condition. The weight loss % (WL) of pellet during immersion in SBF was calculated using equation 3.4

$$WL = \left(\frac{M_0 - M_t}{M_0} \right) \times 100 \quad (3.4)$$

Where, M_0 and M_t was the initial weight and the weight of sample at time 't' respectively.

Table 3.1
Ion concentrations (mmol/dm³) of SBF and human blood plasma

Ionic concentration (mmol/dm³)	Simulated body fluid	Blood plasma
Na ⁺	142	142
K ⁺	5.0	5.0
Mg ⁺	1.5	1.5
Ca ⁺	2.5	2.5
Cl ⁻	147.8	103.0
HCO ₃ ⁻	4.2	27.0
HPO ₄ ⁻	1.0	1.0
SO ₄ ⁻	0.5	0.5

Table 3.2
Reagent used for preparing SBF (1L, pH 7.4)

Order	Reagent	Amount (g/l)
1	NaCl	7.996 g
2	NaHCO ₃	0.350 g
3	KCl	0.224 g
4	K ₂ HPO ₄ ·3H ₂ O	0.228 g
5	MgCl ₂ ·6H ₂ O	0.305 g
6	1M-HCl	40 ml
7	CaCl ₂	0.278 g
8	Na ₂ SO ₄	0.071 g
9	(CH ₂ OH) ₃ CNH ₂	6.057 g

3.2.5 In vitro drug loading experiment:

If the material is biocompatible and biodegradable and have capacity to uptake and release drug in controlled manner then this material have applications in

biomedicines [10, 30, 31]. For that purpose, norfloxacin (widely used antibiotic) was chosen as model drug. In particular, different concentrations (5, 10, 15%) of norfloxacin powder were prepared by dissolving it into 100 mL of de-ionized water. Afterwards, 1 g of CaSiO₃ sample was added to above said drug solutions. The resultant suspensions were stirred for different time (20, 40, 80, 120 minutes) and different temperatures (40, 50, 60, 70°C). Then after, the resultant solution was kept intact for 24 h. The solution was centrifuged in order to separate the precipitate. The drug loaded on CaSiO₃ sample was assessed by knowing the difference in concentration of drug before and after loading. Drug loading (%) on CaSiO₃ was evaluated by following equation:

$$\text{Drug loading (\%)} = [(A-B)/A] \times 100 \quad (3.5)$$

Where, A is the initial and B is the final norfloxacin concentration in aqueous solution.

3.2.6 In vitro drug release experiment:

Time period of 200 hrs was used to evaluate in vitro drug release. 100 mg of drug-loaded CaSiO₃ sample added into a capped glass bottle contains phosphate-buffered (50 mL) saline (PBS) having pH = 7.4 and incubated at 37°C. The stationary mode was used to study drug release. To calculate the released amount of drug, 5 mL of sample were centrifuged and replaced with 5 mL of fresh PBS medium. Afterwards, the actual concentration of Norfloxacin in the supernatant liquid was measured at 274 nm using spectrophotometer.

3.3 Results and discussion:

3.3.1 TGA/DTA analysis:

Thermal stability of CaSiO₃ ceramic sample was examined by thermal decomposition of the powder. The TGA-DTA results as shown in Fig.3.2, it was observed that initial ceramic sample losses 19.35 weight (%) as compared to its initial weight. DTA shows relatively strong exothermic peak with the maximum at 436°C; the weight loss in the temperature range of 26-100°C indicated the evaporation of physically adsorbed water and ethanol molecules. Weight loss at the temperatures 100-350°C can be mainly due to degradation of the residual part of nitrate molecules and the weight loss up to 1000°C were only due to the degradation of ammonia matter in the material [32].

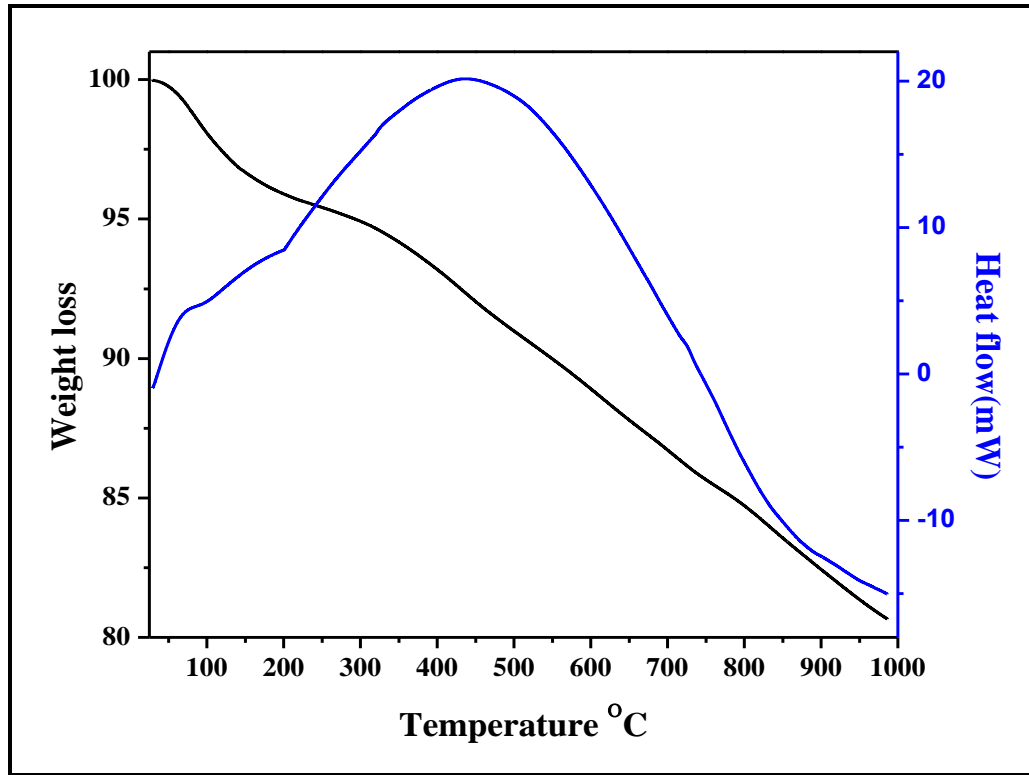


Fig.3.2 Thermal behavior of the CaSiO₃ obtained from TG-DTA measurements

3.3.2 Phase identification:

The X-ray diffraction study and phase purity of synthesized CaSiO₃ bioceramic sample was examined by XRD analysis. Fig.3.3 shows X-ray diffraction pattern of CaSiO₃ system sintered at 1250°C. The XRD data of compound show formation of a single phase crystalline compound and corresponding d_{hkl} and 2θ values was compared with the standard JCPD data Card No. 31-0300 [33]. No any additional peaks are seen in XRD data which confirms that synthesized samples are in pure hexagonal phase. The lattice parameters values ($a = 6.818 \text{ \AA}$ and $c = 19.517 \text{ \AA}$) for synthesized hexagonal CaSiO₃ sample was calculated by using following relation:

$$\frac{1}{d^2} = \frac{4}{3} \left(\frac{h^2 + hk + k^2}{a^2} \right) + \frac{l^2}{c^2} \quad (3.6)$$

The average crystallite size obtained for CaSiO₃ sample calcined at 1250°C was found to be ~ 34 nm. The lattice parameter values of the synthesized material are nearly similar to the constituent phases. Interplanar spacing (d), hkl planes and corresponding θ values of this material are tabulated in Table 3.3.

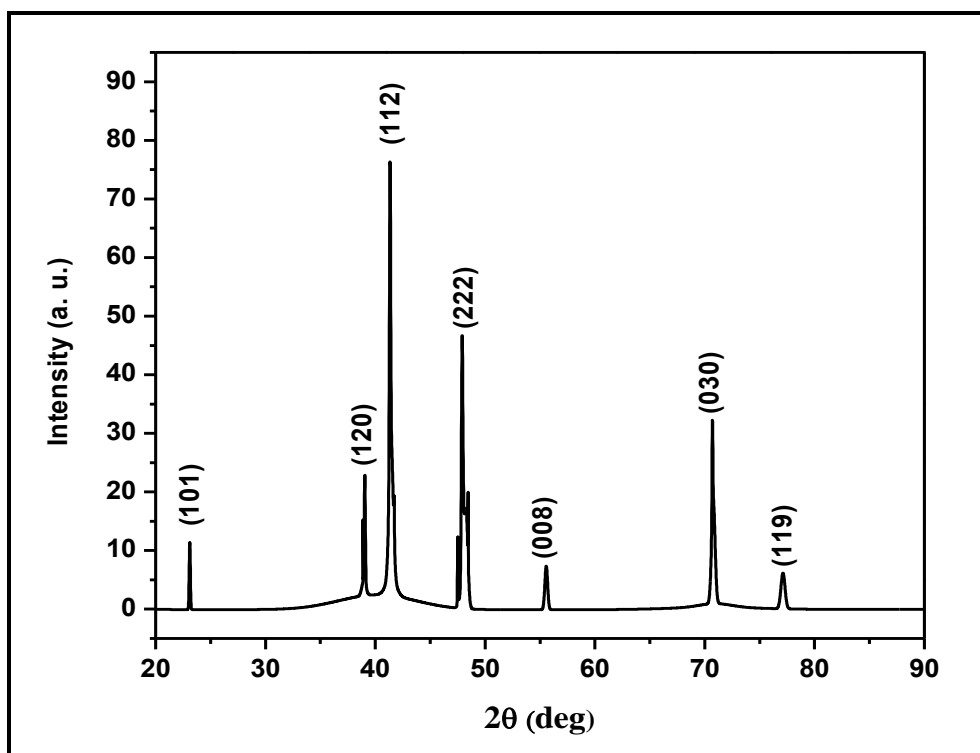


Fig.3.3 X-ray diffraction pattern of CaSiO_3 nanoparticles

Table-3.3
Indexed X-ray diffraction pattern of CaSiO₃

Sr. No.	2 θ	d _{obs} Å	d _{std} Å	h k l Planes
1	18.166	5.682	5.671	101
2	30.354	3.428	3.419	120
3	32.126	3.246	3.235	112
4	37.067	2.822	2.816	222
5	42.876	2.445	2.449	008
6	53.636	1.979	1.984	030
7	58.496	1.839	1.832	119

Structure: Hexagonal Lattice constant: a= 6.818 Å, c= 19.557 Å

3.3.3 TEM analysis:

The shape and size of the particle was clearly examined by using TEM analysis. As prepared sample was therefore characterized by TEM analysis technique and the corresponding TEM micrographs of CaSiO₃ are shown in Fig.3.4 (A-D). It has been seen from the micrographs A-D shows formation of particles in spherical shape which is advantageous in the field of tissue engineering applications. It is interesting to see that such nanospherical particles are randomly oriented and threaded into each other. Further it shows formation of agglomerated particles having size of each particle ~ 40 nm which in agreement with the XRD results.

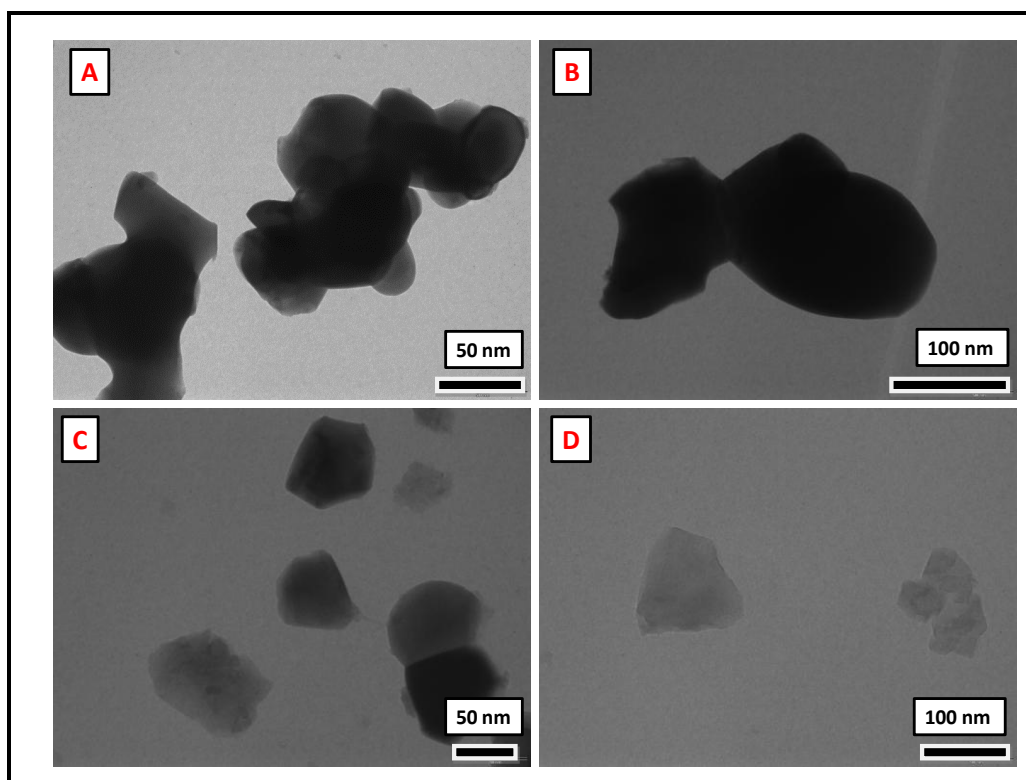


Fig.3.4 TEM (A-D) micrographs of the CaSiO_3 sintered at 1250°C

3.3.4 SEM Analysis:

Surface morphological study of CaSiO_3 sample was characterized by using SEM analysis. Fig.3.5 (A-D) shows SEM images of CaSiO_3 sample at four different magnifications. These images reveal that a randomly oriented crystallites of elongated spherical shape with sharp and clear edges. This is true for all magnifications. Some over growth has been observed to be initiated on the surface of uniformly distributed grains of CaSiO_3 sample.

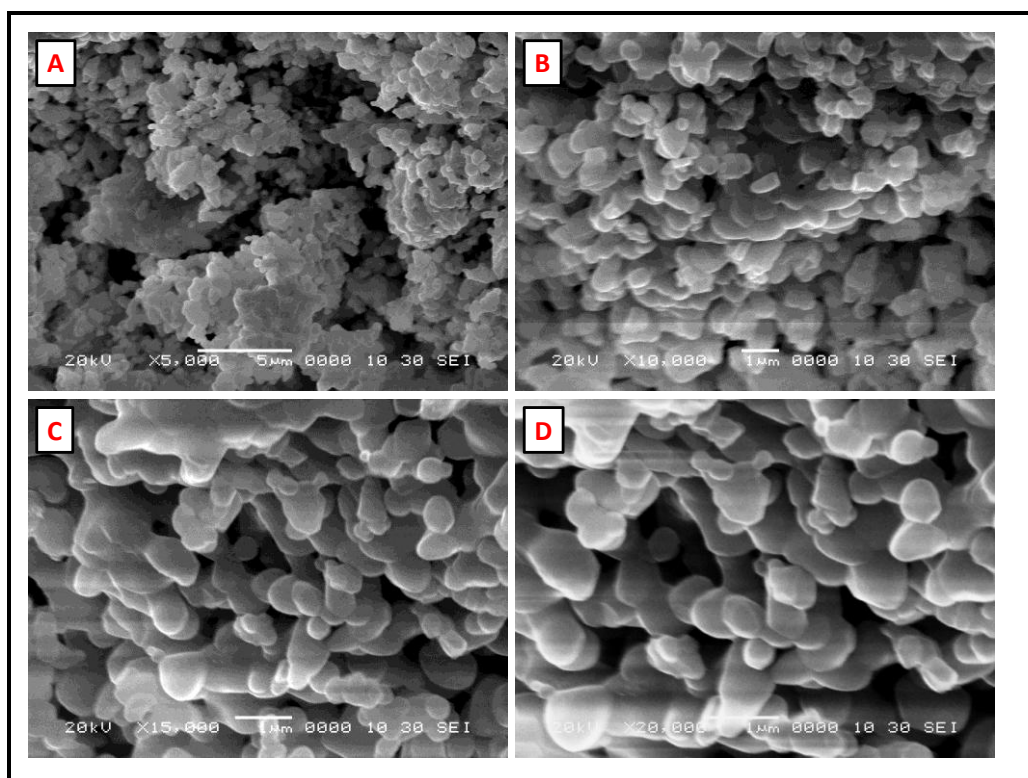


Fig.3.5 SEM images of synthesized nanocrystalline CaSiO_3 ceramic

3.3.5 EDAX analysis:

The elemental composition and homogeneity of particles have significant effects on biocompatibility and bioactivity properties of bioceramic materials. To understand interrelationship between materials properties, composition of the material must be known. This technique was used to analyze CaSiO_3 sample. An EDAX spectrum of this sample is shown in Fig.3.6 and reveals that as synthesized sample confirm the presence of Ca, Si, and O in CaSiO_3 sample.

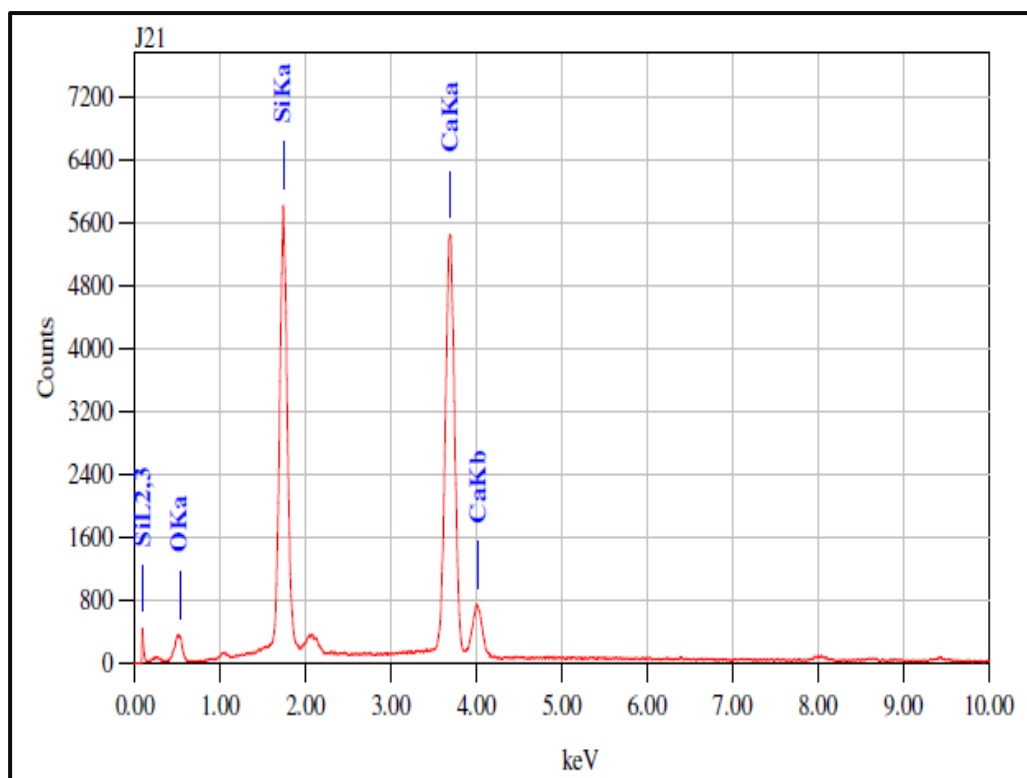


Fig.3.6 Energy dispersive spectra (EDAX) of CaSiO_3 powder

3.3.6 FTIR analysis:

The useful information regarding functional groups and molecular structure of the sample was determined by using FTIR analysis. As synthesized sample was therefore characterized by FTIR analysis and corresponding FTIR spectra of CaSiO_3 sample is shown in Fig.3.7. An FTIR spectrum of this sample was recorded in the wavenumber ranging from 400 cm^{-1} to 4000 cm^{-1} . The spectral data have presented a broad band in the range from 3700 to 3200 cm^{-1} associated with stretching vibrations of OH^- [34, 35]. The absorption bands in the 950 - 1150 cm^{-1} range were allotted to asymmetric stretching vibrations of the Si-O-Si [36]. Moreover, bending mode of Si-O-Si appeared in range of 450 - 480 cm^{-1} [37]. The bending bands of O-Si-O, Si-O and Si-OH are centered at 480 cm^{-1} , 800 cm^{-1} and 950 cm^{-1} respectively [38].

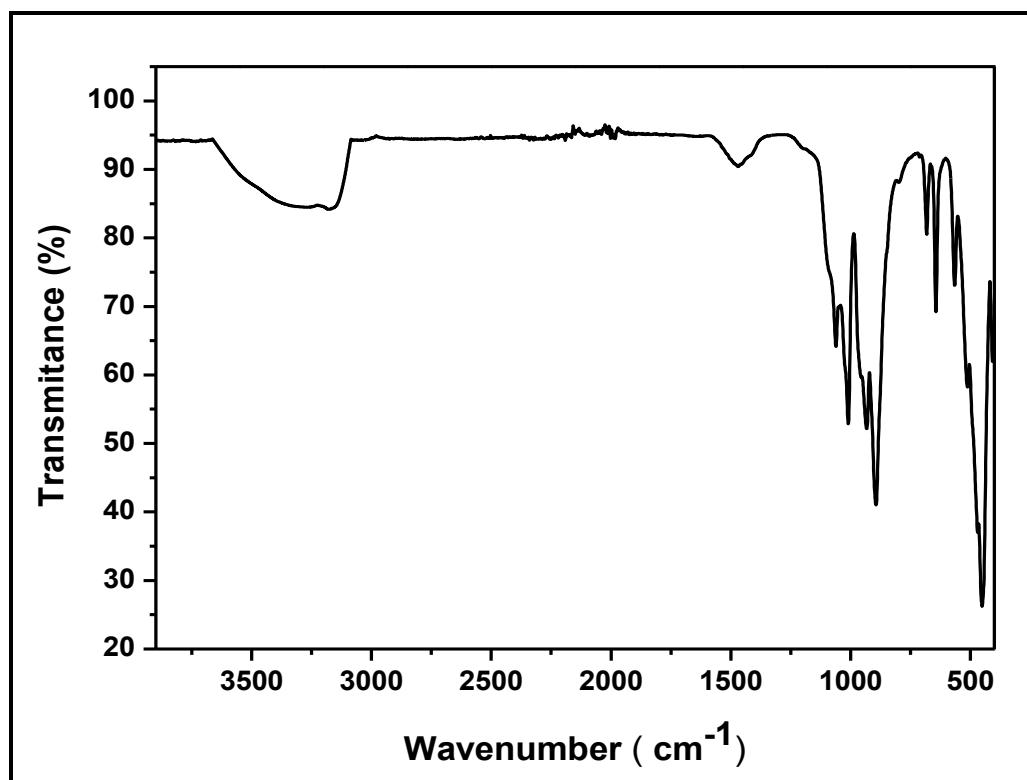


Fig.3.7 FTIR spectrum of CaSiO_3 powder

3.3.7 Wettability studies:

To evaluate the witting behavior of CaSiO_3 sample was measured by contact angle meter Fig.3.8 shows actual photograph of contact angle between CaSiO_3 sample and water droplet. The 0° static contact angle observed for CaSiO_3 confirms its superhydrophilic nature. Due to rough surface nature, CaSiO_3 material has a high surface free energy, quickly absorbs water molecules and its surface gets completely wet. The actual presence of OH groups on the surface of CaSiO_3 is responsible for its superhydrophilic nature [39]. Wettable material supports cell growth and produces required medium.

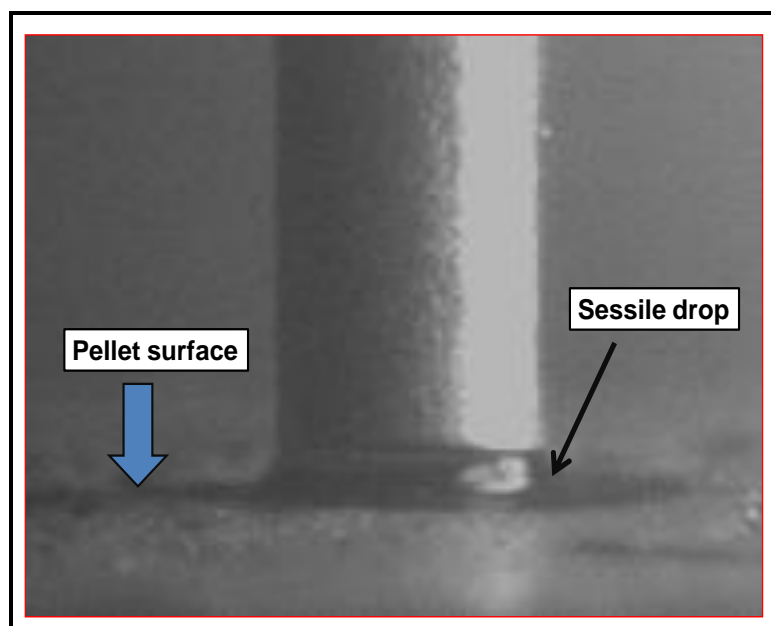


Fig.3.8 Water droplet on the superhydrophilic of CaSiO_3

3.3.8 Cell growth measurement:

MTT assays test were used to evaluate cell proliferation, cell viability of synthesized CaSiO_3 sample that helps to develop new biomedical applications and the result is predicted in Fig.3.9. Mesenchymal stem cells (MSCs) can be distinguished into cell type multiplicity and extensively used in tissue engineering. In present investigation, to evaluate in vitro cytotoxicity, tissue culture plates were used as a reference, and it is compared with synthesized CaSiO_3 nanopowders by using BMMSCs and CBMSCs cells. From the results it is seen that growth rate of cell viability for both the cells are depend upon incubation period and concentration of CaSiO_3 nanopowder. When the concentration of CaSiO_3 nanopowder was $80 \mu\text{g/mL}$ and incubation period was 48 h, the value of cell viability for CBMSCs cells was 98.40 %. However, after 12 and 24 h there is slight decreases in percentage viability of CBMSCs, although it is not statistically significant compared to control. While, BMMSCs showed 82.28 ± 4.95 % viability compared to control. Percentage viability in BMMSCs after 48 h and 12 h was similar. This result was therefore found to be suitable for good biocompatibility of calcium silicate nanoparticles for all concentration. The results were formulated as mean standard deviation (SD) and this result was established at a level of $p < 0.05$.

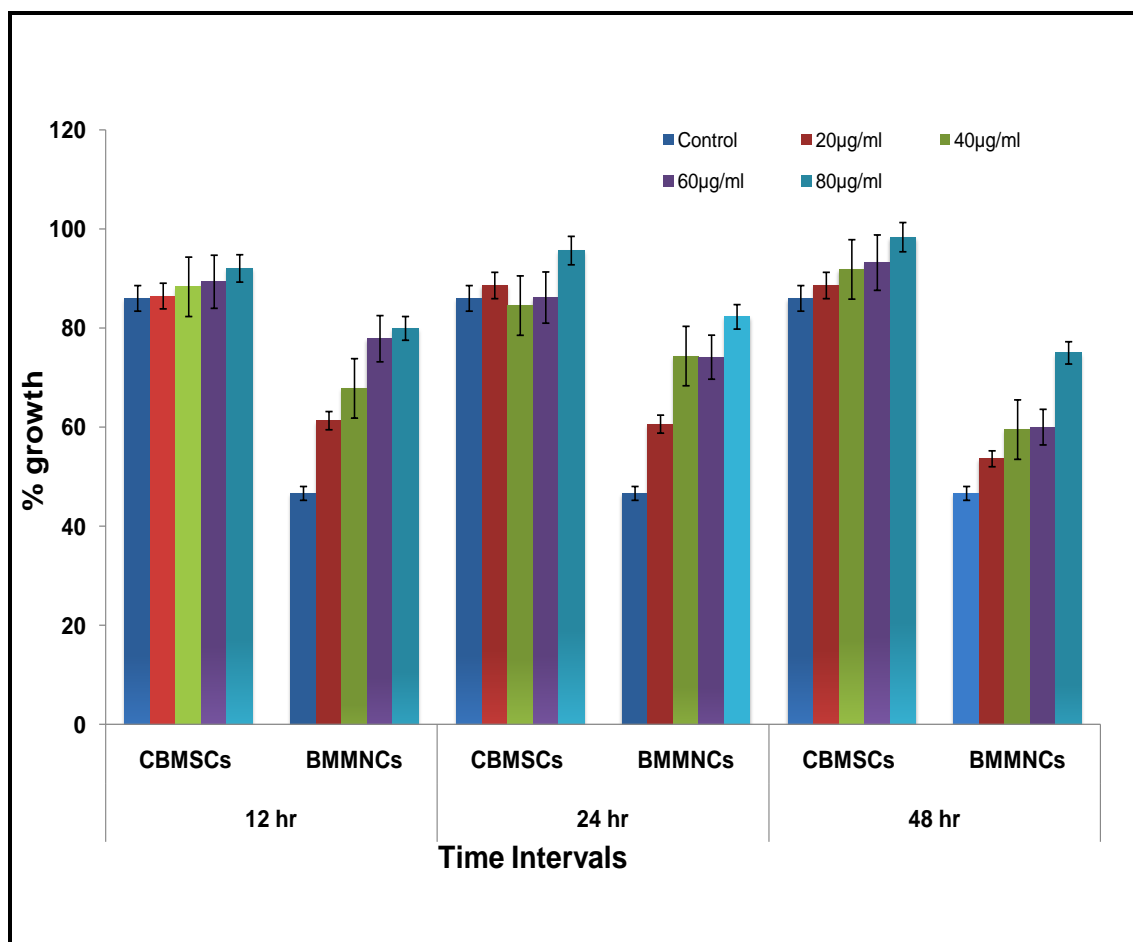


Fig.3.9 MTT assay results showing the human bone marrow mesenchymal stem cells (BMMSCs) and cord blood mesenchymal stem cells (CBMSCs) proliferation on CaSiO_3 sample after 12, 24 and 48 h of culturing

3.3.9 Cell adhesion studies:

Cell adhesion property was used to evaluate the behavior of the MMSCs cells on CaSiO_3 sample after incubation of 3 and 7 days. Fig.3.10 (B) and (C-D) shows the pictures of attachment of cells on sample after cell culture incubated for 3 and 7 days respectively. The captured pictures shows maximum amount attachment of cells on the surface of sample in case of culture incubated for 3 days, while the growth of the MMSCs increases noticeably in cell culture incubated for 7 days. The CaSiO_3 sample shows no any adverse effect on morphology of cell. These result indicated that the CaSiO_3 sample supported MMSCs adhesion which providing an indication of CaSiO_3 biocompatibility property. Such types of results also reported earlier in our laboratory by my colleague R. B. Chavan for plant materials [40]. Fig.3.10 (A) shows the culture medium of the MMSCs without CaSiO_3 sample considered as a positive control.

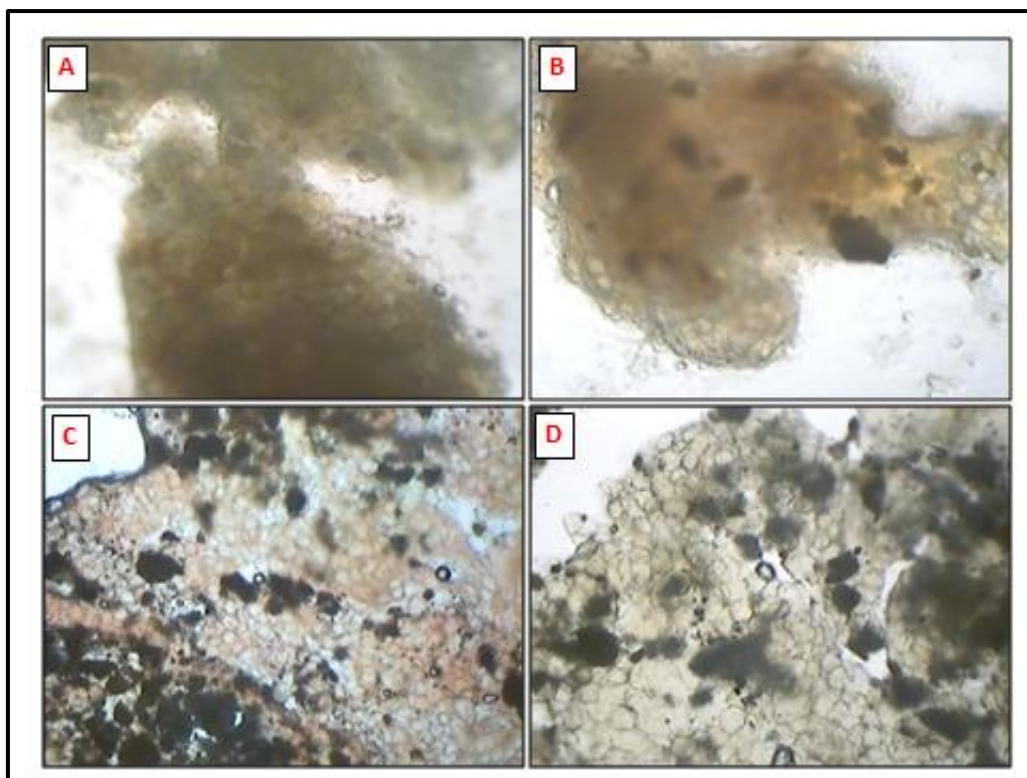


Fig.3.10 The morphological behavior of BMMSCs cells without CaSiO_3 as positive control (A). BMMSCs cells adhering and spreading on CaSiO_3 surface after 3 days (B) and 7 days (C-D)

3.3.10 Degradation study:

Bioceramics or biomaterials undergo degradation in the presence of fluids which leads to, changes in their chemical structure and physical properties [41]. Degradation mechanism of sample depends on its nature. Dissolution-reprecipitation type of degradation takes place when bioactive bioceramics based materials come in contact with human (biological) fluid [30]. In this experiment, *in vitro* degradation behavior of CaSiO_3 pellets were evaluated through analyzing weight loss in SBF. The change of weight loss % of CaSiO_3 with time of immersion is depicted in Fig.3.11. The results revealed that degradation of CaSiO_3 sample takes place continuously through the entire incubation period. Calcium silicate has a higher weight loss with degradation time, reaching up to 13% after 50 days. The results revealed that calcium silicate sample degrades easily in SBF and in orthopaedic field such type of bioactive and biodegradable materials can be applied as scaffolds.

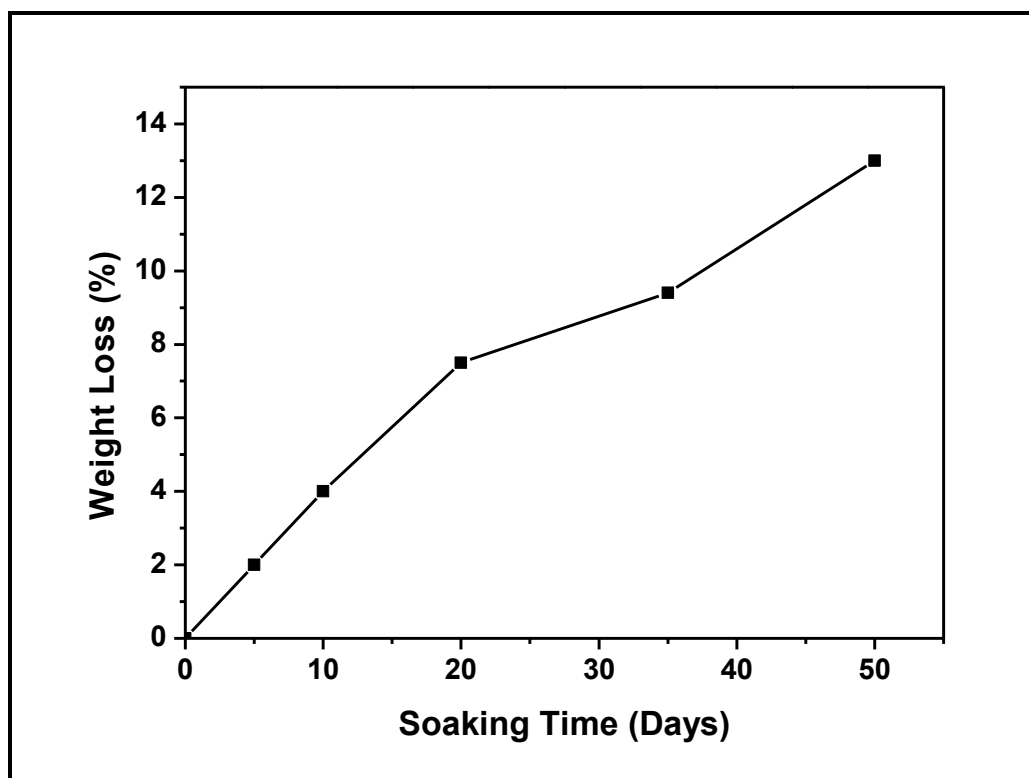


Fig.3.11 Changes in weight loss of CaSiO_3 after immersion in SBF

3.3.11 Drug loading:

The drug concentration and drug to bioceramics ratio are responsible factor for drug uptake efficiency of bioceramics. The drug loading percentage is directly proportional to these parameters and attains maximum value at a particular level. Fig.3.12 (A) shows that variation of drug loading on CaSiO_3 sample with change in drug concentration. 75% of drug is loaded for 5% drug concentration and loading of drug increases up to 80% when concentration of drug increases to 10% then after, it remains constant at 20% drug concentration. Fig.3.12 (B) shows effect of temperature on loading of drug. A maximum 75% drug loading is observed in case of 5% drug concentration at 60°C with 40-min stirring time. As temperature increases there is increase in drug loading percentage afterwards, it attains constant value. Fig. 3.12 (C) shows bar graph of changes in drug loading on CaSiO_3 sample with different stirring time. Therefore, 40-min stirring time and 60°C are considered as optimized parameters for drug loading.

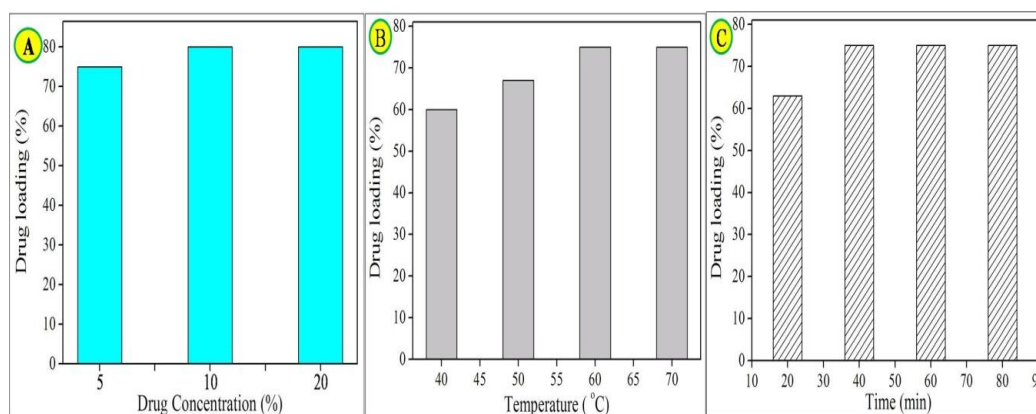


Fig.3.12 Drug loading behavior on CaSiO_3 at different Drug concentration (A) different temperature (B) and at different stirring time (C)

3.3.12 In vitro drug release:

Norfloxacin drug was loaded on CaSiO_3 sample to examine the efficiency of the drug delivery. Fig.3.13 shows different drug release profiles. The approximate drug release percentage in 200 hrs were found to be 55, 43 and 35% from 15, 10 and 5% of drug-loaded samples. The steady release of drug is observed for particular time; afterwards it is more or less constant. At initial time drug release behavior is high, then after, it decreases to attain some constant value. The possible reason for initial high release of Norfloxacin is desorption of Norfloxacin molecules from surface of the sample. The molecules of Norfloxacin do not show any powerful interaction with CaSiO_3 sample. CaSiO_3 sample absorbs surrounding fluid in to it during the in vitro drug release analysis, due to this exclusion and dissolution of norfloxacin is observed. More amounts of norfloxacin get exposed to the fluid because of breaking of large particles of drug into smaller particles. The complete desorption of loosely adsorbed norfloxacin and incorporation between norfloxacin drug with CaSiO_3 nanoparticles leads to slow drug release. Similar results were reported earlier for bioceramics and ceramics based materials due to their excellent bioactivity with bone tissue [42, 43].

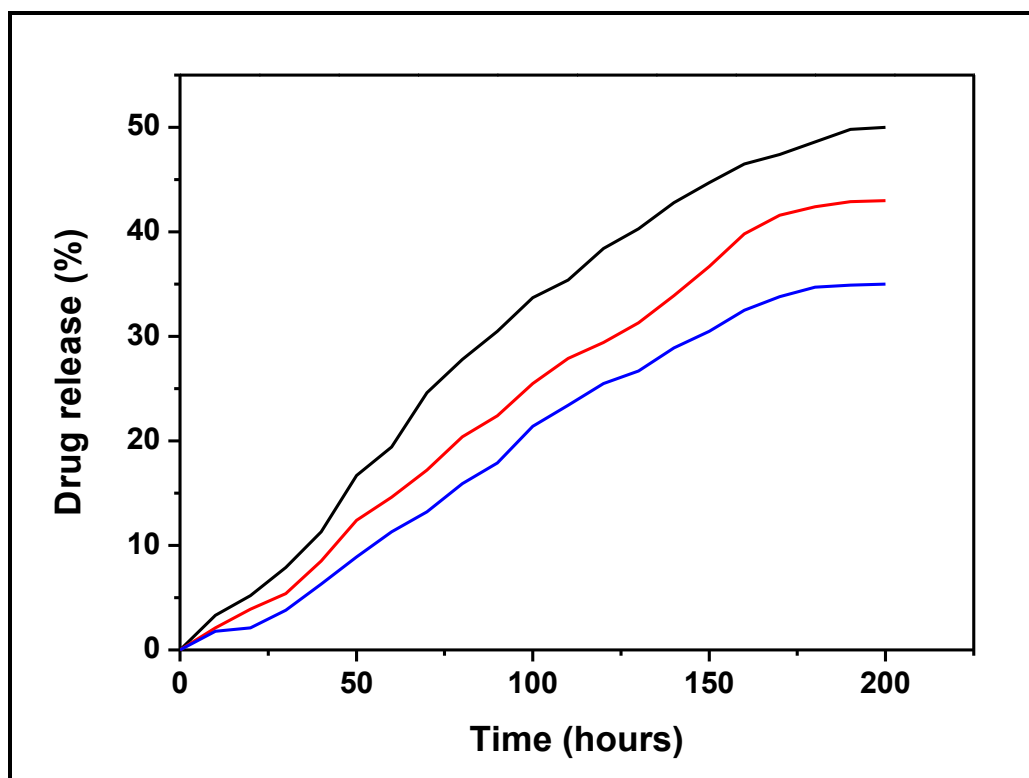


Fig.3.13 Drug release percentage from CaSiO_3

3.4 Conclusions:

1. The present study illustrates that nanosized CaSiO_3 biomaterial was successfully synthesized by the wet-chemical method at room temperature.
2. XRD data confirms hexagonal structure of the synthesized compound. Particle size in this sample, estimated on the basis of experiments, was ~ 40 nm which in good agreement with XRD pattern.
3. Morphology and elemental analysis showed that the grains and metals in the sample were distributed homogenously, maintaining their stoichiometric composition.
4. Wetting experiment revealed that the CaSiO_3 material was superhydrophilic in nature.
5. Cell culture and MTT assay and cell adhesion assay showed that the nanosized CaSiO_3 powder provided a more adequate environment for cell adhesion and proliferation and was characterized by good biocompatibility.
6. The degradability in vitro was evaluated by weight loss in the SBF and it shows that the CaSiO_3 nanoparticles exhibit a higher degradation rate.

7. The present investigation well demonstrated that CaSiO_3 could efficiently adsorb and controlled release of norfloxacin, which suggested its extended applications for other antibiotics.

Chapter - 4

SYNTHESIS, CHARACTERIZATION AND APPLICATIONS OF HYDROXYAPATITE (HAP)

4.1 Introduction:

Biomaterials especially the inorganic, calcium phosphate the one among many does have the extensive applications in medicinal sector [1]. There are different types of bioceramics which are used in orthopedic and dental field [2]. Currently, hydroxyapatite (HAP, $\text{Ca}_{10}(\text{PO}_4)_6(\text{OH})_2$) is an example of promising ceramic biomaterial because of its bioactivity, nontoxic, and non-inflammatory properties [3, 4]. Sinterability, solubility, fracture toughness, castability and absorption are the basic physical properties of HAP. Controlled and calculative tailoring of particle size, morphology along with help of different physical parameters, these can be adapted in various fields [5, 6].

Reporting important advantages of the synthetic HAP, they offer good osteoconductive and osteoinductive capabilities [7, 8]. Taniguchi et al. [9] through the investigations sintered HAP exhibited outstanding biocompatibility with soft tissue like muscles and gums. The mentioned potential of the HAP has made it as supreme contender for orthopaedic and dental implants. Concerning the hard tissues mostly the synthetic HAP has its extensive usage especially for the repair and then on for general usage is the coating of implants, bone augmentation and bone repair also it acts as fillers in bone or teeth [10, 11]. All the discussed applications and the characters it seems to give great importance and a special significance to devise method for the synthesis of HAP that can have precise control over particle size and morphology.

Different synthetic strategies have been explored for the process of synthesizing HAP. This include ultrasound assisted method [12], freezing organic–inorganic soft solution [13], co-precipitation method [14], microwave hydrothermal method [15], mechanochemical method [16], sol-gel method [17] and microemulsion route [18]. From the above read list, considering the size confinement and creating porosity both, auto-combustion method is judged as the best [19]. Auto-combustion method with citric acid enacting as fuel is a simplistic one-pot way to acquire HAP nanoparticles with pure phase and high crystalline.

Biomaterial while its makings do have the link with the porous materials. The progressive improvement of porous materials becomes a key theme for orthopaedic and dental fields. The earlier demonstration suggests that porous structure for the enhancement in the attachment, proliferation and migration of cells. The continuous diffusion of different essential nutrients throughout the entire structure is obtained by

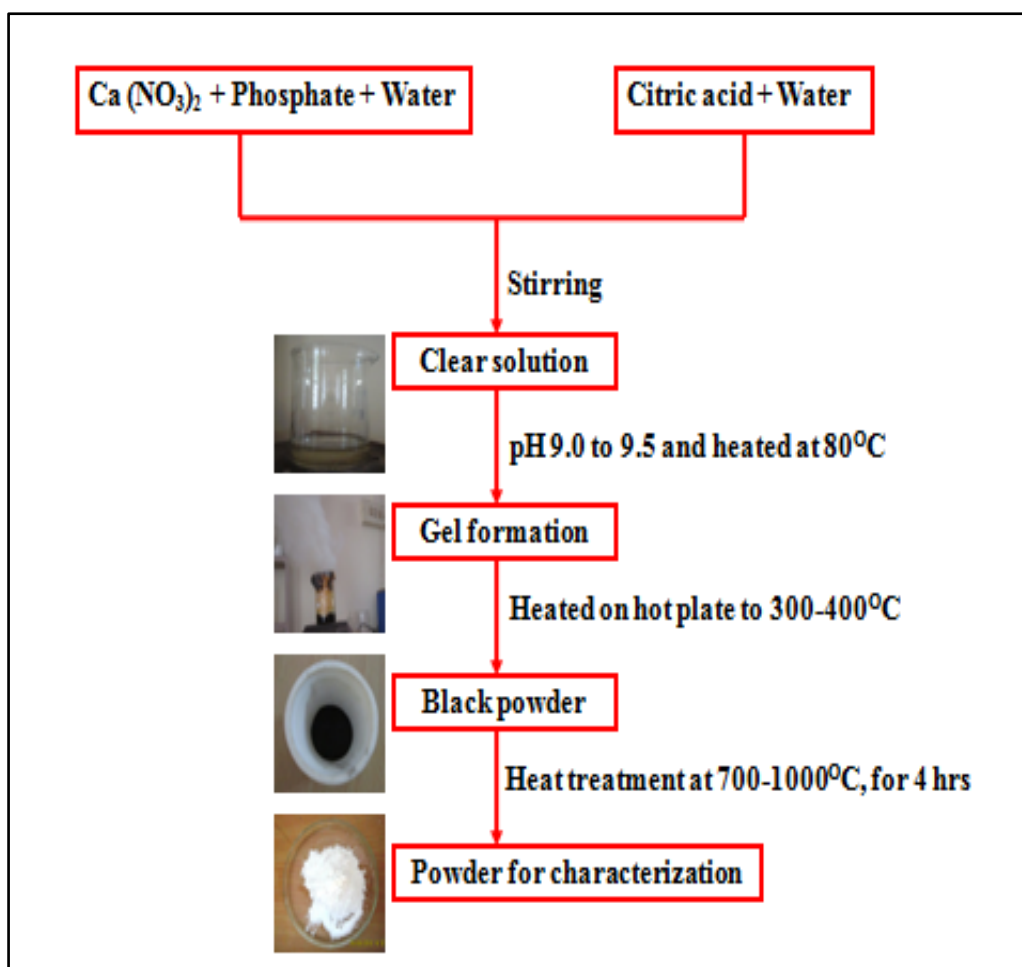
tailoring the porosity, pore size and interconnectivity of synthesized biomaterial [20, 21].

This investigational analysis of ceramics and its practical behavior was necessary to understand. For this study HAP bioceramics prepared by auto-combustion method was carried and the concern sample was investigated by using TG-DTA, XRD, TEM, SEM, EDAX, FTIR and in vitro wettability behaviour to explore their structural properties. The in vitro biocompatibility of HAP is examined by observing effect of HAP nanoparticles on cell viability, adhesion and cell proliferation of human and sheep mesenchymal stem cells. The drug loading, drug release and in vitro biodegradation of HAP nanoparticles were also evaluated.

4.2 Experimental and material details:

Nanostructured HAP sample having general formula $\text{Ca}_{10}(\text{PO}_4)_6(\text{OH})_2$, was synthesized by auto-combustion method. In the typical synthesis calcium nitrate, diammonium hydrogen phosphate and citric acid were used as sources of Ca, P and fuel respectively. All chemical used in synthesis are of analytical Grade. The molar ratio of both metal nitrate and phosphate to citric acid was taken as 1:2. Firstly, stoichiometric amount calcium nitrate and diammonium hydrogen phosphate were dissolved in millipore water with vigorous stirring. Citric acid was weighted stoichiometrically and dissolved in distilled water. The above solution mixed under constant stirring and pH adjusted 9 to 9.5 using ammonia. A homogeneous clear solution was achieved. This clear solution was stirred vigorously and heated up to 80°C for 4 h to obtain gel. Further, dry HAP powder was obtained by heating of gel at 300-400°C. This dried HAP was further sintered at 700-1000°C for 4 h. The pellets were prepared by mixing of calcined HAP with polyvinyl alcohol (1-2%) as a binder. The removal of the binder was done by calcinations of pellets at 250-400°C. HAP in powdered form was used for biological and structural analysis. While the pellets are used for in vitro biodegradation behavior and wettability test.

Auto-combustion technique used for preparation of nanostructured HAP is shown by following flow chart.



Flow chart of auto-combustion synthesis of HAP bioceramics

The thermal decomposition behaviour and required sintering temperature of citrate precursor to phase formation of the sample was checked by thermogravimetric analysis on the SDT Q-600 instrument by heating the powder after auto-combustion in air atmosphere from 20° to 1000°C at the rate of 10°C per min. The X-ray diffraction analysis was used to know phase purity of synthesized material by using PW3710 (Model- Philips) with CuK α radiation ($\lambda = 1.5406\text{\AA}$). Morphology of synthesized HAP sample was studied by TEM analysis (Philips CM-200) at 200 kV. The surface topography and microstructure of the sample was examined by means of electron microscopy scanned with different magnifications (JEOL JSM-6360). These nanoparticles were evaluated for the qualitative and quantitative determination of different elements by energy-dispersive X-ray spectroscopy (JEOL JSM-6360). JASCO FT/IR-6100 type 'A' spectrometer was used for FTIR study of these nanoparticles. In vitro wetting property of HAP sample was evaluated by sessile drop technique using contact angle measurement. A distilled water droplet (0.01 mL) was diffused to the upper surface of HAP and examined with sophisticated goniometer

(Model110, R. hart Instrument Co., USA). UV-Visible spectral measurements of this sample carried out by using UV/Visible spectrophotometer (Systronic AU-2700). The pH of the solution was carried out by using HANNA phep (model H 19).

4.2.1 Cell culture experiments:

In vitro test is an important parameter to study the biocompatibility of HAP sample. Therefore, the present study mainly focuses on in vitro test of as synthesized HAP sample. The human bone marrow mesenchymal stem cells (BMMSCs) and cord blood mesenchymal stem cells (CBMSCs) from a passage 4-6 were analyzed as a test subject. Prior to bioceramic surface cell seeding, cells were revived and cultured in Dulbecco's minimum essential medium (DMEM, Make-Sigma Aldrich) with fetal bovine serum (FBS) 10%, 1mM sodium pyruvate, 2mM L-glutamine, streptomycin (50 mg/mL) and penicillin (50 U/mL) as a supplement. The concentration of 5×10^5 cells per well were used for seeding in 6-well plates with 2 mL of DMEM. Further, incubation of the cells were done for growth and proliferation in CO₂ incubator optimized at 5% CO₂, 90% humidity with temperature at 37°C. The cells were cultured with 20, 60, and 80 µg HAP/ml for 12, 24 and 48 hours (70% confluency) before the assays.

4.2.2 MTT cytotoxicity test:

MTT cytotoxicity test is very important to evaluate cell viability and cell proliferation of bioceramic materials. As synthesized HAP sample was therefore analyzed by MTT cytotoxicity test to study cell cytotoxicity, proliferation and viability. Well-characterized BMMSCs and CBMSCs cells were used and cultured by culture method described previously [22]. Each composition was taken in three replicate. Initially, autoclaved samples were positioned in the well plate and consequently washed with PBS. After that, 96 well plates were seeded with concentration of 5×10^5 cells per mL. Afterward, the incubation of culture plate in CO₂ incubator was done for 12, 24 and 48 hours. Subsequently, the medium was aspirated and then samples were washed with PBS twice. 20 µL of MTT dye solution [(3-(4,5-dimethylthiazol-2-yl) -2,5 diphenyltetrazolium bromide: Make-SIGMA, USA, Cat no.M5655)] and 5 mg per mL phosphate buffer was added to each well so as to pH =7.4. Lastly, the incubation of plate for 15 min and 4 h was done for steady-state confluent cells and exponentially growing cells respectively. After the incubation, the samples were taken off from the well and the crystals were solubilized with help of DMSO (200 µL) and this solution was energetically stirred for

dissolution of the reacted dye. ELISA automated microplate reader was used to check the absorbance of each well at 550 nm (Biorad). All data were given in form of mean \pm SD for three group samples. The culture medium without cells is used as blank to calibrate the spectrophotometer at zero.

The viability of the cell in percentage is related to control wells containing cell culture medium without any addition of nanoparticles and was analyzed using the formula:

$$\text{Cell Viabilities (\%)} = [A] / [AB] \times 100 \quad (4.1)$$

Where, A and [AB] is the absorbance of the test sample and control sample respectively.

4.2.3. Cell adhesion test:

Cell adhesion property of bioceramic samples provides basic information due to which bioceramics were widely used in tissue engineering. Therefore, in vitro cell adhesion test of HAP sample was evaluated using microscopic methods. This property is carried out to examine whether the HAP sample is capable to sustain morphology of the MMSCs. The cells were cultivated in direct contact with the HAP sample. Therefore, mesenchymal stem cells (MMSCs) derived from bone marrow of sheep and plated in to the 50 mL hard glass test tube. The cells were moderately immersed in Dulbecco's modified eagle medium with 10% serum of animal, 100 U per mL penicillin G, 100 μ g per mL streptomycin (invitrogen) and 15 mg of HAP (calcined powder) sprayed on the surface of cultured cells which acts as supplement. These cultured medium was incubated in CO₂ incubator operated at optimized conditions (5% CO₂, 90% humidity) at 37°C for 7 days respectively. After selected time points, for morphological examination surface layer of cultured medium was removed and dried in air after washed with distilled water. The adherent cells on HAP sample were visualized under 40X magnification microscope (Coslab, Model HL-9). Additionally, one culture medium containing MMSCs without studied sample considered as positive control.

4.2.4 In vitro biodegradation behavior:

Degradability of bioceramics is most important parameter in the biomedical field. Therefore, in vitro biodegradation behavior of HAP sample was carried out in simulated body fluid (SBF). Ionic concentrations were used to prepare the SBF

solution which is nearly similar to human blood plasma. It is prepared as per the procedure developed by Kokubo [23-25]. The comparison of human blood plasma with ion concentration of SBF prepared by Kokubo method was displayed in Table 4.1 and Table 4.2 provides appropriate quantities of reagents to be added in de-ionized water to have desired ionic concentration. Reagents are added in stepwise manner Table 4.2. Further, pH of this solution was adjusted to 7.4. The temperature of the SBF solution is maintained at 37°C.

To assess in vitro biodegradation tests the HAP pellets (3 wt%) were added in closed bottle of SBF solution maintained at body temperature and are incubated for 5, 15, 20, 35, and 50 days. Afterwards, the pellets of sample are taken out from SBF solution subsequently rinsing with de-ionized water, and drying in an oven at 100°C-150°C for 24 h was done. At last, weight loss (%) of sample and particulates was calculated by precise electronic balance. Two pellets of each group were rested under the above mentioned condition. The weight loss % (WL) of pellet during immersion in SBF was calculated using equation 4.2

$$WL = \left(\frac{M_0 - M_t}{M_0} \right) \times 100 \quad (4.2)$$

Where, M_0 and M_t was the initial weight and the weight of sample at time 't' respectively.

Table 4.1**Ion concentrations (mmol/dm³) of SBF and human blood plasma**

Ionic concentration (mmol/dm³)	Simulated body fluid	Blood plasma
Na ⁺	142	142
K ⁺	5.0	5.0
Mg ⁺	1.5	1.5
Ca ⁺	2.5	2.5
Cl ⁻	147.8	103.0
HCO ₃ ⁻	4.2	27.0
HPO ₄ ⁻	1.0	1.0
SO ₄ ⁻	0.5	0.5

Table 4.2**Reagent used for preparing SBF (1L, pH 7.4)**

Order	Reagent	Amount (g/l)
1	NaCl	7.996 g
2	NaHCO ₃	0.350 g
3	KCl	0.224 g
4	K ₂ HPO ₄ ·3H ₂ O	0.228 g
5	MgCl ₂ ·6H ₂ O	0.305 g
6	1M-HCl	40 ml
7	CaCl ₂	0.278 g
8	Na ₂ SO ₄	0.071 g
9	(CH ₂ OH) ₃ CNH ₂	6.057 g

4.2.5 In vitro drug loading experiment:

If the material is biocompatible and biodegradable and have capacity to uptake and release drug in controlled manner then this material have wide range of applications in biomedicines [26, 27]. For that purpose, norfloxacin widely used antibiotic was chosen as the model drug. In particular, different concentrations (5, 10, 15%) of norfloxacin powder were prepared by dissolving it into 100 mL of de-ionized water. Afterwards, 1 g of HAP sample was added to above said drug solutions. The resultant suspensions were stirred for different time (20, 40, 80, 120 minutes) and different temperatures (40, 50, 60, 70°C). Then after, the resultant solution was kept intact for 24 h. The solution was centrifuged in order separate the precipitate. The drug loaded on HAP sample was assessed by knowing the difference in concentration of drug before and after loading. Drug loading (%) on HAP was evaluated by following equation:

$$\text{Drug loading (\%)} = [(A-B)/A] \times 100 \quad (4.3)$$

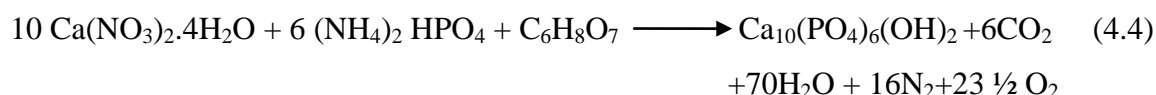
Where, A is the initial and B is the final norfloxacin concentration in aqueous solution.

4.2.6 In vitro drug release experiment:

Time period of 200 hrs was used to evaluate in vitro drug release. 100 mg of drug-loaded HAP sample added into a capped glass bottle contains phosphate-buffered (50 mL) saline (PBS) having pH =7.4 and incubated at 37°C. The stationary mode was used to study drug release. To calculate the released amount of drug, 5 mL of sample were centrifuged and replaced with 5 mL of fresh PBS medium. Afterwards, the actual concentration of Norfloxacin in the supernatant liquid was measured at 274 nm using spectrophotometer.

4.3 Result and Discussion:

The reaction involved in the formation of HAP can be expressed as following equation.

**4.3.1 TGA-DTA Analysis:**

Thermal stability of HAP ceramic sample was examined by thermal decomposition of the powder. The TGA-DTA results as shown in Fig.4.1, it was observed that decomposition of HAP sample below 200°C due to removal of

absorbed water. Decomposition during 200–320°C can be mainly due to degradation of organic residual part. DTA curve shows that thermal decomposition of HAP sample at 100°C, 200°C and 250°C with an endothermic peak and this peak is only due to degradation of residual water from gel. TGA shows weight loss in the temperature range of 100-200°C indicated the reactions (oxidation-reduction) of nitrates with fuel [28].

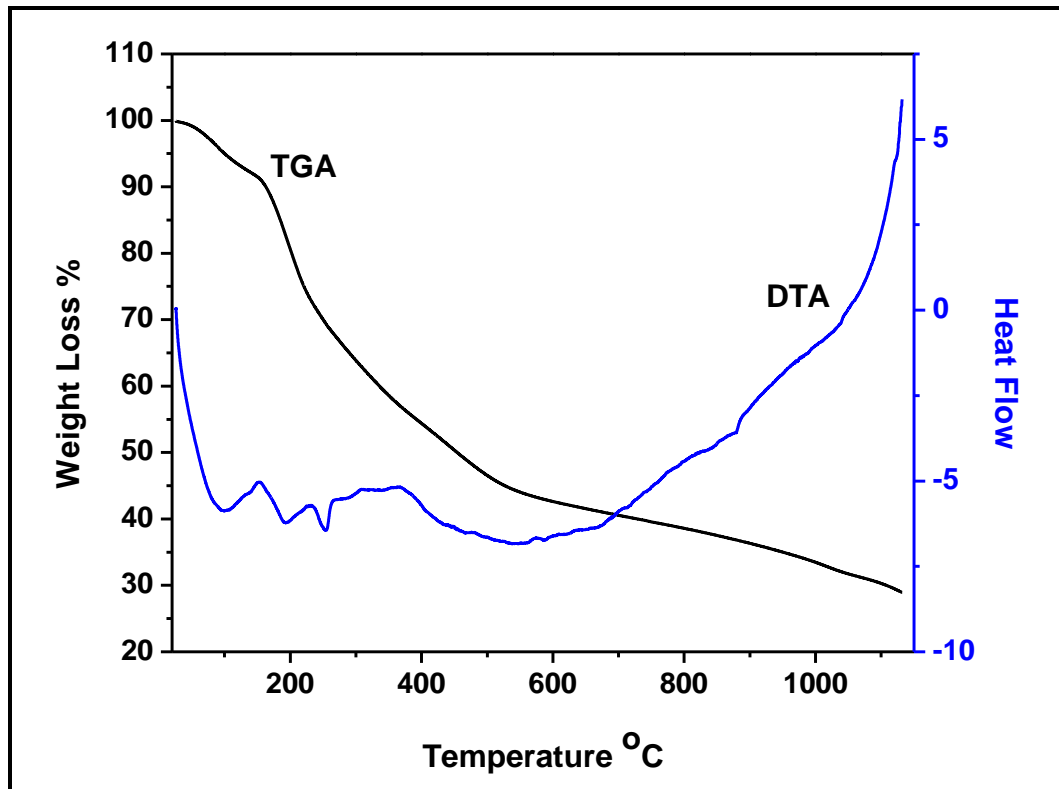


Fig.4.1 TGA-DTA curve of HAP as synthesized powder

4.3.2 Phase identification:

X-ray diffraction study and phase purity of synthesized HAP bioceramic sample was examined by XRD analysis. Fig.4.2 shows X- ray diffraction pattern of HAP sample annealed at different temperatures (750-1000°C). The XRD analysis of these samples exhibit almost similar patterns with each other except changes in peak height and peak width with increases in temperature. This pattern corresponds to peaks of (002), (211), (300), (202), (310), (311), (113), (222), (312), (213), (321), (410), (402) and (004). These polycrystalline HAP nanoparticles exhibit single phase hexagonal structure (JCPDS 09-0432) [29]. Lattice parameters of HAP was found to be $a = 9.418 \text{ \AA}$ and $c = 6.881 \text{ \AA}$. The average crystallite size of synthesized HAP sample was estimated by using Debye Scherrer's formula [30-32].

$$\tau = 0.94 * \lambda / \beta * \cos \theta \quad (4.5)$$

Where, crystallite size (τ) depends upon wavelength λ (1.54 Å for CuK α) of the X- ray and the FWHM (β) of the XRD peak at 2θ . The average crystallite size obtained for HAP sample calcined at 1000°C was found to be ~ 30 nm. No any additional peaks are seen in XRD data which confirms that synthesized HAP samples are in pure form. Interplanar spacing (d), hkl planes and corresponding θ values of this material are tabulated in Table 4.3.

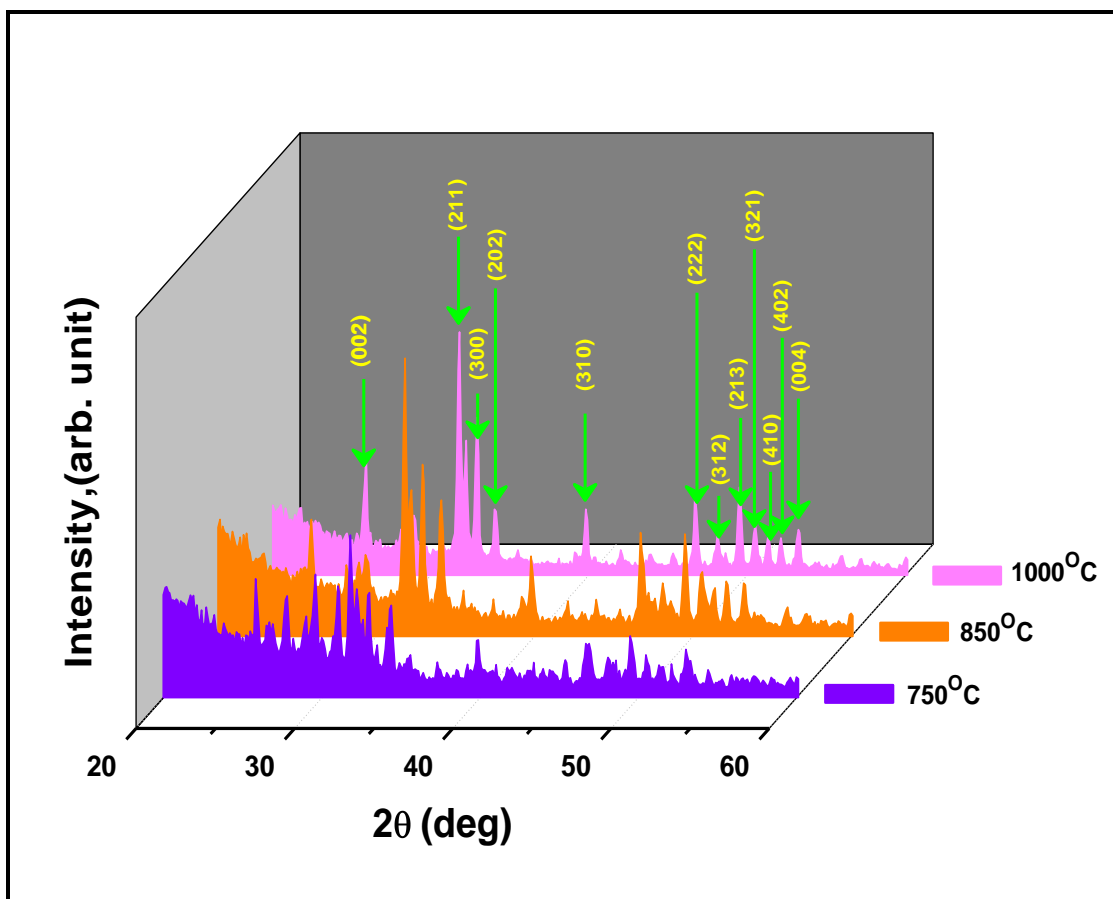


Fig.4.2 XRD patterns of the HAP samples prepared by auto- combustion method

Table 4.3
Indexed X-ray diffraction pattern of HAP

Sr. No.	2θ	d_{obs} Å	d_{std} Å	h k l Planes
1	25.881	3.439775	3.439775	002
2	31.771	2.814233	2.814233	211
3	32.902	2.720032	2.720032	300
4	34.047	2.63113	2.63113	202
5	39.818	2.66208	2.66208	310
6	46.711	1.943068	1.943068	222
7	48.102	1.890076	1.890076	312
8	49.462	1.841244	1.841244	213
9	50.493	1.806039	1.806039	321
10	51.283	1.780057	1.780057	410
11	52.1	1.754049	1.754049	402
12	53.143	1.722056	1.722056	004

Structure: Hexagonal

Lattice constant: a = 9.418 Å, c = 6.881 Å

4.3.3 TEM Analysis:

Transmission electron microscopy (TEM) can provide very useful information about shape and size of the particle. As prepared sample was therefore characterized by TEM analysis technique and the corresponding TEM micrographs of HAP samples are shown in Fig.4.3 (A-B). It has been seen from micrographs the nanoparticles have spherical shape and well dispersed without evident aggregation. The images suggest

that the particle size of around 30-40 nm and this value is in the close vicinity to value obtained from XRD analysis.

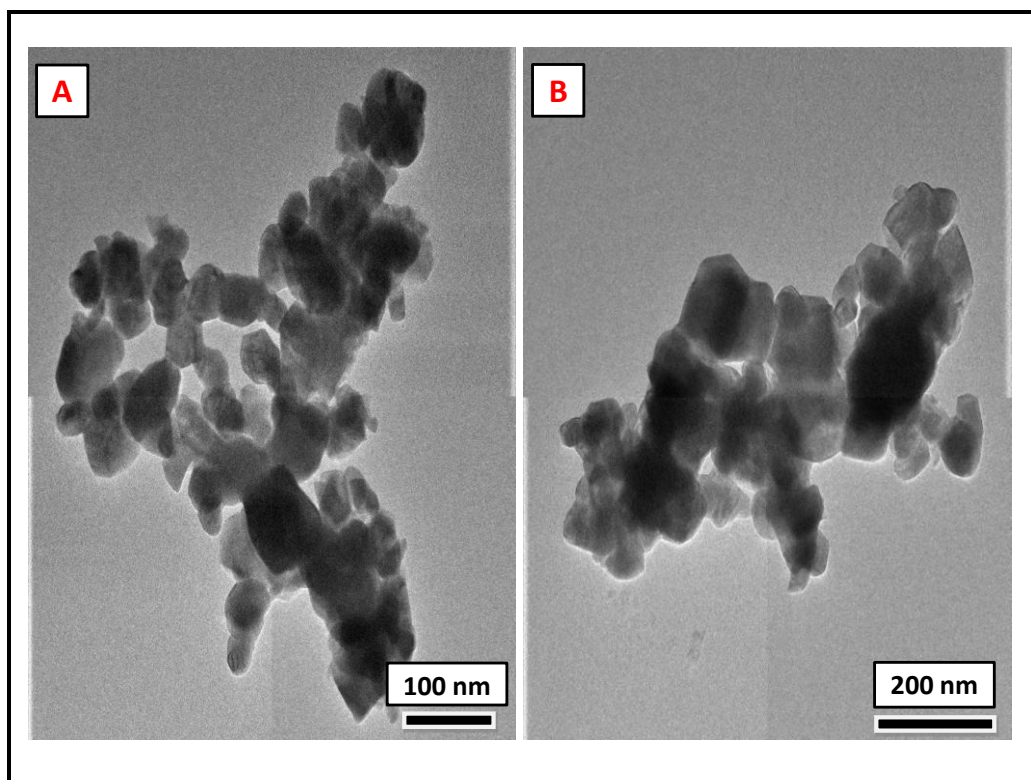


Fig.4.3 (A-B) Transmission electron microscopy images of HAP calcined at 1000°C for 4 h

4.3.4 SEM Analysis:

SEM instrument have been invoked to know the morphology of the obtained HAP. Fig.4.4 (A-D) shows the SEM images of HAP samples and reveals that as prepared HAP product consist of many pores having irregular shape with separated with infinitesimal distance. The formation of pores is beneficial, and finds very useful applications in drug carriers [33] and bone tissue engineering as they would permit the cell adhesion and proliferation [20].

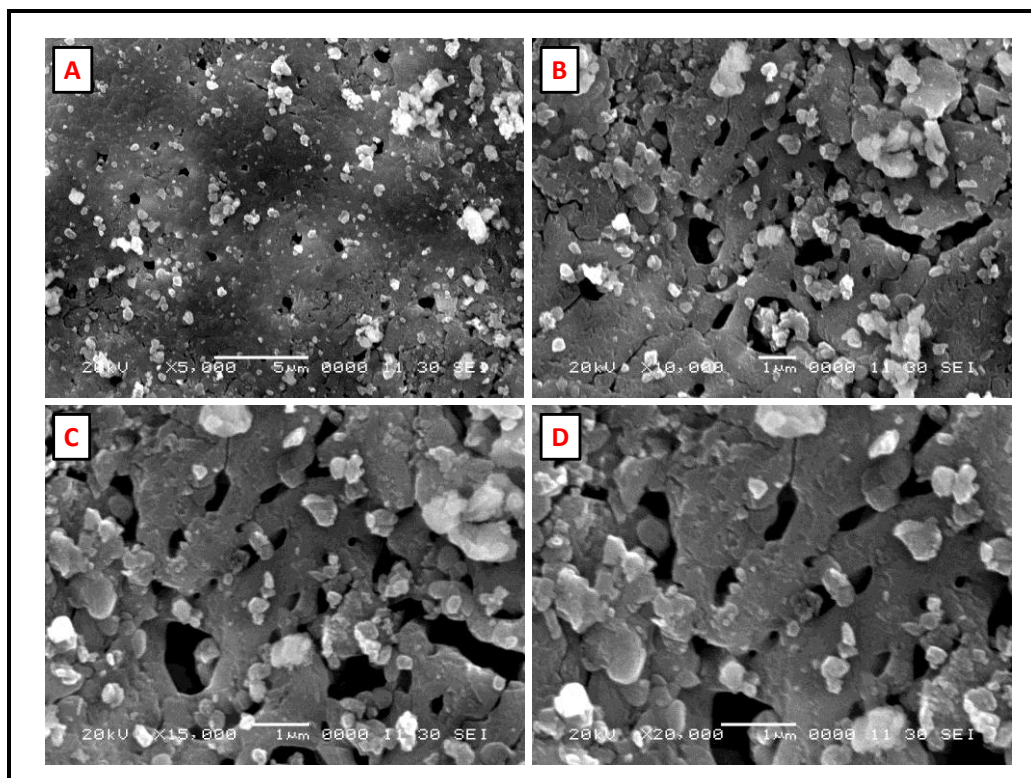


Fig.4.4 SEM micrographs of the porous HAP bioceramics

4.3.5 EDAX Analysis:

The elemental composition and homogeneity of particles have significant effects on biocompatibility and bioactivity properties of bioceramic materials. To understand interrelationship between materials properties, composition of the material must be known. This technique was used to analyze HAP sample. An EDAX spectrum of this sample is shown in Fig.4.5. Biological reactions of a HAP samples are strongly dependent on its chemical composition, i.e., Ca/P ratios; human bone primarily consists of Ca and P with a Ca/P ratio from 1.4 to 1.7 [34]. EDAX result reveals that HAP sample contains Ca, P and O without any impurity. The optimum Ca/P ratio for synthesized sample was found to be 1.73, which is slightly greater than 1.67 (theoretical value) and the same was commonly reported [35].

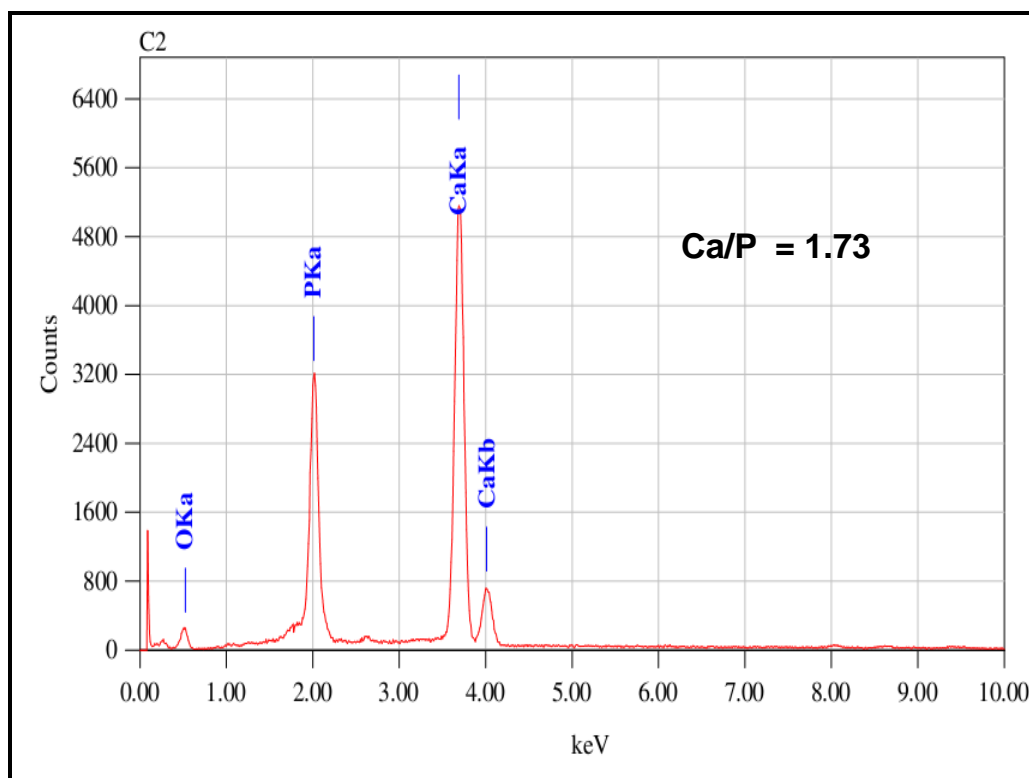


Fig.4.5 Energy dispersive spectra of HAP

4.3.6 FTIR Analysis:

The useful information regarding functional groups and molecular structure of the sample was determined by using FTIR analysis. An FTIR spectrum of this sample was recorded in the wavenumber ranging from 400 cm^{-1} to 4000 cm^{-1} . As synthesized sample was therefore characterized by FTIR analysis and corresponding FTIR spectra of HAP sample is presented in Fig.4.6. Results found to be very similar to those observed by D. Gopi et al and V. Stanic et al [36-37]. The peak located approximately at 3571 cm^{-1} and 632 cm^{-1} corresponds to stretching mode and vibrational mode of the OH^- group. The strong doublet band (shoulder band) at $960\text{--}1100\text{ cm}^{-1}$ was assigned to the P-O stretching vibration of the phosphate group (PO_4^{3-}). The weak band for phosphate bending vibration appears at 473 cm^{-1} . Moreover, the doublet band at $570\text{--}601\text{ cm}^{-1}$ was assigned to the PO_4^{3-} bending mode. A small band at around 1650 cm^{-1} was possibly due to absorbed water. The FTIR result demonstrates that the synthesized HAP sample was in high purity state, similar results were reported by D. Gopi et al [36].

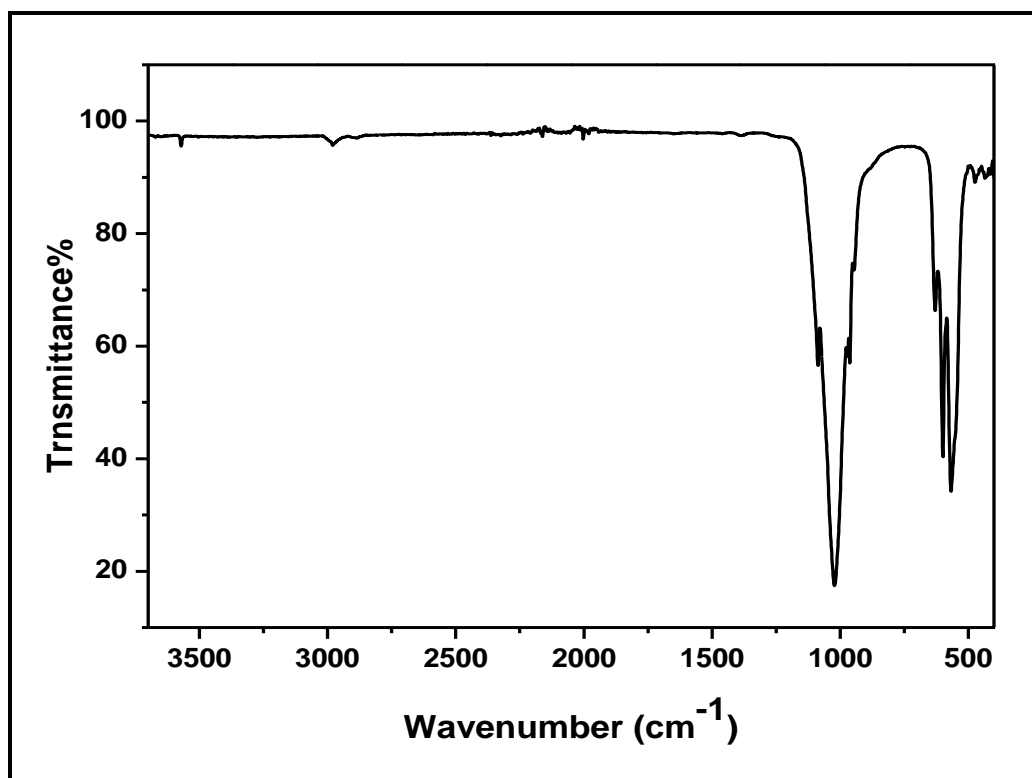


Fig.4.6 FTIR spectrum of HAP powder

4.3.7 Wettability studies:

Behavior of water droplet with surface of HAP sample has been shown in the Fig.4.7. Due to highly porous nature of HAP sample has a high surface free energy, quickly absorbs water molecules and its surface gets completely wet. Water contact angle on a rough surface of HAP exactly equals to 0° . The actual presence of OH groups on the surface of HAP is responsible for its superhydrophilic nature [38]. Wettable material supports cell growth and produces required medium.

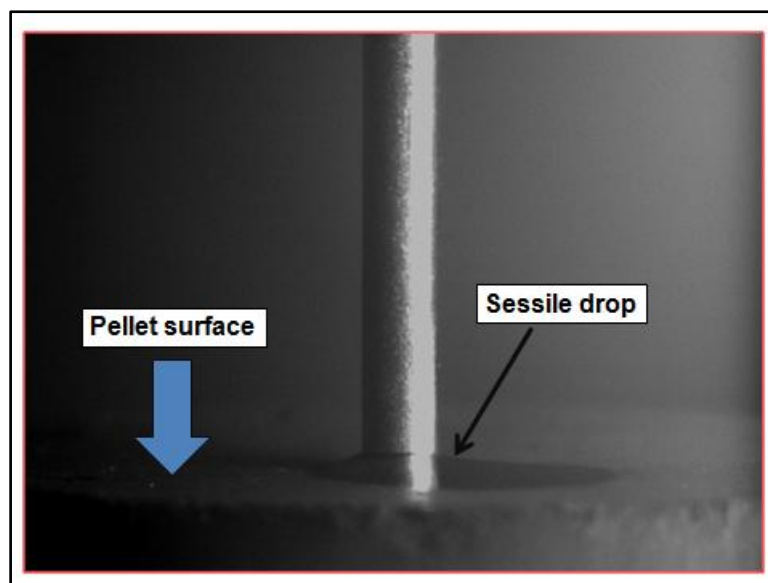


Fig.4.7 Water droplet on the superhydrophilic of HAP

4.3.8 Cell growth measurement:

MTT assay test were used to evaluate cell proliferation, cell viability of synthesized HAP sample that helps to develop new biomedical applications and the result is predicted in Fig.4.8. Mesenchymal stem cells (MSCs) can be distinguished into cell type multiplicity and extensively used in tissue engineering. In present investigation, to evaluate in vitro cytotoxicity, tissue culture plates were used as a reference, and it is compared with synthesized HAP nanopowders by using BMMSCs and CBMSCs cells. From the results it is seen that growth rate of cell viability for both the cells are depend upon incubation period and concentration of HAP nanopowder. When the concentration of HAP nanopowder was 80 $\mu\text{g/mL}$ and incubation period was 48 h, the value of cell viability for CBMSCs cells was 98.42 %. However, after 12 and 24 h there is slight decreases in percentage viability of CBMSCs, although it is not statistically significant compared to control. While, BMMSCs showed $70-77 \pm 4.95$ % viability compared to control. Percentage viability in BMMSCs after 48 h and 12 h was similar. This result was therefore found to be suitable for good biocompatibility of HAP nanoparticles for all concentrations. The results were formulated as mean standard deviation (SD) and this result was established at a level of $p < 0.05$.

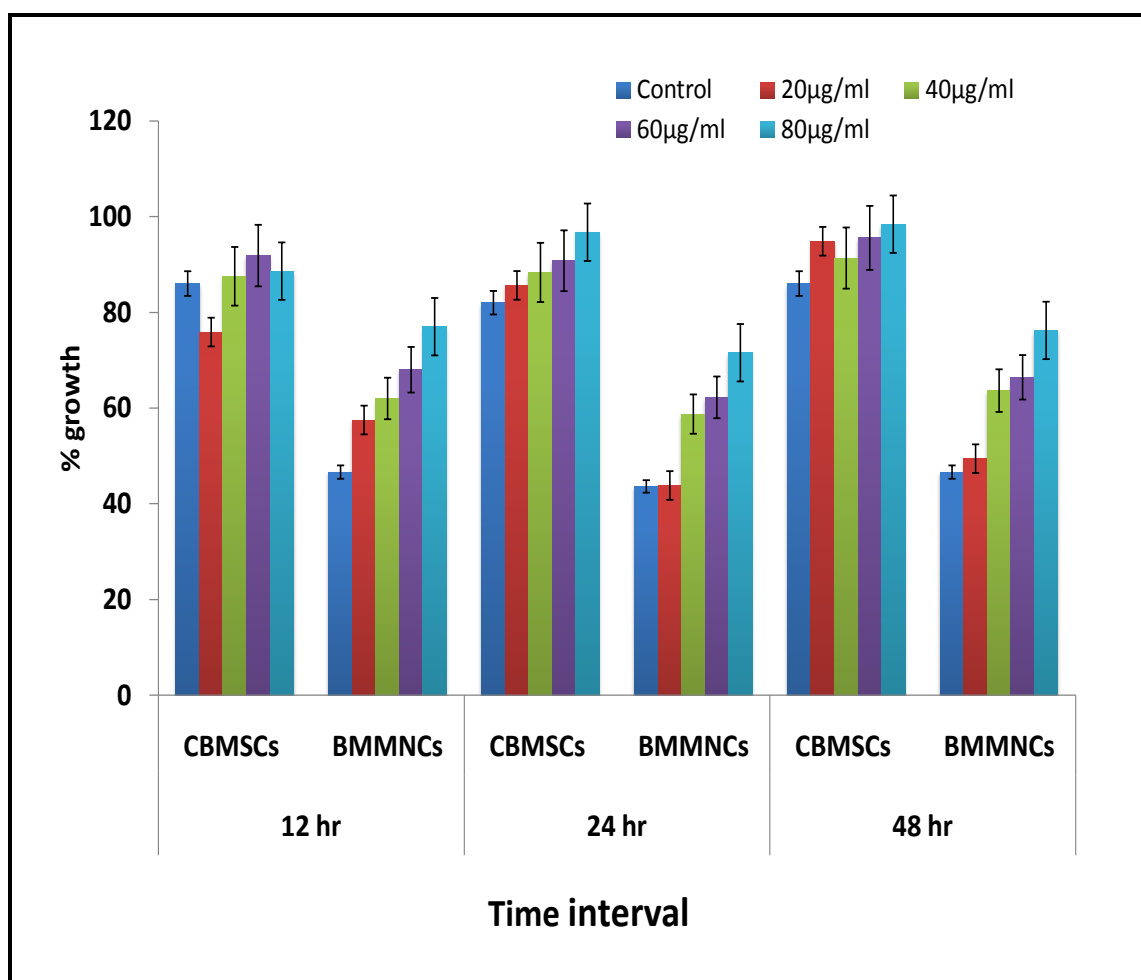


Fig.4.8 MTT assay results showing the human bone marrow mesenchymal stem cells (BMMSCs) and cord blood mesenchymal stem cells (CBMSCs) proliferation on HAP sample after 12, 24 and 48 h of culturing

4.3.9 Cell adhesion studies:

Cell adhesion property was used to evaluate the behavior of the MMSCs cells on HAP sample after incubation of 3 and 7 days. Fig. 4.9 (B) and (C-D) shows the pictures of attachment of cell on sample after cell culture incubated for 3 and 7 days respectively. The captured pictures shows maximum amount attachment of cells on the surface of sample in case of culture incubated for 3 days, while the growth of the MMSCs increases noticeably in cell culture incubated for 7 days. The HAP sample shows no any adverse effect on morphology of cell. These result indicated that the HAP sample supported MMSCs adhesion which providing an indication of HAP biocompatibility property. Fig. 4.9 (A) shows the culture medium of the MMSCs without HAP sample considered as a positive control.

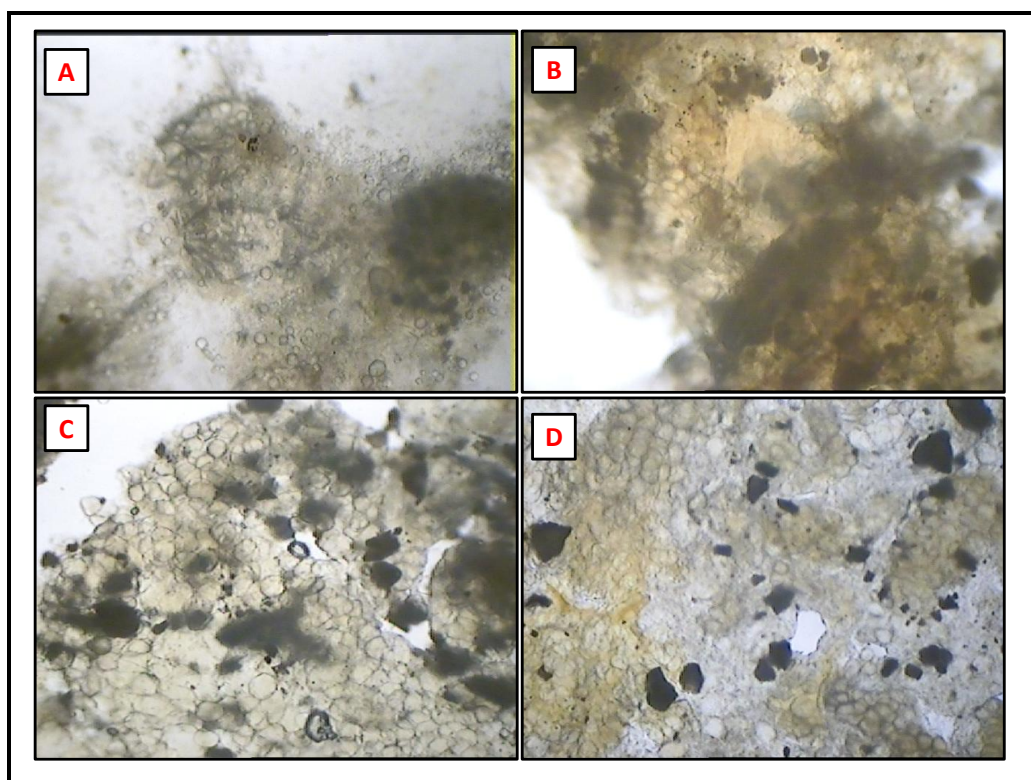


Fig.4.9 The morphological behavior of BMMSCs cells without HAP as positive control (A). BMMSCs cells adhering and spreading on HAP surface after 3 days (B) and 7 days (C-D)

4.3.10 Degradation study:

Biocompatible, bioresorbable and biodegradable materials have been used as an alternative material for internal fixation of human fractures [39, 40]. Bioceramics or biomaterials undergo degradation in the presence of fluids which leads to changes in their chemical structure and physical properties [41]. Degradation mechanism of sample depends on its nature. In contact with biological fluids, bioactive and bioresorbable bioceramics materials degrade through dissolution–reprecipitation mechanisms [26]. In this experiment in vitro degradation behavior of HAP pellet were evaluated through analyzing weight loss in SBF. The change of weight loss % of HAP sample with time of immersion is depicted in Fig.4.10. The results revealed that degradation of HAP sample takes place continuously through entire incubation period. As degradation time increases, the HAP shows higher weight loss. This weight loss reaches up to 10% after 50 days. The results revealed that HAP degrades easily and can be used as a scaffold for orthopedic applications [40].

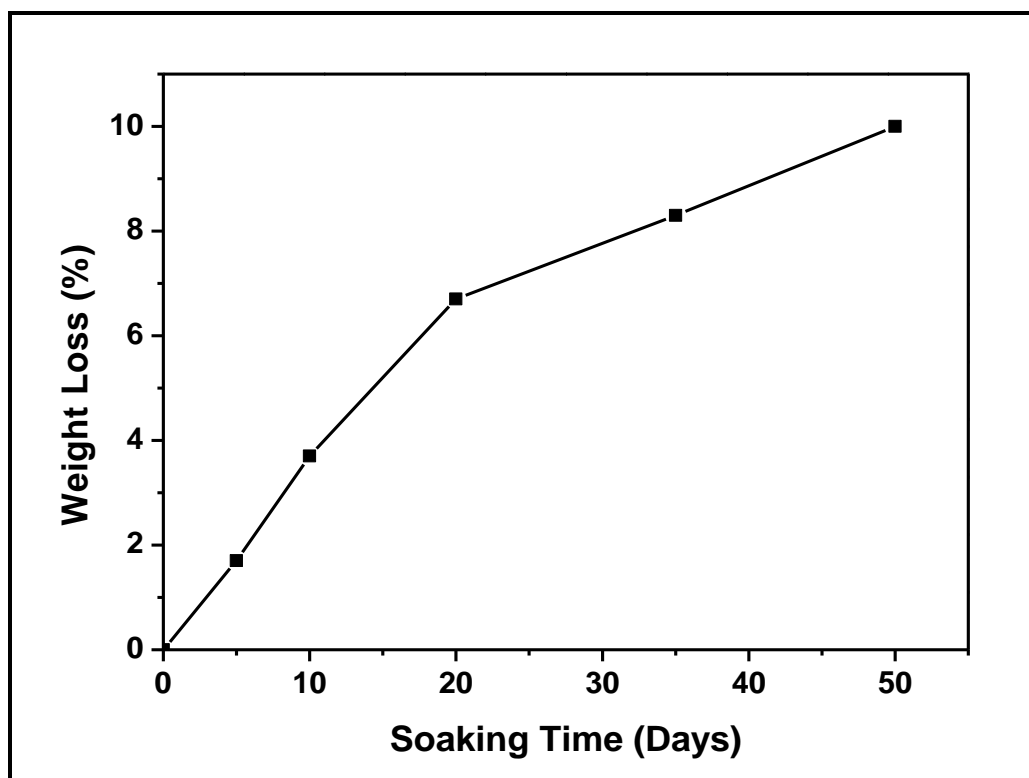


Fig.4.10 Changes in weight loss of HAP after immersion in SBF

4.3.11 Drug loading:

The drug concentration and drug to bioceramics ratio are responsible factor for drug uptake efficiency of bioceramics. The drug loading percentage is directly proportional to these parameters and attains maximum value at a particular level Fig.4.11 (A) shows that variation of drug loading on HAP sample with change in drug concentration. 80% of drug is loaded for 5% drug concentration and loading of drug increases up to 87% when concentration of drug increases to 10% then after, it remains constant at 20% drug concentration. Fig.4.11 (B) shows effect of temperature on loading of drug. A maximum 80% drug loading is observed in case of 5% drug concentration at 60°C with 40-min stirring time. As temperature increases there is increase in drug loading (%) afterwards, it attains constant value. Fig.4.11 (C) shows bar graph of changes in drug loading on HAP sample with different stirring time. Therefore, 40-min stirring time and 60°C are considered as optimized parameters for drug loading.

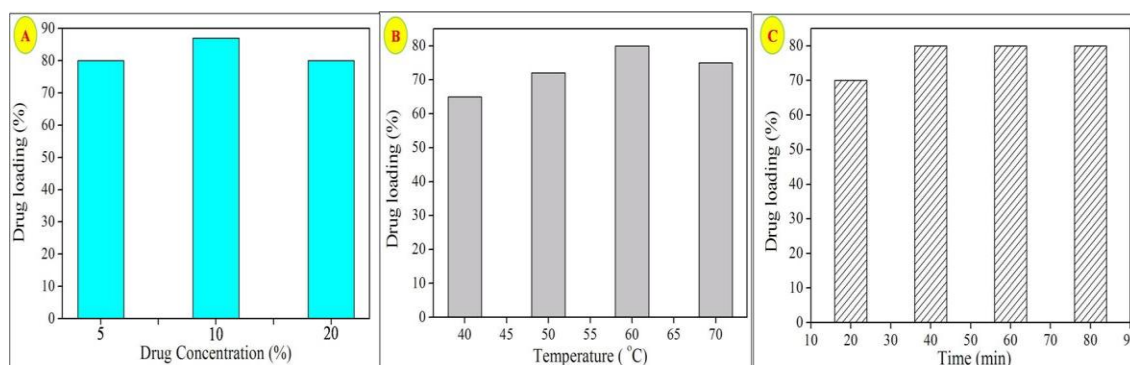


Fig.4.11 Drug loading behavior on HAP at different Drug concentration (A) different temperature (B) and at different stirring time (C)

4.3.12 In vitro drug release:

Norfloxacin drug was loaded on HAP sample to examine the efficiency of the drug delivery. Fig.4.12 shows different drug release profiles. The approximate drug release (%) in 200 h were found to be 60, 48 and 40% from 15, 10 and 5% of drug-loaded samples, respectively. The steady release of drug is observed for particular time; afterwards it is more or less constant. At initial time drug release behavior is high, then after, it decreases to attain some constant value. The possible reason for initial high release of Norfloxacin is desorption of Norfloxacin molecules from surface of the sample. The molecules of Norfloxacin do not show any powerful interaction with HAP sample. HAP sample absorbs the surrounding fluid in to it during the in vitro drug release analysis, due to this exclusion and dissolution of norfloxacin is observed. More amounts of norfloxacin get exposed to the fluid because of breaking of large particles of drug into smaller particles. The complete desorption of loosely adsorbed norfloxacin and incorporation between norfloxacin drugs with HAP nanoparticles leads to slow drug release. In vitro drug delivery experiment for HAP based bioceramics materials are also reported by other scientist for proteins and different antibiotics at different conditions and time [42, 43].

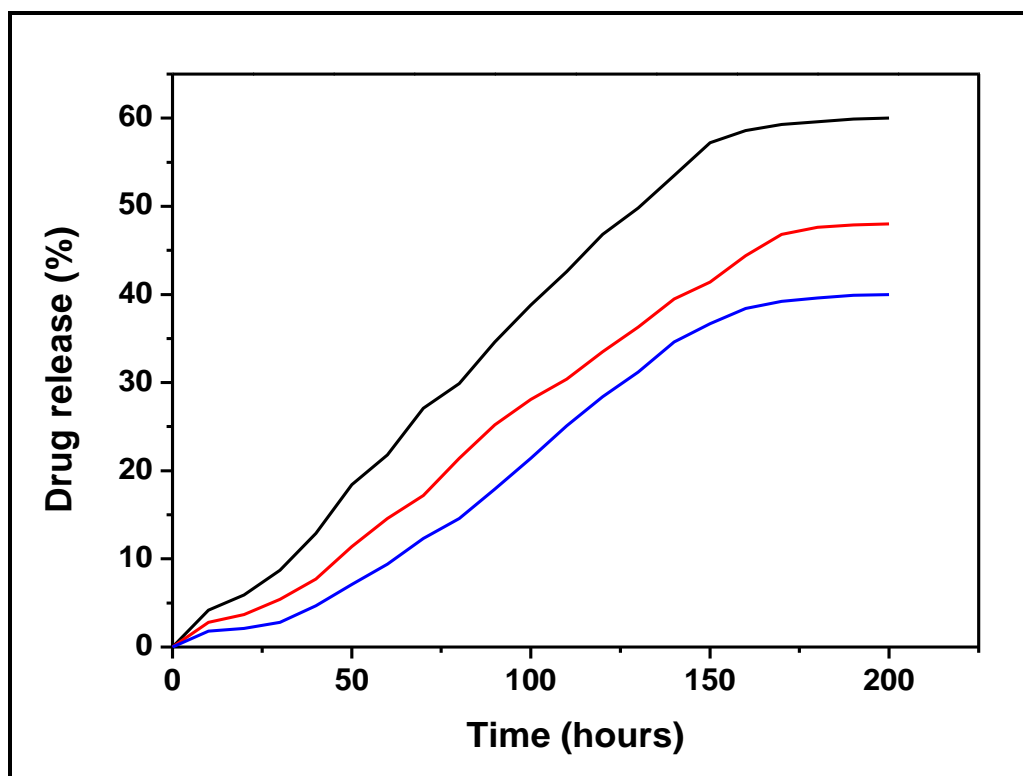


Fig. 4.12 Drug release percentage from HAP

4.4. Conclusions:

1. Hydroxyapatite (HAP) nanoparticles with improved and unique applications in tissue engineering were synthesized by innovative auto-combustion synthesis route.
2. Crystallite size obtained from XRD was found to be 30 nm.
3. The elemental analysis and presence of different elements such as Ca, P and O without any impurity for synthesized nanomaterials was confirmed by EDAX.
4. Wetting experiment revealed that the HAP material was superhydrophilic in nature. Cell culture, MTT and cell adhesion assay showed that the nanosized HAP powder provided a more adequate environment for cell adhesion and proliferation and was characterized by good biocompatibility.
5. The degradability in vitro was evaluated by weight loss in the SBF and it shows that the HAP sample exhibit a higher degradation rate.
6. The present investigation well demonstrated that HAP could efficiently adsorb and controlled release of norfloxacin, which suggested its extended applications for other antibiotics.

Chapter - 5

SYNTHESIS, CHARACTERIZATION AND APPLICATIONS OF Zn DOPED HYDROXYAPATITE

5.1 Introduction

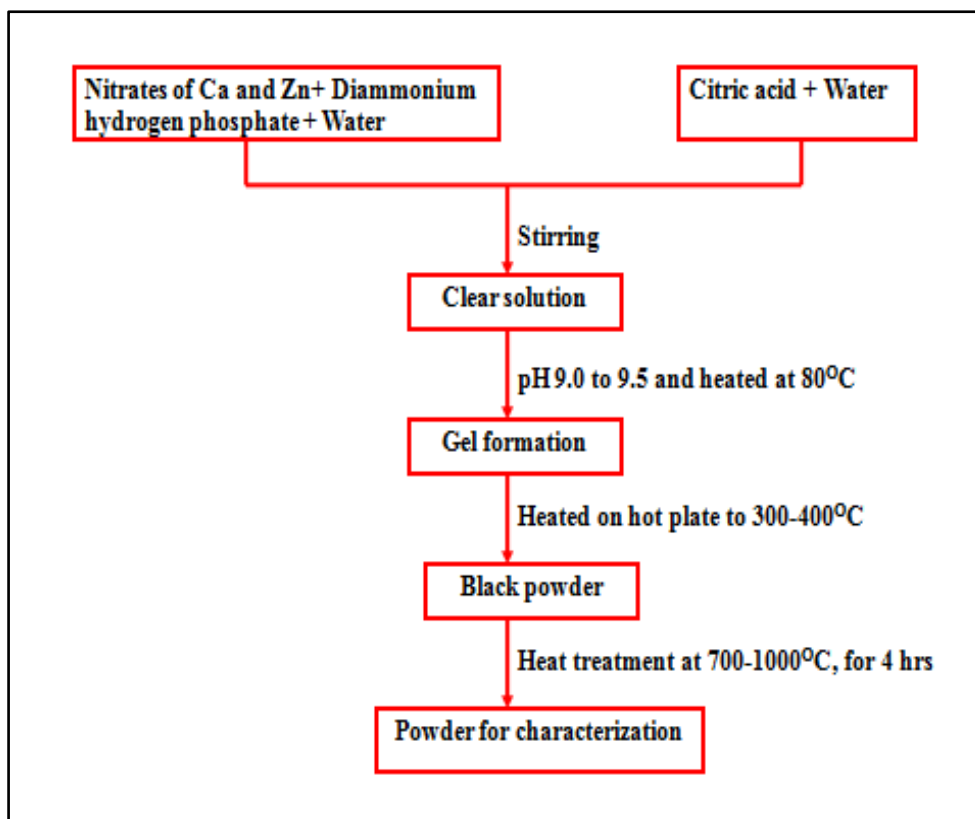
Inorganic biomaterials based on calcium and phosphate can be investigated for its enormous application in medical field [1–3]. The HAP is widely used for the preparation of innovative component, its potential to devise such component is mainly due to its biodegradability, bioactivity, osteoconductivity and chemical similarities with composition of bones [4,5]. Hydroxyapatite is used for filling up the bony defects specifically in orthopedic and dentistry [6–8]. In order to improve their biological properties HAP extensively been used as a coating for metallic prostheses [9–11]. Comparing available elements with the pure HAP sample, it is essential to synthesize nonstoichiometric HAP with substituted elements, which not only mimic bone apatite, but also helps to achieve improved osteoinductivity, bioactivity and biocompatibility. Recently, the researchers are taking considerable efforts for expending and modifying synthetic HAP which will help in enhancing its biodegradability, bioactivity and osteoinductivity by the compositions changed through ionic substitutions [12–14]. Zn, an element, with its great potential has been substituted through all the other available widely. Zn, with all its properties and bone mineral are closely linked together. Bone mineral contains different trace metal out of which Zn is said to be the most abundant. Zinc is an important element for in vitro and in vivo bone formation and it also helps to understand in vivo inhibitory effects on osteoclastic bone resorption [15]. The presence of Zinc in bone composition is important in order to prevent bone loss, increase bone density and bone metabolism [16]. Almost all the tissues of human body contain minor level of zinc. The teeth, bones and the pancreas are the body parts with considerable amount of zinc. About 1.5×10^{-2} mM of zinc is present in Human blood plasma [17]. Zn plays a significant responsibility in gene expression, with it; it does the differentiation and regulation of cellular growth [18]. The reason is the participation of zinc as a co-factor for enzymes counting more than 200, then its implication into the process of metabolism of nucleic acids, carbohydrates and proteins. Deem over, especially bone growth and its need, of the special animals that are inefficient with the zinc. They require this traced element for confirm bone growth, of-course, all this was through the relative observations [19]. Apart from this the enrichment of deficient diets with zinc leads to mineralization and stimulation of bone growth both [20]. For all six classes of metalloenzymes viz. “oxidoreductase, transferase, hydrolase, lyase, isomerase, and

ligase”, zinc is the only metal to be incorporated in their activity [21]. Carbonic anhydrase and alkaline phosphatase (ALP) considered as zinc metalloenzymes which are majorly found in bones, while strong inhibition of tartrate-resistant acid phosphatase also known as TRAP is due to presence of zinc [22, 23]. The process of bone formation, mineralization of bones and the stimulation of ALP activity in calvarial organ cultures [19, 24], takes place only due to presence of zinc along with its unique properties [25]. The growth of osteoblast-like cell cultures [26–28] and the activation of bone DNA polymerase which in turn stimulates the bone DNA synthesis [29] was obtained due to presence of zinc. On the other hand, insufficiency of zinc, initiate about 300% increase in programmed cell death (or apoptosis) in mice [30], and also leads to “apoptosis in hepatocytes, glioma, kidney, monocytes, fibroblasts, and testicular cells”. Zinc, an element is also considered as an antioxidant. Zinc is required in many biomechanical methods and chemical process such as carbohydrate metabolism, blood clotting and protein digestion. A body needs to be immune to anything that it can. Zinc does play crucial role in doing so. So, it would be advantageous to obtain zinc doped hydroxyapatite which helps to enhance different biochemical processes [31]. The various applications of materials mainly depend upon microstructure, surface properties of synthesized sample and method of preparation [32].

There has been an exclusive research working through the element called zinc-substituted HAP but although with available quotes there has been very few evidence. The partial replacement of Ca by Zn in the apatite lattice has been reported and was possibly due to differences in ionic radius of Ca and Zn, this leads to adsorption of Zn on exterior phases of HAP. There is no description available about the structural changes of apatite after replacement by Zn. Therefore, this research focuses that we synthesize zinc doped HAP by auto-combustion method and thorough examination of the effect of Zn^{2+} ions on the synthesis, including TG-DTA, XRD, TEM, SEM, EDAX, and FTIR and in vitro wettability behaviour to explore their structural properties. MTT assay was evaluated to study in vitro biocompatibility. The present researches are taking efforts for developing biocompatible, biodegradable materials for their potentials biomedical applications. Norfloxacin antibiotics were used for assessing the process of drug loading and drug releasing behavior.

5.2 Experimental and material details:

Nanostructured zinc doped HAP samples having the general formula, $\text{Ca}_{10-x}\text{Zn}_x(\text{PO}_4)_6(\text{OH})_2$ was synthesized by auto-combustion method. The synthesis was carried out with the calcium nitrate, zinc nitrate and diammonium hydrogen phosphate as the Ca, Zn and P sources, citric acid used as fuel. The raw materials used in the experiment were all of analytical purity. The molar ratio of metal nitrates and phosphate to citric acid was taken as 1:2. Firstly, stoichiometric amount calcium nitrate, zinc nitrate and diammonium hydrogen phosphate were dissolved in doubly distilled water with vigorous stirring. Citric acid was weighted stoichiometrically and dissolved in distilled water. The above solution mixed under constant stirring and pH adjusted 9 to 9.5 using ammonia. A homogeneous clear solution was achieved. This clear solution was stirred vigorously and heated up to 80°C for 4 h to obtain gel. Further, dry Zn-HAP powder was obtained by heating of gel at 300-400°C. This dried Zn-HAP was further sintered at 700-1000°C for 4 h. The pellets were prepared by mixing of calcined Zn-HAP with polyvinyl alcohol (1-2%) as a binder. The removal of the binder was done by calcinations of pellets at 250-400°C. Zn-HAP in powdered form was used for biological and structural analysis, while the pellets are used for in vitro biodegradation behavior and wettability test. Synthesis route and appearance of powder after calcinations is shown in flowchart and Fig.5.1.



Flowchart of sol-gel auto combustion synthesis of Zn-HAP bioceramics

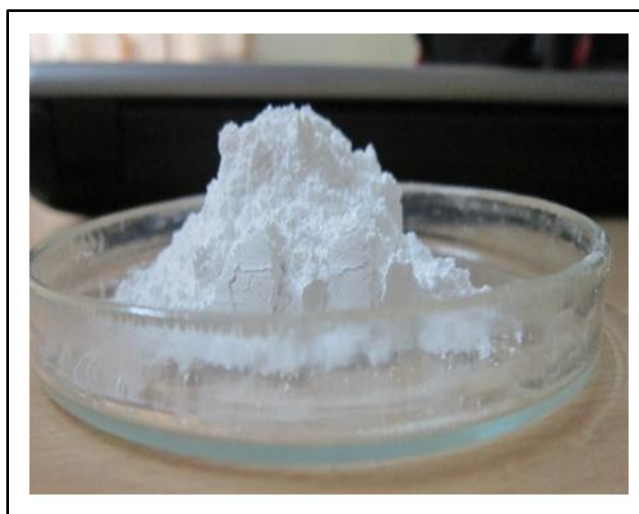


Fig.5.1 Zn-HAP powder calcined at 1000°C

The thermal decomposition behaviour and required sintering temperature of citrate precursor to phase formation of the sample was checked by thermogravimetric analysis on the SDT Q-600 instrument by heating the powder after auto-combustion in air atmosphere from 20° to 1000°C at the rate of 10°C per min. The X-ray diffraction analysis was used to know phase purity of synthesized material by using

PW3710 (Model- Philips) with $\text{CuK}\alpha$ radiation ($\lambda = 1.5406\text{\AA}$). Morphology and particle size of synthesized nanostructure sample was studied by TEM analysis (Philips CM-200) at 200 kV. The surface topography and microstructure of the sample was examined by means of electron microscopy scanned with different magnifications (JEOL JSM-6360). These nanoparticles were evaluated for the qualitative and quantitative determination of different elements by energy-dispersive X-ray spectroscopy (JEOL JSM-6360). JASCO FT/IR-6100 type 'A' spectrometer was used for FTIR study. In vitro wetting property of Zn-HAP samples were evaluated by sessile drop technique using contact angle measurement. A distilled water droplet (0.01ml) was diffused to the upper surface of Zn-HAP and examined with sophisticated goniometer (Model 110, R. hart Instrument Co., USA). UV-Visible spectral measurements of these samples carried out by using UV/Visible spectrophotometer (Systronic AU-2700). The pH of the solutions was carried out by using HANNA phep (model H 19).

5.2.1 Cell culture experiments:

To study the biocompatibility of $\text{Ca}_{10-x}\text{Zn}_x(\text{PO}_4)_6(\text{OH})_2$ ($x = 0.5$ to 2.0), an in vitro test was performed. Therefore, the human bone marrow mesenchymal stem cells (BMMSCs) and cord blood mesenchymal stem cells (CBMSCs) from a passage 4-6 were analyzed as a test subject. Prior to bioceramic surface cell seeding, cells were revived and cultured in Dulbecco's minimum essential medium (DMEM, Make-Sigma Aldrich) with fetal bovine serum (FBS) 10%, 1mM sodium pyruvate, 2mM L-glutamine, streptomycin (50 mg/mL) and penicillin (50 U/mL) as a supplement. The concentration of 5×10^5 cells per well were used for seeding in 6-well plates with 2 mL of DMEM. Further, incubation of the cells was done for growth and proliferation in CO_2 incubator optimized at 5% CO_2 , 90% humidity with temperature at 37°C . The cells were cultured with $40\mu\text{g Ca}_{10-x}\text{Zn}_x(\text{PO}_4)_6(\text{OH})_2/\text{ml}$ for 12, 24 and 48 hours (70% confluency) before the assays.

5.2.2 MTT cytotoxicity test:

For successful human bone substitution, however, it is necessary to know the effect of bioceramic materials on cellular response of human originated cells. Therefore, as synthesized $\text{Ca}_{10-x}\text{Zn}_x(\text{PO}_4)_6(\text{OH})_2$ ($x = 0.5$ to 2.0) samples were analyzed by MTT cytotoxicity test to study cell cytotoxicity, proliferation and viability. Well-characterized BMMSCs and CBMSCs cells were used and cultured by culture method described previously [33]. Each composition was taken in three

replicate. Initially, autoclaved samples were positioned in the well plate and consequently washed with PBS. After that, 96 well plates were seeded with concentration of 5×10^5 cells per mL. Afterward, the incubation of culture plate in CO_2 incubator was done for 12, 24 and 48 hours. Subsequently, the medium was aspirated and then samples were washed with PBS twice. 20 μL of MTT dye solution [(3-(4,5-dimethylthiazol-2-yl)-2,5 diphenyltetrazolium bromide: Make-SIGMA, USA, Cat no.M5655)] and 5 mg per mL phosphate buffer was added to each well so as to $\text{pH} = 7.4$. Lastly, the incubation of plate for 15 min and 4 h was done for steady-state confluent cells and exponentially growing cells respectively. After the incubation, the samples were taken off from the well and the crystals were solubilized with help of DMSO (200 μL) and this solution was energetically stirred for dissolution of the reacted dye. ELISA automated microplate reader was used to check the absorbance of each well at 550 nm (Biorad). All data were given in form of mean \pm SD for three group samples. The culture medium without cells is used as blank to calibrate the spectrophotometer at zero.

The viability of the cell in percentage is related to control wells containing cell culture medium without any addition of nanoparticles and was analyzed using the formula:

$$\text{Cell Viabilities (\%)} = [A] / [AB] \times 100 \quad (5.1)$$

Where, A and [AB] is the absorbance of the test sample and control sample respectively.

5.2.3 Cell adhesion test:

Cell adhesion property of bioceramic samples provides basic information due to which bioceramics were widely used in tissue engineering. Therefore, in vitro cell adhesion test of $\text{Ca}_{10-x}\text{Zn}_x(\text{PO}_4)_6(\text{OH})_2$ ($x = 0.5$ to 2.0) samples were evaluated using microscopic methods. It is necessary to examine whether these bioceramic samples are capable to sustain morphology of the MMSCs. The cells were cultivated in direct contact with the $\text{Ca}_{10-x}\text{Zn}_x(\text{PO}_4)_6(\text{OH})_2$ system. Therefore, mesenchymal stem cells (MMSCs) derived from bone marrow sheep and plated in to the 50 mL hard glass test tube. The cells were moderately immersed in Dulbecco's modified Eagle medium with 10% serum of animal, 100 U per mL penicillin G, 100 μg per mL streptomycin (invitrogen) and 15 mg of Zn-HAP ceramic samples (sintered powder) sprayed on the surface of cultured cells which acts as supplement. These cultured medium was incubated in CO_2 incubator operated at optimized conditions (5% CO_2 , 90%

humidity) at 37°C for 7 days respectively. At the selected time points, for morphological examination surface layer of cultured medium was removed and dried in air after washed with distilled water. The adherent cells on $\text{Ca}_{10-x}\text{Zn}_x(\text{PO}_4)_6(\text{OH})_2$ samples were visualized under 40X magnification microscope (Coslab, Model HL-9). Additionally, one culture medium containing MMSCs without studied sample considered as positive control.

5.2.4 In vitro biodegradation behavior:

Degradability of bioceramics is most important parameter in the biomedical field. Therefore, in vitro biodegradation behavior of $\text{Ca}_{10-x}\text{Zn}_x(\text{PO}_4)_6(\text{OH})_2$ systems with ($x=0.5$ to 2.0) were carried out in simulated body fluid (SBF). Ionic concentrations were used to prepare the SBF solution which is nearly similar to human blood plasma. It is prepared as per the procedure developed by Kokubo [34-36]. The comparison of human blood plasma with ion concentration of SBF prepared by Kokubo method was displayed in Table 5.1 and Table 5.2 provides appropriate quantities of reagents to be added in de-ionized water to have desired ionic concentration. Reagents are added in stepwise manner Table 5.2. Further, pH of this solution was adjusted to 7.4. The temperature of the SBF solution is maintained at 37°C.

To assess in vitro biodegradation tests the zinc doped HAP pellet (3 wt%) were added in closed bottle of SBF solution maintained at body temperature and are incubated for 5, 15, 20,35, and 50 days. Afterwards, the pellets of sample are taken out from SBF solution subsequently rinsing with de-ionized water, and drying in an oven at 100°C-150°C for 24 h was done. At last, weight loss (%) of sample and particulates was calculated by precise electronic balance. Two pellets of each group were rested under the above mentioned condition. The weight loss % (WL) of pellet during immersion in SBF was calculated using equation 5.2

$$WL = \left(\frac{M_0 - M_t}{M_0} \right) \times 100 \quad (5.2)$$

Where, M_0 and M_t was the initial weight and the weight of sample at time 't' respectively.

Table 5.1**Ion concentrations (mmol/dm³) of SBF and human blood plasma**

Ionic concentration (mmol/dm³)	Simulated body fluid	Blood plasma
Na ⁺	142	142
K ⁺	5.0	5.0
Mg ⁺	1.5	1.5
Ca ⁺	2.5	2.5
Cl ⁻	147.8	103.0
HCO ₃ ⁻	4.2	27.0
HPO ₄ ⁻	1.0	1.0
SO ₄ ⁻	0.5	0.5

Table 5.2**Reagent used for preparing SBF (1L, pH 7.4)**

Order	Reagent	Amount (g/l)
1	NaCl	7.996 g
2	NaHCO ₃	0.350 g
3	KCl	0.224 g
4	K ₂ HPO ₄ 3H ₂ O	0.228 g
5	MgCl ₂ 6H ₂ O	0.305 g
6	1M-HCl	40 ml
7	CaCl ₂	0.278 g
8	Na ₂ SO ₄	0.071 g
9	(CH ₂ OH) ₃ CNH ₂	6.057 g

5.2.5 Drug loading experiment:

If the material is biocompatible and biodegradable and have capacity to uptake and release drug in controlled manner then this material have applications in biomedicines. For that purpose, norfloxacin widely used antibiotic was chosen as model drug. In particular, concentrations (5%) of norfloxacin powder were prepared by dissolving it into 100 mL of de-ionized water. Afterwards, 1 g of calcined Zn-HAP

samples were added to above said drug solutions. The resultant suspensions were stirred for 40 minutes at temperatures 60°C. Then after, the resultant solution was kept intact for 24 h. The solution was centrifuged in order separate the precipitate. The drug loaded on Zn-HAP samples were assessed by knowing the difference in concentration of drug before and after loading. Drug loading (%) on Zn-HAP samples were evaluated by following equation:

$$\text{Drug loading (\%)} = [(A-B)/A] \times 100 \quad (5.3)$$

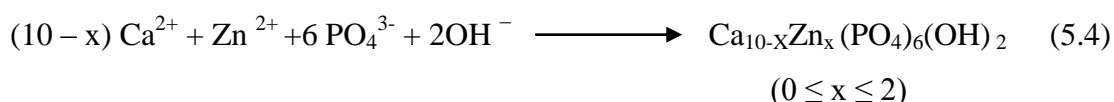
Where, A is the initial and B is the final norfloxacin concentration in aqueous solution.

5.2.6 In vitro drug release experiment:

In vitro drug release was evaluated over a time period of 200 hrs. 100 mg of drug-loaded Zn-HAP samples with (x=0.5 to 2.0) were added into a capped glass bottle contains phosphate-buffered (50 mL) saline (PBS) having pH =7.4 and incubated at 37°C. The stationary mode was used to study drug release. To calculate the released amount of drug, 5 mL of sample were centrifuged and replaced with 5 mL of fresh PBS medium. Afterwards, the actual concentration of Norfloxacin in the supernatant liquid was measured at 274 nm using spectrophotometer.

5.3 Results and Discussion:

The reaction involved in the formation of Zn-HAP can be expressed as following equation.



5.3.1 TGA-DTA Analysis:

To study the effect of zinc on the phase transformations and thermal stability of synthesized $\text{Ca}_{10-x}\text{Zn}_x(\text{PO}_4)_6(\text{OH})_2$ system, TGA-DTA analysis of the dried gel, of x = 0.5, 1.0 and 2.0 samples, were performed. TGA curves Fig.5.2, 5.3 and 5.4 shows thermal decomposition of samples below 200°C due to removal of absorbed water from the pores of gel [37]. The corresponding weight losses in this region were around 11.25%, 19.90% and 24.99% for x = 0.5, 1.0 and 2.0 samples, respectively. TGA curves of all of the three samples shows second weight loss possibly due to adsorbed water which get desorbed and due to thermal decomposition of organic residue within the temperature range between 200 and 320°C, The weight loss in this region is 13.14%, 21.52% and 7.36 % for x = 0.5, 1.0 and 2.0 samples, respectively.

A weight loss takes place is because of nitrates NO_3^- which get thermally decomposed within range from 320°C to 600°C [38]. The DTA curve shows that thermal decomposition of Zn-HAP samples at 100°C , 200°C and 250°C with an endothermic peak and this peak is attributed due to thermal decomposition of residual water from gel [39]. TGA shows weight loss in the temperature range of 100 - 200°C indicated the reactions (oxidation-reduction) of nitrates with fuel [40].

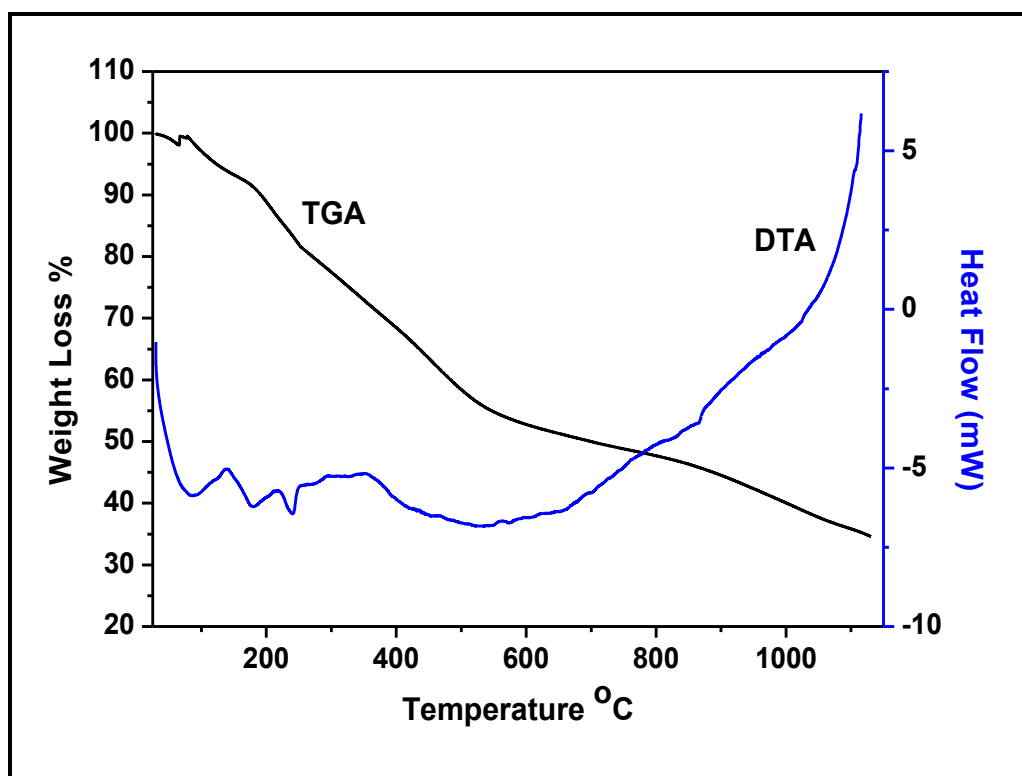


Fig. 5.2 TGA-DTA curve of $\text{Ca}_{10-x}\text{Zn}_x(\text{PO}_4)_6(\text{OH})_2$ system ($x=0.5$)

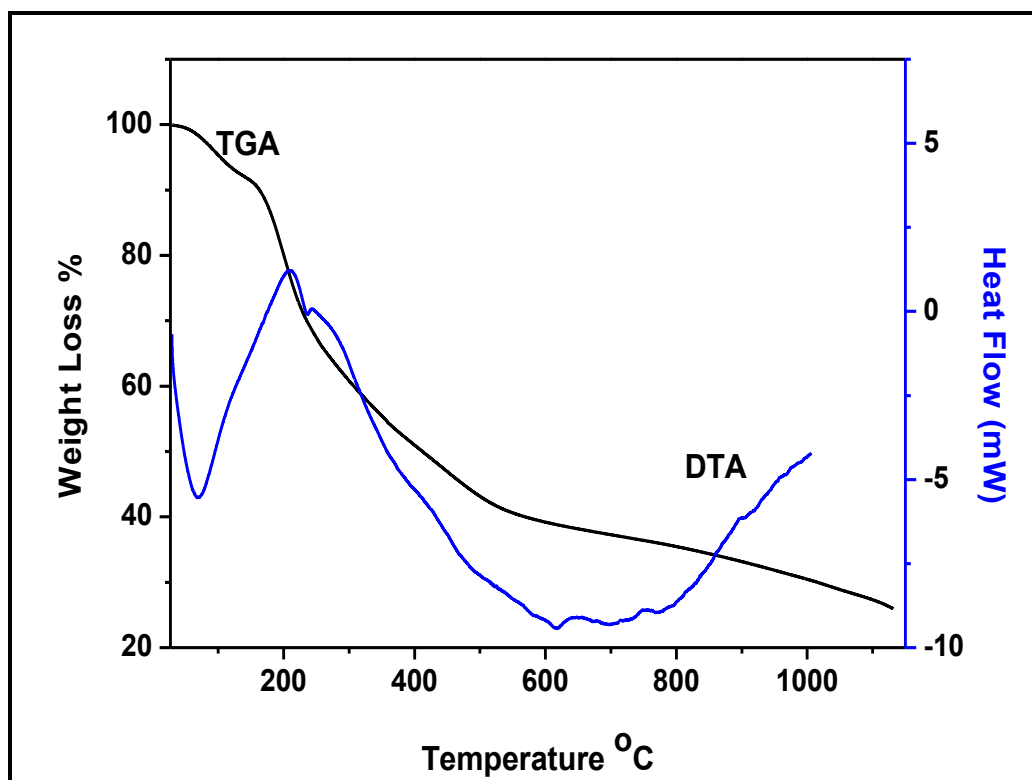


Fig.5.3 TGA-DTA curve of $\text{Ca}_{10-x}\text{Zn}_x(\text{PO}_4)_6(\text{OH})_2$ system ($x=1.0$)

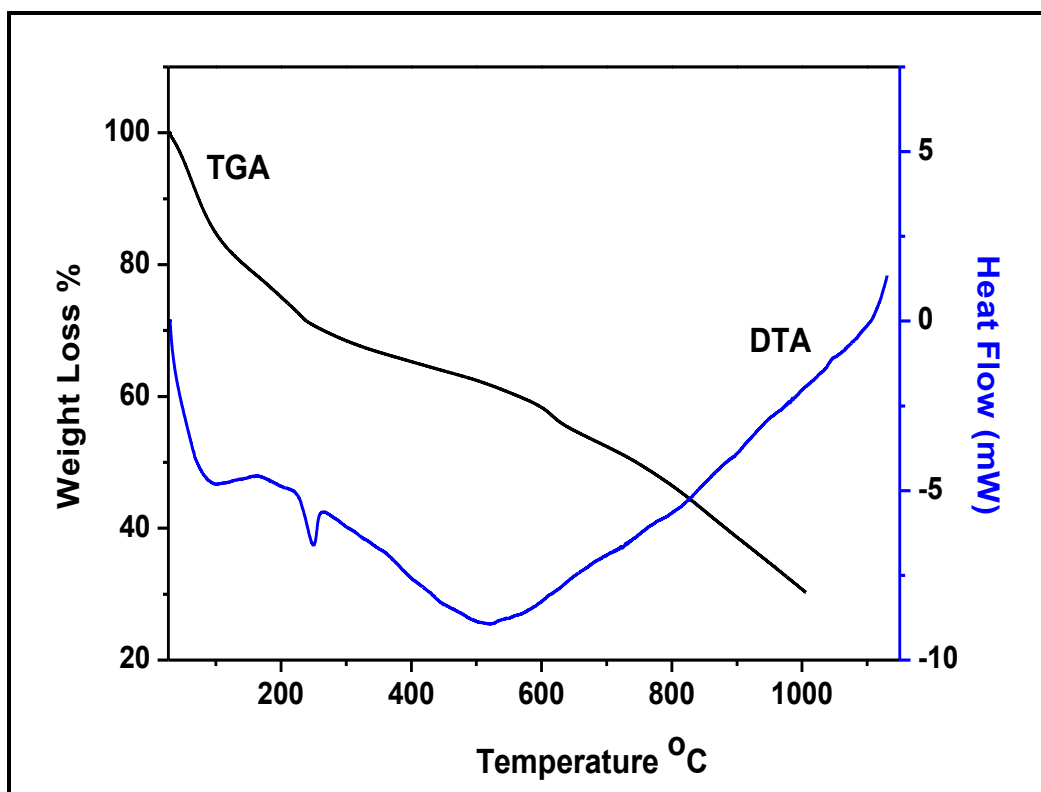


Fig.5.4 TGA-DTA curve of $\text{Ca}_{10-x}\text{Zn}_x(\text{PO}_4)_6(\text{OH})_2$ system ($x=2.0$)

5.3.2 Phase identification:

The X-ray diffraction study and phase purity of synthesized Zn-HAP bioceramic samples were examined by XRD analysis. Fig.5.5 shows X-ray

diffraction pattern of calcined Zn-HAP samples calcined at 1000°C for 4 hours. The peak in XRD patterns were indexed to (002), (211), (300), (202), (310), (311), (113), (222), (312), (213), (321), (410), (402), (004). These polycrystalline Zn-HAP nanoparticles exhibit single phase hexagonal structure (JCPDS 09-0432) [41]. Debye Scherrer's formula was used to estimate crystallite size of synthesized Zn-HAP samples [42- 44].

$$\tau = 0.94 * \lambda / \beta * \cos \theta \quad (5.5)$$

Where, crystallite size (τ) depends upon wavelength λ (1.54 Å for CuK α) of the X- ray and the FWHM (β) of the XRD peak at 2θ . The average crystallite size obtained for Zn-HAP samples [$x = 0.0$ to 2.0] calcined at 1000°C were found to be 30 to 40 nm. Interplanar spacing (d), hkl planes and corresponding θ values of these systems are tabulated in Tables 5.3 to 5.7.

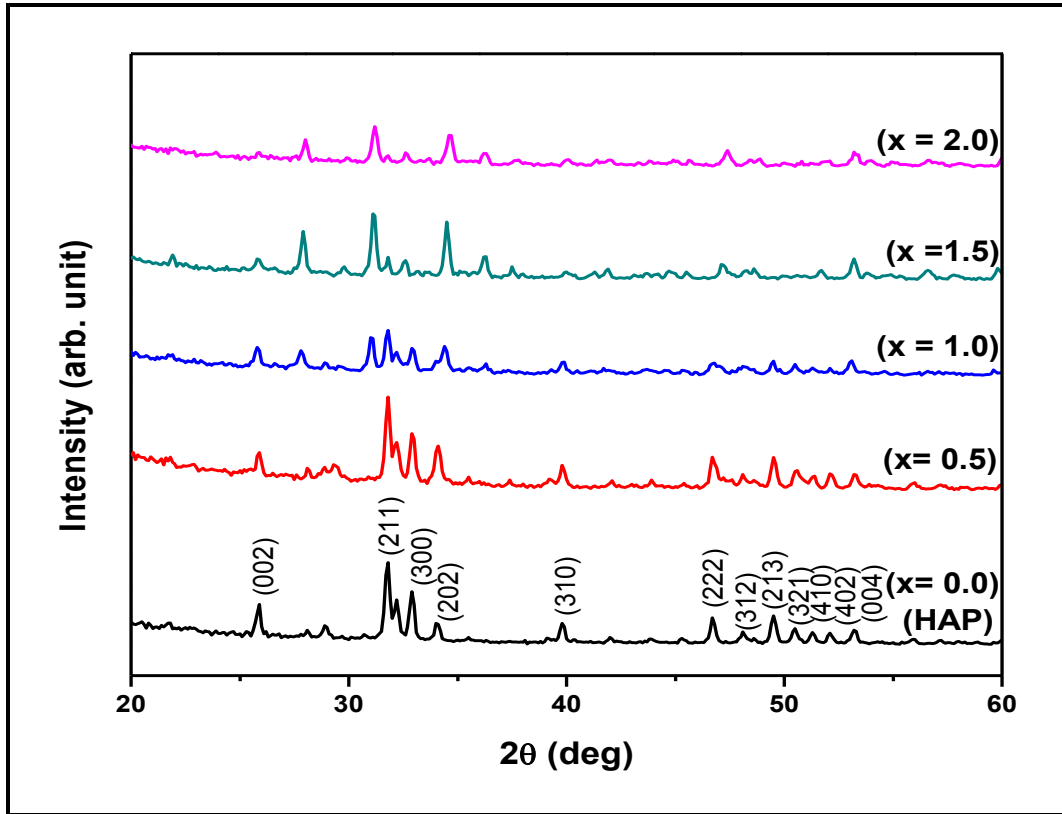


Fig.5.5 XRD pattern for $\text{Ca}_{10-x}\text{Zn}_x(\text{PO}_4)_6(\text{OH})_2$ system ($0 \leq x \leq 2$)

Table 5.3
Indexed X-ray diffraction pattern of $\text{Ca}_{10-x}\text{Zn}_x(\text{PO}_4)_6(\text{OH})_2$ ($x = 0.0$)

Sr. No.	2 θ	$d_{\text{obs}} \text{ \AA}$	$d_{\text{std}} \text{ \AA}$	h k l Planes
1	25.881	3.439775	3.439775	002
2	31.771	2.814233	2.814233	211
3	32.902	2.720032	2.720032	300
4	34.047	2.63113	2.63113	202
5	39.818	2.66208	2.66208	310
6	46.711	1.943068	1.943068	222
7	48.102	1.890076	1.890076	312
8	49.462	1.841244	1.841244	213
9	50.493	1.806039	1.806039	321
10	51.283	1.780057	1.780057	410
11	52.1	1.754049	1.754049	402
12	53.143	1.722056	1.722056	004

Structure: Hexagonal

Lattice constant: $a = 9.418 \text{ \AA}$, $c = 6.881 \text{ \AA}$

Table 5.4
Indexed X-ray diffraction pattern of $\text{Ca}_{10-x}\text{Zn}_x(\text{PO}_4)_6(\text{OH})_2$ ($x = 0.5$)

Sr. No.	2 θ	$d_{\text{obs}} \text{ \AA}$	$d_{\text{std}} \text{ \AA}$	h k l Planes
1	25.818	3.448025	3.439775	002
2	31.816	2.810355	2.814233	211
3	32.998	2.712337	2.720032	300
4	34.164	2.622387	2.63113	202
5	39.845	2.26061	2.26208	310
6	46.813	1.939071	1.943068	222
7	48.146	1.888452	1.890076	312
8	49.562	1.837762	1.841244	213
9	50.662	1.803736	1.806039	321
10	51.297	1.779605	1.780057	410
11	52.145	1.752641	1.754049	402
12	53.213	1.719955	1.722056	004

Structure: Hexagonal

Lattice constant: $a = 9.4051 \text{ \AA}$, $c = 6.879 \text{ \AA}$

Table 5.5

Indexed X-ray diffraction pattern of $\text{Ca}_{10-x}\text{Zn}_x(\text{PO}_4)_6(\text{OH})_2$ ($x = 1.0$)

Sr. No.	2θ	d_{obs} Å	d_{std} Å	h k l Planes
1	25.109	3.437164	3.439775	002
2	31.884	2.804516	2.814233	211
3	33.096	2.704529	2.720032	300
4	34.369	2.607213	2.63113	202
5	39.898	2.257729	2.26208	310
6	46.89	1.936066	1.943068	222
7	48.199	1.886499	1.890076	312
8	49.578	1.837207	1.841244	213
9	50.577	1.803236	1.806039	321
10	53.145	1.721995	1.722056	004

Structure: Hexagonal

Lattice constant: a = 9.379 Å, c = 6.887 Å

Table 5.6
Indexed X-ray diffraction pattern of $\text{Ca}_{10-x}\text{Zn}_x(\text{PO}_4)_6(\text{OH})_2$ ($x = 1.5$)

Sr. No.	2 θ	d_{obs} Å	d_{std} Å	h k l Planes
1	25.92	3.434688	3.439775	002
2	31.89	2.804002	2.814233	211
3	32.556	2.748145	2.720032	300
4	34.497	2.597831	2.63113	202
5	40.055	2.249241	2.26208	310
6	47.12	1.927151	1.943068	222
7	48.339	1.881362	1.890076	312
8	49.35	1.84516	1.841244	213
9	53.266	1.718369	1.722056	004

Structure: Hexagonal

Lattice constant: $a = 9.381$ Å, $c = 6.873$ Å

Table 5.7

Indexed X-ray diffraction pattern of $\text{Ca}_{10-x}\text{Zn}_x(\text{PO}_4)_6(\text{OH})_2$ ($x = 2.0$)

Sr. No.	2θ	d_{obs} Å	d_{std} Å	h k l Planes
1	26.014	3.422489	3.439775	002
2	31.91	2.80229	2.814233	211
3	32.733	2.733688	2.720032	300
4	34.649	2.586782	2.63113	202
5	40.178	2.242638	2.26208	310
6	47.396	1.916571	1.943068	222
7	48.646	1.870204	1.890076	312
8	53.312	1.716994	1.722056	004

Structure: Hexagonal

Lattice constant: a = 9.376Å, c = 6.867Å

5.3.3 TEM Analysis:

TEM images Fig.5.6 to 5.9 clearly depicted the influence of zinc concentration on the morphology and crystallographic features of the HAP. Fig. 5.6 (with $x = 0.5$) clearly shown that synthesized sample consists of spherical shape nanoparticles having an average size of 30 nm. Further, from TEM images Fig.5.7 to 5.9 it can be concluded that with increasing concentration of Zinc from $x=1.0$ to $x=2.0$, the small particles get vanished while rod-like particles were appeared. From the results, it can be conclude that the morphology of $\text{Ca}_{10-x}\text{Zn}_x(\text{PO}_4)_6(\text{OH})_2$ system with ($x=0.5$ to 2.0) changes from spherical to rod like particles. Average diameter of nanorods in the range of 25-45 nm, respectively. Zinc doped HAP with a spherical and nanorod like morphology shows good adsorbability due to larger surface area (Van der Waal's interactions) which leads to enhancement in biocompatibility and bioactivity property

of Zn doped HAP [45] and spherical geometry is important for achieving osseointegration [46, 47].

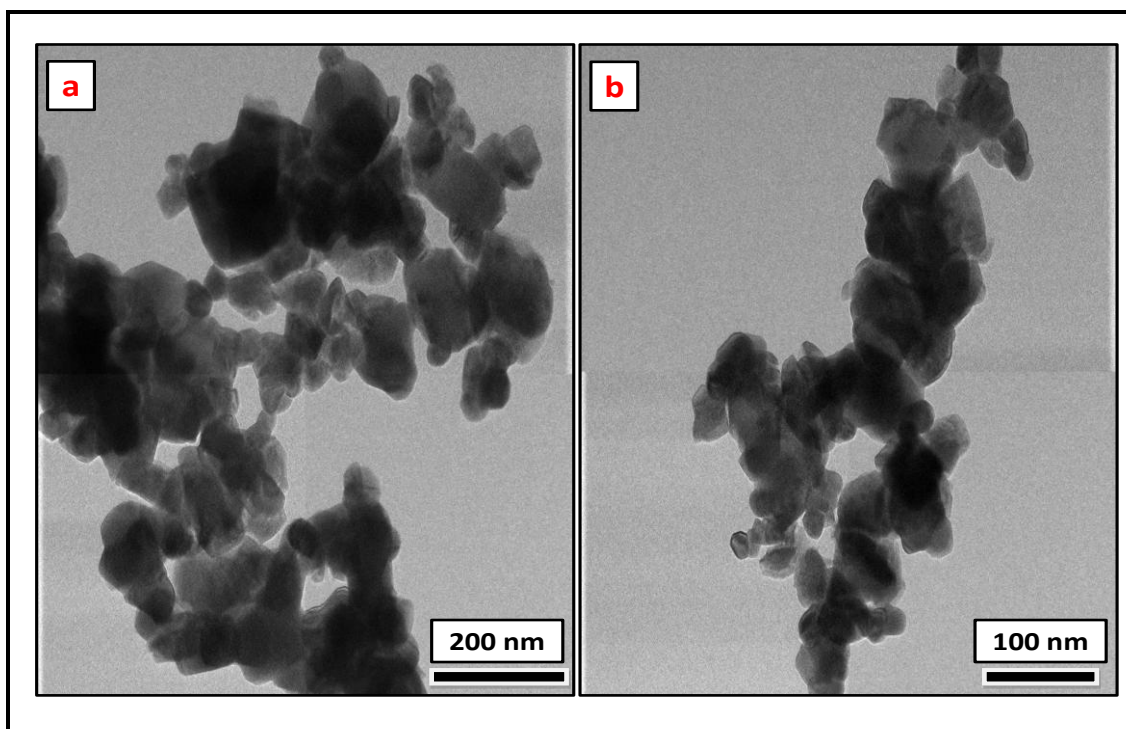


Fig.5.6 Transmission electron spectrum of $\text{Ca}_{10-x}\text{Zn}_x(\text{PO}_4)_6(\text{OH})_2$ system ($x=0.5$)

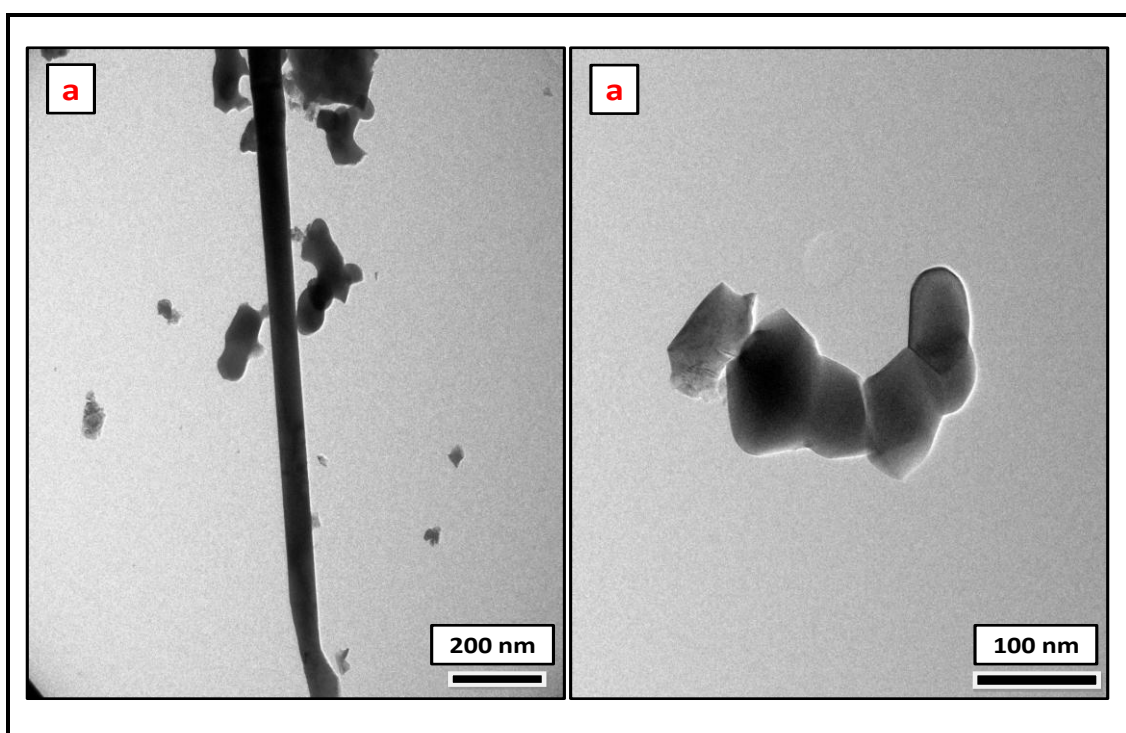


Fig.5.7 Transmission electron spectrum of $\text{Ca}_{10-x}\text{Zn}_x(\text{PO}_4)_6(\text{OH})_2$ system ($x=1.0$)

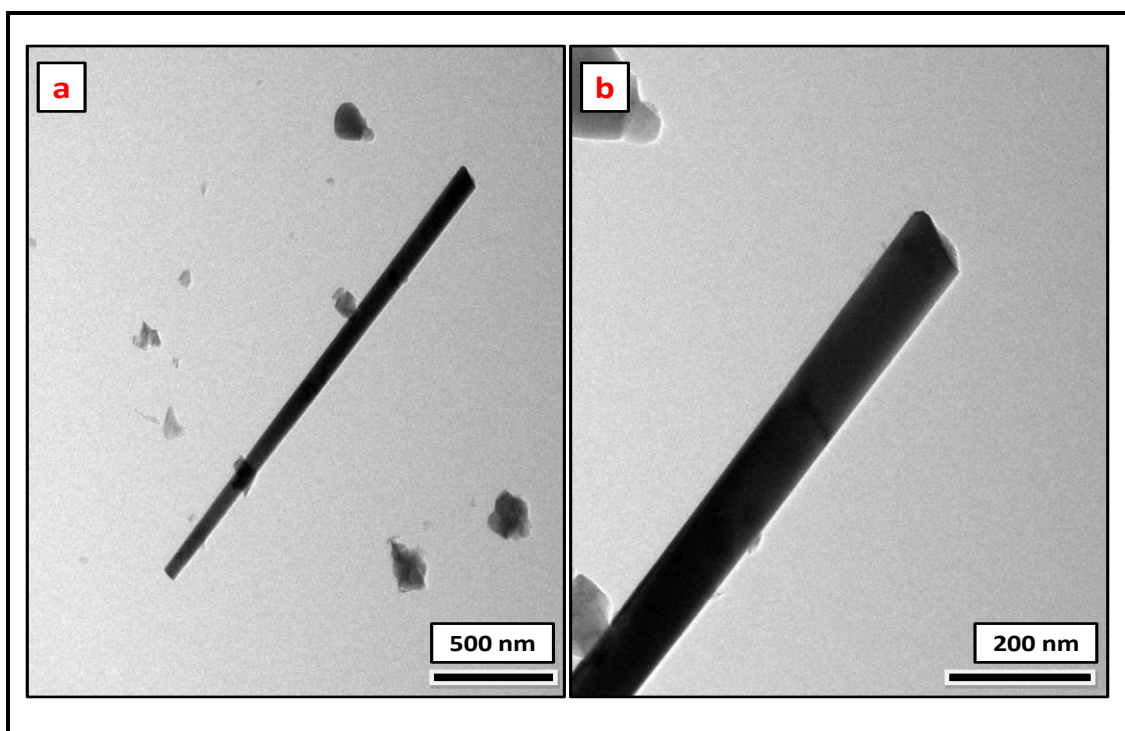


Fig.5.8 Transmission electron spectrum of $\text{Ca}_{10-x}\text{Zn}_x(\text{PO}_4)_6(\text{OH})_2$ system ($x=1.5$)

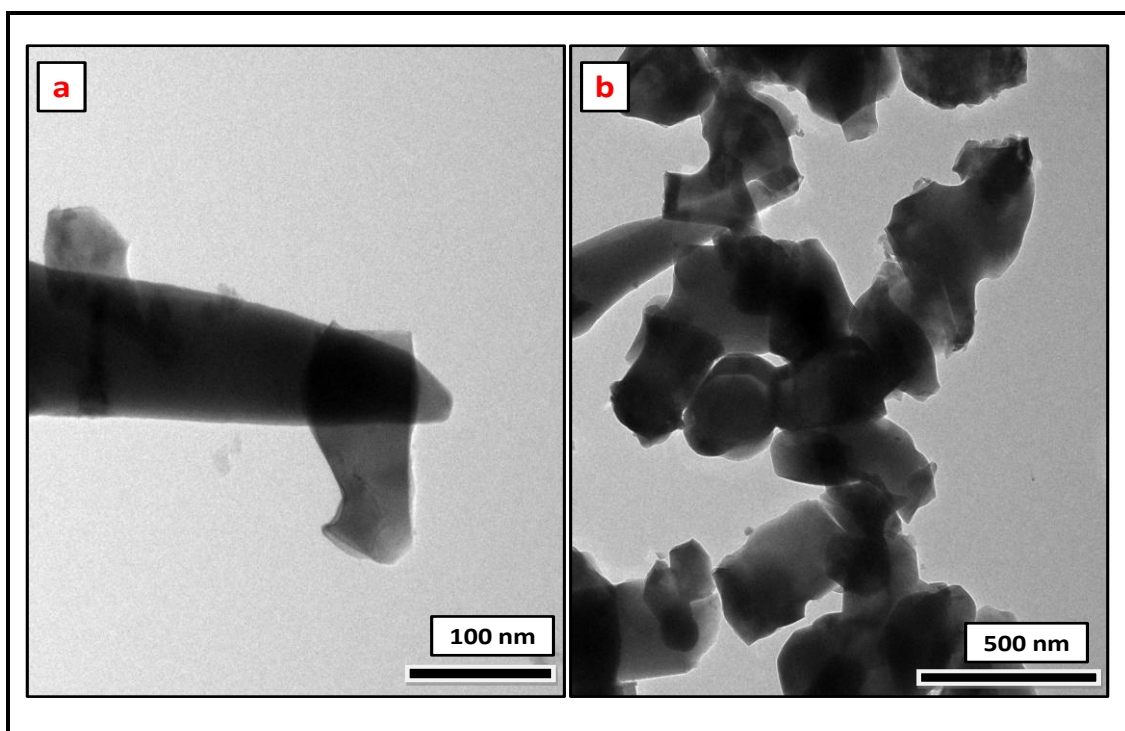


Fig.5.9 Transmission electron spectrum of $\text{Ca}_{10-x}\text{Zn}_x(\text{PO}_4)_6(\text{OH})_2$ system ($x=2.0$)

5.3.4 SEM Analysis:

In the present work, the surface morphological study of Zn-HAP system was examined using SEM. The SEM micrographs of $\text{Ca}_{10-x}\text{Zn}_x(\text{PO}_4)_6(\text{OH})_2$ as

synthesized by auto-combustion method are given in the Fig.5.10 to 5.13. A large number of particles having irregular shape and separated with infinitesimal distance are obtained for Zn-HAP ($x=0.5$) shown in Fig.5.10. The synthesized samples shows monodisperse and uniform nanorod like structures which can be seen from the SEM images. It can be seen that there is a strong correlation between zinc concentration and the product morphology. Large number of particles, which changes to rod like and needle like morphology Fig.5.11 to 5.13 by increasing zinc concentration. HAP based bioceramics having needle like and rod like shapes and morphology are highly preferred because they are the basic “building block” for constructing the microstructure of tooth and bone [48].

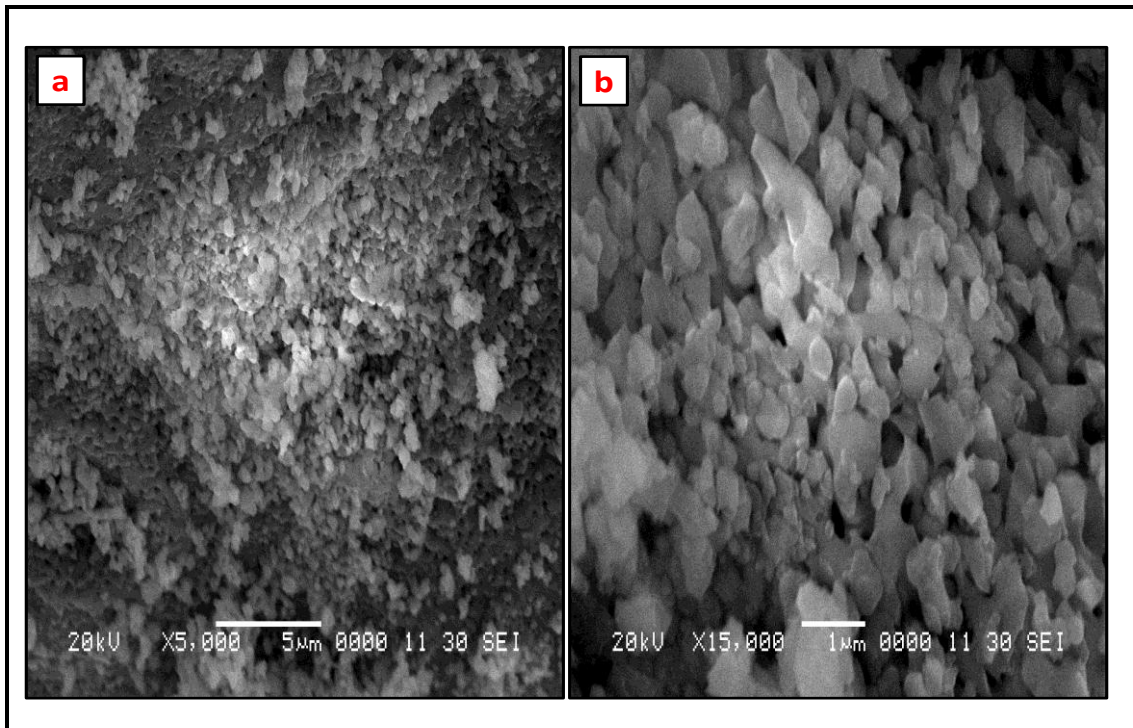


Fig.5.10 SEM micrograph of the $\text{Ca}_{10-x}\text{Zn}_x(\text{PO}_4)_6(\text{OH})_2$ system ($x=0.5$)

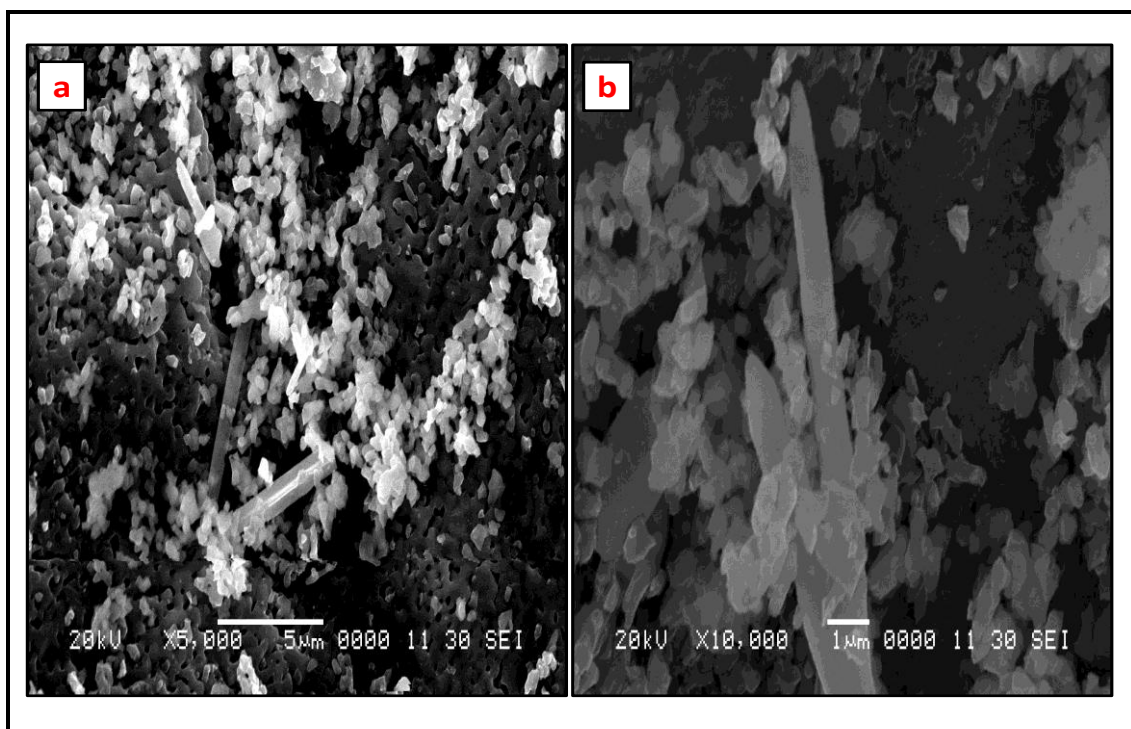


Fig.5.11 SEM micrograph of the $\text{Ca}_{10-x}\text{Zn}_x(\text{PO}_4)_6(\text{OH})_2$ system ($x=1.0$)

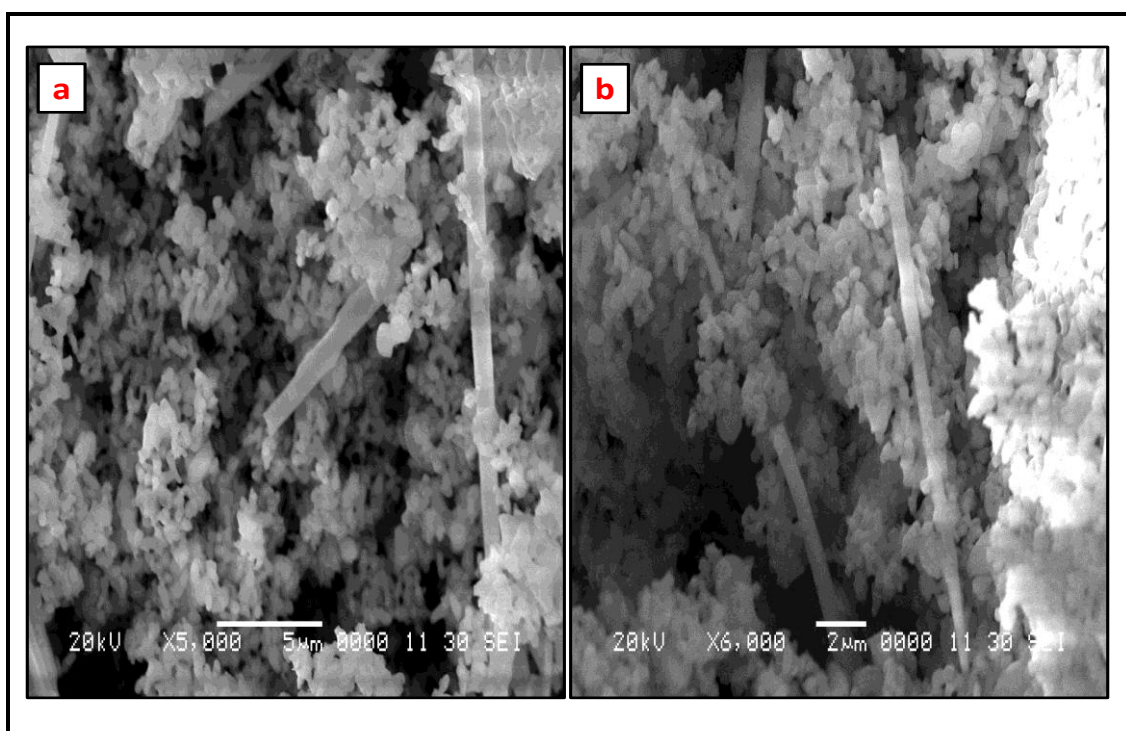


Fig.5.12 SEM micrograph of the $\text{Ca}_{10-x}\text{Zn}_x(\text{PO}_4)_6(\text{OH})_2$ system ($x=1.5$)

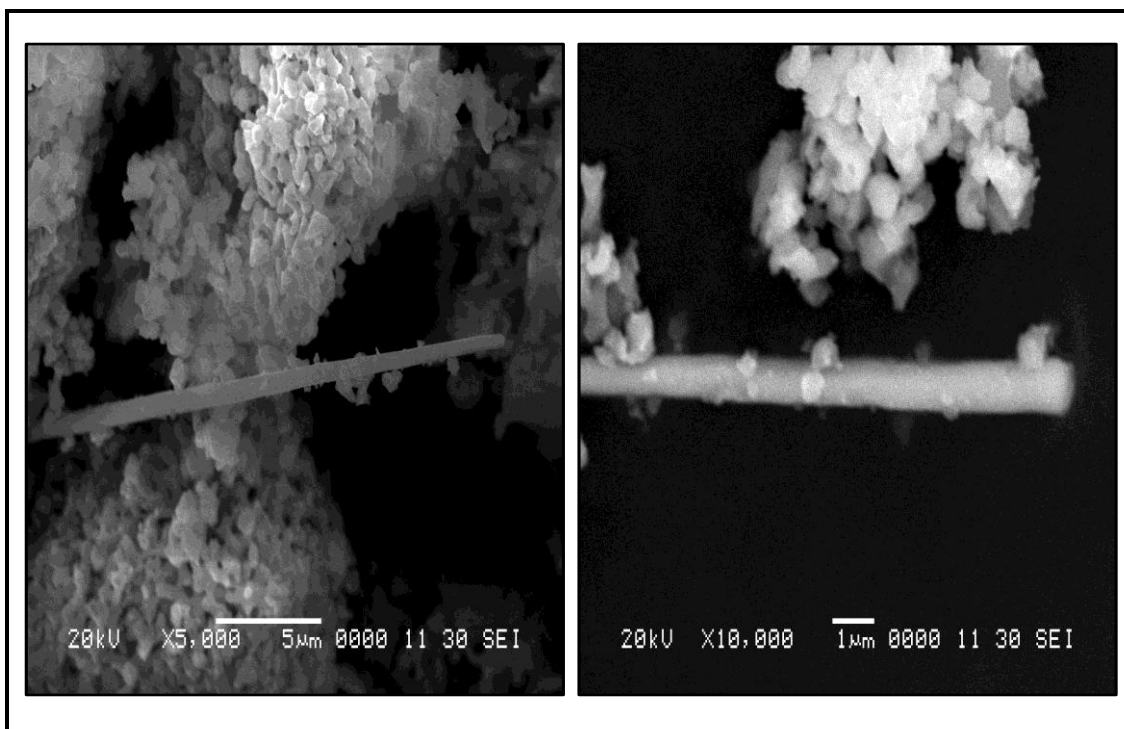


Fig.5.13 SEM micrograph of the $\text{Ca}_{10-x}\text{Zn}_x(\text{PO}_4)_6(\text{OH})_2$ system ($x=2.0$)

5.3.5 EDAX Analysis:

The qualitative and quantitative elemental analysis of the synthesized Zn doped HPA system with ($x= 0.5$ to 2.0) were examined using energy dispersive X-ray spectrometer (EDAX) and shown in Fig.5.14 to 5.17. Figures clearly shows that the synthesized Zn doped HAP samples contain Ca, Zn, P and O without any impurity. The pure HAP contains Ca to P molar ratio within the range 1.67 to 1.7 [49], the corresponding stoichiometry of pure HAP is affected by addition of Zinc which possibly due to replacement of some of Ca by Zn. From EDAX analysis with increasing amount of Zn there is decrease in the (Ca + Zn): P ratio. This might be due to the crystal defects by Zn substitution. The EDAX result reveals that all the obtained values lie within the satisfactory range for the pure hydroxyapatite [50, 51].

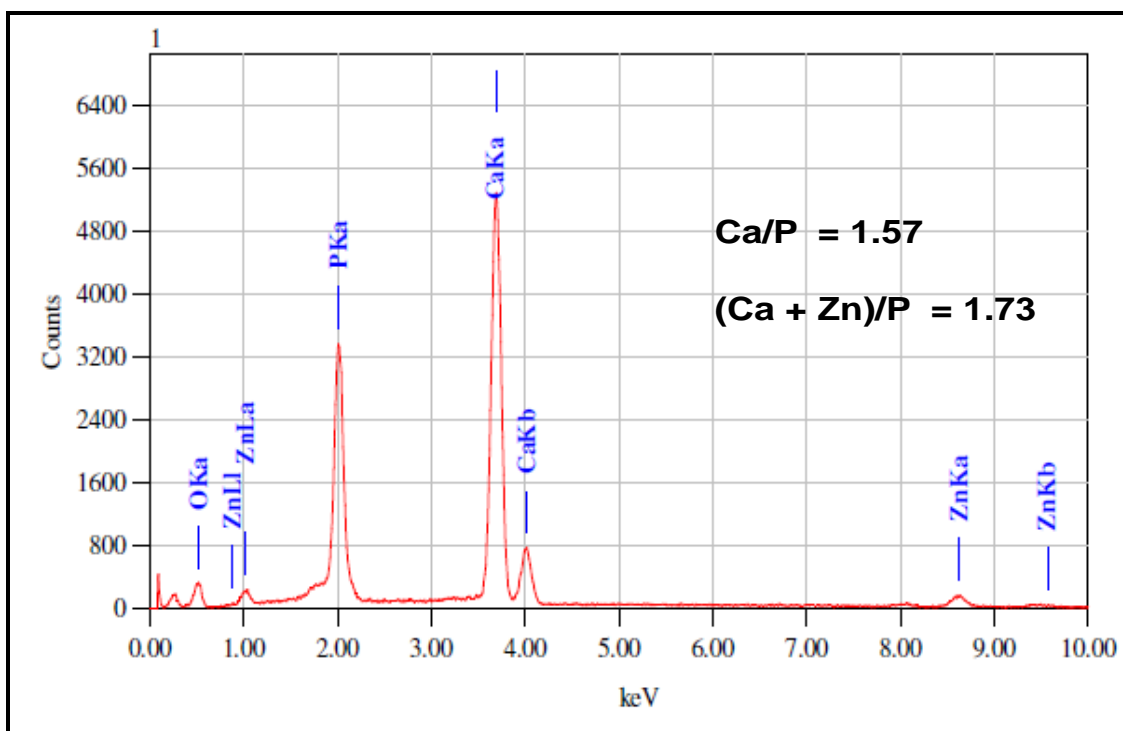


Fig.5.14 Energy dispersive spectra of the $\text{Ca}_{10-x}\text{Zn}_x(\text{PO}_4)_6(\text{OH})_2$ system ($x=0.5$)

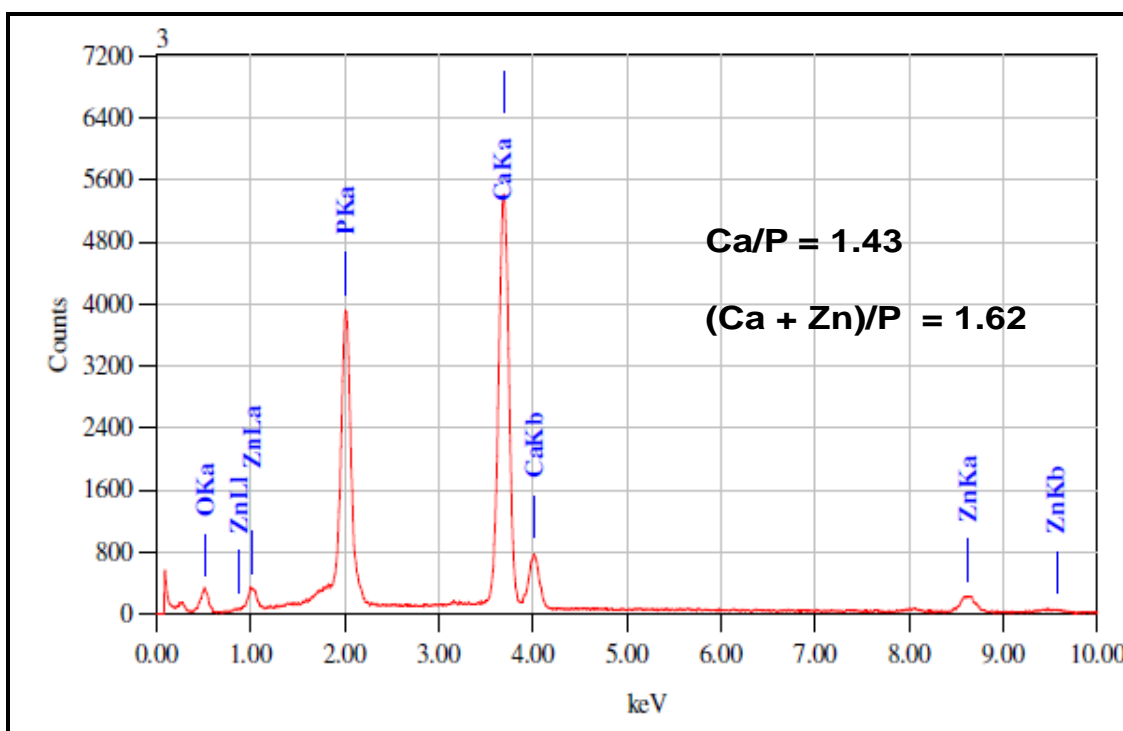


Fig.5.15 Energy dispersive spectra of the $\text{Ca}_{10-x}\text{Zn}_x(\text{PO}_4)_6(\text{OH})_2$ system ($x=1.0$)

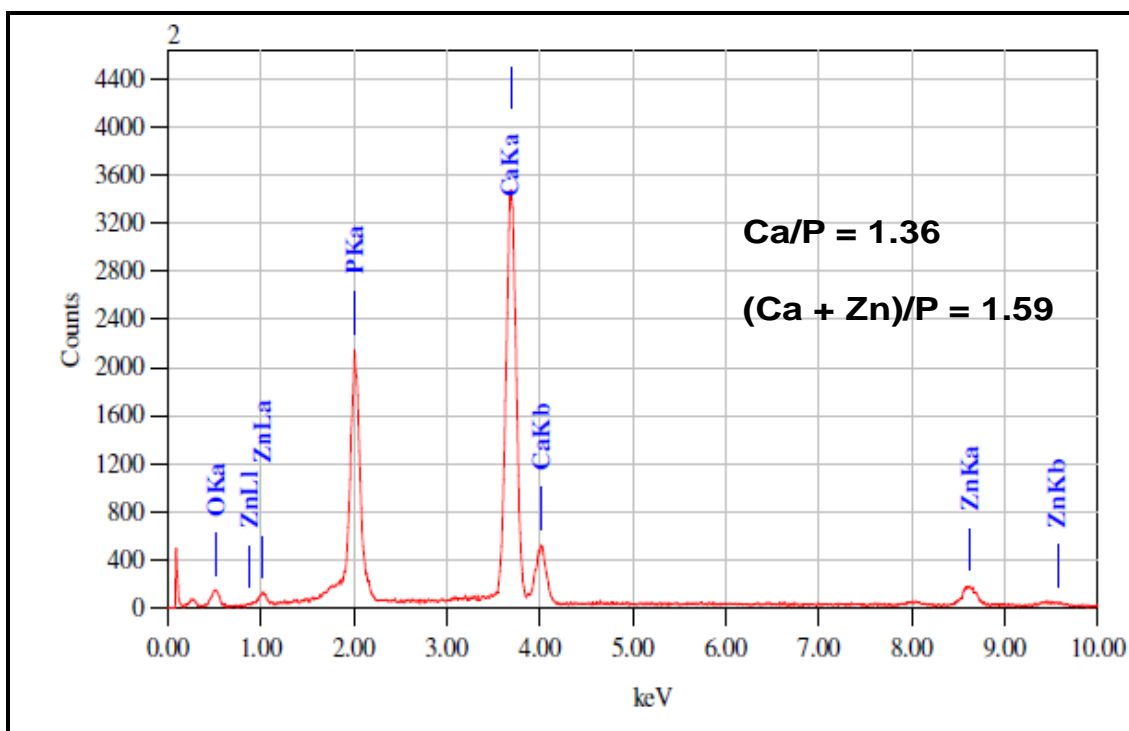


Fig.5.16 Energy dispersive spectra of the $\text{Ca}_{10-x}\text{Zn}_x(\text{PO}_4)_6(\text{OH})_2$ system ($x=1.5$)

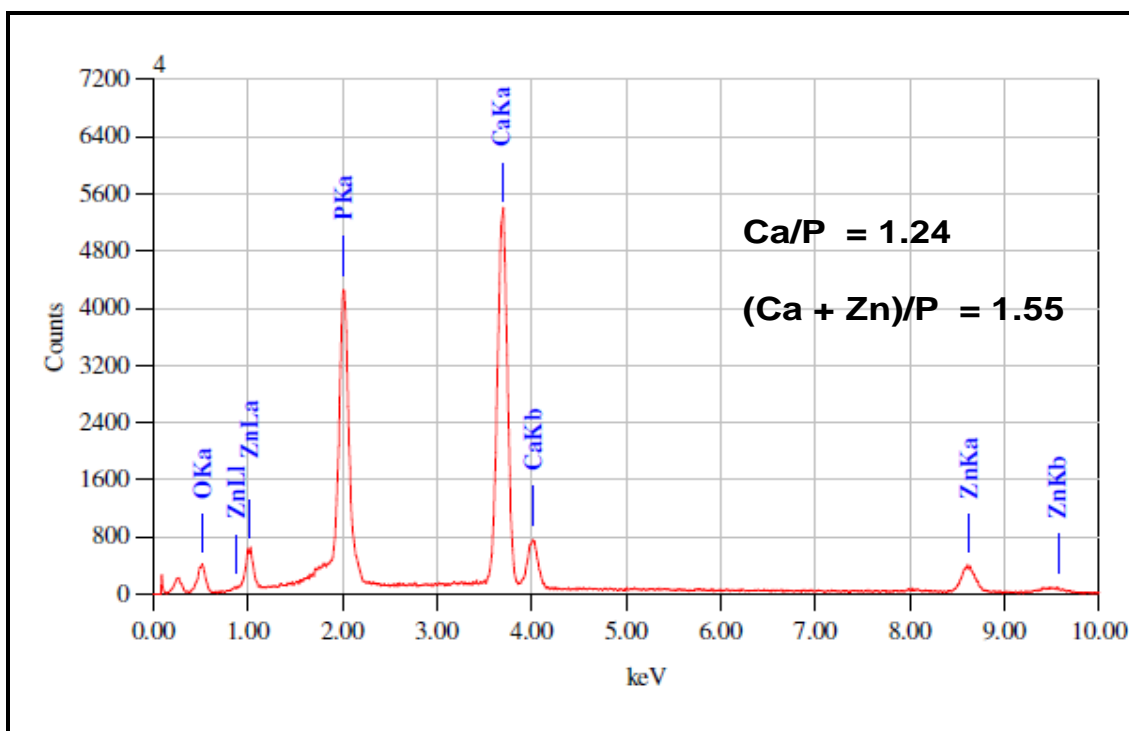


Fig. 5.17 Energy dispersive spectra of the $\text{Ca}_{10-x}\text{Zn}_x(\text{PO}_4)_6(\text{OH})_2$ system ($x=2.0$)

5.3.6 FTIR Analysis:

FTIR scanning of pure HAP and $\text{Ca}_{10-x}\text{Zn}_x(\text{PO}_4)_6(\text{OH})_2$ system with ($x=0.5$, to 2.0) calcined at 1000°C are given in the Fig.5.18 and found to be very similar to those observed by D. Gopi and C. Yang et al [52, 53]. There are distinct differences between the spectra of the HAP and zinc doped HAP. Therefore, one can say there were some changes were taking place in the chemical structure of HAP due to the addition of zinc. All samples shows bands corresponding to HAP, which is confirmed by FTIR spectra. The peak located approximately at 3571 cm^{-1} and 632 cm^{-1} corresponds to the stretching vibration and vibrational mode of OH^- respectively. The strong doublet band or shoulder at $960\text{-}1100\text{ cm}^{-1}$ was assigned to P-O stretching vibration of the phosphate group (PO_4^{3-}). The band at about 473 cm^{-1} (weak) and $570\text{-}601\text{ cm}^{-1}$ (doublet) corresponds to the phosphate bending vibration and PO_4^{3-} bending mode respectively. A small band at around 1650 cm^{-1} was possibly due to absorbed water (bending mode). The FTIR result demonstrates that the synthesized pure HAP and Zn-HAP samples were in high purity state, similar results were reported by C. Yang et al [53].

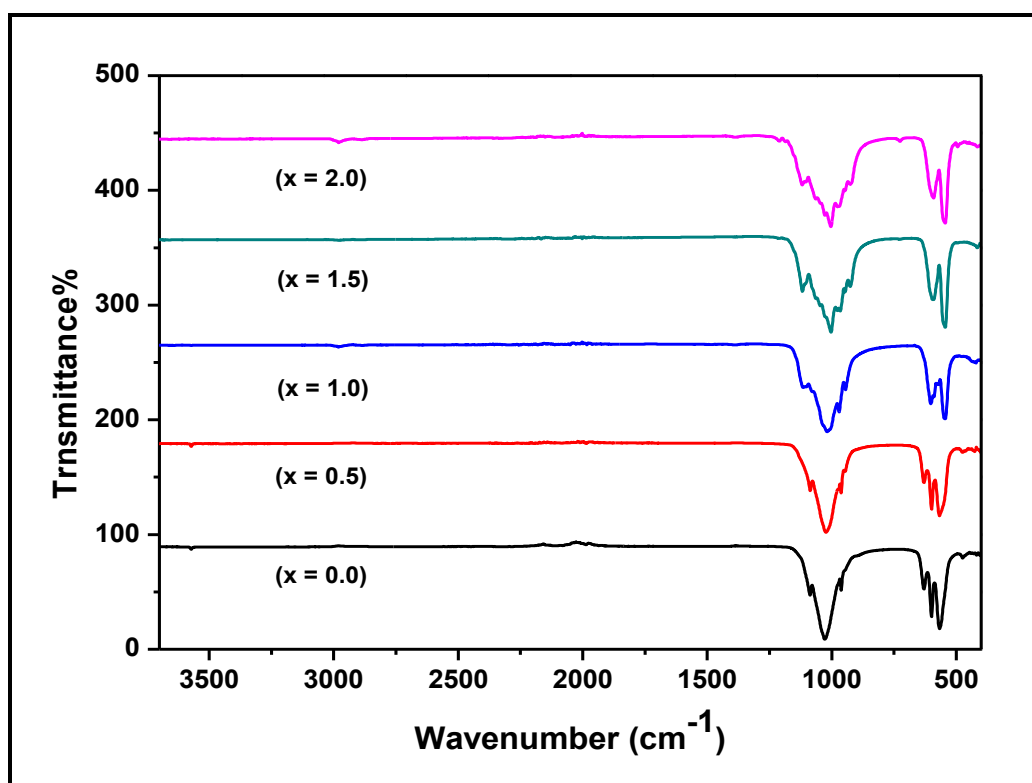


Fig.5.18 FTIR spectrum of $\text{Ca}_{10-x}\text{Zn}_x(\text{PO}_4)_6(\text{OH})_2$ system

5.3.7 Wettability Studies:

The in vitro wettability behavior of $\text{Ca}_{10-x}\text{Zn}_x(\text{PO}_4)_6(\text{OH})_2$ system with ($x=0.5$ and 1.5) has been shown in the Fig.5.19 (a-b). Due to highly porous surface and nanorod structure, Zn-HAP samples has a high surface free energy, quickly absorbs water molecule and its surface gets completely wet. Water contact angle on rough surface of $\text{Ca}_{10-x}\text{Zn}_x(\text{PO}_4)_6(\text{OH})_2$ system is exactly to 0° . It indicates that the system has superhydrophilic ($\theta \leq 5$) in nature. Superhydrophilic nature of $\text{Ca}_{10-x}\text{Zn}_x(\text{PO}_4)_6(\text{OH})_2$ system is also caused by the presence of OH groups on the surface [54]. Wettable material supports cell growth and produces required medium. This result plays a very important role in study of biocompatibility property of bioceramic materials.

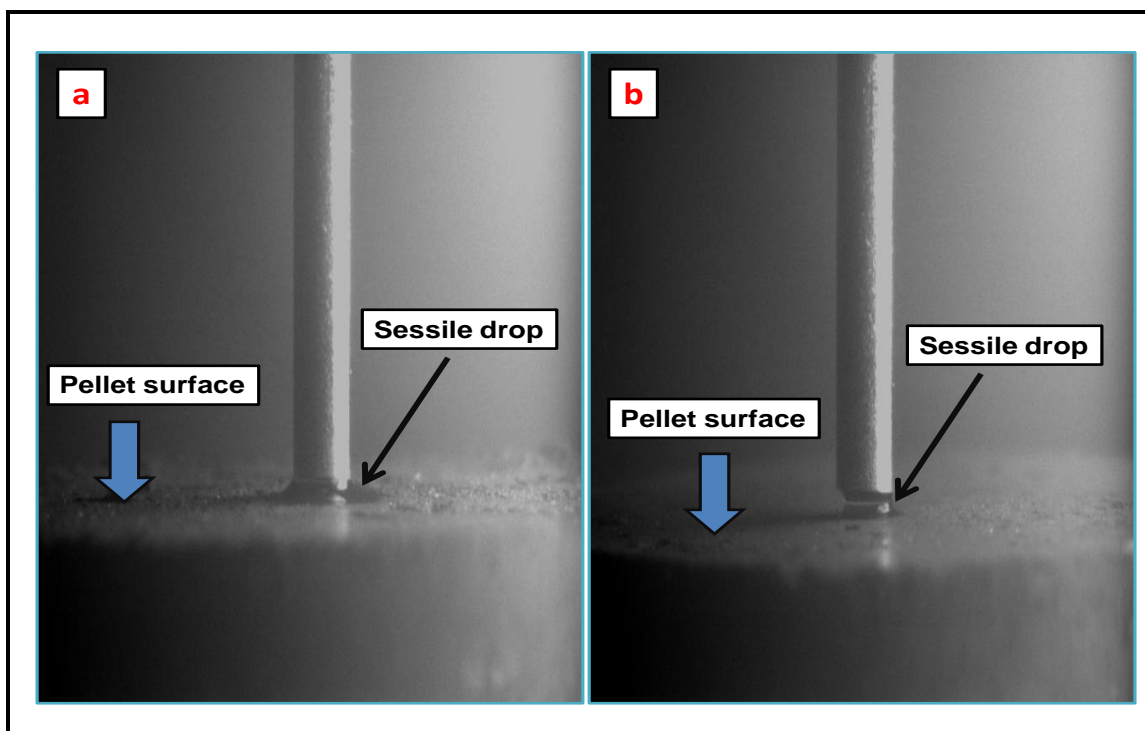


Fig.5.19 (a-b) Photograph of measured contact angle on surface of $\text{Ca}_{10-x}\text{Zn}_x(\text{PO}_4)_6(\text{OH})_2$ ($x=0.5$ and 1.5) (Pellet)

5.3.8 Cell growth measurement:

MTT assays were used to evaluate cell proliferation, cell viability of synthesized $\text{Ca}_{10-x}\text{Zn}_x(\text{PO}_4)_6(\text{OH})_2$ systems for that helps to develop new biomedical applications and results is predicted in Fig.5.20. Mesenchymal stem cells (MSCs) can be distinguished into cell type multiplicity and extensively used in tissue engineering. In present investigation, to evaluate in vitro cytotoxicity, tissue culture plates were

used as a reference, and it is compared with synthesized $\text{Ca}_{10-x}\text{Zn}_x(\text{PO}_4)_6(\text{OH})_2$ nanopowders by using BMMSCs and CBMSCs cells. From the results it is seen that growth rate of cell viability for both the cells are depend upon incubation period and concentration of zinc. From the results it is clear that when zinc concentration has increased from ($x = 0.5$ to $x = 2.0$) and incubation period increased from 12 to 48 h the cell viability value also increased. When $x = 1.5$ and incubation period was 48 h, the value of cell viability for CBMSCs cells was 95.33%. The percentage viability of CBMSCs increases with increasing zinc concentration in pure HAP. BMMSCs showed 70-74% viability, which was statistically significant, compared to the control. Zinc concentration and time of culture plays a significant role in the percentage viability in both the cell types. This may attributed to the good biocompatibility of $\text{Ca}_{10-x}\text{Zn}_x(\text{PO}_4)_6(\text{OH})_2$ samples. The results were formulated as mean of standard deviation (SD) and this result was established at a level of $p < 0.05$.

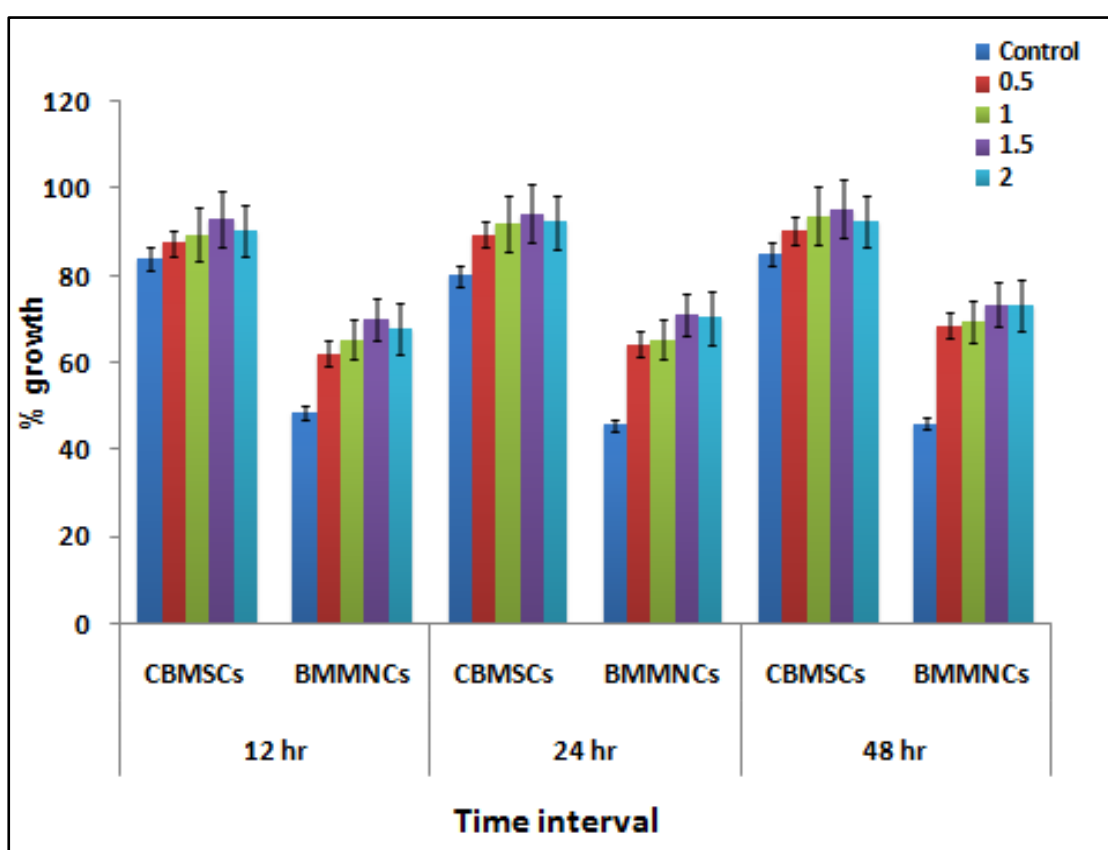


Fig.5.20 MTT assay results showing the human bone marrow mesenchymal stem cells (BMMSCs) and cord blood mesenchymal stem cells (CBMSCs) proliferation on zinc doped HAP sample after 12, 24 and 48 h of culturing

5.3.9 Cell adhesion studies:

Cell adhesion property were used to evaluate the behavior of MMSCs cells on Zn-HAP systems ($x = 0.5$ to 2.0) after incubation of 3 and 7 days. Fig.5.21 (b to i) shows the pictures of attachment of cell on sample after cell culture incubated for 3 and 7 days respectively. The captured pictures shows maximum amount attachment of cells on the surface of sample in case of culture incubated for 3 days, while the growth of the MMSCs increases noticeably in cell culture incubated for 7 days. Perceptibly, the Zn-HAP ($x=0.5$ to $x=2.0$) systems shows no any adverse effect on morphology of cell. Result indicated that the zinc doped HAP system supported MMSCs adhesion which providing an indication of good biocompatibility property. Fig.5.21(a) shows the culture medium of the MMSCs without samples considered as a positive control.

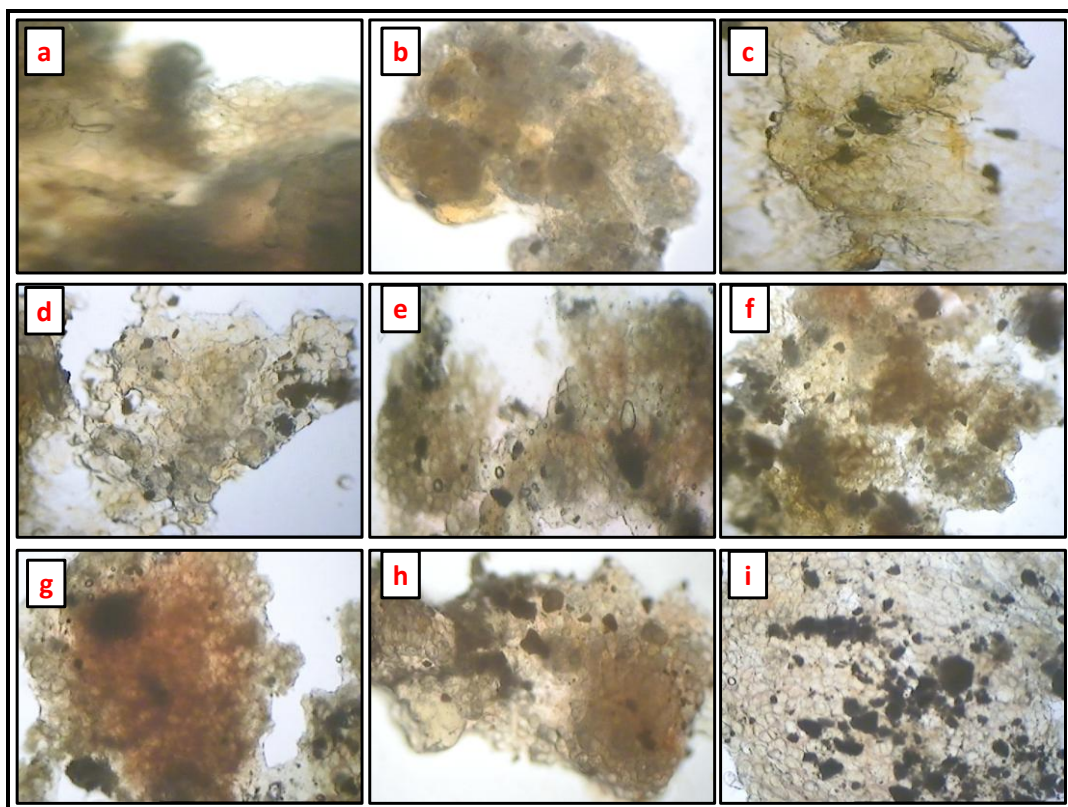


Fig.5.21 The morphological behavior of BMSCs cells without nanoparticles as positive control (a). BMSCs cells adhering and spreading on $\text{Ca}_{10-x}\text{Zn}_x(\text{PO}_4)_6(\text{OH})_2$ system after 3 days [b-($x=0.5$), c-($x=1.0$), d-($x=1.5$), e-($x=2.0$)] and after 7 days [f-($x=0.5$), g-($x=1.0$), h-($x=1.5$), i-($x=2.0$)]

5.3.10 Degradation study:

In bone tissue engineering, bioresorbable HAP based bioceramic materials have been used as temporary carrier for implantation of cells [55] and internal fixation of human fractures [56, 57] due to its unique properties such as a biocompatibility and degradability. Degradation of bioceramics leads to changes in their chemical structure, physical properties and appearance [58], such degradation occurred in the existence of body fluids along with cells. Moreover, Degradation mechanism of sample depends on its nature. In contact with biological fluids, bioactive and bioresorbable bioceramics materials degrade through dissolution-reprecipitation mechanisms [59]. Ionic transfers take place via surface hydration leads to phase change from solid to liquid. It is well known that degradation of bioceramics in the presence of biological fluids is one of the most important characteristics for tissue engineering field [57].

In this experiment degradation study of $\text{Ca}_{10-x}\text{Zn}_x(\text{PO}_4)_6(\text{OH})_2$ systems ($x=0.5$ to 2.0) was assessed by measuring weight loss after soaking. The change of weight loss % of Zn-HAP samples with time of immersion is depicted in Fig.5.22. The results revealed that degradation of Zn-HAP sample take place continuously through entire incubation period. The present study demonstrates that $\text{Ca}_{10-x}\text{Zn}_x(\text{PO}_4)_6(\text{OH})_2$ systems with $(\text{Ca}+\text{Zn} / \text{P})$ ratio 1.55 ($x=2.0$) exhibit higher degradation and loss of 17.40 % of its initial weight after soaking for 50 days, which confirms zinc doped HAP is degradable. In contrast, the systems with ($x = 0.5, 1.0, 1.5$) show 10.6%, 12.4% and 16.2% weight loss respectively, during incubation period. The results show that the degradation of the Zn-HAP system with ($x = 0.5, 1.0, 1.5, 2.0$) is faster than pure HAP bioceramics in simulated body fluid (SBF). This results reveals that $\text{Ca}+\text{Zn} / \text{P}$ ratio obviously affects the degradation of the zinc doped HAP. In the field of bone tissue engineering, there is special interest in preparation of Ca and P based nanostructured porous bioceramics and investigate their degradation behavior, to evaluate the possibility of using these materials as bone scaffolds [60, 61].

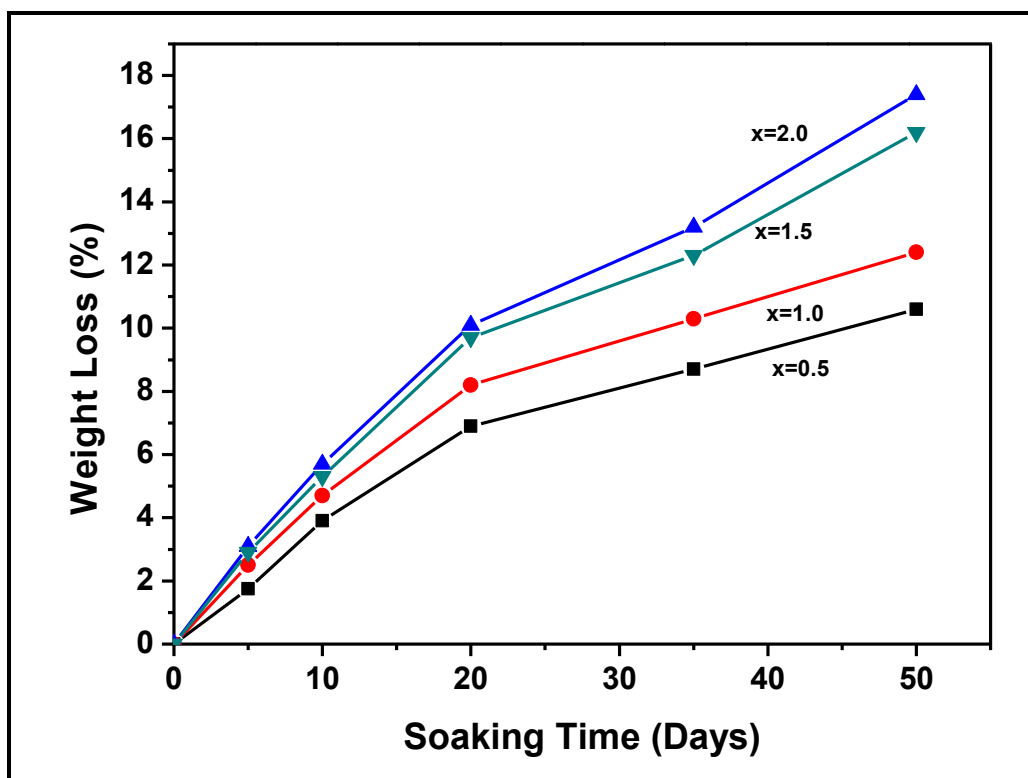


Fig.5.22 Changes in weight loss of $\text{Ca}_{10-x}\text{Zn}_x(\text{PO}_4)_6(\text{OH})_2$ system with ($x=0.5$, $x=1.0$, $x=1.5$, $x=2.0$) after immersion in SBF

5.3.11 Drug loading:

Four different Zn-HAP samples were used for drug loading each having 5% concentration of Norfloxacin. The percentage of drug loading for different Zn-HAP samples ($x=0.5$ to 2.0) was shown in Fig.5.23. From the bar graph it is concluded that there is no significant change occur in the percent drug loading with the incorporation of zinc.

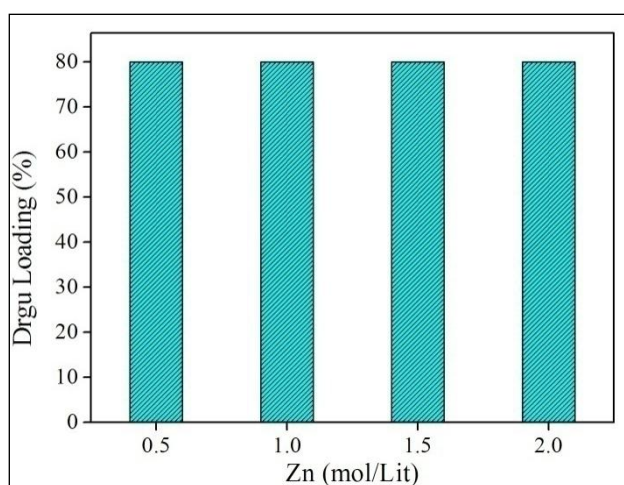


Fig.5.23 Drug loading behavior on Zn-HAP system

5.3.12 In vitro drug release:

Norfloxacin drug was loaded on Zn-HAP samples to examine the efficiency of the drug delivery. The in vitro drug release profile from the $\text{Ca}_{10-x}\text{Zn}_x(\text{PO}_4)_6(\text{OH})_2$ systems is shown in Fig.5.24. The percentage of norfloxacin drug released from zinc doped HAP increases with this composition in pure HAP. Estimated percentages of drug released in 200 hrs were found to be 45, 53, 59 and 63% from $x = 0.5$ to 2.0 samples, respectively. The steady release of drug is observed for particular time; which confirms the release of drug from Zn-HAP in a controlled manner. Norfloxacin release behavior from Zn-HAP increases with Zn composition ($x = 0.5$ to 2.0). The composition of zinc in pure HAP sample is confirmed by the EDAX analysis. The results reveal that the release of drug from Zn-HAP is superior than that of pure hydroxyapatite at optimum temperature and time. In vitro drug delivery experiments for pure HAP and metal doped HAP bioceramics are also reported by other scientists for different antibiotics at different conditions and time [62, 63].

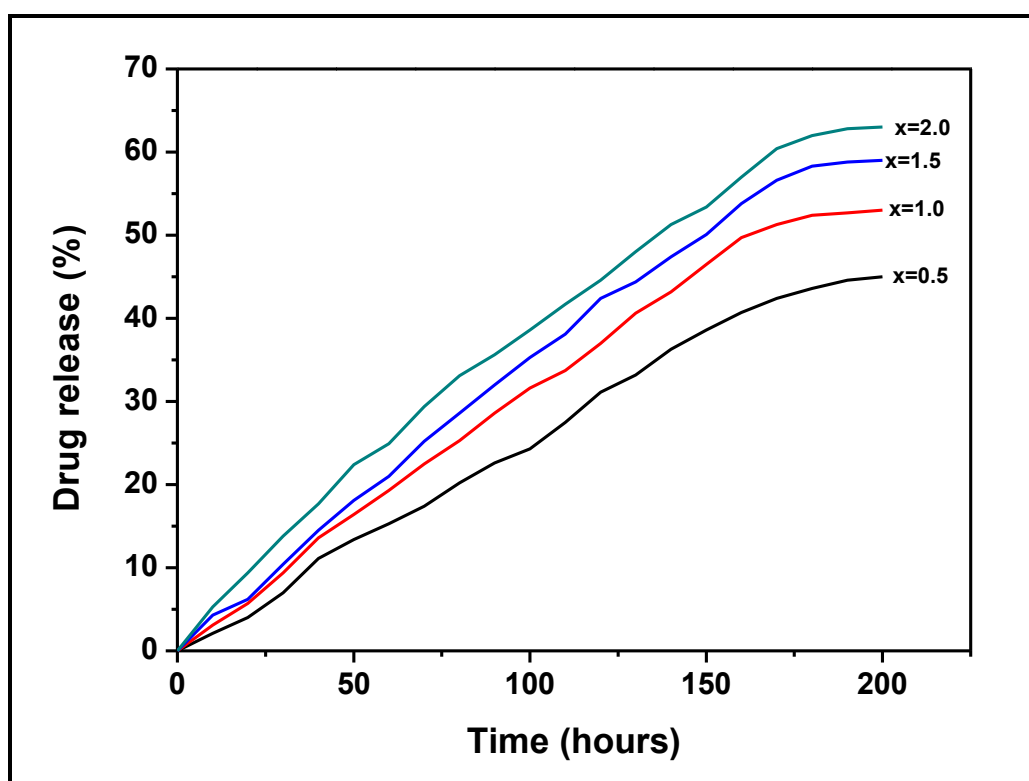


Fig.5.24 Drug release percentage from $\text{Ca}_{10-x}\text{Zn}_x(\text{PO}_4)_6(\text{OH})_2$

5.4 Conclusions:

1. Zinc doped Hydroxyapatite (HAP) nanoparticles were synthesized by innovative auto combustion synthesis route.
2. Crystallite size obtained from XRD was found to be 30 to 40 nm.
3. EDAX analysis of the nanomaterials confirms the qualitative presence of Ca, Zn, P and O without any impurity.
4. The nanorod like morphology of synthesized Zn-HAP samples were confirmed by TEM analysis.
5. Wetting experiment revealed that the Zn-HAP material was superhydrophilic in nature. Cell culture and MTT assay and cell adhesion assay showed that the nanosized Zn- HAP powder provided a more adequate environment for cell adhesion and proliferation and was characterized by good biocompatibility.
6. The degradability in vitro was evaluated by weight loss in the SBF and it shows that the Zn-HAP nanoparticles exhibit a higher degradation rate.
7. As compared to pure HAP, nanorods of Zn doped HAP bioceramics show superior carrier and releasing capacity of antibiotics.
8. In summary, this present research focuses on potential to produce nanorods of zinc doped HAP as a carrier for drug delivery for bone regeneration and other biomedical applications.

Chapter - 6

SYNTHESIS, CHARACTERIZATION AND APPLICATIONS OF Fe DOPED HYDROXYAPATITE

6.1 Introduction

Hydroxyapatite ($\text{Ca}_{10}(\text{PO}_4)_6(\text{OH})_2$ – HAP) bioceramics is one of the basic materials used in bone tissue engineering. Nowadays, HAP nanocomposites are used not only as bone graft substitute but also for numerous engineering applications [1]. Recently, the researchers, had given an attention to magnetic nanoparticles, confining about the usage, on applicative and commercial basis, into the biomedicine sector [2-5]. Drug delivery agent is one applications, [6] and then if enlisted is hyperthermia treatment of cancer [7]. Nanoparticles, as found, are basically semi-crystalline structures, if considered with the dimension, ranges between 10 and 100 nm. Properties of it when characterized are size uniformity, surface area and adsorption kinetics. These can finally be refrained while in the preparation process with its purpose that too specific. Most of the magnetic nanoparticles are found to be used in medicine and biotechnology fields both [8, 9]. When mentioning about the applicative part of the nanoparticles it must get introduced to the blood stream. This does exposes nanoparticles to the bio-safety even. Passivation – the method or the process, especially for the surface of the magnetic nanoparticles can be utilized to augment the biocompatibility of the same. If the HAP with its properties and applications needs to get developed then magnetic ions must be incorporated into it.

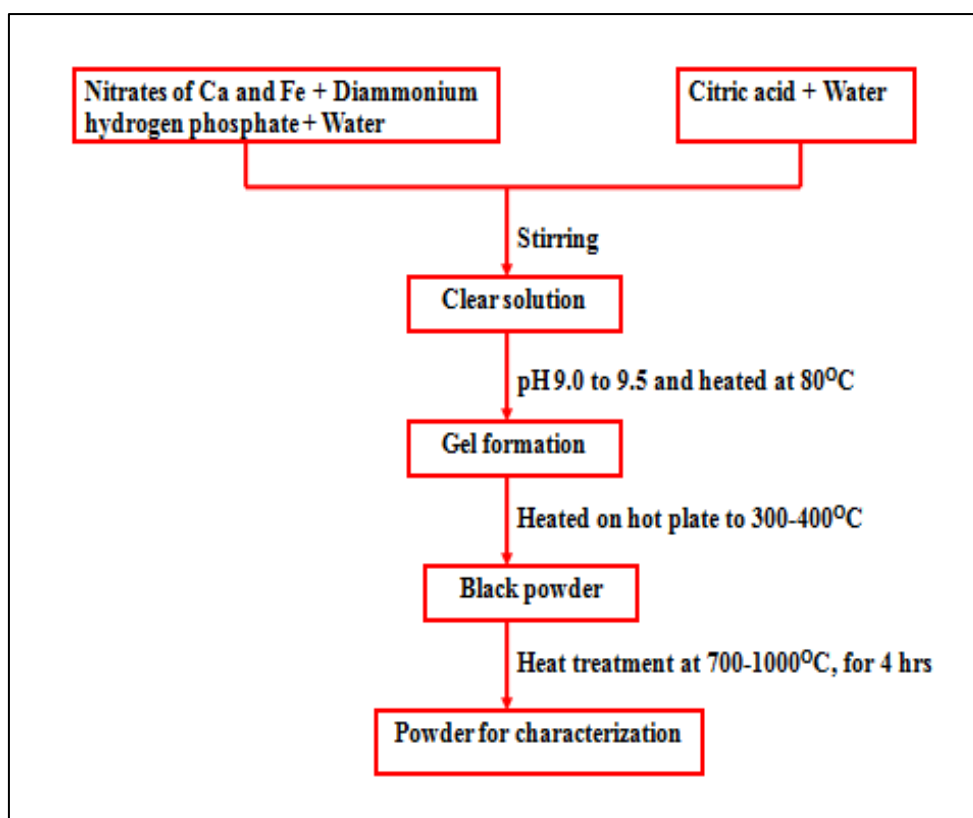
Iron (Fe), though being the metal, it is traced that it is an essential element having its presence in bone and teeth [10]. Considering different biological process, it is needy micronutrient and also an important component of metalloproteins. Almost 60-70% of Iron is present in hemoglobin processing as circulating erythrocytes. The Fe in the intestinal lumen survives as ferrous and ferric salts [11]. Hence when it is bipological functioning of the human body Fe does play an important role. Research paper on the subject reads that the ions present in the iron are toxic to human body functioning through all the sources [12-14], but the reports suggests that the Fe doped HAP are having many separate biomedical applications [15]. The researchers have made available many studies over the synthesis of HAP bioceramics [16-18]. Some researchers even conclude to the insertion of Fe into the HAP [19, 20]. However, literature survey reveals that, no report on synthesis of Fe doped HAP by auto-combustion method.

The present work is focused on the synthesis of an innovative biocompatible Fe ion doped HAP by auto-combustion method and thorough examination of the

effect of Fe ions on the synthesis, including TG-DTA, XRD and FTIR. In vitro cell adhesion test was performed in order to evaluate in vitro biocompatibility. Additionally, in vitro drug storage and release properties also investigated on these systems by using norfloxacin as a model drug.

6.2 Experimental and material details:

Nanostructured Fe doped HAP samples having the general formula, $\text{Ca}_{10-2x}\text{Fe}_{2x}(\text{PO}_4)_6(\text{OH})_2$ was synthesized by auto-combustion method. The synthesis was carried out with the calcium nitrate, iron nitrate and diammonium hydrogen phosphate as the Ca, Fe and P sources, citric acid used as fuel. The raw materials used in the experiment were all of analytical purity. The molar ratio of metal nitrates and phosphate to citric acid was taken as 1:2. Firstly, stoichiometric amount calcium nitrate, iron nitrate and diammonium hydrogen phosphate were dissolved in doubly distilled water with vigorous stirring. Citric acid was weighted stoichiometrically and dissolved in distilled water. The above solution mixed under constant stirring and pH adjusted 9 to 9.5 using ammonia. A homogeneous clear solution was achieved. This clear solution was stirred vigorously and heated up to 80°C for 4 h to obtain gel. Further, dry Fe-HAP powder was obtained by heating of gel at 300-400°C. This dried Fe-HAP was further sintered at 700-1000°C for 4 h. Synthesis route and appearance of powder after calcinations is shown in flowchart and Fig.6.1.



Flowchart of sol-gel auto combustion synthesis of Fe-HAP bioceramics



Fig.6.1 Fe-HAP powder calcined at 1000°C

The thermal decomposition behaviour and required sintering temperature of citrate precursor to phase formation of the sample was checked by thermogravimetric analysis on the SDT Q-600 instrument by heating the powder after auto-combustion in air atmosphere from 20° to 1000°C at the rate of 10°C per min. The X-ray

diffraction analysis was used to know phase purity of synthesized material by using PW3710 (Model- Philips) with $\text{CuK}\alpha$ radiation ($\lambda = 1.5406\text{\AA}$). JASCO FT/IR-6100 type 'A' spectrometer was used for FTIR study. UV-Visible spectral measurements of these samples carried out by using UV/Visible spectrophotometer (Systronic AU-2700). The pH of the solutions was carried out by using HANNA phep (model H 19).

6.2.1 Cell adhesion test:

Cell adhesion property of bioceramic samples provides basic information due to which bioceramics were widely used in tissue engineering. Therefore, in vitro cell adhesion test of $\text{Ca}_{10-2x}\text{Fe}_{2x}(\text{PO}_4)_6(\text{OH})_2$ ($x = 0.1$ to 0.4) samples were evaluated using microscopic methods. It is necessary to examine whether these bioceramic samples are capable to sustain morphology of the MMSCs. The cells were cultivated in direct contact with the $\text{Ca}_{10-2x}\text{Fe}_{2x}(\text{PO}_4)_6(\text{OH})_2$ system. Therefore, mesenchymal stem cells (MMSCs) derived from bone marrow of sheep and plated in to the 50 mL hard glass test tube. The cells were moderately immersed in Dulbecco's modified Eagle medium with 10% serum of animal, 100 U per mL penicillin G, 100 μg per mL streptomycin (invitrogen) and 15 mg of Fe-HAP ceramic samples (sintered powder) sprayed on the surface of cultured cells which acts as supplement. These cultured medium was incubated in CO_2 incubator operated at optimized conditions (5% CO_2 , 90% humidity) at 37°C for 7 days respectively. At the selected time points, for morphological examination surface layer of cultured medium was removed and dried in air after washed with distilled water. The adherent cells on $\text{Ca}_{10-2x}\text{Fe}_{2x}(\text{PO}_4)_6(\text{OH})_2$ samples were visualized under 40X magnification microscope (Coslab, Model HL-9). Additionally, one control culture with no presence of studied materials was grown.

6.2.2 Drug loading experiment:

If the material is biocompatible and biodegradable and have capacity to uptake and release drug in controlled manner then this material have applications in biomedicines. For that purpose, norfloxacin widely used antibiotic was chosen as model drug. In particular, concentration (5%) of norfloxacin powder was prepared by dissolving it into 100 mL of de-ionized water. Afterwards, 1 g of calcined Fe-HAP samples were added to above said drug solutions. The resultant suspensions were stirred for 40 minutes at temperatures 60°C . Then after, the resultant solution was kept intact for 24 h. The solution was centrifuged in order separate the precipitate. The drug loaded on Fe-HAP samples were assessed by knowing the difference in

concentration of drug before and after loading. Drug loading (%) on Fe-HAP samples were evaluated by following equation:

$$\text{Drug loading (\%)} = [(A-B)/A] \times 100 \quad (6.1)$$

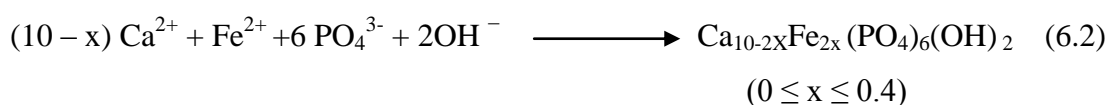
Where, A is the initial and B is the final norfloxacin concentration in aqueous solution.

6.2.3 Drug release-in vitro study:

In vitro drug release was evaluated over a time period of 200 h. 100 mg of drug-loaded Fe-HAP samples with ($x = 0.1$ to 0.4) were added into a capped glass bottle contains phosphate-buffered (50 mL) saline (PBS) having pH = 7.4 and incubated at 37°C . The stationary mode was used to study drug release. To calculate the released amount of drug, 5 mL of sample were centrifuged and replaced with 5 mL of fresh PBS medium. Afterwards, the actual concentration of norfloxacin in the supernatant liquid was measured at 274 nm using spectrophotometer.

6.3 Results and Discussion:

The reaction involved in the formation of Fe-HAP can be expressed as following equation.



6.3.1 TGA-DTA Analysis:

The $\text{Ca}_{10-2x}\text{Fe}_{2x}(\text{PO}_4)_6(\text{OH})_2$ systems heated at the rate $10^\circ\text{C}/\text{minute}$ from 0°C to 1000°C , is given in Fig.6.2 to 6.4. The TGA curves 6.2 to 6.4 shows thermal decomposition of Fe-HAP ($x = 0.1, 0.2$, and 0.4) samples below 200°C due to removal of absorbed water. Decomposition $250\text{--}400^\circ\text{C}$ is due to thermal decomposition of organic residue. The weight loss along with endothermic peak at $700\text{--}750^\circ\text{C}$ indicates that decomposition of CaCO_3 following the reaction [21].



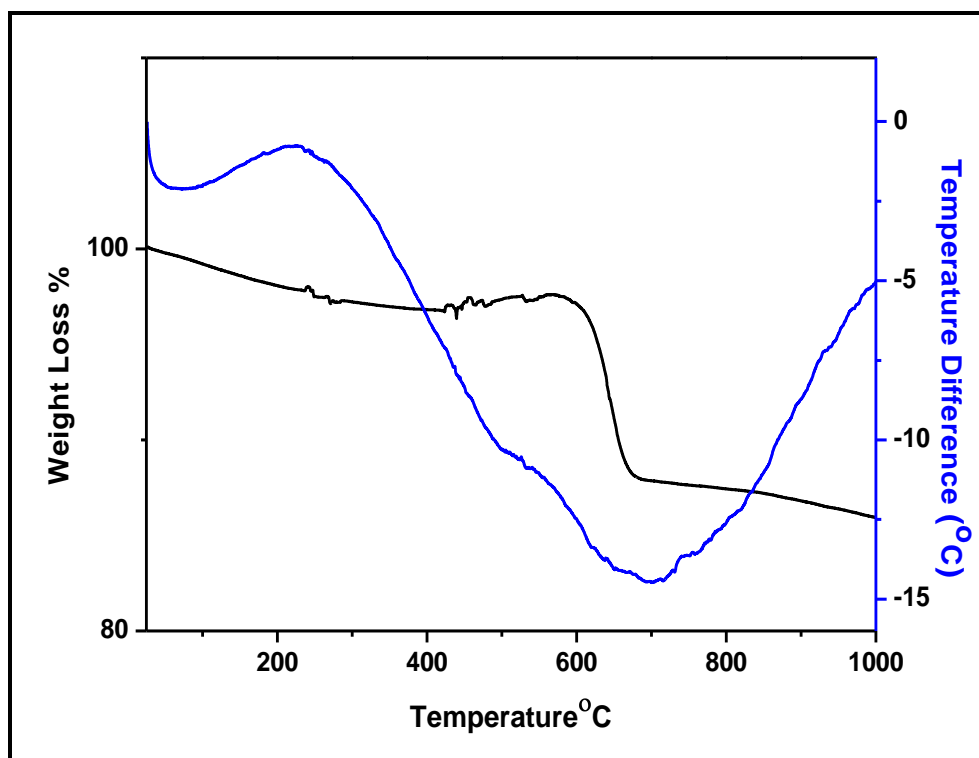


Fig.6.2 TGA-DTA curve of $\text{Ca}_{10-2x}\text{Fe}_{2x}(\text{PO}_4)_6(\text{OH})_2$ system ($x=0.1$)

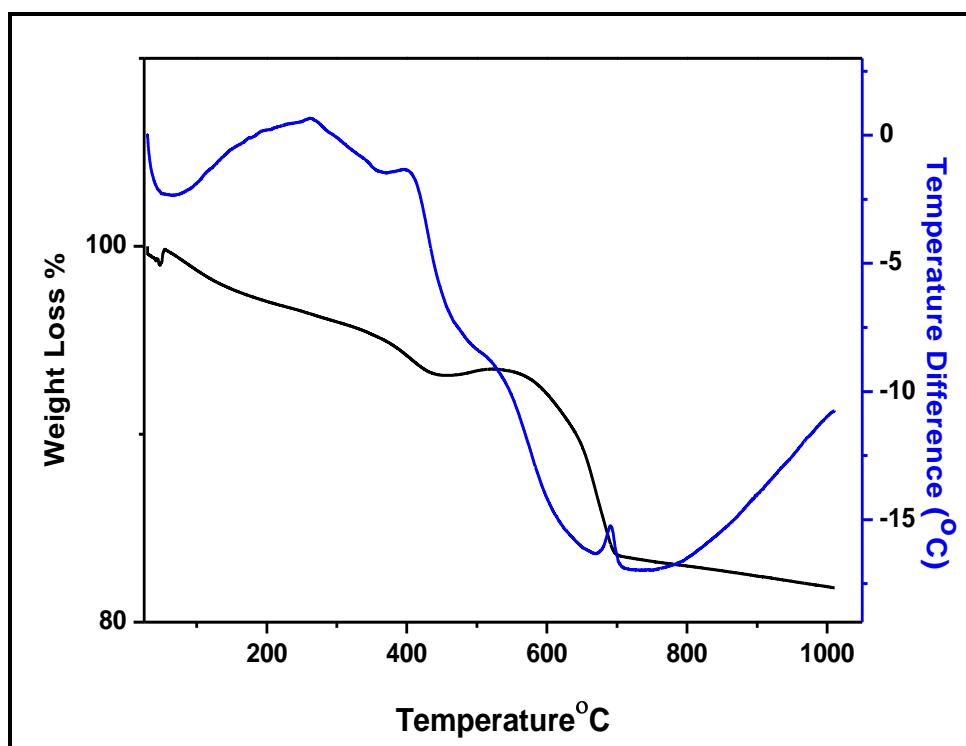


Fig.6.3 TGA-DTA curve of $\text{Ca}_{10-2x}\text{Fe}_{2x}(\text{PO}_4)_6(\text{OH})_2$ system ($x=0.2$)

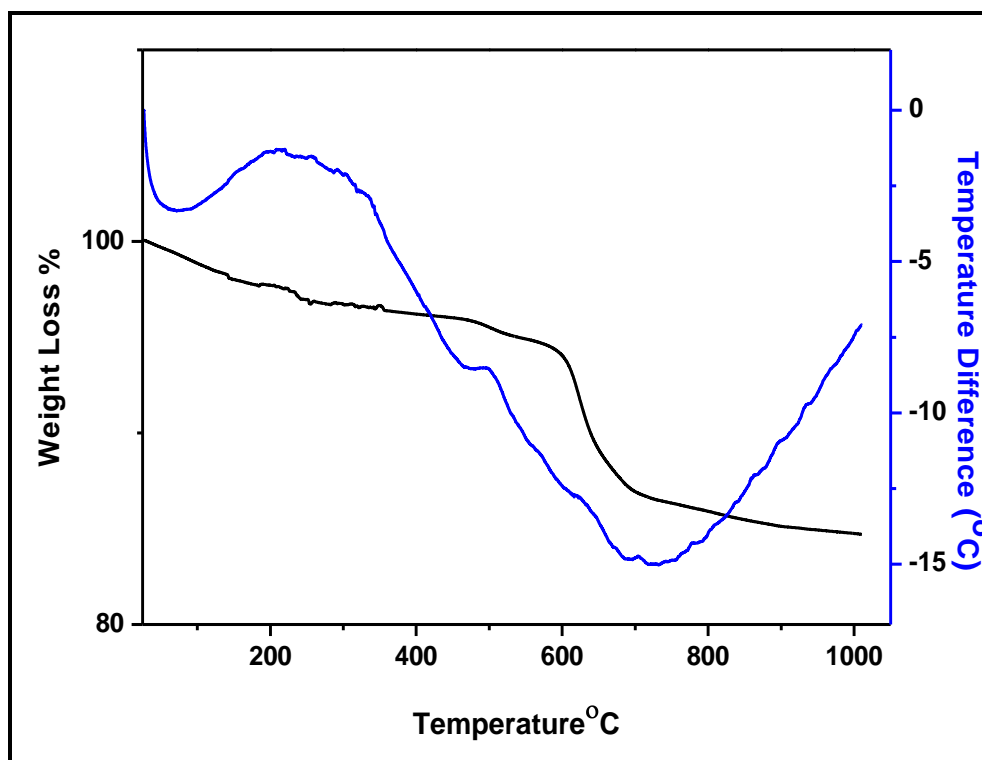


Fig.6.4 TGA-DTA curve of $\text{Ca}_{10-2x}\text{Fe}_{2x}(\text{PO}_4)_6(\text{OH})_2$ system ($x=0.4$)

6.3.2 Phase identification:

The X-ray diffraction study and phase purity of synthesized HAP and Fe doped HAP bioceramic samples were examined by XRD analysis. Fig.6.5 and 6.6 shows X-ray diffraction pattern of pure HAP and Fe doped HAP ($x=0.1$ to 0.4) samples calcined at 1000°C for 4 hours. The peaks in XRD patterns were indexed to (002), (211), (300), (202), (310), (311), (113), (222), (312), (213), (321), (410), (402), (004). These polycrystalline HAP and Fe-HAP nanoparticles exhibit single phase hexagonal structure (JCPDS 09-0432) [22]. Debye Scherrer's formula was used to estimate average crystallite size of synthesized Fe-HAP samples [23-25].

$$\tau = 0.94 * \lambda / \beta * \cos \theta \quad (6.4)$$

Where, crystallite size (τ) depends upon wavelength λ (1.54 \AA for $\text{CuK}\alpha$) of the X-ray and the FWHM (β) of the XRD peak at 2θ . The average crystallite size obtained for Fe-HAP samples [$x = 0.0$ to 0.4] 30 to 25 nm. Interplanar spacing (d), hkl planes and corresponding θ values of these systems are tabulated in Tables 6.1 to 6.4

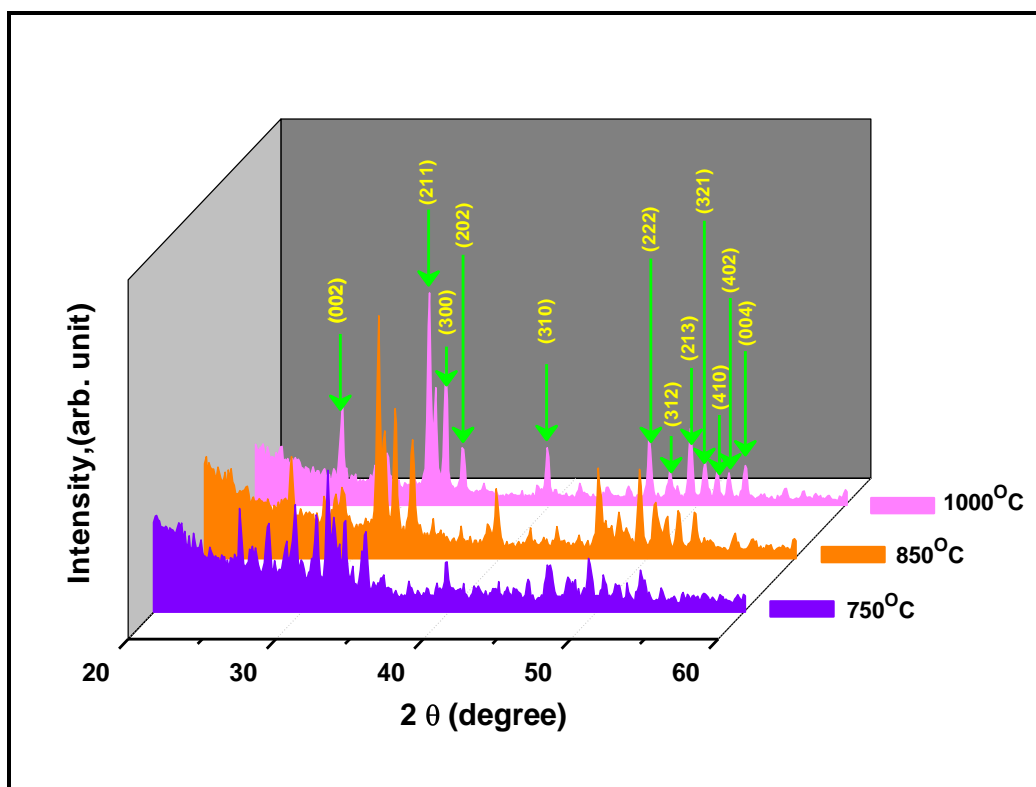


Fig.6.5 XRD patterns of the pure HAP sample

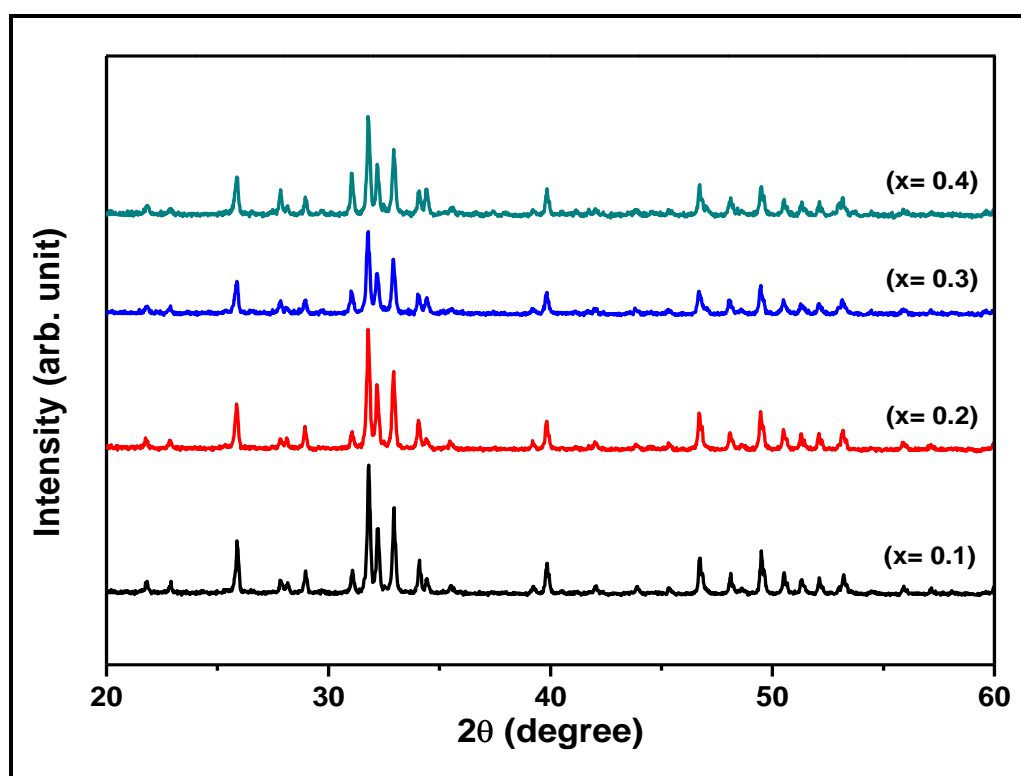


Fig.6.6 XRD pattern for $\text{Ca}_{10-2x}\text{Fe}_{2x}(\text{PO}_4)_6(\text{OH})_2$ system ($0.1 \leq x \leq 0.4$)

Table 6.1
Indexed X-ray diffraction pattern of $\text{Ca}_{10-2x}\text{Fe}_{2x}(\text{PO}_4)_6(\text{OH})_2$ ($x = 0.1$)

Sr. No.	2θ	d_{obs} Å	d_{std} Å	h k l Planes
1	25.884	3.439383	3.439775	002
2	31.789	2.812680	2.814233	211
3	32.932	2.717622	2.720032	300
4	34.130	2.624921	2.63113	202
5	39.873	2.259087	2.26208	310
6	46.738	1.942008	1.943068	222
7	48.105	1.889966	1.890076	312
8	49.520	1.839223	1.841244	213
9	50.614	1.802005	1.806039	321
10	51.309	1.779216	1.780057	410
11	52.166	1.751985	1.754049	402
12	53.210	1.720045	1.722056	004

Structure: Hexagonal

Lattice constant: a = 9.415Å, c = 6.880Å

Table 6.2
Indexed X-ray diffraction pattern of $\text{Ca}_{10-2x}\text{Fe}_{2x}(\text{PO}_4)_6(\text{OH})_2$ ($x = 0.2$)

Sr. No.	2θ	d_{obs} Å	d_{std} Å	h k l Planes
1	25.886	3.439122	3.439775	002
2	31.793	2.812335	2.814233	211
3	32.949	2.716259	2.720032	300
4	34.137	2.624399	2.63113	202
5	39.879	2.258761	2.26208	310
6	46.741	1.941890	1.943068	222
7	48.107	1.889892	1.890076	312
8	49.531	1.838840	1.841244	213
9	50.642	1.801074	1.806039	321
10	51.319	1.778893	1.780057	410
11	52.174	1.751735	1.754049	402
12	53.217	1.719835	1.722056	004

Structure: Hexagonal

Lattice constant: a = 9.414Å, c = 6.879Å

Table 6.3
Indexed X-ray diffraction pattern of $\text{Ca}_{10-2x}\text{Fe}_{2x}(\text{PO}_4)_6(\text{OH})_2$ ($x = 0.3$)

Sr. No.	2θ	d_{obs} Å	d_{std} Å	h k l Planes
1	25.886	3.439122	3.439775	002
2	31.803	2.811474	2.814233	211
3	32.949	2.716259	2.720032	300
4	34.167	2.622163	2.63113	202
5	39.883	2.258543	2.26208	310
6	46.749	1.941517	1.943068	222
7	48.121	1.889375	1.890076	312
8	49.543	1.838423	1.841244	213
9	50.642	1.801074	1.806039	321
10	51.319	1.778893	1.780057	410
11	52.177	1.751642	1.754049	402
12	53.220	1.719745	1.722056	004

Structure: Hexagonal

Lattice constant: a = 9.410Å, c = 6.878Å

Table 6.4
Indexed X-ray diffraction pattern of $\text{Ca}_{10-2x}\text{Fe}_{2x}(\text{PO}_4)_6(\text{OH})_2$ ($x = 0.4$)

Sr. No.	2θ	d_{obs} Å	d_{std} Å	h k l Planes
1	25.890	3.438599	3.439775	002
2	31.884	2.804516	2.814233	211
3	33.041	2.708906	2.720032	300
4	34.236	2.617036	2.63113	202
5	39.883	2.258543	2.26208	310
6	46.760	1.941146	1.943068	222
7	48.121	1.889375	1.890076	312
8	49.571	1.837450	1.841244	213
9	50.657	1.800576	1.806039	321
10	51.325	1.778699	1.780057	410
11	52.181	1.751517	1.754049	402
12	53.223	1.719656	1.722056	004

Structure: Hexagonal

Lattice constant: a = 9.383Å, c = 6.878Å

6.3.3 FTIR Analysis:

FTIR scanning of pure HAP and $\text{Ca}_{10-2x}\text{Fe}_{2x}(\text{PO}_4)_6(\text{OH})_2$ system with ($x=0.1, 0.2, 0.3, 0.4$) calcined at 1000°C are given in the Fig.6.7 and found to be very similar to those observed by D. Gopi et al and C. Yang et al [26-27]. There are distinct differences between the spectra of the HAP and Fe doped HAP. Therefore, one can

say there were some changes were taking place in the chemical structure of HAP due to the addition of Fe. All samples shows bands corresponding to HAP, which is confirmed by FTIR spectra. The peak located approximately at 3571 cm^{-1} and 632 cm^{-1} corresponds to the stretching vibration and vibrational mode of OH^- respectively. The strong doublet band or shoulder at $960\text{--}1100\text{ cm}^{-1}$ was assigned to P-O stretching vibration of the phosphate group (PO_4^{3-}). The band at about 473 cm^{-1} (weak) and $570\text{--}601\text{ cm}^{-1}$ (doublet) corresponds to the phosphate bending vibration and PO_4^{3-} bending mode respectively. A small band at around 1650 cm^{-1} was possibly due to absorbed water (bending mode). The FTIR result demonstrates that the synthesized pure HAP and Fe-HAP samples were in high purity state, similar results were reported by C. Yang et al [27].

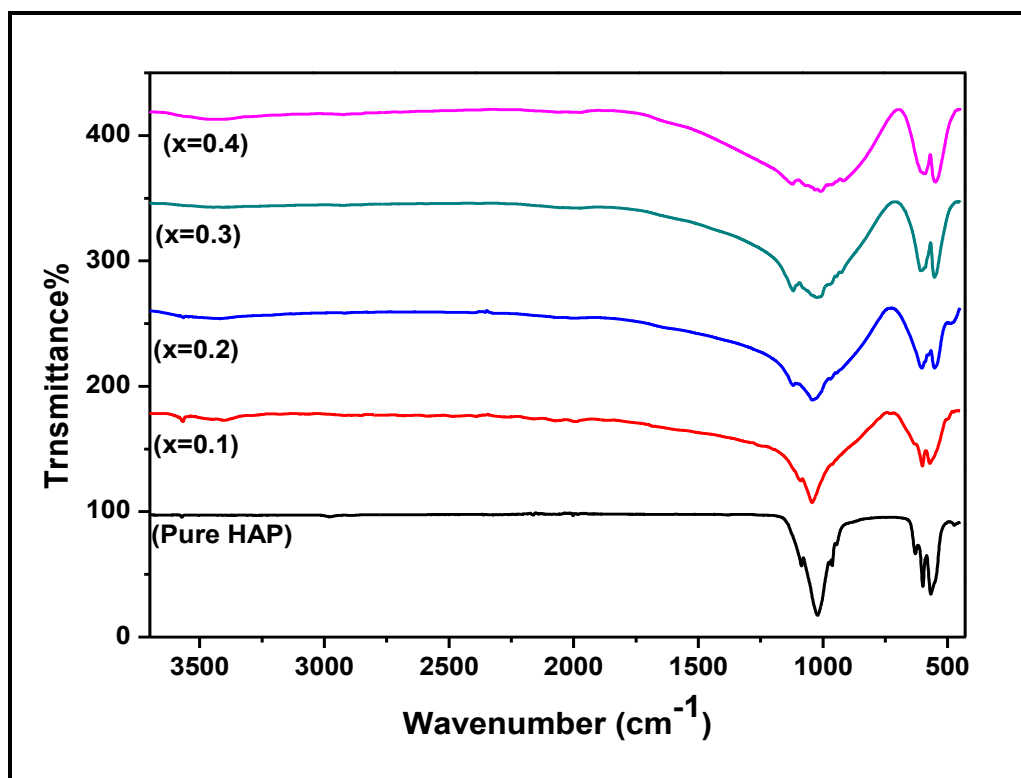


Fig.6.7 FTIR spectrum of $\text{Ca}_{10-2x}\text{Fe}_{2x}(\text{PO}_4)_6(\text{OH})_2$ system ($x=0.1$ to 0.4)

6.3.4 Cell adhesion studies:

Cell adhesion property were used to evaluate the behavior of MMSCs cells on Fe-HAP systems ($x= 0.1$ to 0.4) after incubation of 3 and 7 days (Fig. 6.8 (b to i)). It is well known that higher concentration of Fe is biologically toxic. Therefore, cell morphology and cell adhesion property of Fe doped HAP samples are of great importance. In this study, Fe-HAP with ($x=0.1$ and $x=0.2$) after 3 and 7 days culture

Fig.6.8 (b-c) and Fig.6.8 (f-g), large amount of cells adhere to the substrates and had regular morphological characteristics was observed. When concentration of iron in pure HAP increases from ($x=0.3$ to $x=0.4$) and after 3 and 7 days of culture population of cell adherence are slightly decreases Fig.6.8 (d-e) and Fig.6.8 (h-i). It can be seen that there is a strong correlation between iron concentration and the cell morphology and adherence. The result shows that no signs of cytotoxicity in the case of the all investigated materials. As expected, Fe-HAP with ($x=0.1$ and $x=0.2$) samples are the most biocompatible. After careful analysis of the results of cell response it can be concluded that no negative influence of $\text{Ca}_{10-2x}\text{Fe}_{2x}(\text{PO}_4)_6(\text{OH})_2$ system up to ($x=0.4$) and also all samples were considered nontoxic comparable to the control. Fig.6.7 (a) shows the culture medium of the BMMSCs without samples considered as a positive control.

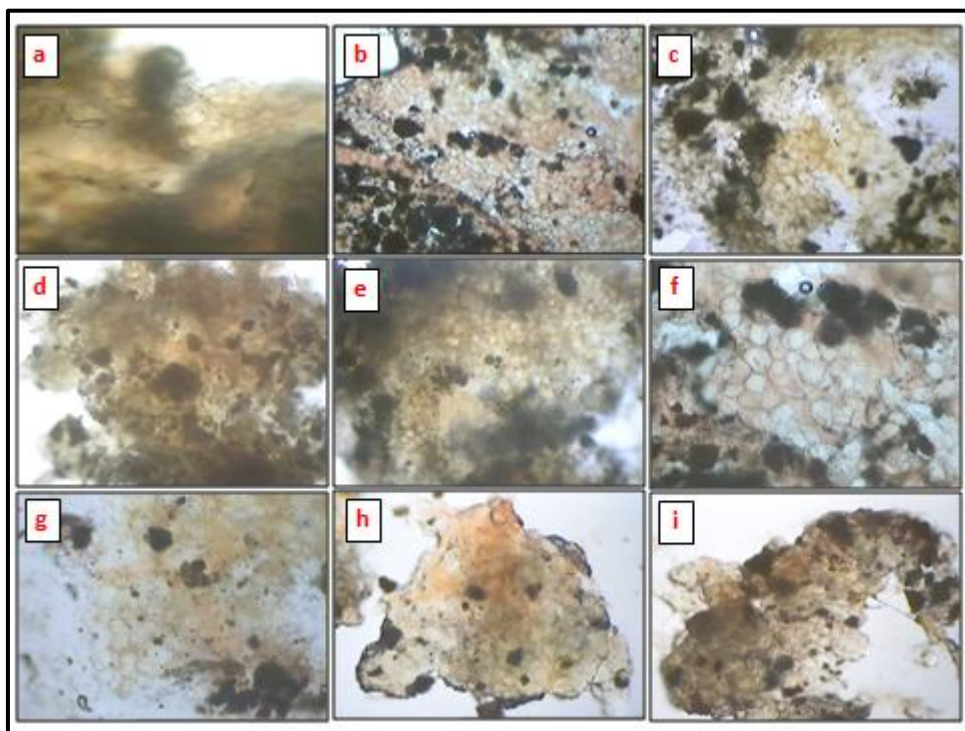


Fig.6.8 The morphological behavior of BMMSCs cells without nanoparticles as positive control (a). BMMSCs cells adhering and spreading on $\text{Ca}_{10-2x}\text{Fe}_{2x}(\text{PO}_4)_6(\text{OH})_2$ system after 3 days [b-($x=0.1$), c-($x=0.2$), d-($x=0.3$), e-($x=0.4$)] and after 7 days [f-($x=0.1$), g-($x=0.2$), h-($x=0.3$), i-($x=0.4$)]

6.3.5 Drug loading:

Four different Fe-HAP samples were used for drug loading each having 5% concentration of Norfloxacin. The percentage of drug loading for different Fe-HAP samples ($x=0.1$ to 0.4) was shown in Fig.6.9. From the bar graph it is concluded that

there is no significant change occur in the percent drug loading with the incorporation of iron.

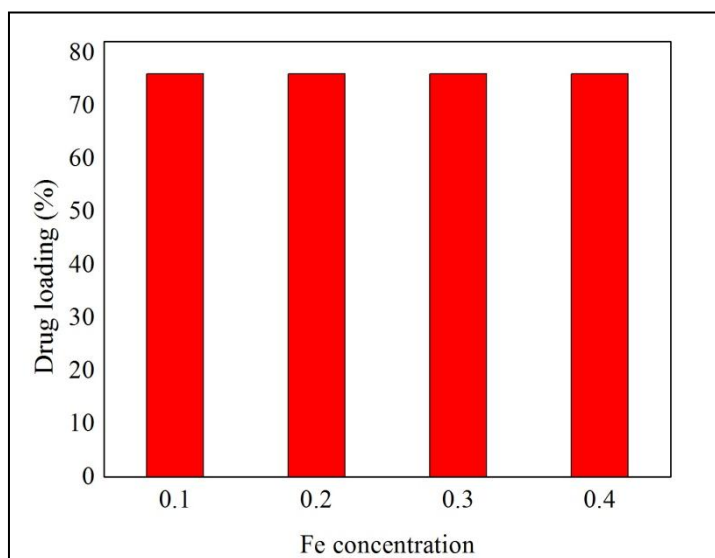


Fig.6.9 Drug loading behavior on Fe-HAP system

6.3.6 In vitro drug release:

Norfloxacin drug was loaded on Fe-HAP samples to examine the efficiency of the drug delivery. The in vitro drug release profile from the $\text{Ca}_{10-2x}\text{Fe}_{2x}(\text{PO}_4)_6(\text{OH})_2$ systems is shown in Fig.6.10. The percentage of norfloxacin drug released from Fe doped HAP increases with this composition in pure HAP. Estimated percentages of drug released in 200 hrs were found to be 40, 44, 50 and 54% from $x=0.1$ to $x=0.4$ samples, respectively. The steady release of drug is observed for particular time; which confirms the release of drug from Fe-HAP in a controlled manner. Norfloxacin release behavior from Fe-HAP increases with Fe composition ($x=0.1$ to 4.0). The results reveal that the release of drug from Fe doped HAP is superior to that of pure HAP optimum temperature and time.

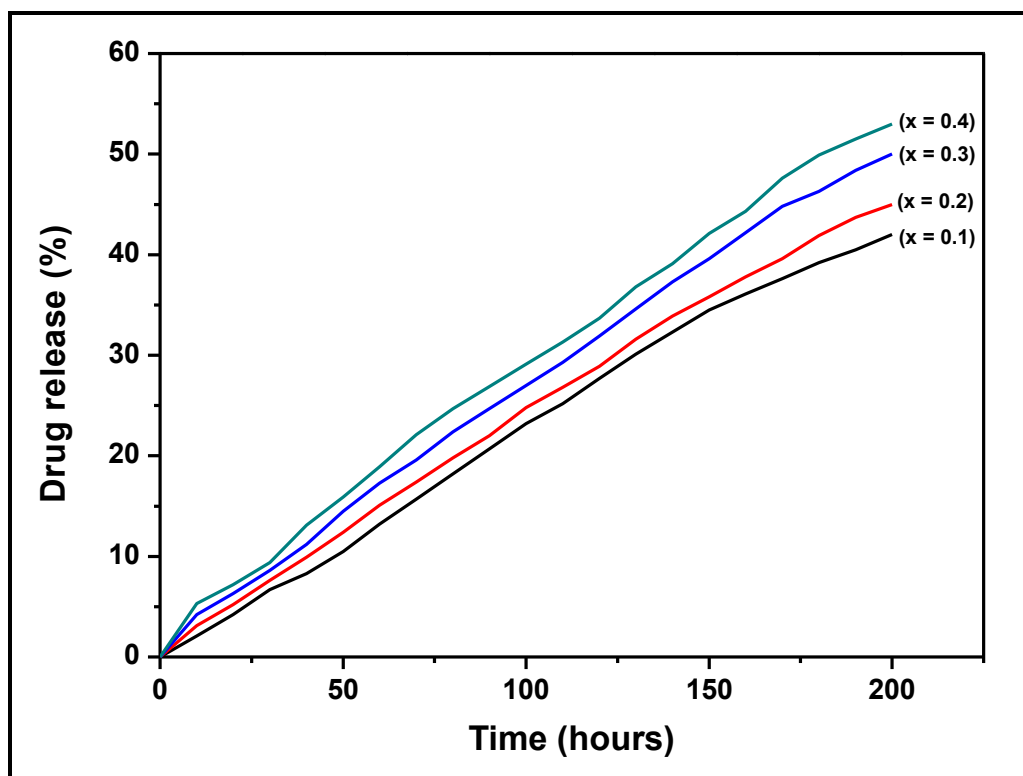


Fig.6.10 Drug release percentage from $\text{Ca}_{10-2x}\text{Fe}_{2x}(\text{PO}_4)_6(\text{OH})_2$ ($x = 0.1$ to 0.4)

6.4 Conclusions:

1. Auto-combustion method was used to synthesis of Fe doped hydroxyapatite (HAP) precursor nanopowder.
2. This technique is very simple, inexpensive and without any additional surfactant, template or base.
3. Crystallite size obtained from XRD was found to be 30 to 25 nm.
4. Cell adhesion assay showed that the Fe doped HAP nanocomposites with low concentration had good biocompatibility.
5. Nanocrystalline Fe doped HAP bioceramics show much higher carrier and releasing capacity of antibiotics than pure HAP. This facilitates their future applications in biomedicines.

Chapter - 7

SUMMARY AND CONCLUSIONS

Summary and conclusions

Throughout life, the human body's muscular-skeleton system is constantly being formed and resorbed; with increasing age this leads to a reduction in bone mass and density and need to replace or repair the degenerated bone and restore its biologic function. Techniques to combat this serious problem have now become a major clinical need. Bioceramics are a class of advanced ceramics, which are defined as "the substance that confirm completely to the human body's environment are those manufactured by the body itself (autogenous) and any other substance that is recognized as foreign, and initiates some type of reaction". With the increase in clinical demands for dental and orthopaedic implant surgery, different types of bioceramic based materials are developed during the past decades. Nowadays, bioceramics and tissue engineering science aim to develop materials which can be implanted in the human body to replace damaged tissues. It is known that the reactivity of solids begins on their surface. This general statement is of particular importance in the field of bioceramics, since they will be in contact with an aqueous medium and in presence of cells and proteins.

Currently, there has been a great deal of interest in synthesis of different types of bioceramic materials for biomedical applications. Hydroxyapatite (HAP) of the chemical formula $\text{Ca}_{10}(\text{PO}_4)_6(\text{OH})_2$ has received much attention in tissue engineering. In fact, it is used as a bioceramic because of its bioactivity and osteoconductive properties. Compared to other bioceramics as bioglass, the advantage of HAP use as a bioceramic or biomaterial is its chemical similarity to the inorganic component of bone and tooth. It also exhibits no cytotoxic effects and shows excellent biocompatibility with hard tissues, skin and muscle tissues. Therefore, HAP has been applied clinically not only as a dense, sintered material but also as a coating on metallic implants. Moreover, an enormous number of substitutions, especially the composites resulting from the cationic substitution are of potential application in the fields of dental and bone substitution, luminescence, drug delivery, and catalysis because of the high stability and flexibility of the apatitic structure. However, use of HAP in biomedical fields is limited by its relatively slow rate of biological interaction, and there is also a requirement to improve the success rate of HAP implants, an approach to improve the osseointegration is to modify chemically the HAP by doping with low levels of beneficial elements which are found in human

bone. These doped elements can modify the surface structure of HAP, with potential influence on the material in biological environment. Among the elements that have been substituted, Zn and Fe are considered to have great potential. Also the nanoparticles of calcium silicate (CaSiO_3) ceramics have been investigated as new bioceramics for bone regeneration. The metal ion distribution and physical properties of the materials also depend upon the preparative method. Although conventional methods for the synthesis of bioceramics, have not received importance because of the use of expensive raw materials and many processing steps. Therefore in this work we have focused on the synthesis, characterization and applications of calcium silicate and hydroxyapatite based bioceramic materials.

Chapter – 1:

This chapter includes information about the bioceramics in brief. Types and applications of bioceramics are also discussed. Biocompatibility, biodegradation, drug delivery and clinical uses of bioceramics are also included. Literature survey regarding the applications and preparation methods such as auto-combustion and wet chemical precipitation of bioceramics are also included.

Chapter – 2:

This chapter deals with the details of characterization techniques such as TGA/DTA, X-ray analysis, SEM, EDAX, TEM, FTIR, Wettability measurement and UV-visible spectroscopy are included with instrumentation and working. Determination of lattice parameter and crystallite size by using XRD study also discussed.

Chapter – 3:

This chapter consists of wet chemical technique for the preparation of CaSiO_3 nanoparticles followed by fabrication of pellets. The X-ray diffraction analysis shows single phase hexagonal structure. The average crystallite size obtained for CaSiO_3 sample calcined at 1250°C was found to be ~ 34 nm. Spherical shape morphology and microstructure of the synthesized sample was studied by TEM and SEM analysis. EDAX and FTIR analysis of the synthesized nanomaterial corroborates that the material is composed of Ca, Si and O without any impurity. In vitro wetting experiment revealed that the CaSiO_3 material was superhydrophilic in nature. Cell culture, MTT assay and cell adhesion assay showed that the nanosized CaSiO_3 powder provided a more adequate environment for cell adhesion and proliferation and was characterized by good biocompatibility. The degradability in vitro was evaluated

by weight loss in the SBF and it shows that the CaSiO_3 nanoparticles exhibit a higher degradation rate. CaSiO_3 could efficiently adsorb and controlled release of norfloxacin, which suggested its extended applications for other antibiotics.

Chapter – 4:

It consists of synthesis of hydroxyapatite (HAP) bioceramics by auto-combustion technique by using citric acid as a fuel. Crystallite size obtained from XRD was found to be 30 nm. The porous microstructure of synthesized HAP material which is beneficial for cell growth was examined by SEM analysis. EDAX and FTIR analysis of the synthesized nanomaterial corroborates that the material is composed of Ca, P and O without any impurity. TEM analysis was found to be good agreement with the value obtained from XRD pattern. Wetting experiment revealed that the HAP material was superhydrophilic in nature. Cell culture, MTT and cell adhesion assay showed good biocompatibility of HAP nanoparticles. The degradability in vitro was evaluated by weight loss in the SBF and it shows that the HAP sample exhibit a higher degradation rate. Drug loading and drug release behavior of HAP nanoparticles show good uptake and release capacity.

Chapter –5:

In this chapter we have employed the simple auto-combustion technique using citric acid to synthesize zinc doped hydroxyapatite $(\text{Ca}_{10-x}\text{Zn}_x(\text{PO}_4)_6(\text{OH})_2)$ nanoparticles. Crystallite size obtained from XRD was found to be 30 to 40 nm. EDAX analysis confirms that the material is composed of Ca, P, O and Zn. Formations of nanorod like structure by increasing zinc concentration in pure HAP were studied by SEM and TEM analysis. The results reveal that there is a strong correlation between zinc concentration and the product morphology. Effect of zinc concentration on in vitro biocompatibility, in vitro biodegradation and in vitro drug delivery were also observed.

Chapter – 6:

This chapter deals with synthesis of $\text{Ca}_{10-2x}\text{Fe}_{2x}(\text{PO}_4)_6(\text{OH})_2$ by using auto-combustion method and its characterization. From the XRD result, it is confirmed that the synthesized material forms single hexagonal phase with average crystallite size 30 to 25 nm. The FTIR result shows distinct differences between the spectra of the HAP and Fe doped HAP due to the addition of Fe. Cell adhesion studies shows that no negative influence of $\text{Ca}_{10-2x}\text{Fe}_{2x}(\text{PO}_4)_6(\text{OH})_2$ system up to $x=0.4$ which indicate

good biocompatibility. In vitro drug delivery was also investigated by using norfloxacin drug.

Future Scope

While the past 40 years has seen a major move forward both in the quantity of bioceramics used in clinical application and also the quality of bone repair that they offer, there is still potential for major advances to be made in the field. These include a requirement for the

- Evaluation of in vivo performance and clinical trials of newly prepared nanostructured bioceramics materials.
- Improvement in their performance in terms of their stability and ability to deliver biological agents.
- Development of smart nanomaterials capable of combining sensing with bioactivity.
- Development of improved biomimetic composites.

However, there is still need for a better understanding of the biological system. If we were able to fully understand the fundamentals of bone response to specific ions and the signals they activate, then we would be able to design better bioceramics for the future.

BIBLIOGRAPHY

Bibliography

Chapter – 1

- [1] M. Vallet-Regi, **(2001)** “Ceramics for medical applications”, J. Chem. Soc. Dalton. Trans., 97-108.
- [2] R. H. Doremus, **(1992)** “Review bioceramics”, J. Mater. Sci., 27: 285-97.
- [3] S. M. Best, A. E. Porter, E. S. Thian, J. Huang, **(2008)** “Bioceramics: past, present and for the future”, J. Eur. Ceram. Soc., 28: 1319-27.
- [4] M. N. Rahaman, A. Yao, B. S. Bal, J. P. Garino, M. D. Ries, **(2007)** “Ceramics for prosthetic hip and knee joint replacement”, J. Am. Ceram. Soc., 90: 1965-88.
- [5] S. V. Dorozhkin, **(2010)** “Bioceramics of calcium orthophosphates”, Biomaterials, 31: 1465-85.
- [6] B. Ben-Nissan, **(2004)** “Biomimetics and bioceramics, learning from nature how to design new implantable biomaterials”, Kluwer Academic Publishers, 89-103.
- [7] K. D. Jandt, **(2007)** “Evolutions, revolutions and trends in biomaterials science a perspective”, Adv. Eng. Mater., 9: 1035-50.
- [8] S. Mann, **(1996)** “Biomimetic materials chemistry”, UK: Wiley-VCH.
- [9] M. Vallet-Regi, **(2008)** “Bioceramics: where do we come from and which are the future expectations”, Key. Eng. Mater., 377: 1-18.
- [10] M. A. Meyers, P. Y. Chen, A. Y. M. Lin, Y. Seki, **(2008)** “Biological materials: structure and mechanical properties”, Prog. Mater. Sci., 53: 1-206.
- [11] H. Kawahara, **(1979)** “Today and tomorrow of bioceramics”, J. Oral Implantol, 8: 411-32.
- [12] P. Ducheyne, **(1987)** “Bioceramics: material characteristics versus in vivo behavior”, J. Biomed. Mater. Res., 21(Suppl. A2): 219-36.
- [13] L. L. Hench, **(1991)** “Bioceramics: from concept to clinic”, J. Am. Ceram. Soc., 74: 1487-510.
- [14] W. Cao, L. L. Hench, **(1996)** “Bioactive materials”, Ceram. Int., 22: 493-507.
- [15] L. L. Hench, **(1998)** “Bioceramics”, J. Am. Ceram. Soc., 81: 1705-28.
- [16] R. B. Heimann, **(2002)** “Materials science of crystalline bioceramics: a review of basic properties and applications”, CMU J., 1: 23-46.

- [17] P. Ducheyne, Q. Qiu, **(1999)** “Bioactive ceramics: the effect of surface reactivity on bone formation and bone cell function”, *Biomaterials*, 20: 2287-303.
- [18] The world orthopaedic market 2000-2001, **(2002)** “Dorland’s biomedical / knowledge enterprises”, Philadelphia.
- [19] L. L. Hench, Molecular design of bioactive glasses and ceramics for implants, in W. Soga and A. Kato (eds.), **(1991)** “Ceramics: towards the 21st century”, *J. Ceram. Soc. Japan*, 519-34.
- [20] J. W. Boretos, **(1987)** “Advances in bioceramics”, *Adv. Ceram. Mater.*, 2: 15-24.
- [21] R. Z. LeGeros, **(1988)** “Calcium phosphate materials in restorative dentistry: A review”, *Adv. Den. Res.*, 2: 164-83.
- [22] H. Aoki, **(1978)** “CaO-P₂O₅ Apatite”, Japanese Patent JP 7810999.
- [23] M. Jarcho, C. H. Bolen, M. B. Thomas, J. F. Bobick, J. F. Key, and R. H. Doremus, **(1976)** “Hydroxyapatite synthesis and characterization in dense polycrystalline form”, *J. Mater. Sci.*, 11: 2027-35.
- [24] T. Kokubo, M. Shigematsu, Y. Nagashima, M. Tashiro, T. Nakamura, T. Yamamuro, and S. Higashi, **(1982)** “Apatite-wollastonite containing glass ceramic for prosthetic application”, *Bull. Inst. Chem. Res., Kyoto Univ.*, 60: 260-8.
- [25] T. Kokubo, **(1991)** “Novel biomaterials derived from glasses”, in W. Soga and A. Kato (eds.), *ceramics: Towards the 21st century*, *J. Ceram. Soc. Japan*, 500-18.
- [26] L. L. Hench, R. J. Splinter, W. C. Allen and T. K. Greenlee, **(1972)** “Bonding mechanism at the interface of ceramics prosthetic materials”, *J. Biomed Mater. Res. Sym.*, 2: 117-41.
- [27] P. Lutton, and B. Ben-Nissan, **(1997)** “The status of biomaterials for orthopaedic and dental applications: Part II – bioceramics in orthopaedic and dental applications”, *Mater. Tech.*, 12: 107-11.
- [28] F. C. M. Driessens, **(1980)** “The mineral in bone, dentin and tooth enamel”, *Bull. Soc. Chim. Belg.*, 89: 663-89.
- [29] W. F. De Jong, **(1926)** “The mineral substance in bones”, *Rec. Trav. Chim.*, 45: 445-8.

- [30] A. S. Posner, **(1969)** “Crystal chemistry of bone mineral”, *Physiol. Rev.*, 49: 760-92.
 - [31] A. S. Posner, A. Perloff, and A. F. Dionio, **(1958)** “Refinement of the hydroxyapatite structure”, *Acta Cryst.*, 11: 308-9.
 - [32] I. M. Kay, R. A. Young, and A. S. Posner, **(1964)** “Crystal structure of hydroxyapatite”, *Nature*, 204: 1050-2.
 - [33] Y. Sun, H. Yang, D. Tao, **(2011)** “Microemulsion process synthesis of lanthanide-doped hydroxyapatite nanoparticles under hydrothermal treatment”, *Ceram. Int.*, 37: 2917-20.
 - [34] V. Stanic, D. Janackovic, S. Dimitrijevic, S. B. Tanaskovic, M. Mitric, M. S. Pavlovic, A. Krstic, D. Jovanovic, S. Raicevic, **(2011)** “Synthesis of antimicrobial monophasic silver-doped hydroxyapatite nanopowders for bone tissue engineering”, *Applied Surface Science*, 257: 4510-8.
 - [35] Y. Jeong, W. A. Brantley, H. Choe, **(2013)** “AC impedance behavior of silicon- hydroxyapatite doped film on the Ti–35Nb–xZr alloy by EB-PVD method”, *Surface and Coatings Technology*, 228: 505-10.
 - [36] S. Ligot, T. Godfroid, D. Music, E. Bousser, J. M. Schneider, R. Snyders, **(2012)** “Tantalum-doped hydroxyapatite thin films: Synthesis and characterization”, *Acta Materialia*, 60: 3435-43.
 - [37] A. Tampieri, T. D’Alessandro, M. Sandri, S. Sprio, E. Landi, L. Bertinetti, S. Panseri, G. Peponi, J. Goettlicher, M. Banobre-Lopez, J. Rivas, **(2012)** “Intrinsic magnetism and hyperthermia in bioactive Fe-doped hydroxyapatite”, *Acta Biomaterialia*, 8: 843-51.
 - [38] M. A. Pogossova, P. E. Kazin, Y. D. Tretyakov, **(2012)** “Synthesis and characterization of copper doped Ca–Li hydroxyapatite”, *Nuclear Instruments and Methods in Physics Research B*, 284: 33-5.
 - [39] T. W. Bauer, R. C. Geesink, R. Zimmerman, J. T. McMahon, **(1991)** “Hydroxyapatite-coated femoral stems. Histological analysis of components retrieved at autopsy”, *J. Bone Joint Surg.*, 73: 1439-52.
 - [40] H. Zhou, J. Lee, **(2011)** “Nanoscale hydroxyapatite particles for bone tissue engineering”, *Acta Biomaterialia*, 7: 2769-81.
 - [41] M. Bohner, **(2000)** “Calcium orthophosphates in medicine: from ceramics to calcium phosphate cements”, *Injury-Int. J. Care Injured*, 31: 37-47.
-

- [42] S. V. Dorozhkin, **(2009)** “Calcium orthophosphate-based biocomposites and hybrid Biomaterials”, *J. Mater. Sci.*, 44: 2343-87.
- [43] S. V. Dorozhkin, **(2009)** “Calcium orthophosphates in nature, biology and medicine”, *Materials*, 2: 399-498.
- [44] M. P. Ginebra, M. Espanol, E. B. Montufar, R. A. Perez, G. Mestres, **(2010)** “New processing approaches in calcium phosphate cements and their applications in regenerative medicine”, *Acta Biomaterialia*, 6: 2863-73.
- [45] A. J. W. Johnson, B. A. Herschler, **(2011)** “A review of the mechanical behavior of CaP and CaP/polymer composites for applications in bone replacement and repair”, *Acta Biomaterialia*, 7: 16-30.
- [46] R. Z. Legeros, **(1993)** “Biodegradation and bioresorption of calcium phosphate ceramics”, *Clin. Mater.*, 14: 65-88.
- [47] C. Sikalidis, **(2011)** “Advances in ceramics—electric and magnetic ceramics, bioceramics ceramics and environment”, 360.
- [48] A. Gatti and J. Knowles, **(2002)** “Biocompatibility and biological tests, in: integrated biomaterials science (capitol di un libro) ed. by barbucci, kluwer academic/plenum publishers”, ISBN 0-306- 46678-3, New York, USA, 793-813.
- [49] D. F. Williams, **(2008)** “On the mechanisms of biocompatibility”, *Biomaterials*, 20: 2941-53.
- [50] D. F. Williams, **(1999)** “The williams dictionary of biomaterials”, Liverpool University Press, Liverpool.
- [51] M. Jakob, O. Demarteau, D. Schafer, B. Hintermann, W. Dick, M. Heberer, I. Martin, **(2001)** “Specific growth factors during the expansion and redifferentiation of adult human articular chondrocytes enhance chondrogenesis and cartilaginous tissue formation in vitro”, *J. Cell. Biochem.*, 81: 368-77.
- [52] J. C. Le Huec, D. Clement, B. Brouillaud, N. Barthe, B. Dupuy, B. Foliguet, B. Basse-Cathalinat, **(1998)** “Evolution of the local calcium content around irradiated beta-tricalcium phosphate ceramic implants: in vivo study in the rabbit”, *Biomaterials*, 19: 733-8.
- [53] K. Hyakuna, T. Yamamuro, Y. Kotoura, M. Oka, T. Nakamura, T. Kitsugi, T. Kokubo, H. Kushitani, **(1990)** “Surface reactions of calcium phosphate ceramics to various solutions”, *J. Biomed. Mater. Res.*, 24: 471-88.

- [54] S. Raynaud, E. Champion, D. Bernache-Assolant, D. Tetard, **(1998)** “Dynamic fatigue and degradation in solution of hydroxyapatite ceramics”, *J. Mater. Sci. Mater. Med.*, 9: 221-7.
- [55] R. K. Tang, G. H. Nancollas, C. A. Orme, **(2001)** “Mechanism of dissolution of sparingly soluble electrolytes”, *J. Am. Chem. Soc.*, 123: 5437-43.
- [56] D. S. Brauer, C. Russel, S. Vogt, J. Weisser, M. Schnabelrauch, **(2007)** “Fabrication and in vitro characterization of porous biodegradable composites based on phosphate glasses and oligolactide-containing polymer networks”, *J. Biomed. Mater. Res. A*, 80: 410-20.
- [57] I. I. Slowing, B. G. Trewyn, S. Giri, V. S. Y. Lin, **(2007)** “Mesoporous silica nanoparticles for smart drug delivery”, *Adv. Funct. Mater.*, 17: 1225-36.
- [58] A. G. Gristina, **(1987)** “Biomaterial-centered infection: microbial adhesion versus tissue integration”, *Science*, 237: 1588-95.
- [59] N. N. Mohomed, J. Barrett, J. N. Katz, J. A. Baron, J. Wright, E. Losina, **(2005)** “Epidemiology of total knee replacement in the united states medicare population”, *J. Bone Joint Surg. Am.*, 87: 1222-8.
- [60] C. B. Phillips, J. A. Barrett, E. Losina, N. N. Mohomed, E. A. Lingard, E. Guadagnoli, **(2003)** “Incidence rates of dislocation, pulmonary embolism, and deep infection during the first six months after elective total hip replacement”, *J. Bone Joint Surg. Am.*, 85: 20-6.
- [61] N. Fletcher, D. Sofianos, M. B. Berkes, W. T. Obrebsky, **(2007)** “Prevention of perioperative infection”, *J. Bone Joint Surg. Am.*, 89: 1605-18.
- [62] D. Williams, **(1990)** “An introduction to medical and dental materials, Concise Encyclopedia of Medical and Dental Materials”, D. Williams, Ed., Pergamon Press and the MIT Press, 17-20.
- [63] R. Z. LeGeros, **(2002)** “In: Calcium phosphate ceramics in dentistry and medicine”, 40th Symposium on basic science of ceramics, convention center, Osaka University, Jan. 22-23.
- [64] S. V. Dorozhkin, **(2007)** “Calcium orthophosphates”, *J. Mater. Sci.*, 42: 1061-95.
- [65] P. W. Brown, B. Constantz, editors, **(1994)** “Hydroxyapatite and related materials”, Boca Raton, FL: CRC Press, 343.

- [66] F. C. M. Driessens, M. G. Boltong, E. A. P. De Maeyer, R. Wenz, B. Nies, J. A. Planell, **(2002)** “The Ca/P range of nanoapatitic calcium phosphate cements”, *Biomaterials*, 23: 4011-17.
- [67] T. J. Brunner, M. Böhner, C. Dora, C. Gerber, W. J. Stark, **(2007)** “Comparison of amorphous TCP nanoparticles to micron-sized α -TCP as starting materials for calcium phosphate cements”, *J. Biomed. Mater. Res. (Appl Biomater)*, 83B: 400.
- [68] R. Nemoto, L. Wang, T. Ikoma, J. Tanaka, M. Senna, **(2004)** “Preferential alignment of hydroxyapatite crystallites in nanocomposites with chemically disintegrated silk fibroin”, *J. Nanopart Res.*, 6: 259-65.
- [69] H. R. R. Ramay, M. Zhang, **(2004)** “Biphasic calcium phosphate nanocomposite porous scaffolds for load-bearing bone tissue engineering”, *Biomaterials*, 25: 5171-80.
- [70] Y. M. Sung, Y. K. Shin, J. J. Ryu, **(2007)** “Preparation of hydroxyapatite / zirconia bioceramic nanocomposites for orthopaedic and dental prosthesis applications”, *Nanotechnology*, 18: 065602 [6 pages].
- [71] T. Livingston, P. Ducheyne, J. Garino, **(2002)** “In vivo evaluation of a bioactive scaffold for bone tissue engineering”, *J. Biomed. Mater. Res.*, 62: 1-13.
- [72] I. Pountos, P. V. Giannoudis, **(2005)** “Biology of mesenchymal stem cells”, *Injury*, 36: 8-12.
- [73] B. J. Martin, M. F. Pittenger, **(2006)** “Bone marrow-derived stem cell for myocardial regeneration: preclinical experience. In stem cell therapy and tissue engineering for cardiovascular repair from basic research to clinical applications”, N. Dib, D. A. Taylor and E. B. Diethrich (Eds.) Springer, New York: 137-57.
- [74] C. T. Gomillion, K. J. L. Burg, **(2006)** “Stem cells and adipose tissue engineering”, *Biomaterials*, 27: 6052-63.
- [75] R. Chen, J. A. Hunt, **(2007)** “Biomimetic materials processing for tissue-engineering processes”, *J. Mater. Chem.*, 17: 3974-79.
- [76] W. J. Li, R. Tuli, X. X. Huang, P. Laquerriere, R. S. Tuan, **(2005)** “Multilineage differentiation of human mesenchymal stem cells in a three dimensional nanofibrous scaffold”, *Biomaterials*, 26: 5158-66.

- [77] H. H. K. Xu, M. D. Weir, L. Sun, **(2007)** “Nanocomposite with Ca and PO₄ release: effects of reinforcement, dicalcium phosphate particle size and silanization”, *Dental Mater.*, 23: 1482-91.
- [78] L. L. Hench, **(1993)** “Bioceramics: From concept to clinic”, *Amer. Ceram. Soc. Bull.*, 72: 93-98.
- [79] D. J. Verret, Y. Ducic, L. Oxford, J. Smith, **(2005)** “Hydroxyapatite cement in craniofacial reconstruction”, *Otolaryngol Head Neck Surg.*, 133: 897-9.
- [80] R. A. Giordano, **(1996)** “Dental ceramic restorative systems”, *Compendium of Continuing Education in Dentistry*, 17: 779-82.
- [81] S. Hansen, **(2000)** “Preparation for cerc 3: Where are the limits?”, *International Journal of Computerized Dentistry*, 3: 197-205.
- [82] J. R. Kelly, **(1997)** “Ceramics in restorative and prosthetic dentistry”, *Annual Review of Materials Science*, 27: 443-68.
- [83] J. G. Ironside, M. V. Swain, **(1998)** “Ceramics in dental restorations—a review and critical issues”, *J. Australialasian Ceram. Soc.*, 34: 78-91.
- [84] K. J. Anusavice, **(1993)** “Recent developments in restorative dental ceramics”, *J. Am. Dent. Assoc.*, 124: 72-74.
- [85] M. A. Rauschmann, T. A. Wichelhaus, V. Stirnal, E. Dingeldein, L. Zichner, R. Schnettler, V. Alt, **(2005)** “Nanocrystalline hydroxyapatite and calcium sulphate as biodegradable composite carrier material for local delivery of antibiotics in bone infections”, *Biomaterials*, 26: 2677-84.
- [86] P. Yang, Z. Quan, C. Li, X. Kang, H. Lian, J. Lin, **(2008)** “Bioactive, luminescent and mesoporous europium-doped hydroxyapatite as a drug carrier”, *Biomaterials*, 29: 4341-47.
- [87] S. Lepretre, F. Chai, J. C. Hornez, G. Vermet, C. Neut, M. Descamps, H. F. Hildebrand, B. Martel, **(2009)** “Prolonged local antibiotics delivery from hydroxyapatite functionalised with cyclodextrin polymers”, *Biomaterials*, 30: 6086-93.
- [88] G. D. Venkatasubbu, S. Ramasamy , V. Ramakrishnan, J. Kumar, **(2011)** “Nanocrystalline hydroxyapatite and zinc-doped hydroxyapatite as carrier material for controlled delivery of ciprofloxacin”, *Biotech.*, 1: 173-186.
- [89] R. J. Narayan, P. N. Kumta, C. Sfeir, D. H. Lee, D. Choi, D. Olton, **(2004)** “Nanostructured ceramics in medical devices: applications and prospects”, *JOM*, 56: 38-43.

- [90] O. C. Wilson, J. R. Hull, **(2008)** “Surface modification of nanophase hydroxyapatite with chitosan” *Mater. Sci. Eng. C*, 28: 434-37.
- [91] J. G. Liao, X. J. Wang, Y. Zuo, L. Zhang, J. Q. Wen, Y. B. Li, **(2008)** “Surface modification of nano-hydroxyapatite with silane agent”, *J. Inorg. Mater.*, 23: 145-9.
- [92] M. Kester, Y. Heakal, T. Fox, A. Sharma, G. P. Robertson, T. T. Morgan, **(2008)** “Calcium phosphate nanocomposite particles for in vitro imaging and encapsulated chemotherapeutic drug delivery to cancer cells”, *Nano Lett.*, 8: 4116-21.
- [93] H. T. Ong, J. S. C. Loo, F. Y. C. Boey, S. J. Russell, J. Ma, K. W. Peng, **(2008)** “Exploiting the high affinity phosphonate – hydroxyapatite nanoparticles interaction for delivery of radiation and drugs”, *J. Nanopart Res.*, 10: 141-50.
- [94] T. T. Morgan, H. S. Muddana, E. I. Altinoglu, S. M. Rouse, A. Tabakovic, T. Tabouillot, **(2008)** “Encapsulation of organic molecules in calcium phosphate nanocomposite particles for intracellular imaging and drug delivery”, *Nano Lett.*, 8: 4108-15.
- [95] B. Palazzo, M. Iafisco, M. Laforgia, N. Margitta, G. Natile, C. L. Bianchi, **(2007)** “Biomimetic hydroxyapatite-drug nanocrystals as potential bone substitutes with antitumor drug delivery properties”, *Adv. Funct. Mater.*, 17: 2180-8.
- [96] S. P. Victor, T. S. S. Kumar, **(2008)** “Tailoring calcium-deficient hydroxyapatite nanocarriers for enhanced release of antibiotics”, *J. Biomed. Nanotechnol.*, 4: 203-9.
- [97] O. Kilian, V. Alt, C. Heiss, T. Jonuleit, E. Dingeldein, I. Flesch, **(2005)** “New blood vessel formation and expression of VEGF receptors after implantation of platelet growth factor-enriched biodegradable nanocrystalline hydroxyapatite”, *Growth Factors*, 23: 125-33.
- [98] V. V. Sokolova, M. Eppler, **(2008)** “Inorganic nanoparticles carriers of nucleic acids into cells”, *Angew. Chem. Int. Ed.*, 47: 1382-95.
- [99] J. Czupryna, A. Tsourkas, **(2006)** “Suicide gene delivery by calcium phosphate nanoparticles. A new method of targeted therapy for gastric cancer”, *Cancer Biol. Ther.*, 5: 1691-2.

- [100] D. Olton, J. Li, M. E. Wilson, T. Rogers, J. Close, L. Huang, **(2007)** “Nanostructured calcium phosphates (NanoCaPs) for non-viral gene delivery: Influence of the synthesis parameters on transfection efficiency”, *Biomaterials*, 28: 1267-79.
- [101] E. H. Chowdhury, T. Akaike, **(2007)** “High performance DNA nano-carriers of carbonate apatite: multiple factors in regulation of particle synthesis and transfection efficiency”, *Int. J. Nanomed.*, 2: 101-6.
- [102] E. H. Chowdhury, **(2007)** “PH-sensitive nanocrystals of carbonate apatite for smart and cell-specific transgene delivery”, *Expert Opin. Drug Deliv.*, 4: 193-6.
- [103] H. Urch, S. Franzka, D. Dahlhaus, N. Hartmann, E. Hasselbrink, M. Epple, **(2006)** “Preparation of two-dimensionally patterned layers of functionalised calcium phosphate nanoparticles by laser direct writing”, *J. Mater. Chem.*, 16: 1798-802.
- [104] V. V. Sokolova, A. Kovtun, R. Heumann, M. Epple, **(2007)** “Tracking the pathway of calcium phosphate/DNA nanoparticles during cell transfection by incorporation of red-fluorescing tetramethylrhodamine isothiocyanate bovine serum albumin into these nanoparticles”, *J. Biol. Inorg. Chem.*, 12: 174-9.
- [105] V. V. Sokolova, A. Kovtun, O. Prymak, W. Meyer-Zaika, E. A. Kubareva, E. A. Romanova, **(2007)** “Functionalisation of calcium phosphate nanoparticles by oligonucleotides and their application for gene silencing”, *J. Mater. Chem.*, 7: 721-7.
- [106] I. Roy, S. Mitra, A. Maitra, S. Mozumdar, **(2003)** “Calcium phosphate nanoparticles as novel non-viral vectors for targeted gene delivery”, *Int. J. Pharm.*, 250: 25-33.
- [107] S. P. Thompson, S. J. Day, J. E. Parker, A. Evans, C. C. Tang, **(2012)** “Fine-grained amorphous calcium silicate CaSiO_3 from vacuum dried sol–gel–production, characterisation and thermal behaviour”, *J. Non-Crystalline Solids*, 358: 885-92.
- [108] H. Zhong, L. Wang, Y. Fan, L. He, K. Lin, W. Jiang, J. Chang, L. Chen, **(2011)** “Mechanical properties and bioactivity of $\beta\text{-Ca}_2\text{SiO}_4$ ceramics synthesized by spark plasma sintering”, *Ceram. Int.*, 37: 2459-65.
- [109] M. A. Sainz, P. Pena, S. Serena, A. Caballero, **(2010)** “Influence of design on bioactivity of novel $\text{CaSiO}_3\text{--CaMg}(\text{SiO}_3)_2$ bioceramics: In vitro simulated

- body fluid test and thermodynamic simulation”, *Acta Biomaterialia*, 6: 2797-2807.
- [110] N. Jia, S. M. Li, M. G. Ma, R. C. Sun, L. Zhu, **(2011)** “Green microwave-assisted synthesis of cellulose/calcium silicate nanocomposites in ionic liquids and recycled ionic liquids”, *Carbohydrate Research*, 346: 2970-74.
- [111] G. E. Poinern, R. K. Brundavanam, N. Mondinos, Z. Jiang, **(2009)** “Synthesis and characterisation of nanohydroxyapatite using an ultrasound assisted method”, *Ultrasonics Sonochemistry*, 16: 469-74.
- [112] D. Gopi, J. Indira, V. Collins Arun Prakash, L. Kavitha, **(2009)** “Spectroscopic characterization of porous nanohydroxyapatite synthesized by a novel amino acid soft solution freezing method”, *Spectrochimica Acta, Part A*, 74: 282-84.
- [113] S. Ali Poursamar, M. Azami, M. Mozafari, **(2011)** “Controllable synthesis and characterization of porous polyvinyl alcohol/hydroxyapatite nanocomposite scaffolds via an in situ colloidal technique”, *Colloids and Surfaces B: Biointerfaces*, 84: 310-16.
- [114] C. N. R. Rao, **(1994)** “Chemical approaches to synthesis of inorganic materials”, (Wiley Eastern Ltd.), New Age International Ltd., New Delhi.
- [115] A. S. Mukasyan, C. Costello, K. P. Sherlock, D. Lafarga A. Varma, **(2001)** “Perovskite membranes by aqueous combustion synthesis: synthesis and properties”, *Separation and Purification Technology*, 25: 117-26.
- [116] S. T. Aruna, M. Mathuraman and K. C. Patil, **(2000)** “Studies on combustion synthesised LaMnO_3 – LaCoO_3 solid solutions”, *Mater. Res. Bull.*, 35: 289-96.
- [117] M. M. A. Sekar and A. Halliyal, **(1998)** “Low-Temperature synthesis, characterization, and properties of lead-based ferroelectric niobates”, *J. Am. Ceram. Soc.*, 81: 380-88.
- [118] S. T. Aruna, M. Mathuraman and K. C. Patil, **(1997)** “Combustion synthesis and properties of strontium substituted lanthanum manganites, $\text{La}_{1-x}\text{Sr}_x\text{MnO}_3$ ($0 \leq x \leq 0.3$)”, *J. Mater. Chem.*, 7: 2499-503.
- [119] S. Bhaduri, S. B. Bhaduri and E. Zhou, **(1998)** “Auto ignition synthesis and consolidation of Al_2O_3 – ZrO_2 nano/nano composite powders”, *J. Mater. Res.*, 13: 156-65.

- [120] A.G. Merzhanov, **(1993)** “Combustion: New manifestation of an ancient process, In Rao CNR (ed.), Chemistry of Advanced Materials”, Blackwell Scientific, Oxford, 19.
- [121] A. G. Merzhanov (ed.), **(1999)** “SHS Research and Development; Handbook, Institute of structural macrokinetics and materials science”, Russian Academy of Sciences, Chernogolovka, Russia.
- [122] J. J. Kingsley, K.C. Patil, **(1988)** “A novel combustion process for the synthesis of fine particle α -alumina and related oxide materials”, Mater. Lett., 6: 427-432.
- [123] J. Huang, S.M. Best, W. Bonfield, Tom Buckland **(2010)**, Development and characterization of titanium-containing hydroxyapatite for medical applications, Acta Biomaterialia, 6: 241–249.
- [124] M. Jarcho, J. F. Kay, K. I. Gumaer, R. H. Doremus, H. P. Drobeck, **(1977)** “Tissue, cellular and subcellular events at a bone-ceramic hydroxylapatite interface”, J. Bioeng., 2: 79-92.
- [125] S. H. Maxian, J. P. Zawadsky, M. G. Dunn, **(1994)** “Effect of Ca/P coating resorption and surgical fit on the bone/implant interface”, J. Biomed. Mater. Res., 28: 1311-19.
- [126] M. Jarcho, C. H. Bolen, M. B. Thomas, J. Bobick, J. F. Kay, R. H. Doremus, **(1976)** “Hydroxylapatite synthesis and characterization in dense polycrystalline form”, J. Mater. Sci., 11: 2027-35.
- [127] Y. Hu, X. Miao, **(2004)** “Comparison of hydroxyapatite ceramics and hydroxyapatite/borosilicate glass composites prepared by slip casting”, Ceram. Int., 30: 1787-91.
- [128] M. Akao, H. Aoki, K. Kato, **(1981)** “Mechanical properties of sintered hydroxyapatite for prosthetic applications”, J. Mater. Sci., 16: 809-12.
- [129] R. M. Pilliar, J. E. Davies, D. C. Smith, **(1991)** “The bone-biomaterial interface for load-bearing implants”, MRS Bull., 16: 55-61.
- [130] E. Boanini, P. Torricelli, M. Gazzano, R. Giardinob, A. Bigi, **(2008)** “Alendronate–hydroxyapatite nanocomposites and their interaction with osteoclasts and osteoblast-like cells”, Biomaterials, 29: 790-96.
- [131] X. Chen, T. Wu, Q. Wang, J. W. Shen, **(2008)** “Shield effect of silicate on adsorption of proteins onto silicon-doped hydroxyapatite (100) surface”, Biomaterials, 29: 2423-32.

- [132] S. Sebti, R. Tahir, R. Nazih, A. Saber, S. Boulaajaj, **(2002)** “Hydroxyapatite as a new solid support for the knoevenagel reaction in heterogeneous media without solvent”, *Appl. Catal. A: Gen.*, 228: 155-159.
- [133] Y. Matsumura, S. Sugiyama, H. Hayashi, J. B. Moffat, **(1995)** “Lead-Calcium hydroxyapatite: Cation effects in the oxidative coupling of methane”, *J. Solid State Chem.*, 114: 138-45.
- [134] B. A. Mulla, P. S. Jain, K. A. Deshpande and V. S. Darshane, **(1984)** *Ind. J. Chem.*, 23A: 339.

Chapter – 2

- [1] A. Blazek, **(1973)** “Thermal analysis”, Van Norstrand, Reinhold Co. London.
- [2] W. W. Wendalandt, **(1964)** “Thermal Analysis”, Interscience.
- [3] P. D. Garn, **(1973)** “Thermoanalytical methods of investigation”, Academic press, NewYork.
- [4] C. J. Keattch and D. Dollimore, **(1975)** “An introduction to thermogravimetry”, Heyden London.
- [5] S. R. Dharwadkar, **(2002)** “THERMANS 2002”, Published by BARC, Mumbai.
- [6] M. D. Judd and M. I. Pope, **(1977)** “Differential thermal analysis”, Heyden London.
- [7] S. M. Khetre, **(2012)** “Catalytic and structural studies of non-stoichiometric mixed oxides of rare earths and transition metals”, Ph.D. Thesis, Shivaji University, Kolhapur.
- [8] M. Shyamala, S. R. Dharawadkar and M. S. Chandrasekharaiah, **(1982)** “Proceeding of 5th international conference on thermal analysis”, Ed.B. Miller, ohn Willey, NewYork, 220.
- [9] V. M, Raghavan, **(1998)** “Materials science and engineering (ed)”, Prentice-Hall of India, New Delhi.
- [10] L. V. Azaroff, **(1968)** “Element of X-ray crystallography” Mc Graw-Hill Book Company, New York.
- [11] C. Whiston, **(1987)** “X-ray methods” John Willey and Sons, UK.
- [12] B. D. Culity, **(1967)** “X-ray diffraction”,Addisen Wesley Publisher Co. Inc.
- [13] L. S. Dent, Glasser, **(1977)** “Crystallography and its application” Van Nostrand Reinhold Company Ltd. London.
- [14] R. E. Lee, **(1993)** “Scanning electron microscopy and X-ray microanalysis” PTR Prentice Hall. Englewood Cliffs, New Jersey.
- [15] G. Lewes, **(1987)** “Scanning electron microscopy and X-ray microanalysis” John Willey and Sons, UK.
- [16] N. Yao, Z. L. Wang, **(2005)** “Handbook of microscopy for nanotechnology”.
- [17] J. H. Spence, **(1980)** “High-resolution electron microscopy” Oxford press.
- [18] C. P. S., Hsu, “Handbook of instrumental techniques for analytical chemistry, Infrared spectroscopy” chapter 15 (Ed.) F.A. Settle Prentice Hall New Jersey.
- [19] S. Baruah and J. Dutta, **(2009)** Sci. Technol. Adv. Mater., 10: 013001.

- [20] G. R. Chatwal and S. K. Anand, **(2006)** “Instrumental methods of chemical analysis”, Himalaya Publishing House, New Delhi.
- [21] S. N. Das, J. H. Choi, J. P. Kar and J. M. Myoung, **(2009)** “Tunable and reversible surface wettability transition of vertically aligned ZnO nanorod arrays”, *Applied Surface Science*, 255: 7319-22.
- [22] C. H. Sun, A. Gonzalez, N. C. Linn, P. Jiang and B. Jiang, **(2008)** “Templated biomimetic multifunctional coatings”, *Appl. Phys. Lett.*, 92: 051107 (1-3).
- [23] B. Bhushan and Y. C. Jung, **(2011)** “Natural and biomimetic artificial surfaces for superhydrophobicity, self cleaning, low adhesion, and drag reduction”, *Progress in Materials Science*, 56: 1-108.
- [24] W. H. Bragg and W. L. Bragg, **(1913)** “The intensity of reflection of X-rays by crystals”, *Proc. Roy. Soc. London (A)*, 88: 428-38.
- [25] C. N. Banwell and E. M. McCash, “Fundamentals of molecular spectroscopy”, Fourth Edition ed. Tata Mc-Graw-Hill Publishing Company limited.
- [26] B. E. Douglas and H. Darl, Mc Daniel, **(1970)** “Concepts and models of inorganic chemistry”, Oxford and IBH Publishing Co. PVT. Ltd.
- [27] R. D. Waldron, **(1955)** “Infrared red spectra of ferrites”, *Phys. Rev.*, 99: 1727-34.
- [28] P. N. Jagadale, S. R. Kulal, M. G. Joshi, P. P. Jagtap, S. M. Khetre, S. R. Bamane, **(2013)** “Synthesis and characterization of nanostructured CaSiO_3 biomaterial”, *Material Science-Poland*, 31: 269-275.

Chapter – 3

- [1] S. H. Mansur, H. S. Costa, **(2008)** “Nanostructured poly (vinyl alcohol) /bioactive glass and poly(vinyl alcohol)/chitosan/bioactive glass hybrid scaffolds for biomedical applications”, Chem. Eng. J., 137: 72-83.
- [2] B. Ben-Nissan, **(2004)** “Biomimetics and bioceramics, learning from nature how to design new implantable biomaterials”, Kluwer Academic Publishers, 89-103.
- [3] E. Lynch, D. S. Brauer, N. Karpukhina, D. G. Gillam, R. G. Hill, **(2012)** “Multi-component bioactive glasses of varying fluoride content for treating dentin hypersensitivity”, Dent. Mater., 28: 168-78.
- [4] C. Wu, Y. Zhou, W. Fan, P. Han, J. Chang, J. Yuen, M. Zhang, Y. Xiao, **(2012)** “Hypoxia-mimicking mesoporous bioactive glass scaffolds with controllable cobalt ion release for bone tissue engineering”, Biomaterials, 33: 2076-85.
- [5] S. Fagerlund, J. Massera, N. Moritz, L. Hupa, M. Hupa, **(2012)** “Phase composition and in vitro bioactivity of porous implants made of bioactive glass S53P4”, Acta Biomaterialia, 8: 2331-9.
- [6] H. Zhong, L. Wang, Y. Fan, L. He, K. Lin, W. Jiang, J. Chang, L. Chen, **(2011)** “Mechanical properties and bioactivity of β -Ca₂SiO₄ ceramics synthesized by spark plasma sintering”, Ceram. Int., 37: 2459-65.
- [7] S. Ni, J. Chang, L. Chou, **(2006)** “A novel bioactive porous CaSiO₃ scaffold for bone tissue engineering”, J. Biomed. Mater. Res. A, 76: 196-205.
- [8] C. K. Chang, D. L. Mao, J. S. Wu, **(2000)** “Characteristics of crystals precipitated in sintered apatite/wollastonite glass ceramics”, Ceram. Int., 26: 779-85.
- [9] W. Zhai, H. Lu, L. Chen, X. Lin, Y. Huang, K. Dai, K. Naoki, G. Chen, J. Chang, **(2012)** “Silicate bioceramics induce angiogenesis during bone regeneration”, Acta Biomaterialia, 8: 341-49.
- [10] W. Xue, A. Bandyopadhyay, S. Bose, **(2009)** “Mesoporous calcium silicate for controlled release of bovine serum albumin protein”, Acta Biomaterialia, 5: 1686-96.
- [11] A. Balamurugan, G. Sockalingum, J. Michel, J. Faure, V. Banchet, L. Wortham, S. Bouthors, D. Laurent-Maquin, G. Balossier, **(2006)** “Synthesis and characterisation of sol gel derived bioactive glass for biomedical applications”, Mat. Lett., 60: 3752-57.

- [12] H. Oonishi, L. L. Hench, J. Wilson, F. Sugihara, E. Tsuji, M. Matsuura, **(2000)** “Quantitative comparison of bone growth behavior in granules of bioglass®, A-W glass-ceramic, and hydroxyapatite”, *J. Biomed. Mater. Res. A*, 51: 37-46.
- [13] A. K. Lynn, T. Nakamura, N. Patel, A. E. Porter, A. C. Renouf, P. R. Laity, S. M. Best, R. E. Cameron, Y. Shimizu, W. Bonfield, **(2005)** “Composition-controlled nanocomposites of apatite and collagen incorporating silicon as an osseopromotive agent”, *J. Biomed. Mater. Res. A*, 74: 447-53.
- [14] K. Lin, J. Chang, Z. Liu, Y. Zeng, R. Shen, **(2009)** “Fabrication and characterization of 45S5 bioglass rein-forced macroporous calcium silicate bioceramics”, *J. Eur. Ceram. Soc.*, 29: 2937-43.
- [15] C. Wang, Y. Xue, K. Lin, J. Lu, J. Chang, J. Sun, **(2012)** “The enhancement of bone regeneration by a combination of osteoconductivity and osteostimulation using β -CaSiO₃/ β -Ca₃(PO₄)₂ composite bioceramics”, *Acta Biomaterialia*, 8: 350-60.
- [16] X. Y. Liu, C. X. Ding, P. K. Chu, **(2004)** “Mechanism of apatite formation on wollastonite coatings in simulated body fluids”, *Biomaterials*, 25: 1755- 61.
- [17] G. Balasundaram, M. Sato, T. J. Webster, **(2006)** “Using hydroxyapatite nanoparticles and decreased crystallinity to promote osteoblast adhesion similar to functionalizing with RGD”, *Biomaterials*, 27: 2798-805.
- [18] T. J. Webster, T. A. Smith, **(2005)** “Increased osteoblast function on PLGA composites containing nanophase titania”, *J. Biomed. Mater. Res. A*, 74: 677-86.
- [19] S. P. Thompson, S. J. Day, J. E. Parker, A. Evans, C. C. Tang, **(2012)** “Fine-grained amorphous calcium silicate CaSiO₃ from vacuum dried sol-gel – production, characterisation and thermal behaviour”, *J. Non-Crystalline Solids*, 358: 885-92.
- [20] M. A. Sainz, P. Pena, S. Serena, A. Caballero, **(2010)** “Influence of design on bioactivity of novel CaSiO₃-CaMg(SiO₃)₂ bioceramics: In vitro simulated body fluid test and thermodynamic simulation”, *Acta Biomaterialia*, 6: 2797-807.
- [21] N. Jia, S. M. Li, M. G. Ma, R. C. Sun, L. Zhu, **(2011)** “Green microwave-assisted synthesis of cellulose/calcium silicate nanocomposites in ionic liquids and recycled ionic liquids”, *Carbohydrate Research*, 346: 2970-74.
- [22] K. Lin, W. Zhai, S. Ni, J. Chang, Y. Zeng, W. Qian, **(2005)** “Study of the mechanical property and in vitro biocompatibility of CaSiO₃ ceramics”, *Ceram. Int.*, 31: 323-26.
- [23] C. Hammond, **(1997)** “The basics of crystallography and diffraction”, Oxford University Press, Oxford.
- [24] B. D. Cullity, **(1956)** “Elements of X-ray diffraction”, Addison-Wesley, London, 99.

- [25] A. L. Patterson, **(1939)** “The scherrer formula for X-ray particle size determination”, Phys. Rev., 56: 978-82.
- [26] P. N. Jagadale, S. R. Kulal, M. G. Joshi, P. P. Jagtap, S. M. Khetre, S. R. Bamane, **(2013)** “Synthesis and characterization of nanostructured CaSiO₃ biomaterial”, Materials Science-Poland, 31: 269-75.
- [27] C. Ohtsuki, Y. Aoki, T. Kokubo, Y. Bando, M. Neo, T. Nakamura, **(1995)** “Transmission electron microscopic observation of glass-ceramic A-W and apatite layer formed on its surface in a simulated body fluid”, J. Ceram. Soc. Japan, 103: 449-54.
- [28] B. Vaidhyanathan, K. J. Rao, **(1996)** “Rapid microwave assisted synthesis of hydroxyapatite”, Bull. Mater. Sci., 19: 1163-65.
- [29] P. N. Chavan, M. M. Bahir, R. U. Mene, M. P. Mahabole, R. S. Khairnar, **(2010)** “Study of nanobiomaterial hydroxyapatite in simulated body fluid: Formation and growth of apatite”, Mater. Sci. and Eng. B, 168: 224-30.
- [30] J. C. Le Huec, D. Clement, B. Brouillaud, N. Barthe, B. Dupuy, B. Foliguet, B. Basse-Cathalinat, **(1998)** “Evolution of the local calcium content around irradiated beta-tricalcium phosphate ceramic implants: in vivo study in the rabbit”, Biomaterials, 19: 733-8.
- [31] H. T. Schmidt, B. L. Gray, P. A. Wingert, A. E. Ostafin, **(2004)** “Assembly of aqueous-cored calcium phosphate nanoparticles for drug delivery”, Chem. Mater., 16: 4942–7.
- [32] A. Meiszterics, K. Sinko, **(2008)** “Sol-gel derived calcium silicate ceramics”, Colloids and Surfaces A: Physicochemical and Engineering Aspects, 319: 143- 48.
- [33] United Steel Companies Ltd., Research and Development Dept., Swinden Labs., Rotherham, Private Communication, **(1967)**.
- [34] A. A. P. Mansur, D. B. Santos, H. S. Mansur, **(2007)** “A microstructural approach to adherence mechanism of poly(vinyl alcohol) modified cement systems to ceramic tiles”, Cem. Concr. Res., 37: 270-82.
- [35] V. C. Farmer, **(1974)** “The infrared spectra of minerals”, Adlard and Son Ltd, London.
- [36] W. Xia, J. J. Chang, **(2007)** “Preparation and characterization of nano-bioactive-glasses (NBG) by a quick alkali-mediated sol–gel method”, Mater. Lett., 61: 3251-3.

- [37] D. Arcos, D. C. Greenspan, M. Vallet-Regi, **(2002)** “Influence of the stabilization temperature on textural and structural features and ion release in $\text{SiO}_2\text{--CaO--P}_2\text{O}_5$ sol–gel glasses”, *Chem. Mater.*, 14: 1515-22.
- [38] S. P. Hudson, R. F. Padera, R. Langer, D. S. Kohane, **(2008)** “The biocompatibility of mesoporous silicates”, *Biomaterials*, 29: 4045-55.
- [39] S. A. Mahadik, M. S. Kavale, S. K. Mukherjee, A. Venkateswara Rao, **(2010)** “Transparent superhydrophobic silica coatings on glass by sol–gel method”, *Applied Surface Science*, 257: 333-39.
- [40] R. B. Chavan, **(2012)** “Studies on medicinal plant Tit-berry (*Allophylus* species)”, Ph.D. Thesis, Shivaji University, Kolhapur.
- [41] D. F. Williams, **(1999)** “The Williams Dictionary of biomaterials”, Liverpool University Press, Liverpool.
- [42] W. Xia, J. Chang, **(2006)** “Well-ordered mesoporous bioactive glasses (MBG): a promising bioactive drug delivery system”. *J. Controlled Release* 110: 522–30.
- [43] C. Barbe, J. Bartlett, L. G. Kong, K. Finnie, H. Q. Lin, M. Larkin, **(2004)** “Silica particles: a novel drug-delivery system”, *Adv. Mater.*, 16: 1959-66.

Chapter – 4

- [1] M. Vallet-Regi, J. M. Gonzalez-Calbet, **(2004)** “Calcium phosphates as substitution of bone tissues”, *Progress in Solid State Chem.*, 32: 1-31.
- [2] S. V. Dorozhkin, **(2009)** “Nanodimensional and nanocrystalline apatites and other calcium orthophosphates in biomedical engineering”, *Biology and Medicine, Materials*, 2: 1975-2045.
- [3] Y. R. Cai, R. K. Tang, **(2008)** “Calcium phosphate nanoparticles in biomineralization and biomaterials”, *J. Mater. Chem.*, 18: 3775-87.
- [4] J. S. Earl, D. J. Wood, S. J. Milne, **(2006)** “Hydrothermal synthesis of hydroxyapatite”, *J. Phys: Conference Series*, 26: 268-71.
- [5] H. Aoki, **(1991)** “Science and medical application of hydroxyapatite”, Tokyo, Japan: Japanese Association of Apatite Science, 179-92.
- [6] R. Z. LeGeros, **(1991)** “Calcium phosphates in oral biology and medicine”, monographs in oral sciences; Myers, H., Ed.; Karger: Basel, Switzerland, 15: 109-27.
- [7] A. Blom, **(2007)** “(V) Which scaffold for which application?”, *Current Orthopaedics*, 21: 280-87.
- [8] H. Pamela, G. de Klaas, **(2007)** “Osteoinductive biomaterials—properties and relevance in bone repair”, *J. of Tissue Engineering and Regenerative Medicine*, 1: 25-32.
- [9] M. Taniguchi, H. Takeyema, I. Mizunna, N. Shinagawa, J. Yura, N. Yoshikawa, H. Aoki, **(1991)** “The clinical application of intravenous catheter with percutaneous device made of sintered hydroxyapatite”, *Jpn. J. Artif. Organs*, 20: 460-4.
- [10] R. V. Silva, J. A. Camilli, C. A. Bertran, N. H. Moreira, **(2005)** “The use of hydroxyapatite and autogenous cancellous bone grafts to repair bone defects in rats”, *International J. Oral and Maxillofacial Surg.* 34: 178-84.
- [11] S. V. Kenneth, Z. Xing, B. M. Jennifer, W. Mark, W. K. Choll, **(2007)** “Conversion of bulk seashells to biocompatible hydroxyapatite for bone implants”, *Acta Biomaterialia*, 3: 910-18.
- [12] G. E. Poinern, R. K. Brundavanam, N. Mondinos, Z. Jiang, **(2009)** “Synthesis and characterisation of nanohydroxyapatite using an ultrasound assisted method”, *Ultrasonics Sonochemistry*, 16: 469-74.
- [13] D. Gopi, J. Indira, V. Collins Arun Prakash, L. Kavitha, **(2009)** “Spectroscopic characterization of porous nanohydroxyapatite synthesized by a novel amino acid

- soft solution freezing method”, *Spectrochimica Acta Part A: Molecular and Biomolecular Spectroscopy*, 74: 282-84.
- [14] S. Ali Poursamar, M. Azami, M. Mozafari, **(2011)** “Controllable synthesis and characterization of porous polyvinyl alcohol/hydroxyapatite nanocomposite scaffolds via an in situ colloidal technique”, *Colloids and Surfaces B: Biointerfaces*, 84: 310-6.
- [15] Y. Z. Wang, Y. Fu, **(2011)** “Microwave-hydrothermal synthesis and characterization of hydroxyapatite nanocrystallites”, *Mater. Lett.*, 65: 3388-90.
- [16] B. Nasiri-Tabrizi, P. Honarmandi, R. Ebrahimi-Kahrizsangi, P. Honarmandi, **(2009)** “Synthesis of nanosize single-crystal hydroxyapatite via mechanochemical Method”, *Mater. Lett.*, 63: 543-6.
- [17] S. K. Padmanabhan, A. Balakrishnan, M. C. Chu, Y. J. Lee, T. N. Kim, S. J. Cho, **(2009)** “Sol–gel synthesis and characterization of hydroxyapatite nanorods”, *Particuology*, 7: 466-70.
- [18] G. C. Koumoulidis, A. P. Katsoulidis, A. K. Ladavos, P. J. Pomonis, C. C. Trapalis, A. T. Sdoukos, T. C. Vaimakis, **(2003)** “Preparation of hydroxyapatite via microemulsion route”, *J. Colloid Interface Sci.*, 259: 254-60.
- [19] S. V. Bangale, D. R. Patil and S. R. Bamane, **(2011)** “Nanostructured spinel ZnFe_2O_4 for the detection of chlorine gas”, *Sensors & Transducers Journal*, 134: 107-19.
- [20] A. A. P. Mansur, H. S. Mansur, **(2010)** “Preparation, characterization and cytocompatibility of bioactive coatings on porous calcium-silicate-hydrate scaffolds”, *Mater. Sci. and Eng. C*, 30: 288-94.
- [21] S. K. Swain, S. Bhattacharyya, **(2013)** “Preparation of high strength macroporous hydroxyapatite scaffold”, *Mater. Sci. and Eng. C*, 33: 67-71.
- [22] P. N. Jagadale, S. R. Kulal, M. G. Joshi, P. P. Jagtap, S. M. Khetre, S. R. Bamane, **(2013)** “Synthesis and characterization of nanostructured CaSiO_3 biomaterial”, *Material Science-Poland*, 31: 269-275.
- [23] C. Ohtsuki, Y. Aoki, T. Kokubo, Y. Bando, M. Neo, T. Nakamura, **(1995)** “Transmission electron microscopic observation of glass-ceramic A-W and apatite layer formed on its surface in a simulated body fluid”, *J. Ceram. Soc. Japan*, 103: 449-54.
- [24] B. Vaidhyanathan, K.J. Rao, **(1996)** “Rapid microwave assisted synthesis of hydroxyapatite”, *Bull. Mater. Sci.*, 19: 1163-65.

- [25] P. N. Chavan, M. M. Bahir, R. U. Mene, M. P. Mahabole, R. S. Khairnar, **(2010)** “Study of nanobiomaterial hydroxyapatite in simulated body fluid: Formation and growth of apatite”, *Mater. Sci. and Eng. B*, 168: 224-30.
- [26] B. Kundu, D. Ghosh, M. K. Sinha, P. S. Sen V. K. Balla, N. Das, **(2013)** “Doxorubicin - intercalated nano-hydroxyapatite drug delivery system for liver cancer: An animal model”, *Cerm. Int.*, 39: 9557-9566.
- [27] H. T. Schmidt, B. L. Gray, P. A. Wingert, A. E. Ostafin, **(2004)** “Assembly of aqueous-cored calcium phosphate nanoparticles for drug delivery”, *Chem. Mater.*, 16: 4942–7.
- [28] N. S. Gajbhiye, U. Bhattacharyya, V. S. Darshane, **(1995)** “Thermal decomposition of zinc-iron citrate precursor”, *Thermochim Acta*, 264: 219-30.
- [29] Y. Sun, H. Yang, D. Tao, **(2011)** “Microemulsion process synthesis of lanthanide-doped hydroxyapatite nanoparticles under hydrothermal treatment”, *Ceram. Int.*, 37: 2917-20.
- [30] C. Hammond, **(1997)** “The basics of crystallography and diffraction”, Oxford University Press, Oxford.
- [31] B. D. Cullity, **(1956)** “Elements of X-ray diffraction”, Addison-Wesley, London, 99.
- [32] A. L. Patterson, **(1939)** “The scherrer formula for X-ray particle size determination”, *Phys. Rev.*, 56: 978-82.
- [33] E. J. Lee, Y. H. Koh, B. H. Yoon, H. E. Kim, H. W. Kim, **(2007)** “Highly porous hydroxyapatite bioceramics with interconnected pore channels using camphene-based freeze casting”, *Mater. Lett.*, 61: 2270-3.
- [34] J. P. Chen, Y. S. Chang, **(2011)** “Preparation and characterization of composite nanofibers of polycaprolactone and nanohydroxyapatite for osteogenic differentiation of mesenchymal stem cells”, *Colloids and Surfaces B: Biointerfaces*, 86: 169-75.
- [35] H. R. Ramay, M. Zhang, **(2003)** “Preparation of porous hydroxyapatite scaffolds by combination of the gel-casting and polymer sponge methods”, *Biomaterials*, 24: 3293-302.
- [36] D. Gopi, S. Nithiya, E. Shinyjoy, L. Kavitha, **(2012)** “Spectroscopic investigation on formation and growth of mineralized nanohydroxyapatite for bone tissue engineering applications”, *Spectrochimica Acta Part A*, 92: 194-200.
- [37] V. Stanic, D. Janackovic, S. Dimitrijevic, S. B. Tanaskovic, M. Mitric, M. S. Pavlovic, A. Krstic, D. Jovanovic, S. Raicevic, **(2011)** “Synthesis of antimicrobial

- monophase silver-doped hydroxyapatite nanopowders for bone tissue engineering”, *Applied Surface Science*, 257: 4510–18.
- [38] S. A. Mahadik, M. S. Kavale, S. K. Mukherjee, A. Venkateswara Rao, **(2010)** “Transparent superhydrophobic silica coatings on glass by sol–gel method”, *Applied Surface Science*, 257: 333-39.
- [39] P. Rokkanen, O. Bostman, S. Vainionpaa, E. A. Makela, E. Hirvensalo, E. K. Partio, K. Vihtonen, H. Patiala, P. Tormala, **(1996)** “Absorbable devices in the fixation of fractures”, *J. Trauma.*, 40: 123-7.
- [40] N. Zhang, H. L. Nichols, S. Tylor, X. Wen, **(2007)** “Fabrication of nanocrystalline hydroxyapatite doped degradable composite hollow fiber for guided and biomimetic bone tissue engineering”, *Mater. Sci. and Eng. C*, 27: 599-606.
- [41] D.F. Williams, **(1999)** “The Williams Dictionary of Biomaterials, Liverpool University Press”, Liverpool.
- [42] K. I. Intema, W. J. M. Heuvelsland, C. A. M. C. Dirix, A. P. Sam, **(1994)** “Hydroxyapatite microcarriers for biocontrolled release of protein drugs”, *International Journal of Pharmaceutics*, 112: 215-24.
- [43] A. J. Melville, L. M. Rodriguez-Lorenzo, J. S. Forsythe, **(2008)** “Effects of calcinations temperature on the drug delivery behavior of ibuprofen from hydroxyapatite powders”, *J. Mater. Sci. Mater. Med.*, 19: 1187–95.

Chapter – 5

- [1] S. V. Dorozhkin, **(2009)** “Calcium orthophosphates in nature”, *Biology and Medicine Materials*, 2: 399-498.
- [2] M. Vallet-Regi, J. M. Gonzalez-Calbet, **(2004)** “Calcium phosphates as substitution of bone tissues”, *Progress in Solid State Chem.*, 32: 1-31.
- [3] S. V. Dorozhkin, **(2009)** “Nanodimensional and nanocrystalline apatites and other calcium orthophosphates in biomedical engineering”, *Biology and Medicine Materials*, 2: 1975-2045.
- [4] S. Nath, R. Tripathi, B. Basu, **(2009)** “Understanding phase stability, microstructure development and biocompatibility in calcium phosphate–titania composites, synthesized from hydroxyapatite and titanium powder mix”, *Mater. Sci. Eng. C*, 29: 97-107.
- [5] S. Nath, K. Biswas, B. Basu, **(2008)** “Phase stability and microstructure development in hydroxyapatite–mullite system”, *Scr. Mater.*, 58: 1054-57.
- [6] L. L Hench, **(1998)** “Bioceramics”, *J. Am. Ceram. Soc.*, 81: 1705-28.
- [7] C. D. Friedman, P. D. Costantino, C. H. Snyderman, L. C. Chow, S. Takagi, Reconstruction of the frontal sinus and frontofacial skeleton with hydroxyapatite cement, *Arch. Facial Plast. Surg.*, 2 **(2000)** 124-9.
- [8] N. A. Zakharov, I. A. Polunina, K. E. Polunin, N. M. Rakitina, E. I. Kochetkova, N. P. Sokolova, V. T. Kalinnikov, **(2004)** “Calcium hydroxyapatite for medical applications”, *Inorg. Mater.*, 40: 641-8.
- [9] D. Tanaskovic, B. Jokic, G. Socol, A. Popescu, I. N. Mihailescu, R. Petrovic, D. Janackovic, **(2007)** “Synthesis of functionally graded bioactive glass-apatite multistructures on Ti substrates by pulsed laser deposition”, *Appl. Surf. Sci.*, 254: 1279-82.
- [10] K. Hayashi, T. Mashima, K. Uenoyama, **(1999)** “The effect of hydroxyapatite coating on bony ingrowth into grooved titanium implants”, *Biomaterials*, 20: 111-9.
- [11] H. F. Morris, S. Ocbi, **(1998)** “Hydroxyapatite-coated implants: a case for their use”, *J. Oral Maxillofac. Surg.*, 56: 1303-11.
- [12] J. C. Elliott, **(1994)** “Studies in inorganic chemistry”, vol. 18. Amsterdam: Elsevier.
- [13] R. Z. LeGeros, **(1991)** “Monographs in oral science”, vol. 15. Basel: Karger.

- [14] S. Koutsopoulos, **(2002)** "Synthesis and characterization of hydroxyapatite crystals: a review study on the analytical methods", *J. Biomed. Mater. Res. A*, 62: 600-12.
- [15] A. Ito, M. Otsuka, H. Kawamura, M. Ikeuchi, H. Ohgushi, Y. Sogo, N. Ichinose, **(2005)** "Zinc-containing tricalcium phosphate and related materials for Promoting bone formation", *Curr. Appl. Phys.*, 5: 402-6.
- [16] R. Z. Legeros, **(2008)** "US Patent" 7, 419, 680.
- [17] S. Cin, E. Unal, A. Pamir, B. Kologlu, A. O. Cavdar, **(2001)** "Blood zinc (plasma, red blood cell zinc) and insulin-like growth factor-1 in children from an "impoverished" area in ankara", *J. Trace Elem. Exp. Med.*, 14: 31-4.
- [18] M. Hambidge, **(2000)** "Human zinc deficiency", *J. Nutr.*, 130: 1344-9.
- [19] G. Oner, B. Bhaumick, R. M. Bala, **(1984)** "Effect of zinc-deficiency on serum somatomedin levels and skeletal growth in young rats", *Endocrinology*, 114: 1860-3.
- [20] M. Yamaguchi, H. Oishi, Y. Suketa, **(1987)** "Stimulatory effect of zinc on bone formation in tissue culture", *Biochem. Pharmacol.*, 36: 4007-12.
- [21] B. L. Vallee, K. H. Falchuk, **(1993)** "The biochemical basis of zinc physiology", *Physiol. Rev.*, 73: 79-118.
- [22] A. Togari, S. Arakawa, M. Arai, S. Matsumoto, **(1993)** "Alteration of in vitro bone metabolism and tooth formation by zinc", *Gen. Pharmacol.*, 24: 1133-40.
- [23] W. R. Holloway, F. M. Collier, R. E. Herbst, J. M. Hodge, G. C. Nicholson, **(1996)** "Osteoblast-mediated effects of zinc on isolated rat osteoclasts: inhibition of bone resorption and enhancement of osteoclast number", *Bone*, 19: 137- 42.
- [24] M. Yamaguchi, A. Igarashi, S. Uchiyama, **(2004)** "Bioavailability of zinc yeast in rats: Stimulatory effect of bone calcification in vivo", *J. Health. Sci.*, 50: 75-81.
- [25] D. L. Bougle, J. P. Sabatier, G. G. Souquieres, F. G. Metz, D. Laroche, P. Jauzac, F. Bureau, **(2004)** "Zinc status and bone mineralisation in adolescent girls", *J. Trace Elem. Med. Biol.*, 18: 17-21.
- [26] M. Yamaguchi, H. Miwa, **(1991)** "Stimulatory effect of beta-alanyl-L-histidinato zinc on bone formation in tissue culture", *Pharmacology*, 42: 230-40.
- [27] Z. J. Ma, M. Yamaguchi, **(2000)** "Alternation in bone components with increasing age of newborn rats: role of zinc in bone growth", *J. Bone Miner. Metab.*, 18: 264-70.

- [28] Z. J. Ma, M. Yamaguchi, **(2001)** “Role of endogenous zinc in the enhancement of bone protein synthesis associated with bone growth of newborn rats”, *J. Bone Miner. Metab.*, 19: 38-44.
- [29] Z. J. Ma, M. Yamaguchi, **(2001)** “Stimulatory effect of zinc on deoxyribonucleic acid synthesis in bone growth of newborn rats: enhancement with zinc and insulin-like growth factor-I”, *Calcif. Tissue Int.*, 69: 158-63.
- [30] P. J. Fraker, **(2005)** “Roles for cell death in zinc deficiency”, *J. Nutr.*, 135: 359-62.
- [31] S. C. J. Loo, Y. E. Siew, S. Ho, F. Yin Chiang Boey, **(2008)** “Synthesis and hydrothermal treatment of nanostructured hydroxyapatite of controllable sizes”, *J. Mater. Sci. Mater. Med.*, 19: 1389-97.
- [32] B. K. Das, **(1981)** “Preparation and characterization of mater”, (Ed) J. M. Honing and C. N. R. Rao, New York, Academic Press.
- [33] P. N. Jagadale, S. R. Kulal, M. G. Joshi, P. P. Jagtap, S.M. Khetre, S. R. Bamane, **(2013)** “Synthesis and characterization of nanostructured CaSiO_3 biomaterial”, *Materials Science-Poland*, 31: 269-75.
- [34] C. Ohtsuki, Y. Aoki, T. Kokubo, Y. Bando, M. Neo, T. Nakamura, **(1995)** “Transmission electron microscopic observation of glass-ceramic A-W and apatite layer formed on its surface in a simulated body fluid”, *J. Ceram. Soc. Japan*, 103: 449-54.
- [35] B. Vaidhyanathan, K. J. Rao, **(1996)** “Rapid microwave assisted synthesis of hydroxyapatite”, *Bull. Mater. Sci.*, 19: 1163-5.
- [36] P. N. Chavan, M. M. Bahir, R. U. Mene, M. P. Mahabole, R. S. Khairnar, **(2010)** “Study of nanobiomaterial hydroxyapatite in simulated body fluid: Formation and growth of apatite”, *Mater. Sci. and Eng. B*, 168: 224-30.
- [37] A. M. El-Kady, A. F. Ali, R. A. Rizk, M. M. Ahmed, **(2012)** “Synthesis, characterization and microbiological response of silver doped bioactive glass nanoparticles”, *Ceram. Int.*, 38: 177-88.
- [38] A. Saboori, M. Rabiee, F. Moztarzadeh, M. Sheikhi, M. Tahriri, M. Karimi, **(2009)** “Synthesis, characterization and in vitro bioactivity of sol-gel derived $\text{SiO}_2\text{-CaO-P}_2\text{O}_5\text{-MgO}$ bioglass”, *Mater. Sci. Eng. C*, 29: 335-40.

- [39] K. Haberko, M. M. Bu'cko, J. Brzezi'nska-Miecznik, M. Haberko, W. Mozgawa, T. Panz, **(2006)** "Natural hydroxyapatite—its behaviour during heat treatment", *J. Eur. Ceram. Soc.*, 26: 537-42.
- [40] N. S. Gajbhiye, U. Bhattacharyya and V. S. Darshane, **(1995)** "Thermal decomposition of zinc-iron citrate precursor", *Thermochim Acta.*, 264: 219-30.
- [41] Z. Feng, Y. Li, Y. Huang, H. Jin Seo, **(2011)** "Luminescence properties of Eu^{2+} and Eu^{3+} doped calcium-deficient hydroxyapatite prepared in air", *J. Alloys and Compounds*, 509: 7087-92.
- [42] A. L. Patterson, **(1939)** "The Scherrer formula for X-ray particle size determination", *Phys. Rev.*, 56: 978-82.
- [43] C. Hammond, **(1997)** "The basics of crystallography and diffraction, Oxford University Press", Oxford.
- [44] B. D. Cullity, **(1956)** "Elements of X-ray diffraction", Addison-Wesley, London, 99.
- [45] M. Zandi, H. Mirzadeh, C. Mayer, H. Urch, M. B. Eslaminejad, F. Bagheri, H. Mivehchi, **(2010)** "Biocompatibility evaluation of nano-rod hydroxyapatite/gelatin coated with nano-HAP as a novel scaffold using mesenchymal stem cells, *J. Biomedical Materials Research Part A*, 92A: 1244-55.
- [46] V. S. Komlev, S. M. Barinov, V. P. Orlovskii, S. G. Kurdyumov, **(2001)** "Porous ceramic granules of hydroxyapatite", *Refractories and Industrial Ceramics.*, 42: 195-7.
- [47] S. Nayar, M. K. Sinha, D. Basu, A. Sinha, **(2006)** "Synthesis and sintering of biomimetic hydroxyapatite nanoparticles for biomedical applications", *J. Mater. Sci. Mater. Med.*, 17: 1063-8.
- [48] Y. Zhang, J. Lu, J. Wang, S. Yang, Y. Chen, **(2009)** "Synthesis of nanorod and needle-like hydroxyapatite crystal and role of pH adjustment", *J. Crystal Growth*, 311: 4740-6.
- [49] J. P. Chen, Y. S. Chang, **(2011)** "Preparation and characterization of composite nanofibers of polycaprolactone and nanohydroxyapatite for osteogenic differentiation of mesenchymal stem cells", *Colloids and Surfaces B: Biointerfaces*, 86: 169-75.
- [50] M. D. Francis, N. C. Webb, **(1971)** "Hydroxyapatite formation from a hydrated calcium monohydrogen phosphate precursor", *Calc. Tiss. Res.*, 6: 335-42.

- [51] F. Ren, R. Xin, X. Ge, Y. Leng, **(2009)** “Characterization and structural analysis of zinc-substituted hydroxyapatites”, *Acta Biomaterialia*, 5: 3141-9.
- [52] D. Gopi, S. Nithiya, E. Shinyjoy, L. Kavitha, **(2012)** “Spectroscopic investigation on formation and growth of mineralized nanohydroxyapatite for bone tissue engineering applications”*F, Spectrochimica Acta Part A*, 92: 194-200.
- [53] C. Yang, P. Yang, W. Wang, S. Gai, J. Wang, M. Zhang, J. Lin, **(2009)** “Synthesis and characterization of Eu-doped hydroxyapatite through a microwave assisted microemulsion process”, *Solid State Sciences*, 11: 1923–28.
- [54] S. A. Mahadik, M. S. Kavale, S. K. Mukherjee, A. Venkateswara Rao, **(2010)** “Transparent superhydrophobic silica coatings on glass by sol–gel method”, *Applied Surface Science*, 257: 333-39.
- [55] D. S. Brauer, C. Russel, S. vogt, J. Weisser, M. Schnabelrauch, **(2007)** “Fabrication and in vitro characterization of porous biodegradable composites based on phosphate glasses and oligolactide-containing polymer networks”, *J. Biomed. Mater. Res. A*, 80: 410-20.
- [56] P. Rokkanen, O. Bostman, S. Vainionpaa, E. A. Makela, E. Hirvensalo, E. K. Partio, K. Vihtonen, H. Patiala, P. Tormala, **(1996)** “Absorbable devices in the fixation of fractures”, *J. Trauma.*, 40: 123-7.
- [57] N. Zhang, H. L. Nichols, S. Tylor, X. Wen, **(2007)** “Fabrication of nanocrystalline hydroxyapatite doped degradable composite hollow fiber for guided and biomimetic bone tissue engineering”, *Mater. Sci. and Eng. C*, 27: 599- 606.
- [58] D. F. Williams, **(1999)** “The williams dictionary of biomaterials, Liverpool University Press, Liverpool.
- [59] J. C. Le Huec, D. Clement, B. Brouillaud, N. Barthe, B. Dupuy, B. Foliguet, B. Basse-Cathalinat, **(1998)** “Evolution of the local calcium content around irradiated beta-tricalcium phosphate ceramic implants: in vivo study in the rabbit”, *Biomaterials*, 19: 733-8.
- [60] H. Guo, J. Su, J. Wei, H. Kong, C. Liu, **(2009)** “Biocompatibility and osteogenicity of degradable Ca-deficient hydroxyapatite scaffolds from calcium phosphate cement for bone tissue engineering”, *Acta Biomaterialia*, 5: 268-78.

- [61] A. M. El-Kady, A. F. Ali, R. A. Rizk, M. M. Ahmed, **(2012)** “Synthesis, characterization and microbiological response of silver doped bioactive glass nanoparticles”, *Ceram. Int.*, 38: 177-88.
- [62] G. D. Venkatasubbu, S. Ramasamy, V. Ramakrishnan, J. Kumar, **(2011)** “Nanocrystalline hydroxyapatite and zinc-doped hydroxyapatite as carrier material for controlled delivery of ciprofloxacin”, *Biotech*, 1: 173-86.
- [63] W. C. Liu, C. T. Wong, M. K. Fong, W. S. Cheung, R. Y. Kao, K. D. Luk, W. W. Lu, **(2010)** “Gentamicin-loaded strontium-containing hydroxyapatite bioactive bone cement—an efficient bioactive antibiotic drug delivery system”, *J. Biomed. Mater. Res. B Appl. Biomater.*, 9: 397-406.

Chapter – 6

- [1] A. Nakahira, S. Nakamura, M. Horimoto, (2007) “Synthesis of modified hydroxyapatite (HAp) substituted with Fe ion for DDS application”, *IEEE Trans Mag.*, 43: 2465–7.
- [2] A. Tampieri, T. D. Alessandro, M. Sandri, S. Sprio, E. Landi, L. Bertinetti, S. Panseri, G. Pepponi, J. Goettlicher, M. Banobre-Lopez, J. Rivas, (2012) “Intrinsic magnetism and hyperthermia in bioactive Fe-doped hydroxyapatite”, *Acta Biomater.*, 8: 843-51.
- [3] J. L. Corchero, A. Villaverde, (2009) “Biomedical applications of distally controlled magnetic nanoparticles”, *Trends Biotechnol.*, 27: 468–76.
- [4] M. Ajeesh, B. F. Francis, J. Annie, P. R. Harikrishna Varma, (2010) “Nano iron oxide hydroxyapatite composite ceramics with enhanced radiopacity”, *J. Mater. Sci. Mater. Med.*, 21: 1427–34.
- [5] M. Johannsen, A. Jordan, R. Scholz, M. Koch, M. Lein, S. Deger, J. Roigas, K. Jung, S. Loening, (2004) “Evaluation of magnetic fluid hyperthermia in standard rat model of prostate cancer”, *J. Endourol.*, 18: 495-500.
- [6] P. N. Kumta, C. Sfeir, D. H. Lee, D. Olton, D. Choi, (2005) “Nanostructured calcium phosphates for biomedical applications: Novel synthesis and characterization”, *Acta Biomater.*, 1: 65-83.
- [7] A. Ito, T. Kobayashi, (2008) “Intracellular hyperthermia using magnetic nanoparticles: A novel method for hyperthermia cancer”, *Jap. Soc. Thermal Med.*, 24: 113–29.
- [8] Q. A. Pankhurst, J. Connolly, S. K. Jones, J. Dobson, (2003) “Applications of magnetic nanoparticles in biomedicine”, *J. Phys. D. Appl. Phys.*, 36: 167–81.
- [9] C. N. Ramchand, P. Priyadarshini, P. Kopcansky, R. V. Metha, (2001) “Applications of magnetic fluids in medicine and biotechnology”, *Indian J. Pure Appl. Phys.*, 39: 683–9.
- [10] R. Morrissey, L. M. Rodriguez-Lorenzo, K. A. Gross, (2005) “Influence of ferrous iron incorporation on the structure of hydroxyapatite”, *J. Mater. Sci. Mater. Med.*, 16: 387-92.
- [11] P. T. Lieu, M. Heiskala, P. A. Peterson, Y. Yang, (2001) “The roles of iron in health and disease”, *Mol. Aspects Med.*, 22: 1-87.

- [12] K. Yamasaki, H. Hagiwara, **(2009)** “Excess iron inhibits osteoblast metabolism”, *Toxicol. Lett.*, 191: 211–5.
- [13] C. C. Berry, **(2005)** “Possible exploitation of magnetic nanoparticle–cell interaction for biomedical applications”, *J. Mater. Chem.*, 15: 543–7.
- [14] J. Dobson, **(2001)** “Nanoscale biogenic iron oxides and neurodegenerative disease”, *FEBS Lett.*, 496: 1–5.
- [15] K. A. Gross, R. Jackson, J. D. Cashion, L. M. Rodriguez-Lorenzo, **(2002)** “Iron substituted apatites: A resorbable biomaterial with potential magnetic properties”, *Eur. Cells Mater.*, 3: 114–7.
- [16] E. S. Kawasaki, T. A. Player, **(2005)** “Nanotechnology, nanomedicine, and the development of new, effective therapies for cancer”, *Nanomed. Nanotech. Biol. Med.*, 1: 101-9.
- [17] I. Mobasherpour, M. S. Heshajin, A. Kazemzadeh, M. Zakeri, **(2007)** “Synthesis of nanocrystalline hydroxyapatite by using precipitation method”, *J. Alloys Compd.*, 430: 330-3.
- [18] A. Siddharthan, S. K. Seshadri, T. S. Sampath Kumar, **(2006)** “Influence of microwave power on nanosized hydroxyapatite particles”, *Scripta Materialia.*, 55: 175-8.
- [19] W. Pon-On, S. Meejoo, I. M. Tang, **(2007)** “Incorporation of iron into nano hydroxyapatite particles synthesized by the microwave process”, *Int. J. Nanosci.*, 6: 9-16.
- [20] W. Pon-On, S. Meejoo, I. M. Tang, **(2008)** “Substitution of manganese and iron into hydroxyapatite: core/shell nanoparticles”, *Mater. Res. Bull.*, 43: 2137-44.
- [21] A. M. El-Kady, A. F. Ali, R.A. Rizk, M. M. Ahmed, **(2012)** “Synthesis, characterization and microbiological response of silver doped bioactive glass nanoparticles”, *Ceram. Int.*, 38: 177-88.
- [22] Z. Feng, Y. Li, Y. Huang, H. Jin Seo, **(2011)** “Luminescence properties of Eu^{2+} and Eu^{3+} doped calcium-deficient hydroxyapatite prepared in air”, *J. Alloys and Compd.*, 509: 7087-92.
- [23] A. L. Patterson, **(1939)** “The Scherrer formula for X-ray particle size determination”, *Phys. Rev.*, 56: 978-82.
- [24] C. Hammond, **(1997)** “The basics of crystallography and diffraction”, Oxford University Press, Oxford.
- [25] B. D. Cullity, **(1956)** “Elements of X-ray diffraction”, Addison-Wesley, London, 99.

- [26] D. Gopi, S. Nithiya, E. Shinyjoy, L. Kavitha, **(2012)** “Spectroscopic investigation on formation and growth of mineralized nanohydroxyapatite for bone tissue engineering applications”, *Spectrochimica Acta Part A*, 92: 194-200.
- [27] C. Yang, P. Yang, W. Wang, S. Gai, J. Wang, M. Zhang, J. Lin, **(2009)** “Synthesis and characterization of Eu-doped hydroxyapatite through a microwave assisted microemulsion process”, *Solid State Sciences*, 11: 1923–28.

**PATENTS FILED, PUBLICATIONS
AND CONFERENCES ATTENDED**

Patents Filed

- 1) Title of the invention: - [Invention of nanostructured calcium silicate as drug delivery agent.](#)

Application no: - 123/MUM/2012

Date of filing: - 13/01/2012

Date of publication: - 23/03/2012.

- 2) Title of the Invention: - [Invention of nanorods of zinc doped hydroxyapatite biomaterial.](#)

Application no: - 2171/MUM/2012

Date of filing: - 30/07/2012

Date of publication: - 07/09/2012.

Publications

- 1) Synthesis, characterization and in vitro drug delivery of nanostructured Fe-doped hydroxyapatite bioceramics, P. N. Jagadale, P. P. Jagtap, and S. R. Bamane, *Der, Chemica Sinica*, 6: (2015) 28-36.
- 2) Synthesis and characterization of nanostructured CaSiO_3 Biomaterial, P. N. Jagadale, S. R. Kulal, S. M. Khetre, M. G. Joshi, P. P. Jagtap and S. R. Bamane, *Materials Science-Poland*, 31: (2013) 269-275.
- 3) Nanoporous calcium silicate: Potentially an efficient biomaterial for antibiotics carrier, P. N. Jagadale, S. R. Kulal, S. R. Bamane and V. V. Dhapte *Journal of Pharmacy Research*, 5: (2012) 360-362.
- 4) Calcium hydroxyapatite bioceramics and evaluation of their in vitro biocompatibility, P. N. Jagadale and S. R. Bamane, *J. of Pharm, biological and Chemical Science*, 2: (2011) 180-186.
- 5) Novel synthesis and characterization of hydroxyapatite bioceramics nanocrystallites, P. N. Jagadale, P. P. Jagtap, M. G. Joshi, S. R. Bamane, *Advance Materials Letters – Communicated*.
- 6) Synthesis, characterization and electrical properties of nanostructured LaAlO_3 by sol–gel auto combustion method, K. A. Khamkar, P. N. Jagadale, V. V. Dhapte and S. R. Bamane, *J. Mat. Sci: Mat. Elec.*, 24: (2013) 4482-4487.
- 7) Synthesis of Dy doped Co–Zn ferrite by sol–gel auto combustion method and its characterization, S. R. Kulal, S. S. Khetre, P. N. Jagadale and S. R. Bamane, *Materials Letters*, 84: (2012) 169–172.

**Seminars/conferences
attended**

1. Participation in the 18th DAE-BRNS *International Symposium* on “Thermal Analysis (THERMANS-2012)” held at Training School Hostel, Anushaktinagar, Mumbai, (31st – 2nd Feb. 2012).
2. Participation and Paper presented in *1st International Conference* on “Physics of Materials and Materials Based Device Fabrication” organized by Dept. of Physics, Shivaji University, Kolhapur (17-19th Jan. 2012).
3. Participation and Paper presented in *National Workshop* on “Nanoscience and Nanotechnology” Organized by MAEER’s MIT College of Engineering, Pune (6-7th Jan. 2012).
4. Participation and Paper presented in *International Conference* on “Nanoscience, Technology and Societal Implications” organized by C. V. Raman College of Engineering, Bhubaneswar, India (8-10 Dec. 2011).
5. Participation and Paper presented in *National Symposium* on “Advances in Synthetic Methodologies and New materials” organized by Department of Chemistry Shivaji University, Kolhapur (21-22nd Jan 2011).
6. Participation and Paper presented in *National Seminar* on “Advanced Materials” organized by Shivaji University, Kolhapur (19-20th Mar 2010).
7. Participation and Paper presented in *National Conference* on “Recent Trends in Material Synthesis & Characterization” organized by Bhalerao Science College, Saoner (Nagpur) (4-5th Dec 2009).